海洋開発及地球科学技術調査研究促進費

地球科学技術特定調査研究

アジアモンスーン機構に関する研究

JAPANESE EXPERIMENT ON ASIAN MONSOON

(JEXAM)

(平成元年度～平成１０年度)
(FY1989 ～ FY1998)

最終成果報告書
FINAL REPORT

平成１２年３月
March 2000

科学技術庁研究開発局

Research and Development Bureau
Science and Technology Agency
Japan

はじめに

大規模な季節変動として知られているアジアモンスーンは、インド洋・東南アジア周辺の海洋とチベット・ヒマラヤを始めとしたアジア大陸の地表面が、大気を媒体として熱・水蒸気等の交換を行うことにより、相互に影響を及ぼし合って発生している現象です。その活動の年々変動は、東南アジア地域や日本を始めとした周辺地域の気候のみならず、大気大循環を介して世界の気候に大きな影響を与えています。また、アジアモンスーンの活動が西部熱帯太平洋域の大気・海洋変動を引き起こし、太平洋上で発生するエル・ニーニョ南方振動の引き金になっている可能性があるという指摘もあり、この点からも注目されています。しかし、これらの地域・海域は広大であり、また観測環境が厳しいこと等から観測体制の整備が遅れており、気象・海象・陸象に関するデータの収集は必ずしも十分に行われていませんでした。

このため科学技術庁では、海洋開発及地球科学技術調査研究促進費により「アジアモンスーン機構に関する研究」を平成元年度より開始し、さらに、平成５年に「『アジアモンスーン機構に関する研究』プロジェクトに関する日本国科学技術庁と中華人民共和国国家気象局との間の実施取極」を結び、日中の協力体制を整えて、観測・解析を進めてきました。

本研究の成果が、アジアモンスーン機構の解明に寄与し、さらには気候変動に対する理解を深めることを期待しています。

最後になりましたが、本研究に携わっていただいた関係各位に対し感謝するとともに、今後の「アジアモンスーン」研究の更なる発展を祈念いたします。

平成１２年３月

科学技術庁研究開発局長
池田　要

目　次

Contents

研究計画の概要

Outline of the Study Plan

I．研究の趣旨

アジアモンスーンは、インド洋・東南アジア周辺の海洋とチベット・ヒマラヤを始めとしたアジア大陸の地表面が、その熱的特性の相違により大気を媒体とした熱・水蒸気等の交換を通じて、それぞれ相互に影響を及ぼし合う結果、東南アジア・東アジア地域における季節的な現象として発現している。その活動の年次の変動は、東南アジア地域や、日本を始めとした周辺地域の気候の変動に大きな影響を及ぼすばかりでなく、大気大循環変動を介して世界の気候にも大きな影響を与えている。また最近、アジアモンスーンの活動の異常は西部熱帯太平洋域の大気・海洋変動を引き起こし、これが太平洋規模で発生するエル・ニーニョ南方振動の引き金となっている可能性があるという研究報告もあり、この点からも注目する必要がある。しかしながら、これらの地域・海域は、対象域の広大さや観測環境の厳しさ等から観測体制が整備されておらず、気象・海象・陸象の基本的な要素に係るデータの収集が必ずしも十分に行なわれているとは言えない。

従って、アジアの一員であり、アジアモンスーンの直接的影響を受け、大気・海洋観測の十分なポテンシャルを有する我が国が、世界の気候を形成する複雑なシステムの一つであるアジアモンスーンの機構を解明するため長期的・総合的な研究を実施することが緊要となっている。本研究を実施することにより、我が国を含むアジア地域における旱ばつや長雨といった異常気象発現の予測技術のみならず、世界的規模の気候変動を予測する技術の発展に寄与することが期待される。

以上のような状況を踏まえて、本研究は平成元年度より10年間の計画で実施した。

I . General Introduction

Asian Monsoon is caused by the thermal contrast between the Indian Ocean and surrounding oceans, and the land surface of Asian Continent. These two land and ocean areas interact with each other through the exchange of the heat and moisture. Its consequence is observed as a seasonal phenomenon in the regions of Southeast Asia and East Asia, including Japan.

The year-to-year variation of the Asian Monsoon has a significant influence not only on the climate of Southeast Asia and the surrounding area including Japan, but also on the worldwide climate through the global atmospheric circulations. Furthermore, it is recently reported that the anomalous activities of the Asian Monsoon causes the atmospheric/oceanic variations over the tropical western Pacific which, in turn, trigger the El Nino/Southern Oscillation events over the whole Pacific Ocean.

Though it is recognized that Asian Monsoon plays an important role in the global climate system, its mechanism has not yet been made clear. This is mainly attributable to the fact that the atmospheric and oceanographic data are sparse over those regions due to the technical difficulties in the observations and the insufficiencies of conventional observation network.

Japan, as a member of the Asian countries, is situated under the direct influence of the Asian monsoon and has a capability to conduct the atmospheric and oceanographic observations. Therefore, it is an important role of Japan to carry out the research projects for the study on Asian Monsoon in cooperation with the countries such as China and India.

This project is expected to make a contribution for the improvement of the long-range forecast of the global climate change as well as the forecasting technique of the unusual weather, such as drought and long spell of rain.

Based on the understandings as mentioned above, Science and Technology Agency (STA) of Japan has launched this ten-year research project since April 1989.

Ⅱ．研究の概要

1．大気・海洋・陸域間相互作用の諸過程に関する観測・解析研究

(1) 大気における諸過程に関する観測・解析研究

・　静止気象衛星資料をデータベース化し、モンスーン活動の年々変動、降水システム、エルニーニョとの関連についての解析を行う。

・　前期に観測した対流雲のデータを解析し、対流雲の構造、対流雲による熱、水、運動量の輸送過程を明らかにする。

(2) 海洋における諸過程に関する観測・解析研究

・　東南アジア周辺海域及びインド洋を航行する公庁船、商船及び漁船により海洋表層水温の通年観測を行う。

・　インド洋に漂流ブイを放流し、大規模海流循環の通年観測を行う。

・　上記で取得した海洋データの標準化、データベース化を促進する。また、インド洋及び東南アジア周辺海域の海洋観測情報交換システムを構築し、取得データを交換する。

(3) 陸域における諸過程に関する観測・解析研究

・　チベット地域における気象及び陸面の観測を行い、大気陸面間のエネルギー収支を見積もる。

・　商船委託により、インド洋から東南アジア周辺に至る海域での海上気象・高層気象観測、及びウィンドプロファイラーにより下層大気の観測を行い、大気海洋間、大気陸面間のエネルギー収支を見積もる。

・　極軌道地球観測衛星資料から、積雪、雲分布、土壌水分量を算出し、解析する。

・　中国の代表流域の水文資料、水文・気象データを収集し、水収支解析及び蒸発発散解析を行う。

2．数値モデルによる大気・海洋・陸域間相互作用の実験研究

(1) 数値モデルによる４次元資料同化システムの開発に関する研究

・　現在の４次元資料同化システムに、現在使用されていない衛星データ等を組み込めるように高度化を図り、得られた物理量からモンスーン機構を考察する。

(2) 広域水収支モデルの開発に関する研究

・　前期に開発した流出量モデル、蒸発散量モデルへの検証・改良を行うと共に、積雪・流出量サブモデルを開発し、積雪地域への広域水収支モデルの適用を図る。

3．大気・海洋・陸面間の相互作用に関する総合研究

(1) 大規模モデルによる大気・海洋・陸面間の相互作用に関する実験研究

・　前期に用いたモデルの改良を行う。また、大気海洋結合モデルを導入し、アジアモンスーンの機構に対する海洋や陸面の役割を評価する。さらに高分解能の大気大循環モデルを開発し、地表面状態や対流活動の影響を評価する。

(2) モンスーンのエネルギー収支に関する解析研究

・　モデルのシミュレーション結果を衛星観測データの解析結果によって検証し、モンスーン機構のエネルギー収支解析を行う。

(3) モンスーン循環系の総合解析

・　海洋や雪氷分布の変動と、モンスーン循環を含む大気大循環や日本の天候の関連を調査する。また、高層・地上・海洋・陸面観測データを用いて総合的に解析することによって、モンスーン循環系を解明する。

Ⅱ. Outline of the Study

1. Observation and Analysis on the Process of the Atmosphere-Ocean-Land Interactions

(1) Observation and Analysis on the Process in the Atmosphere

-To construct a database of the Japanese and Indian satellites and make an analysis of the large scale cloudiness changes.

-To observe and three dimensional structures of the tropical convective clouds related to the heat budget of the atmosphere-ocean interaction by wind Doppler radar.

(2) Observation and Analysis on the Process over the Ocean

-To observe sub-surface temperature throughout the year by voluntary, official, commercial and fishing ships over the Southeast Asia and the Indian Ocean.

-To observe larg-scale oceanic current throughout the year by drifting buoys over the Indian Ocean.

-To standardize and construct a database of the oceanic data and promote a data exchange. To construct an information exchange systemconcerning to the observation in the Indian Ocean.

(3) Observation and Analysis on the Process over the Land

-To observe weather and land surface conditions over the Tibetan area and estimate an energy budget of the atmosphere-land interaction.

-To observe three dimensional structures of low level air flow related to the heat budget of the atmosphere-land interaction by wind profiler.

-To promote a maritime meteorological observation by voluntary commercial ships and estimate an energy budget of the atmosphere-ocean interaction.

-To construct a database of the polar orbiting earth observation satellites and make an analysis of the atmosphere-ocean-land situations related to the large scale hydrological variations.

-To collect daily hydro-meteorological data over the Yangtze River basin and make an analysis of the long-term variations.

2. Experiment of the Atmosphere-Ocean-Land Interactions by the Use of Numerical Models

(1) Development of the Four Dimensional Data Assimilation System by the Use of Numerical Model

-To develop the four dimensional data assimilation system by the use of numerical models for the analysis on the process of the atmosphere-ocean-land interactions.

(2) Development of the Water Balance Model over the Wide Area

-To develop numerical models for the investigation of the large scale hydrological budget over the Tibet,India and Southeast Asia related to the heat transport.

3. Synthetic Study on the Atmosphere-Ocean-Land Interactions

(1) Experiment of the Atmosphere-Ocean-Land Interactions by the Use of General Circulation Models

-To perform numerical experiments of the effect of intraseasonal 30-60 day variation on Asian monsoon.

-To perform numerical experiments by the atmosphere-ocean coupled model for the investigation of the effects of oceanic conditions on the long-term variation of the atmosphere-land condition.

(2) Analysis of the Energy Balance of Monsoon

-To construct a database of Earth radiation budget through the polar orbiting meteorological satellites and make an analysis of an effect of the monsoon variation.

(3) Synthetic Study of the Monsoon Circulations

-To make a comprehensive analysis of the monsoon circulation by the use of the standardized data.

III. 研究実施体制
Research Items and Institutes

研究項目 Research Items	担当機関 Research Institutes
I．大気・海洋・陸域間相互作用の諸過程に関する観測・解析研究 Observation and Analysis on the Process of the Atmosphere-Ocean-Land Interactions	
1．大気における諸過程に関する観測・解析研究 Observation and Analysis on the Process in the Atmosphere	
(1) 大規模積雲対流活動と降水系に関する解析研究 Analysis on the Large scale Convective Activity and Precipitation Systems	気象庁 気象研究所 Meteorological Research Institute (MRI), Japan Meteorological Agency (JMA)
(2) 大規模雲域内における対流雲構造に関する観測研究 Observation of Structure of Convective Clouds in Large-scale Cloud Systems	気象庁 気象研究所 MRI/JMA
(3) モンスーン域対流雲の維持過程と水収支に関する研究 Analysis on the evolution of Convective cloud systems	科学技術庁 防災科学技術研究所 National Research Institute for Earth Science and Disaster Prevention (NIED), Science and Technology Agency (STA)
2．海洋における諸過程に関する観測・解析研究 Observation and Analysis on the Process over the Ocean	
(1) 表層水温に関する観測研究 Observation on Subsurface Temperature by Voluntary Ships	水産庁 遠洋水産研究所 Far seas Fisheries Research Laboratory, Fisheries Agency 気象庁 気候・海洋気象部 Climate & Marine Department (CMD), JMA
(2) 海流循環に関する観測研究 Observation on Oceanic Currents with Drifting Buoys	海上保安庁 水路部 Hydrographic Department (HD), Maritime Safety Agency (MSA)
(3) 海洋データの標準化及び海洋データ交換の推進 Standardization of Oceanic Data and Promotion of Exchange of Oceanic Data and Information	海上保安庁 水路部 HD/MSA
3．陸域における諸過程に関する観測・解析研究 Observation and Analysis on the Process over the Land	
(1) チベット・ヒマラヤにおける水文変動に関する観測研究 Observation on Hydrology over the Tibetan Plateau and Himalayas	科学技術庁 防災科学技術研究所 NIED/STA

研究項目 Research Items	担当機関 Research Institutes
(2) 地表面熱収支に関する観測研究 Observation on Regional Surface Heat Budget Observational Study of the Ground Surface Heat Budgets	気象庁 気象研究所 MRI/JMA 郵政省 通信総合研究所 Communications Research Laboratory, Ministry of Posts and Telecommunications
(3) モンスーン循環広域条件及び雪氷変動状況に関する解析研究 Analysis on Environmental Condition and Snow-Ice Cover Changes Affecting Monsoon Cycle in Asia	科学技術庁 防災科学技術研究所 NIED/STA
(4) 地域水収支に関する解析研究 Analytical study of water balance on representative river basins	科学技術庁 防災科学技術研究所 NIED/STA
Ⅱ. 数値モデルによる大気・海洋・陸域間相互作用の実験研究 Experiment of the Atmosphere-Ocean-Land Interactions by the Use of Numerical Models	
1. 数値モデルによる４次元資料同化システムの開発に関する研究 Development of the Four Dimensional Data Assimilation System by the Use of Numerical Model	気象庁 予報部 Forecasting Department (FD), JMA
2. 広域水収支モデルの開発に関する研究 Development of the Water Balance Model over the Wide Area	科学技術庁 防災科学技術研究所 NIED/STA
Ⅲ. 大気・海洋・陸面間の相互作用に関する総合研究 Synthetic Study on the Atmosphere-Ocean-Land Interactions	
1. 大規模モデルによる大気・海洋・陸面間の相互作用に関する実験研究 Experiment of the Atmosphere-Ocean-Land Interactions by the Use of General Circulation Models	気象庁 気象研究所 MRI/JMA
2. モンスーンのエネルギー収支に関する解析研究 Analysis of the Energy Balance of Monsoon	気象庁 気象研究所 MRI/JMA
3. モンスーン循環系の総合解析 Synthetic Study of the Monsoon Circulations	気象庁 気候・海洋気象部 CMD/JMA
Ⅳ. 検討委員会の開催等 Research Steering Committee	気象庁 気象研究所 MRI/JMA 科学技術庁 研究開発局 Research and Development Bureau, STA

IV. 研究検討委員会

Research Steering Committee

委　員　名 Membership		所　　属 Affiliation
委員長 Chairman:	浅井　冨雄 Dr. Tomio Asai	「地球変動のメカニズム」戦略的基礎研究推進事業研究事務所研究統括 Core Research for Evolutional Science and Technology, JST
委員 Member:	稲掛　伝三 Dr. Denzo Inagake	水産庁遠洋水産研究所海洋・南大洋部低緯度域海洋研究室長 National Research Institute of Far Seas Fisheries
	大畑　哲夫 Dr. Tetsuo Oh'hata	北海道大学低温科学研究所寒冷陸域科学部門 Institute of Low Temperature Science, Hokkaido University
	加藤　内蔵進 Dr. Kuranoshin Kato	岡山大学教育学部助教授 School of Education, Okayama University
	岸井　徳雄 Dr.Tokuo Kishii	科学技術庁防災科学技術研究所気圏·水圏地球科学技術研究部陸域水循環モデルチーム長 National Research Institute for Earth Science and Disaster Prevention
	久保田　雅久 Prof. Masahisa Kubota	東海大学海洋学部教授 School of Marine Science and Technology, Tokai University
	近藤　洋輝 Dr. Hiroki Kondo	気象庁気象研究所気候研究部長 MRI/JMA
	住　　明正 Prof. Akimasa Sumi	東京大学気候システム研究センター長 Center for Climate System Research, University of Tokyo
	竹内　義明 Dr. Yoshiaki Takeuchi	気象庁予報部数値予報課予報官 FD/JMA

委 員 名 Membership	所 属 Affiliation
西田 英男 Mr. Hideo Nishida	海上保安庁水路部企画課沿岸調査課長 HD/MSA
萩野谷 成徳 Dr. Shigenori Haginoya	気象庁気象研究所物理気象研究部主任研究官 MRI/JMA
藤谷 徳之助 Dr. Tokunosuke Fujitani	気象庁気候・海洋気象部海洋課長 CD/JMA
増田 悦久 Dr. Yoshihisa Masuda	郵政省通信総合研究所沖縄電波観測所長 Communications Research Laboratory, Ministry of Posts and Telecommunications
松浦 五朗 Dr. Goro Matsuura	海上保安庁水路部海洋情報課上席海洋情報官 HD/MSA
安成 哲三 Prof. Tetsuzoh Yasunari	筑波大学地球科学系教授 Institute of Geosciences, Tsukuba University
山形 俊男 Prof. Toshio Yamagata	東京大学大学院理学系研究科教授 Graduate School of Science, University of Tokyo
中村 雅人 Mr. Masato Nakamura	科学技術庁研究開発局海洋地球課地球科学技術推進調整官 Ocean and Earth Division, Research and Development Bureau, STA

研究成果報告

Result of the Study

Ⅰ.Observation and analysis on the process of the atmosphere-ocean-land interactions
大気・海洋・陸域間相互作用の諸過程に関する観測・解析研究

1. Observation and analysis on the process in the atmosphere
大気における諸過程に関する観測・解析研究

（1）Analysis on the Large scale Convective Activity and Precipitation Systems
大規模積雲対流活動と降水系に関する解析研究

Meteorological Research Institute,
Nobuo Yamazaki, Toshiro Inoue,
Minoru Tanaka, Kiyotoshi Takahashi
Hiroaki Ueda, Tetsuo Nakazawa
Japan Meteorological Agency
Masato Murakami
Meteorological Satellite Center
Kiyoshi Sasamoto
気象庁　気象研究所
山崎信雄、井上豊志郎、田中実、高橋清利、
植田宏昭、中澤哲夫
気象庁
村上勝人
気象衛星センター
笹本清

Abstract

Using 3 hourly mean GMS infrared data, diurnal variations of convvective clouds and the influence of the intraseasonal variations to the diurnal variations are investigated over the Asian monsoon region. It is found that phase of the diurnal variations propagate from land areas to off shores over the Bay of Bengal and the west of Sumatra Island. The intraseasonal variations influence the diurnal variations such that the phase of the diurnal variation is delayed (advanced) over land (ocean) at the active phase of the intraseasonal variation. Multi- level cloudiness data derived from GMS infrared histogram data revealed that the diurnal variations of convective activities over the oceans depend strongly upon the cloud height : two peaks are observed for the cloudiness variations with moderate cloud- top temperature (～250K), while a single peaks is observed for very deep convective cloudiness variations (～210K).

By using the sea surface wind data obtained by the NASA scatterometer (NSCAT) on board the Advanced Earth Observing Satellite, it is found that the onset of 1997/98 ENSO is closely related to the atmospheric Madden-Julian Oscillation (MJO), which accompanies enhanced convective activity and low-level tropospheric westerly over the western Pacific in March 1997.

The split window (11 and 12μm in combination) on board NOAA was used to see the interannual variations of the Indian monsoon. It is found that Sea Surface temperature (SST) off Somalia and over the Arabian Sea decreases as the monsoon wearily strengthens. Interannual variations of the Indian monsoon shows good correlation with water vapor amount over the Arabian Sea.

The analysis of the precipitation systems was carried out with emphasis on the interannual and interdecadal variations and its relationship to El Nino and La Nina. The onset of the summer monsoon over the western north Pacific near 15N is early in the La Nina years and late in the El Nino years. Significant positive correlation between the July rainfall in the northern part of Kyusyu and NINO3 SST are observed for a 30-year period from 1963 to 1992, implying that the Baiu rainfall is heavy in the El Nino years.

Using Singular Value Decomposition (SVD) method between variations of SST and Asian monsoon activities, the Indian and Southeast Asian monsoon in El Nino years are generally shown to be suppressed, while the East Asian monsoon is enhanced in July.

1. Objectives

This study aims at revealing the large-scale features of the Asian Monsoon by using satellite data and the objective analysis data. The diurnal and intraseasonal variations (ISV) are known as principle variations in the tropical convective activity.

It is now widely recognized that the ENSO has a profound effect on the activity of the Asian monsoon and the cause of the ENSO onset is one of the hot issues related to the air-sea interaction. We describe the MJO during spring of 1997, and explore the effect on the onset of the 1997/1998 ENSO.

The objective of this part is also to study characteristic features of SST, water vapor amount and convective activity associated with Asian summer monsoon over the 40S-40N, 40E-150E area using split window (11mm and 12mm) data. Split window data is effective to classify convective clouds and non-precipitating cold cirrus clouds. Convective activity can be assessed more reliably by split window than single infrared data. Split window measurement is also effective in estimating Sea Surface Temperature (SST) and water vapor amount over the cloud-free ocean area.

It has been emphasized that large-scale differential heating between continent and the surrounding ocean is fundamental importance for establishment of the Asian summer monsoon. However, we have revealed that the ocean also plays a consequential role in seasonal evolution of the "oceanic monsoon" over the western subtropical Pacific. Our purposes are how interannual variation of the Indian summer monsoon is influenced by the ocean and how the seasonal change of SST is related to surface wind speed.

For the analysis of annual and decadal variations of monsoon systems the objects in this study are to analyze the precipitation systems in the Asian and adjacent monsoon region and to investigate the possible relationship to the ENSO and the interdecadal changes in the climate system.

The basin scale SST variations are known to influences on the seasonal march of the Asian monsoon. The SVD method between monthly mean SST, and circulation fields and convective activities are used to describe how SST affects annual variations the Asian monsoon in the each

region in Asia.

2. Methods

In the analysis of diurnal variation, one-degree square mesh 3 hourly mean equivalent black body temperature (TBB) data were used. Analysis area is from 80E to 180W in longitude and from 15S to 35N in latitude. Analysis period is summer season (May - September) for 14 years (1980-1994, excluding 1984). To avoid the influence of temperature variation of the ground and sea surface, we defined the index (hereafter referred as IC255), in the similar way as Nitta and Sekine (1994), as follows.

$$IC255 = \begin{cases} |255-TBB| & \text{if } TBB < 255K \\ 0 & \text{if } TBB > 255K. \end{cases}$$

The amplitudes and phases of diurnal variations were calculated by the Fourier analysis of 3 hourly data, the first and second components corresponding to diurnal and semi-diurnal ones respectively.

Multi-level cloudiness data with different thresholds for cloud-top temperature derived from GMS IR histogram data is also used to study the dependence of diurnal variations on cloud- top heights. Their spatial and temporal resolutions are 0.25 degree and 3 hourly, respectively. We have compiled that data for 1984-1998.

The active and inactive periods of the ISV were decided on each mesh based on 30-60 day-filtered anomaly of daily mean IC255. We defined the period as active (inactive) when the filtered anomaly is larger (less) than 1K(-1K). The composites were made at both phases of the ISV respectively, and were compared with each other.

The sea surface wind data obtained by the NSCAT on board the ADEOS from September 16, 1996 to June 30, 1997 are used for the atmospheric signals during the early stage of the 1997/98 ENSO event. We used the NSCAT level 3 data set derived via the NSCAT-1 algorithm. The advantages of ADEOS/NSCAT data are wide spatial coverage (90% global in 2 days) and accuracy (2m/s in wind speed of 3-20 m/s, 20 degree in wind direction).

The interannual variations of the Indian summer monsoon were analyzed using split window on board NOAA polar orbiting satellite as well as SSM/I and COADS data sets. Infrared (IR) measurements from satellite give us information on clouds. Therefore, IR data from satellite are widely used for the analysis of convective activity over the tropics. However, we cannot tell the difference between cold non-precipitating cirrus clouds and convective clouds from the single infrared measurements. Split window (11 and 12μm in combination) is effective in classifying optically thin cirrus clouds and optically thick cumulus clouds.

Convection index was estimated using the brightness temperature optically thick cumulus clouds classified by the split window method. Non-precipitating cirrus clouds classified by the split window were discarded in estimating this convection index. SSTs were retrieved using the NOAA multi-channel SST algorithm for daytime. Cloud free ocean areas were classified by the spatial coherence method. Water vapor amount was also retrieved.

Using the 5-day mean rainfall and sea-level pressure data, the analysis of the precipitation systems was carried out with emphasis on the interannual and interdecadal variations, and its relationship to the ENSO.

The analysis of the monsoon systems using the 5-day mean GMS high-cloud amount, sea-level pressure, and precipitation data were carried out with emphasis on the interannual and interdecadal variation and its relationship to the ENSO.

The data used for the analysis of relationship of SST with the monsoon variability are monthly mean SST, OLR and stream function at 850 hPa from 1980 to 1995.

3. Results

Fig. 1 shows the summer-time diurnal phase of cloud top variations derived from one degree square mesh 3 hourly TBB data for 14 years. The local times of the lowest TBB are depicted. This figure reproduces the well-known phase pattern of the diurnal variations such as the maximum cloud activity in the evening to midnight (in the early morning) over land (ocean) areas. In the ocean near the coastal lines as in the Bay of Bengal, off the Sumatra, the South China Sea (SCS) and the equatorial Western Pacific, the phase of diurnal variations advance from land to ocean. Consequently in these oceanic regions cloud activities reach maximum from early morning to noon. These suggest diurnal variations have structure of local circulation similar to land-sea breeze. Note that there seems no one-to-one correspondence between background mean wind and the phase change, as seen over the Bay of Bengal.

Semi-diurnal variations as well as diurnal variations are found to exist in the tropical convections. Over the land and the ocean adjacent to the land diurnal component is predominant. On the other hand, over the ocean far from the land like the central Pacific and the Indian Ocean existence of semi-diurnal component becomes clear. Especially over the Bay of Bengal and the South China Sea diurnal component prevails.

The phase change of the diurnal variation due to the intraseasonal variation (ISV) tends to be delayed over the sea and advanced over the land at the inactive phase of the ISV. This pattern of the phase change is seen over the Indian subcontinent, the Bay of Bengal, the Indochina peninsula and the South.

Multi- level cloudiness data reveals that over the ocean two peaks are observed in IC255 or cloudiness with 255K threshold as in the mean TBB data. One peak appears around the early morning and the other is around the late afternoon. As the threshold temperature for cloudiness becomes lower, the morning peak becomes more predominant and the late-afternoon peak tends to diminish. Especially in the case of 210K threshold, only the morning peak is observed almost all oceanic regions.

Over the land, especially in the regions where diurnal variations of convective activity are predominant, cloudiness changes with each threshold is very similar to each other and IC255.

Using multi-cloudiness data, seasonal variation of convective activity depicted with the cloudiness with 210K threshold over the equatorial Indian ocean was different from the one with IC255. That is, in IC255 enhanced convective activity can be observed during the monsoon season, while in May the maximum appears in the cloudiness with 210K threshold (Fig. 2).

To study the influence of the ISV on the diurnal variations we show the differences in amplitudes and phases of the diurnal variations in Figs. 3 and 4, respectively. Dotted areas denote the values where the diurnal amplitude was enhanced (suppressed) at the inactive (active) phase. One cannot see the much contrast of the diurnal amplitude between the land and sea clearly in the figures.

It is seen from Fig. 4 that the phase of the diurnal variation tends to be delayed over the sea and advanced over the land at the inactive phase of the ISV. This pattern of the phase change is seen

over the Indian subcontinent, the Bay of Bengal, the Indochina Peninsula and the South China Sea.

We analyzed intraseasonal variations of the Indian monsoon. Figs. 5a and 5b show the monthly mean distribution of cumulonimbus cloud in July of 1987 and 1988. Larger cloud amounts are seen along the west coast of Indian in 1988, while less cloud amounts are seen over south India in 1987. The difference of cloud cover distribution in 1987 and 1988 shows general agreement with the seasonal GPI rainfall difference between 1987 and 1988 (Janowiak and Arkin, 1991). The winds of the operational global analysis (GANAL) by JMA show big difference of low level monsoon westerly. The wind at 850 hPa over east of Somalia was about 18 m/s in 1987 and was about 27 m/s in 1988. There is the big difference of water vapor amount over the Arabian Sea between 1987 and 1988, although SST was a little colder in 1988. The larger amount of water vapor over the Arabian Sea corresponds to enhanced convective activity over the south India. Figs. 6a and 6b show the monthly mean total precipitable water vapor (TPW) estimated from SSM/I. The TPW over the Arabian Sea is about 45 mm in 1987 and is about 55 mm in 1988. These results are consistent with the split window measurements. Further, we can see about 20% increase of water vapor amount in comparison between east of Somalia and Arabian Sea. This suggests the importance of Arabian Sea in terms of moisture supply for the Indian summer monsoon.

Fig. 7 shows the interannual variation of surface wind speed by SSM/I and SST to the east of Somalia (47E, EQ) on July. We can see very good negative correlation between the two. When the wind speed is strong the SST to the east of Somalia becomes cool due to the up welling. However, the magnitude of SST change seems depending on year to year as seen in 1993 and 1994. Further, we cannot see any good correlation between the wind and SST over the middle of Arabian Sea (67E, 10N).

Fig. 8 shows good correlation between surface wind and water vapor amount over the middle of Arabian Sea. The stronger wind corresponds to larger amount of water vapor. Fig. 9 shows the variations of rainfall over the south India and those of the wind speed. Except 1990, we can see good correlation between rainfall over the south India and wind speed, water vapor. This confirms our former result that the rainfall over south India correlates with water vapor and wind rather than SST.

ENSO is considered to be an unstable coupled atmosphere-ocean system. Necessary preconditions for instability include (a) piling-up of warm water in the western Pacific in response to strong easterly trades and (b) persistent westerly winds over the western Pacific. A likely source for westerly wind forcing on the ocean is the Madden-Julian Oscillation (MJO). We examine the importance of the MJO in the onset of ENSO because:

(1) The MJO time scale (30-60 days per global circuit) is sufficiently long to permit ocean-atmosphere coupling in a westerly wind regime;
(2) The MJO is seasonal, i.e., active in summer hemispheres and crossing the equator in spring (going N) or fall (going S). Coupling relevant to ENSO should occur on the equator, suggesting that MJO affects ENSO onset in spring or fall; and
(3) The MJO initiates in the Indian Ocean and propagates to the western Pacific. Atmosphere-ocean coupling important for ENSO occurs in the western/central Pacific, suggesting the potential for short-term predictability.

From the sea surface wind from NSCAT data (see Fig. 10), we found that the onset of 1997/98 ENSO is closely related to the atmospheric MJO, which accompanies enhanced convective activity and low-level tropospheric westerly over the western Pacific in March 1997. There was another MJO in December 1996, which might also contribute to the onset of 1997/98 ENSO.

It is found that two times abrupt enhancements of large-scale convective activities occur over

the southeast Asia region in the climatological mean data . The first activation is seen over the Arabian Sea(north of equator)-around Indochina Peninsula-South China Sea during middle May before the Indian monsoon onset, the latter one is recognizable over the Arabian Sea(westward of the Indian sub-continent)-the Bay of Bengal during early June which correspond to onset of the Indian monsoon.

Seasonal changes of SST have intriguing features. Over the North Indian ocean, the maximum temperature in excess of 30℃ appears from late April to late May which are accompanied by weakening of northeasterly wind associated the winter monsoon system. On the other hand, the SST abruptly decreases after early June because of the active convection through evaporative cooling and turbulent mixing in addition to decrease of solar insolation.

The interannual variations of the Indian summer monsoon are modified by pre-monsoon condition of SST. From correlation analysis, the typical(atypical) onset is closely associated with warm(cold) anomaly of SST around 15。N form March to May, especially middle May.

Lag correlation between SST and surface wind speed in weekly time-scale revealed that the change of wind speed precedes about 3 to 5 weeks before the change of SST. On the other hand, wind speed delays about 10 weeks for the change of SST over the Indian Ocean, which suggests an existence of monsoonal feedback between atmosphere and ocean.

Interannual variations of the precipitation system was analyzed using the 5-day mean GMS high-cloud amount data, sea-level pressure data from 1978 to 1992 and rainfall data from 1963 to 1992. The onset of convection near 20N, 150E are early in the La Nina years (1978,84,85,88) and are delayed by 20 to 25 days during the El Nino years as shown in Fig. 11. Similar delay in the ending dates of the Baiu season was observed near Japan. The onset of the western north Pacific summer monsoon defined by the sea-level pressure difference (10N minus 20N) at 140E (see Fig. 12) are also delayed by about 20-25 days in the El Nino years compared to the La Nina. The rainfall correlation NINO3 SST (4° N-4° S,150° W-90° W)showed large areas of negative correlation in October (Figure 13) and delayed onset of the monsoon rain in Southeast Asia in May. Further, the Baiu convection is under the strong influence of interannual variations of the NINO3 SST (4° N-4° S, 150° W-90° W) during this period as seen in Fig. 14.

The heterogeneous correlation maps of the OLR (SST) of 1st mode of SVD analysis between monthly OLR from May to August and SST in March is shown in Fig.15(a). From Fig.15(b) the 1st mode corresponds to El Nino pattern. Fig. 15(a) of the correlation map with OLR shows convective activity is suppressed from May to July in India through Indonesian region, while over East Africa and South Indian Ocean enhanced convections are seen. In August convection is enhanced around India. In East Asia the Baiu activity is suppressed in June except the northern part of Kyushu in Japan, while enhanced in July and August.

Fig. 16 shows the result for the low level stream function. The pattern consistent with the OLR result can be seen: low-level westerly (easterly) anomalies are seen over regions with the enhanced (suppressed) convective activity.

4. **Discussions**

The diurnal variation is dominant over the land and semi-diurnal variation is recognized clearly over the equatorial ocean region. The result that the phase of the diurnal variation is delayed (advanced) at the active phase of the intraseasonal variation (ISV) is consistent with a hypothesis that diurnal variation is caused by solar heating over the land and by nocturnal cooling over the sea.

The difference of the characteristics of the morning and late afternoon peaks over the ocean suggests the different mechanisms. More detailed analyses will be needed to clarify mechanisms.

Many researches have been conducted using OLR or TBB to describe the convective activity in monsoon study. However, the behavior of deep convection depicted by the cloudiness with 210K threshold was found to be different from the one by OLR or TBB. It is interesting to reconsider the depiction of monsoon activity and its evolution with multi-level cloudiness data.

Using the NSCAT sea surface wind data, we found the MJO has an important role in the onset of the 1997/1998 ENSO event. This is derived from the NSCAT wind data, which are good quality as well as wide spatial coverage over the ocean.

Cumulus type clouds classified by split window show reasonable agreement with convective rain area. Our study using the NOAA split window data has shown the interannual variations of the Indian monsoon is closely related to the water vapor rather than the SST, consistent with the result from the SSM/I and COADS data.

Establishment of the Indian monsoon is closely connected with pre-monsoon condition of SST. It is important to clarify the basic variation such as seasonal variation before we examine the anomaly fields. In addition, a slight modulation of monsoon system brings severe damage for human beings in Asian region.

We found that the SST in the equatorial eastern Pacific significantly influences the western north Pacific summer monsoon and Baiu activity in the East Asia.

It is found that the influence of the SST variations on the seasonal march of the Asian monsoon depends on both spatial location and season of the monsoon evolution.

5. References

1) Nitta, T. and S. Sekine, 1994: Diurnal Variations of Convective Activity over the Tropical Western Pacific, J. Meteor. Soc. Japan, Vol.72, p627-641

6. Publications

6.1 Domestic Journal (8 papers)

T. Nakazawa:Tropical Super Cloud Cluster and ENSO
Kaiyo Vol.21.8 1989

T. Nakazawa, K. M. Lau, L. Peng and C. H. Sui: Dynamics of Super Cloud Clustes, Westerly Wind Bursts, 30- 60 Day Oscillations and ENSO : An Unified View
J. Meteor. Soc. Japan, Vol.67, April 1989

T. Nakazawa: Seasonal phase lock of intraseasonal variation during the Asian summer monsoon
J. Meteor. Soc. Japan, Vol.70, No.1B February 1992

M. Tanaka: Intraseasonal Oscillation and the Onset and Retreat Dates of the Summer Monsoon over East, Southeast Asia and the Western Pacific Region using GMS High Cloud Amount Data
J. Meteor. Soc. Japan, Vol.70, No.1B February 1992

T. Nitta, T. Mizuno and K. Takahashi: Multi- Scale Convective Systems duringthelnitial Phase of the 1986/87 El Nino
J. Meteor. Soc. Japan, Vol.70, No.1B, 447-466 February 1992

M. Tanaka: The onset and retreat dates of the Austral summer monsoon over Indonesia, Australia and New Guinea
J. Meteor. Soc Japan 1994, Vol.72, 255- 267

M. Tanaka: Interannual and interdecadal variations of the Western North Pacific monsoon and Baiu rainfall and their relationship to the ENSO cycles.
J. Meteor. Soc. Japan, Vol.75, 1109- 1123. December 1997.

Wu. P. and T. Nakazawa: El Nino observed by NASA Scatterometer on ADEOS・Midori satellite.
Journal of Remote Sensing Society of Japan, Vol. 17, 122- 125

6.2 Foreign Journal (3 papers)
T. C. Chen, K. Takahashi: Diurnal variation of outgoing longwave radiation in the vicinity of the South China Sea: Effect of intraseasonal oscillation
Mon. Wea. Rev. 1995, Vol.123,566- 577

T. Inoue: Contrast of 87/88 Indian summer monsoon observed by split window measurements.
1997 Advances in Space Research, 19, 447- 455

T.C.Chen, S. P. Weng, S. Kiehneand N. Yamazaki: Interannnal Variation in the Tropical CycloneFormation over the Western North Pacific
Mon.Wea.Rev.Vol.126 1080- 1090

7. International Cooperation

The cooperation with China was carried out based on the agreement signed in 1993 between Japan Science and Technology Agency and China Meteorological Administration. During these cooperation period, 14 Chinese experts were invited to MRI and performed the joint study on the Baiu/Meiyu activity and air-sea interaction of Asian monsoon by using the GMS satellite data. From Japanese side, 8 research officials visited China and performed the joint study on the analysis of monsoon related rainfall activity.

(和文要旨)

3時間毎のGMSの赤外データを用いて、積雲対流の日変化,及び季節内変動がこの日変化に及ぼす影響をアジアモンスーン域で調べた。ベンガル湾やスマトラ島の西では日変化の位相が陸上から海上に伝搬してゆくことがわかった。陸上（海上）の日変化の位相は季節内変動の活発期に遅れる（進む）ことがわかった。GMSの赤外ヒストグラムデータから得られた閾値別雲量データから海洋上の日変化の位相は雲頂に大きく依存することがわかった：250K程度の雲頂温度に対応する雲量変動には１日２回のピークが見られるが、非常に背の高い（210K程度）雲量変動には１つのピークのみが見られた。

ADEOS衛星に搭載されたNSCATから得られた海上風のデータを用いて、1997/98 ENSOは、1997年３月に西太平洋上で活発な対流活動と下層西風を伴った大気のマデンージュリアン振動に密接に関連していたことがわかった。

NOAA衛星（米国）搭載のスプリットウィンドウのデータを用いて、インドモンスーンの年々変動を調べた。ソマリ沖やアラビア海の海面水温はモンスーン西風の強化とともに降下し、インドモンスーンの年々変動はアラビア海の水蒸気量とよい相関を示すことがわかった。

アジアモンスーンの年々変動、１０年変動、及びエルニーニョ・ラニーニャとの関連に焦点を当てながら降水系の解析を行った。15°N 付近の北西太平洋上の夏季モンスーンはラニーニャ（エルニーニョ）年に早く（遅く）に始まることがわかった。1963年から1992年の30年間のデータから、東太平洋赤道上のNINO3の海面水温と九州北部の７月の降水量との間には大きな正の相関があり、エルニーニョ年には梅雨による降水量は増大することがわかった。

アジアモンスーンとインド洋及び太平洋における海面水温間の特異値解析を行い、エルニーニョ年にはインドと東南アジアのモンスーンは一般的に弱くなり、東アジアモンスーンは７月に強化されることがわかった。

Fig.1. Horizontal distribution of summer (May-September) mean diurnal phase of the TBB for 14 years. Diurnal amplitude less than 0.5 degree is suppressed.

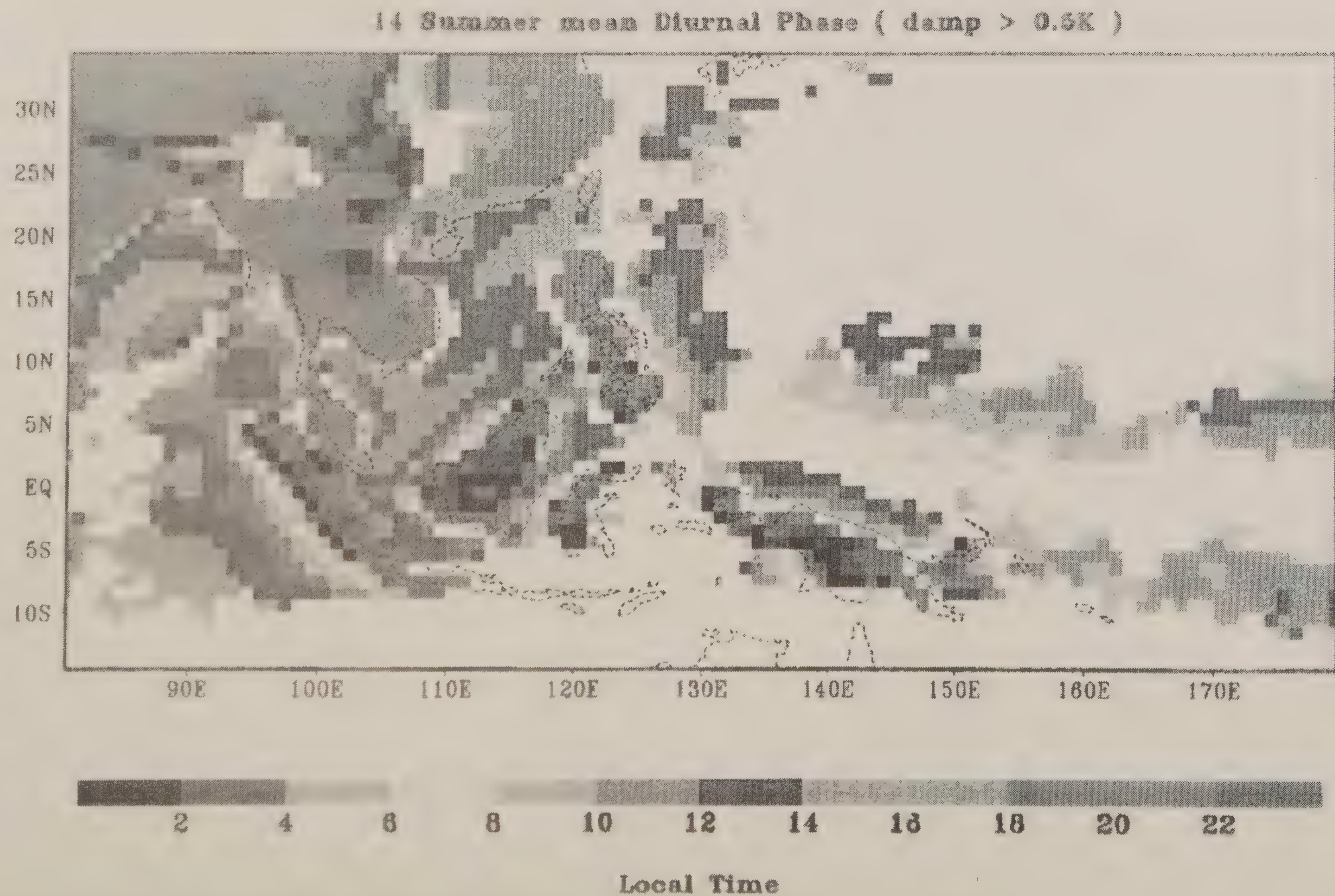
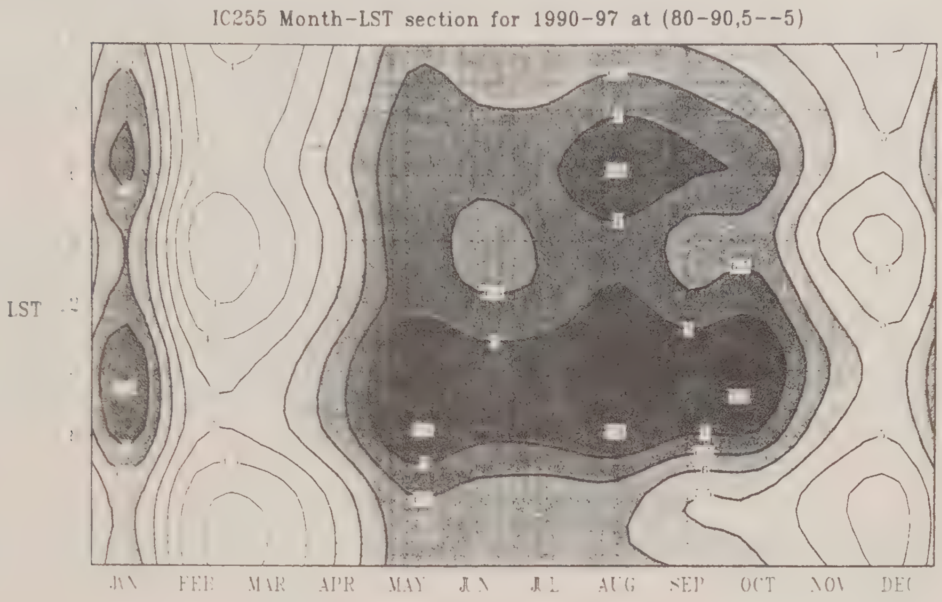
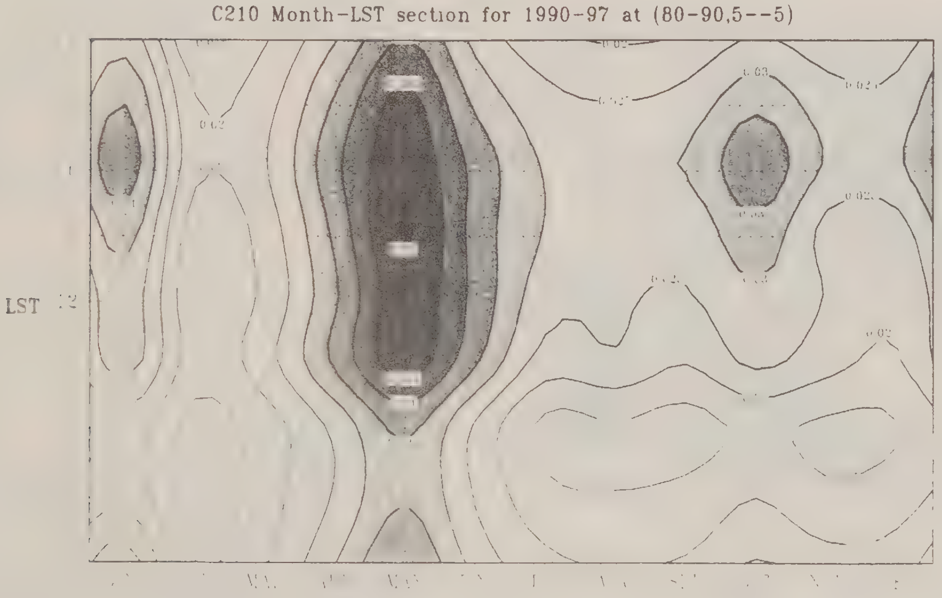


Fig. 2 Local time-Month cross section of monthly averaged IC255 (Upper) and cloudiness with 210K (Lower)





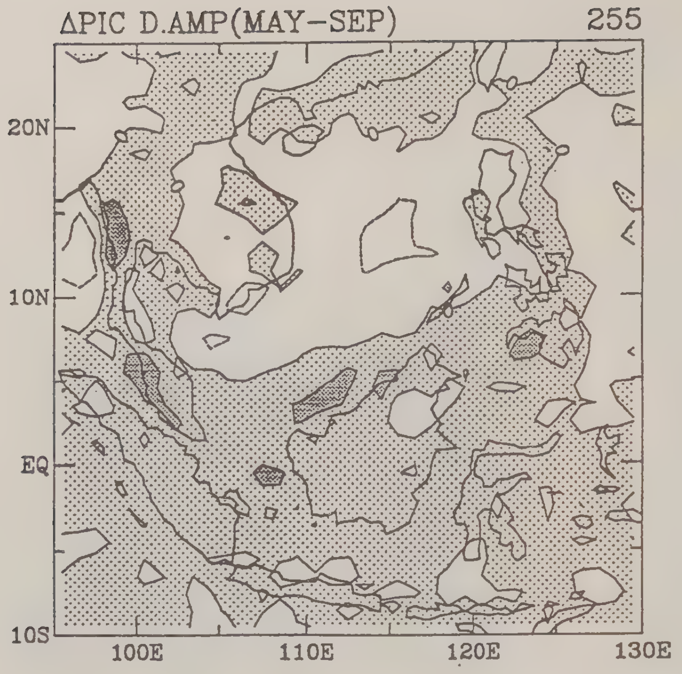


Fig. 3 Summer horizontal distribution of differences of diurnal amplitudes defined by subtraction of the active phase's one from the inactive.

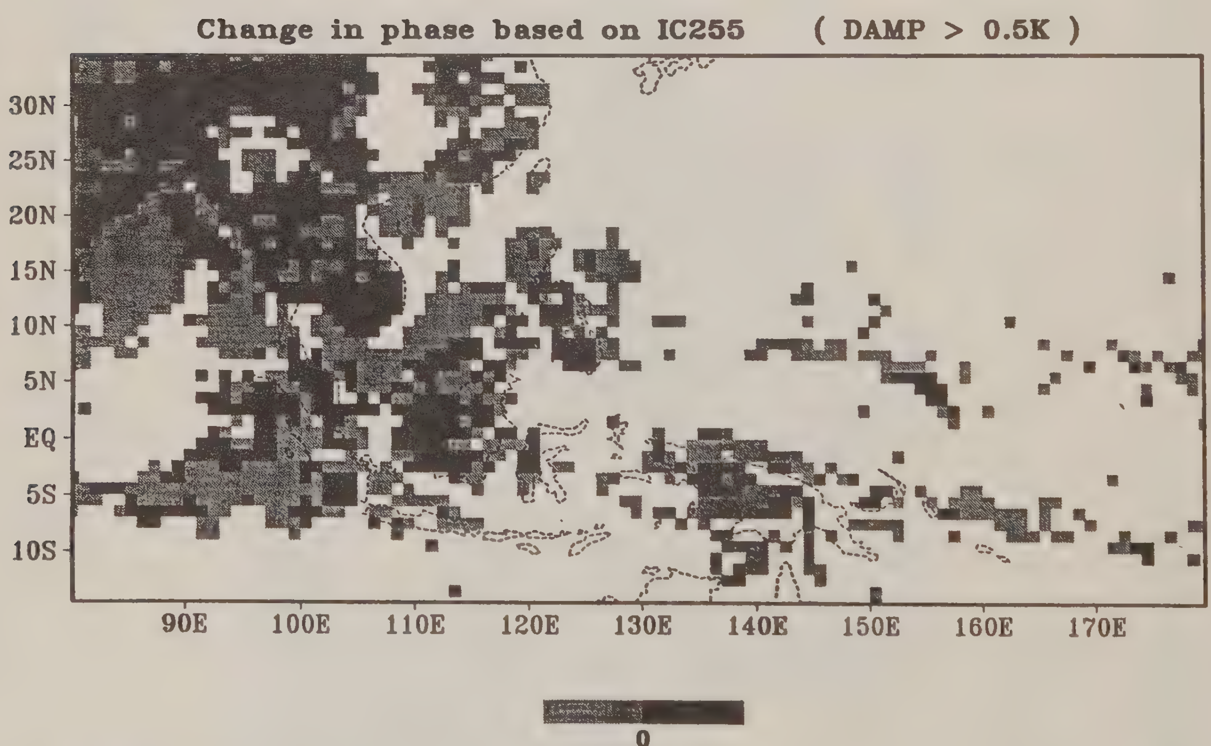


Fig. 4 The distribution of the difference of diurnal phase between active and inactive phases of the ISV (30-60 day mode). Dense(Light) shaded region is the one where diurnal phase is advanced(delayed) at the inactive phase of the ISV. The meshes with larger than 0.3K diurnal amplitude are plotted.

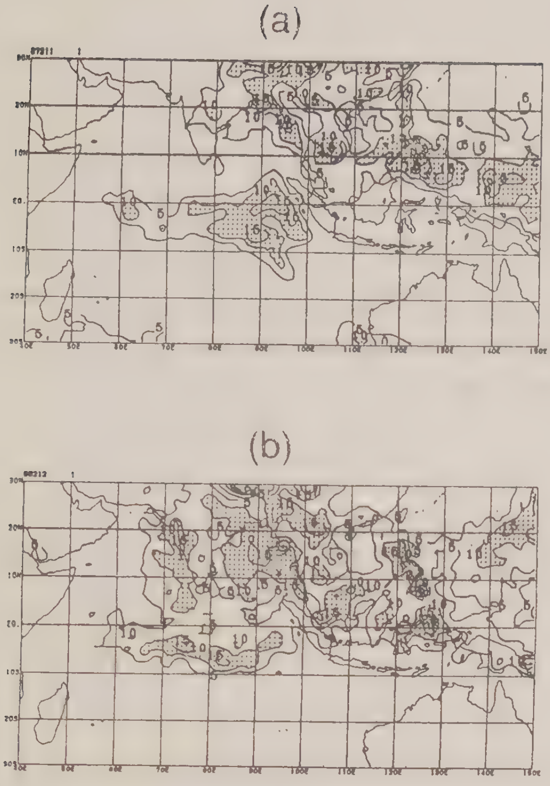


Fig. 5 The monthly mean distribution of cumulonimbus cloud in July of 1987 (a) and 1988 (b).

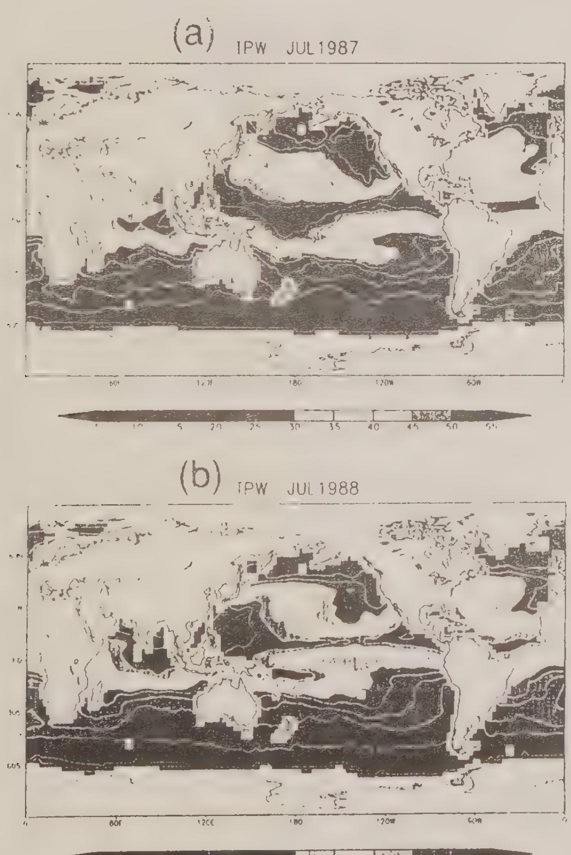


Fig. 6 The monthly mean total precipitable water vapor (TPW) estimated from SSM/I in July of 1987 (a) and 1988 (b).

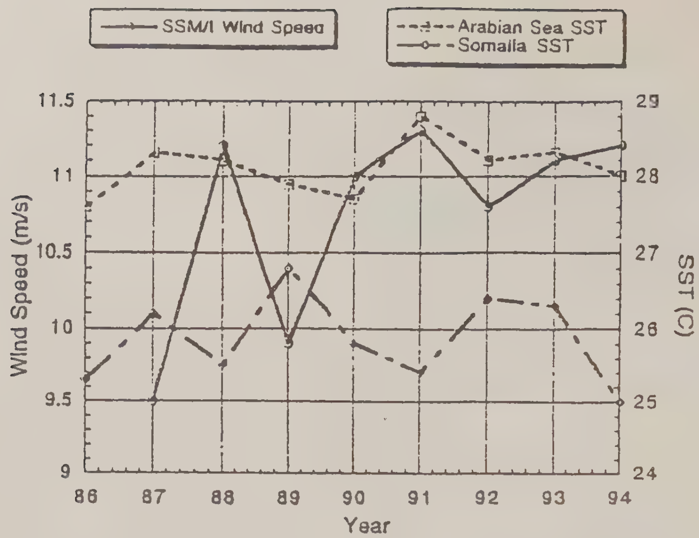


Fig. 7 Interannual variations of July's monthly mean of surface wind and SST over Arabian Sea and east of Somalia.

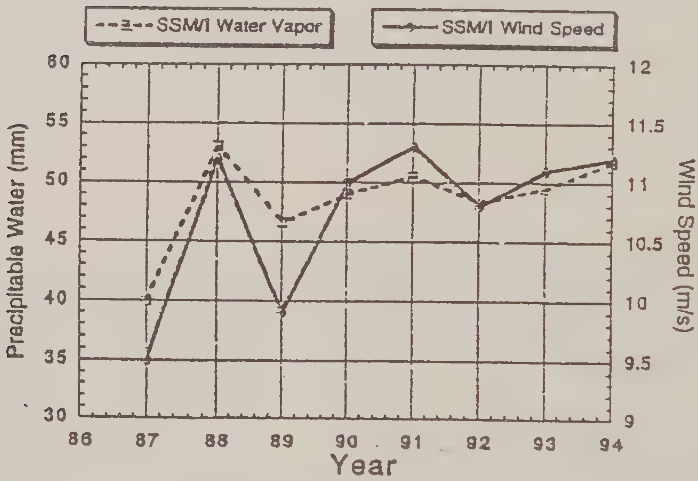


Fig. 8 Same as Fig.7 but water vapor and wind speed.

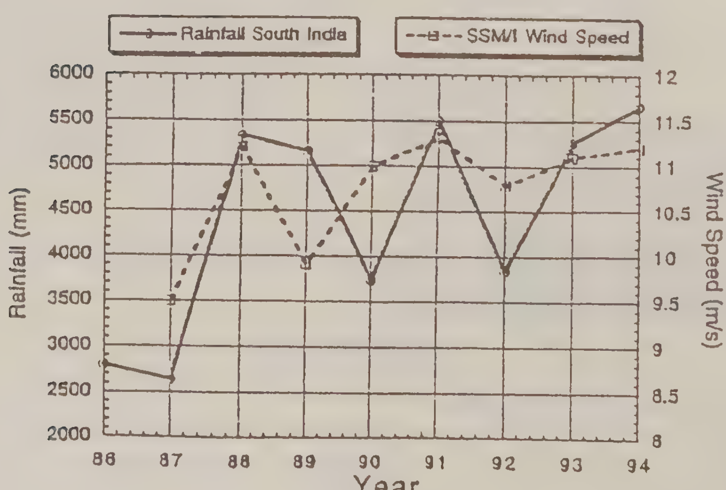


Fig. 9 Same as Fig.7 but rainfall over south India and wind speed.

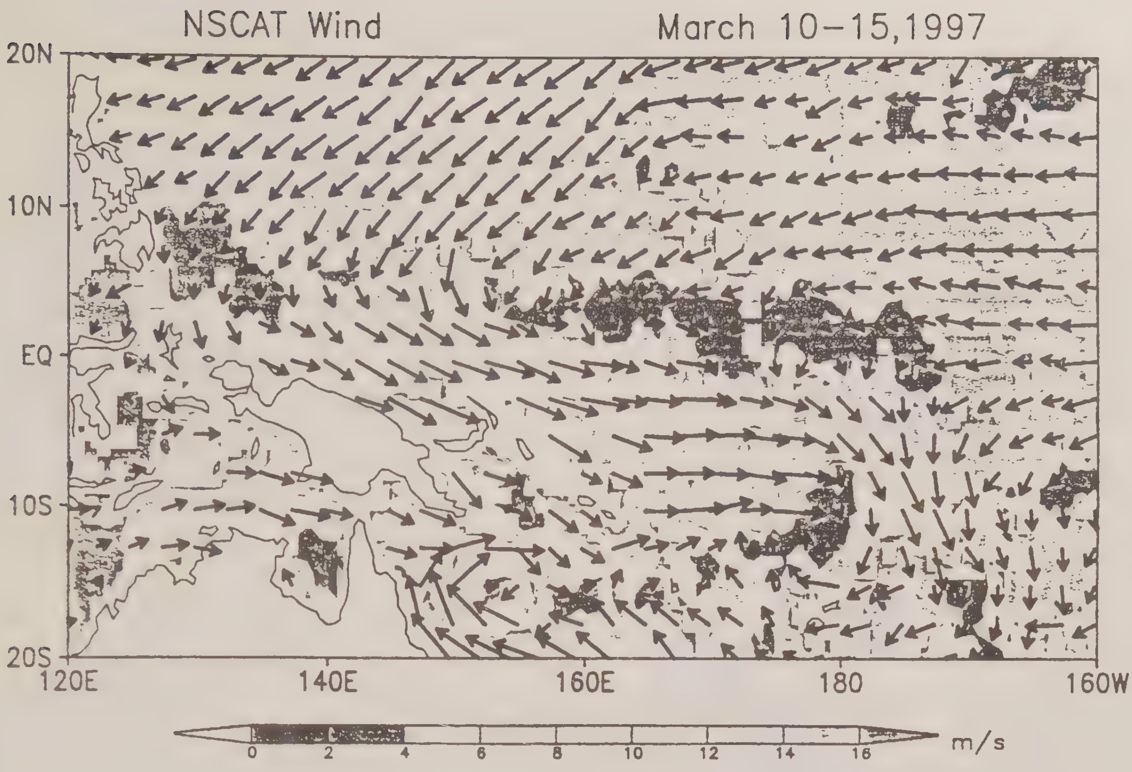


Fig. 10 Sea surface Wind and wind speed averraged over March 10-15, 1997 observed by the NSCAT.

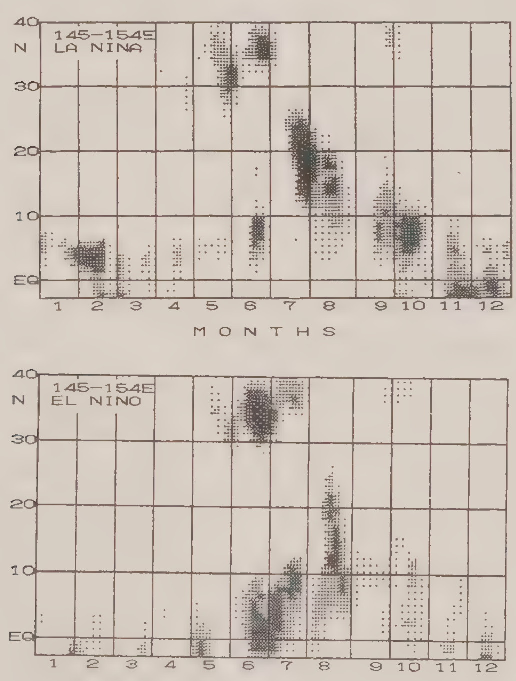


Fig. 11 Composite latitude-time cross section of the GMS high-cloud-amount for La Nina years (1978, 84, 85, 88; upper) and El Nino years (1982, 83, 87, 91, 92; lower) for the longitude 145-154E.

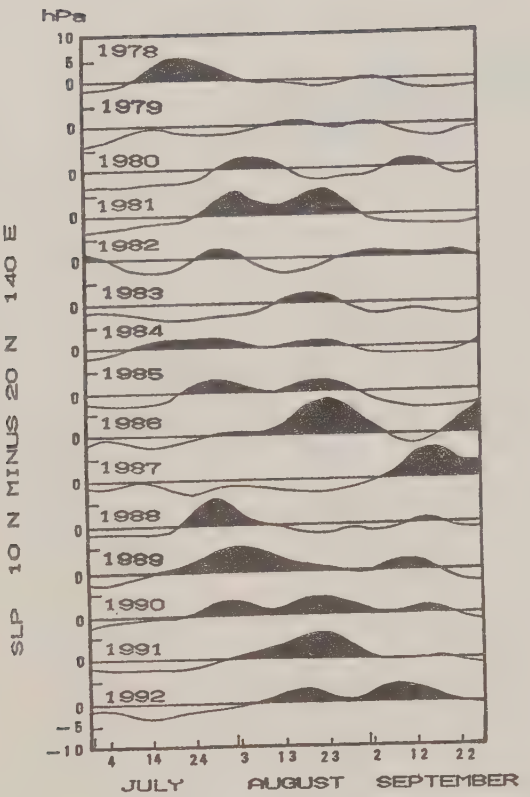


Fig. 12 Year-to-year change in the 1-2-1 filtered 5-day mean sea level pressure difference (10N minus 20N) at 140E from 1978 to 1992. Shaded areas show the period of westerly geostrophic winds at 15N.

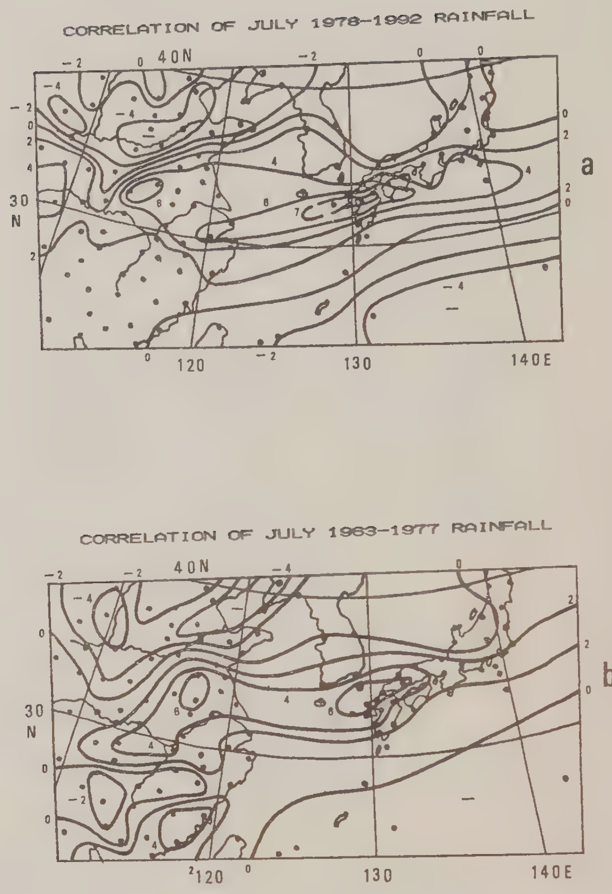


Fig. 13 Lag-correlations between the July rainfall in East Asia and NINO3 SST (4°N-4°S,150°W-90°W)

a) Rainfall for 1978-1992 and September NINO3 SST

b) Rainfall for 1963-1977 and May NINO3 SST

Fig. **14** Correlations between October sea-level pressure and NINO3 SST (solid lines, number indicates correlation x10) and the rainfall (black areas are more then 0.45 negative correlations to NINO3 SST)

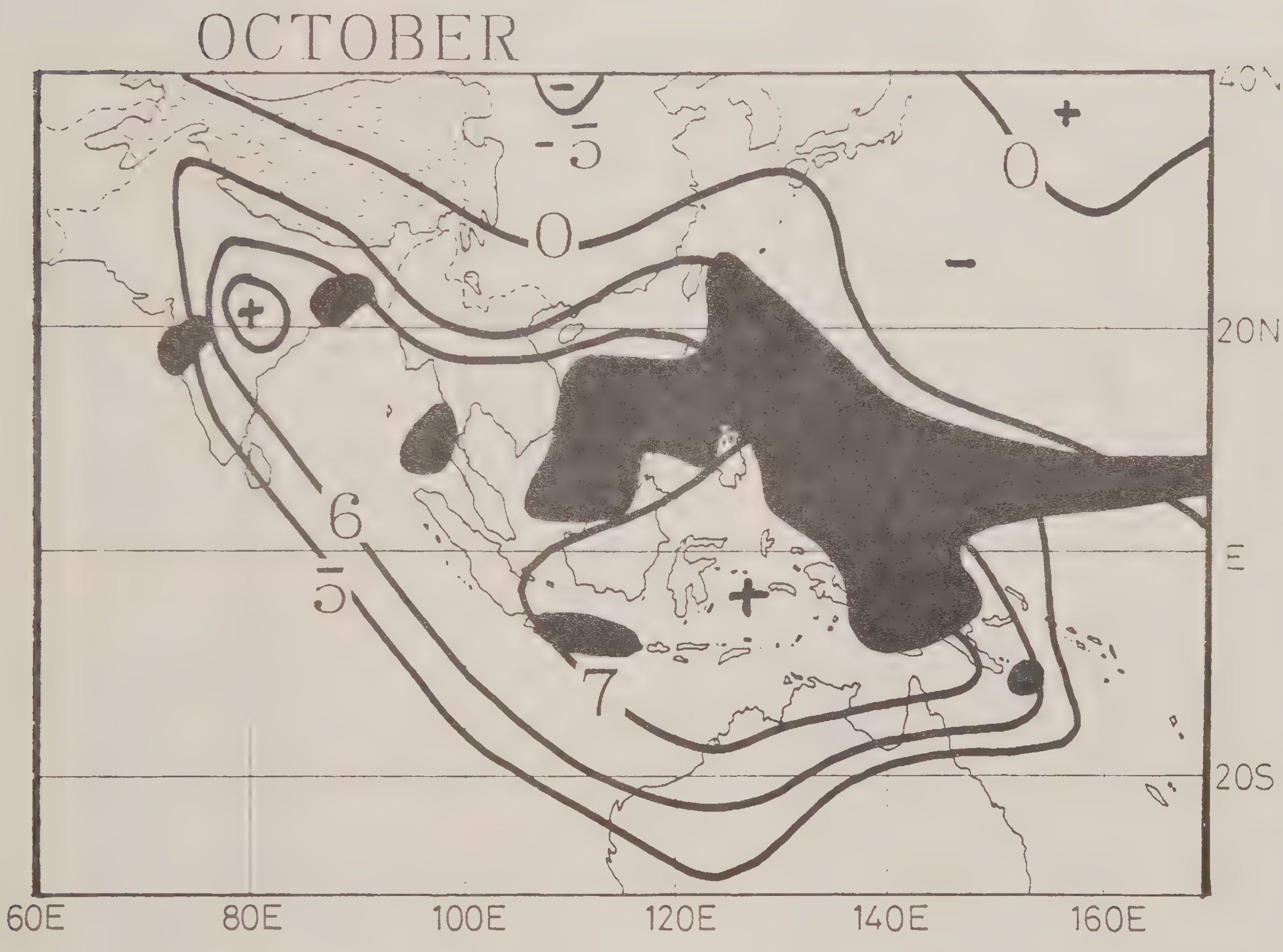


Fig. 15 (a) Heterogeneous correlation map of the OLR from May to August with the 1st SVD mode. (b) Heterogeneous correlation map of the SST in March with the 1st SVD mode. Contour intervals are 0.2 and areas less than -0.2 are shaded.

(a)

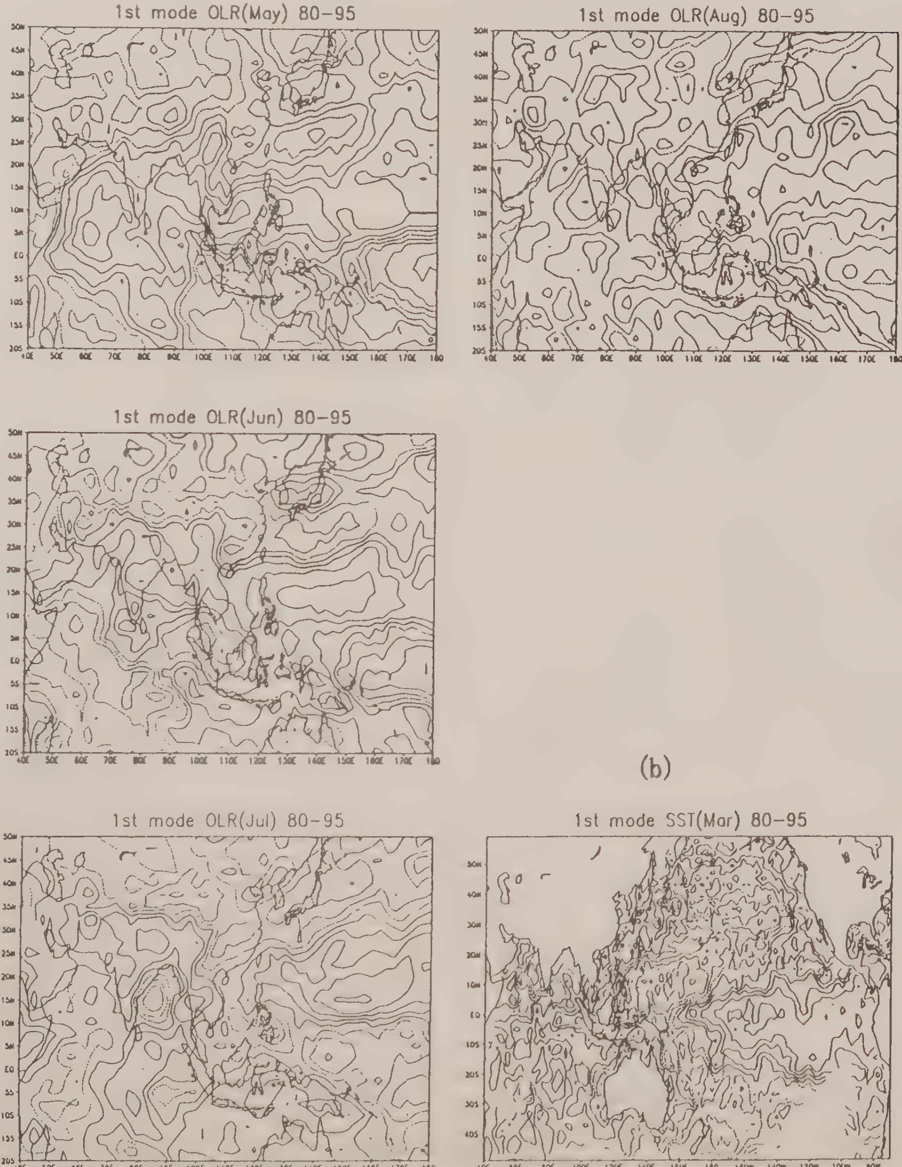
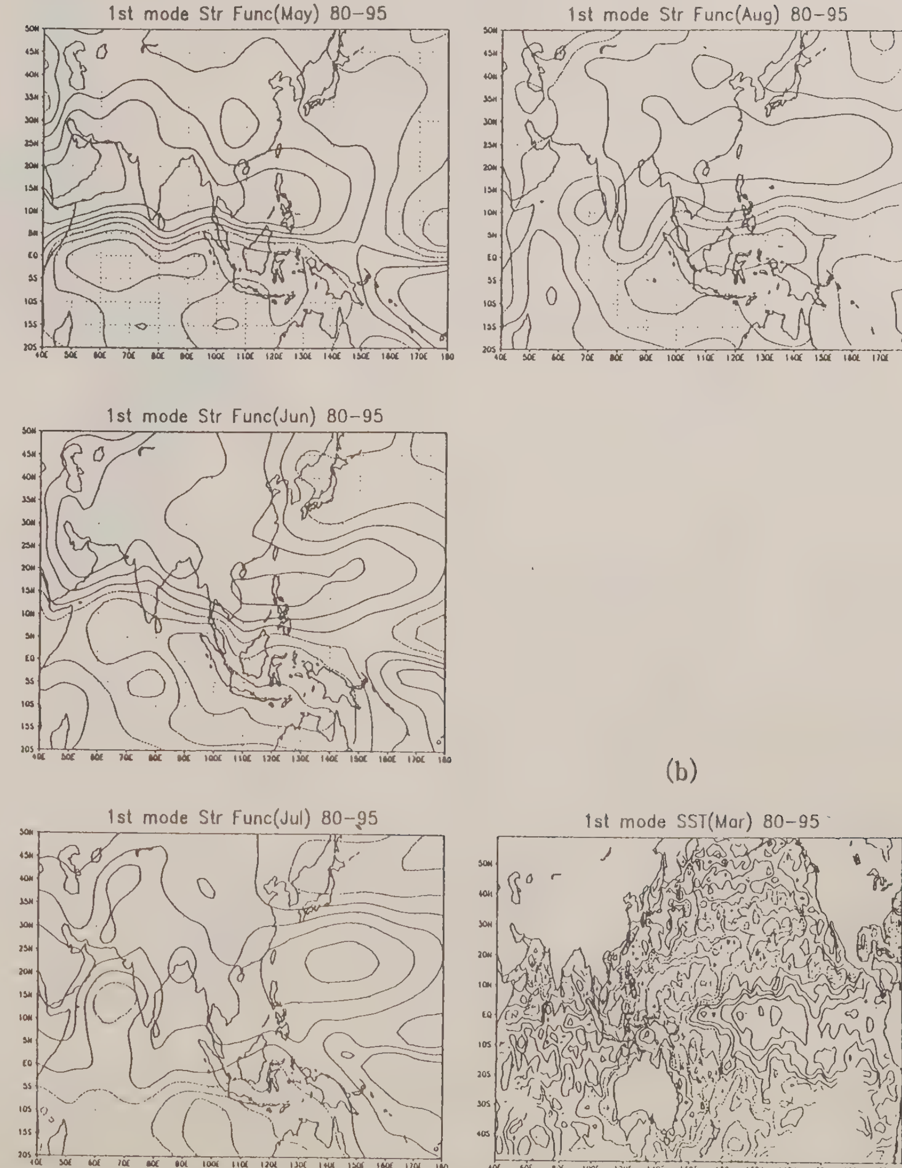


Fig. 16 The same as Fig. 6 except for stream function at 850 hPa.

(a)



I. Observation and analysis on the process of the atmosphere-ocean-land interactions
大気・海洋・陸域間相互作用の諸過程に関する観測・解析研究

1. Observation and analysis on the process in the atmosphere
大気における諸過程に関する観測・解析研究

(2) Observation of structure of convective clouds in large-scale cloud systems
大規模雲域内における対流雲構造に関する観測研究

Meteorological Research Institute,
Japan Meteorological Agency
H.Sakakibara, A.Tabata, H.Okamura, K.Mori, K.Akaeda,
M.Ishihara, Y.Shimazu, Y.Tanaka, K.Bessho
気象庁気象研究所
榊原均、田畑明、岡村博文、森一正、赤枝健治、石原正仁、
島津好男、田中恵信、別所康太郎

(Abstract)

Large-scale cloud systems (cloud clusters) are important in producing precipitation and transporting heat and water substances vertically in the Asian monsoon area. In order to reveal the structure of convective clouds in cloud clusters which are the main component active in producing precipitation and transporting heat and water, MRI and NIED carried out Doppler radar and upper air observation in the island of Miyako (24.8°N, 125.4°E) in 1990-92. Typhoons and cloud clusters during the Baiu season were observed.

Typhoons are composed of mesoscale precipitation systems (MPSs) classified as eyewall, inner rainband and outer rainband. MPSs had inherent features in airflow and precipitation structure in each MPS type in spite of their various appearances in different typhoons. Eyewall clouds contain outward sloping updrafts and convective clouds. Inner rainbands are further subdivided into three categories according to airflow and precipitation structure, (a) convective rainbands with convergence near the surface, (b) convective rainbands with convergence at middle levels and (c) stratiform rainbands. Inner rainbands are frequently observed in stratiform precipitation areas. Outer rainbands are associated with remarkable convergence near the surface and contain convective clouds.

Environment, evolution and structure of the cloud clusters associated with the Baiu front in 1992 were examined. The Baiu cloud zone roughly corresponded to low-level positive vorticity area and sharp latitudinal gradient zone of equivalent potential temperature (θ e). Two types of cloud clusters were studied. A stationary cloud cluster which formed apart from the Baiu front was maintained by repeated evolution of MPSs. Each MPS first formed at the western edge of the cloud cluster, moved eastward and then decayed. Three MPSs passed the island. In the first two MPSs middle-level flow entered from the front of the system and passed through it to the rear. Convective cloud repeatedly developed at low level convergence area and moved rearward according to the middle-level front-to-rear flow. In the last MPS middle-level inflow from the front was blocked by rear inflow to form a deep convergence layer up to 8km. This deep convergence maintained one quasi-steady convective band. Two cloud clusters were formed in cold-frontal zones during the observation period. In these cloud clusters repeated evolution of MPSs was not remarkable.

1. Objectives

Large-scale cloud systems (cloud clusters) which form and develop over the warm sea transport upward heat and water vapor supplied at the sea surface. Latent heat released by condensation of water vapor heats the air in the cloud cluster. This heating is not only the energy source of the cloud cluster but also one of the energy sources of monsoon. In this study we aimed to reveal the structure of convective clouds in cloud clusters which are the main component in producing precipitation and transporting heat and water.

2. Methods

The X-band Doppler radar and omega-sonde equipment of MRI are installed in the island of Miyako (24.8°N, 125.4°E) where the possibility to observe mature typhoons is the highest in Japan. Convective clouds in typhoons were observed in 1990-91. In 1992 typhoons and cloud clusters associated with the Baiu front were also observed in the island by two Doppler radars of MRI and NIED. These data were analyzed to reveal the structure of convective clouds in cloud clusters.

Large-scale environments of cloud clusters in the Baiu-frontal zone were analyzed by using routinely collected data of satellite (GMS) and conventional radar and global objective analysis data (GANAL) made every twelve hours by the Numerical Prediction Division (NPD), Japan Meteorological Agency (JMA).

3. Results

3.1 Typhoons

We observed convective clouds associated with six typhoons and one severe tropical storm (Fig.1). Among them, four typhoons, that is, Typhoon 9015 (Abe), Typhoon 9020 (Gene), Typhoon 9110 (Ellie) and Typhoon 9119 (Mireille), passed over or near the island of Miyako. Typhoons 9015, 9020 and 9119 were in the mature stage when they approached the island. Typhoon 9110 was in the weakening stage. Radar echo pattern of the four typhoons near the island was shown in Fig.2. The size of the typhoons are various and mesoscale precipitation systems (MPSs) included in them also seems to be various.

In spite of their various appearances, MPSs have several types in airflow and precipitation structure. We simply classify the observed MPSs into (1) eyewall clouds, (2) inner rainbands and (3) outer rainbands based on the location relative to the storm center. Airflow and precipitation features for each type are summarized as follows. Eyewall clouds contain outward sloping updrafts and convective clouds. Inner rainbands are further subdivided into three categories according to airflow and precipitation structure, (a) convective rainbands with convergence near the surface, (b) convective rainbands with convergence at middle levels and (c) stratiform rainbands. Inner rainbands are frequently observed in stratiform precipitation areas. Outer rainbands are associated with remarkable convergence near the surface and contain convective clouds. Airflow and precipitation structure of typical typhoon MPSs are shown in the following subsections.

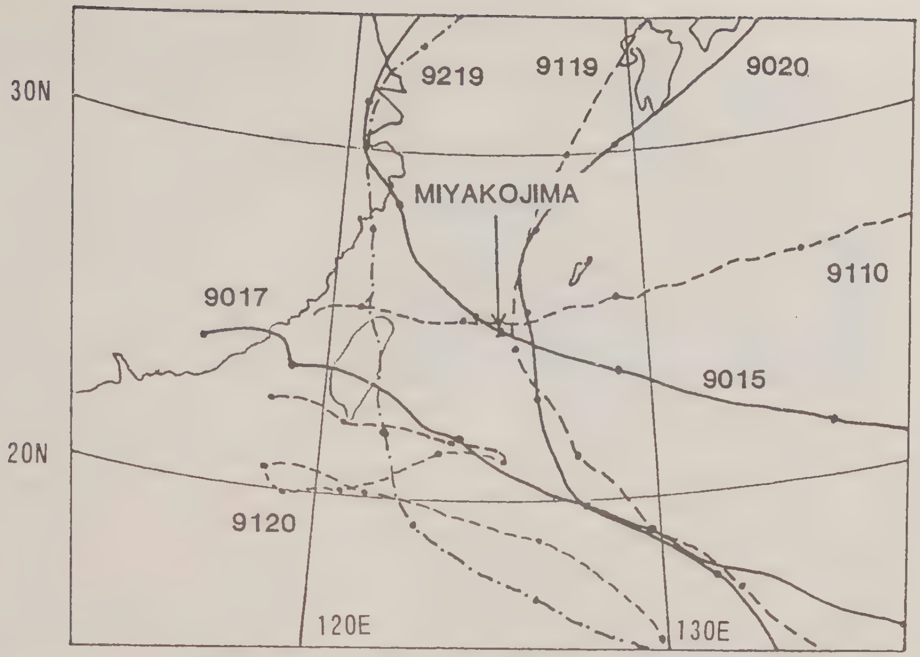


Fig.1 Tracks of the typhoons of which mesoscale precipitation systems were observed by the Doppler radar in the island of Miyako.

(1) Eyewall

Figure 3 shows the eyewall of Typhoon 9015 which was in the mature stage during its passage over the island. Vertical cross section of the eyewall shows that there were frictional inflow just above the surface, outward sloping updraft and convective and stratiform precipitation areas below the updraft. The convective precipitation area was below a strong updraft (85-90km from the typhoon center). These features are very similar to those observed in mature hurricanes (e.g. Jorgensen, 1984b). Similar features were seen in other typhoons. For example, even in the little typhoon T9110 (Diameter ~300km), outward sloping updraft, a convective precipitation area and stratiform precipitation areas were seen in its southeastern portion.

(2) Inner rainbands

Typical inner rainbands in Typhoon 9119 are shown in Fig.4. As shown in this figure, inner rainbands are often embedded in stratiform precipitation areas. There were large differences of the vertical structure between these rainbands. The innermost rainband at 225km was convective and corresponding convergence was seen at middle levels. The outermost rainband at 255km was shallow and convective. Convergence was seen in the lowest layer. The rainband between them seems rather stratiform in nature and does not accompany remarkable convergence.

Similar features of inner rainbands are seen in other rainbands. Figure 5 shows the inner rainbands in Typhoon 9015. The inner rainbands at 155km and 205km are convective and remarkable convergence is seen at middle levels, while the rainband around 180km was stratiform. In the latter rainband low-level convergence is seen in a wide area corresponding to the rainband, so there seems to be a mesoscale updraft in the rainband. Therefore, this stratiform rainband is different from the above-mentioned stratiform rainband in Typhoon 9119 in the formation mechanism.

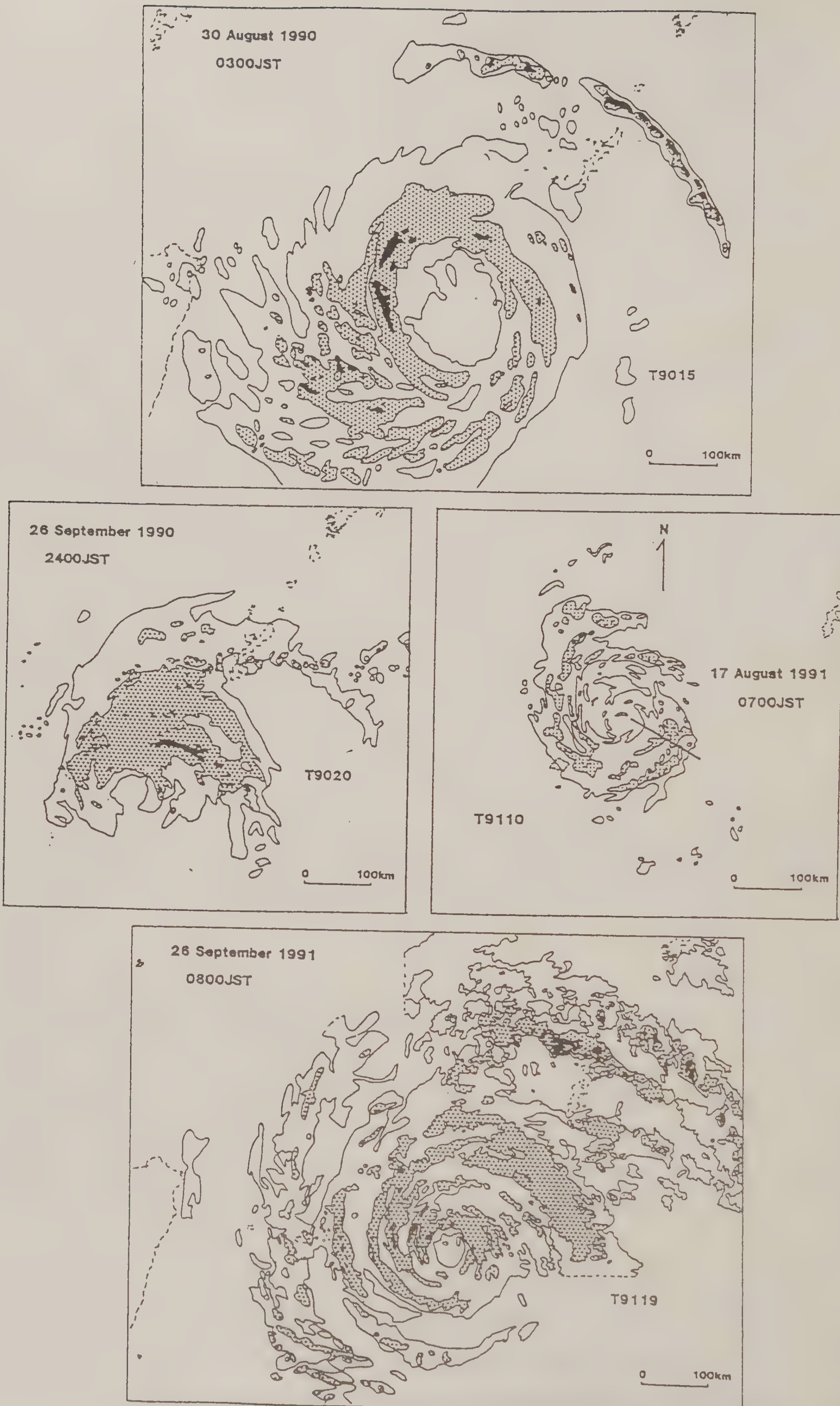


Fig.2 Composited radar echoes of Typhoons 9015, 9020, 9110 and 9119 near the island of Miyako observed by three conventional radars of Japan Meteorological Agency.

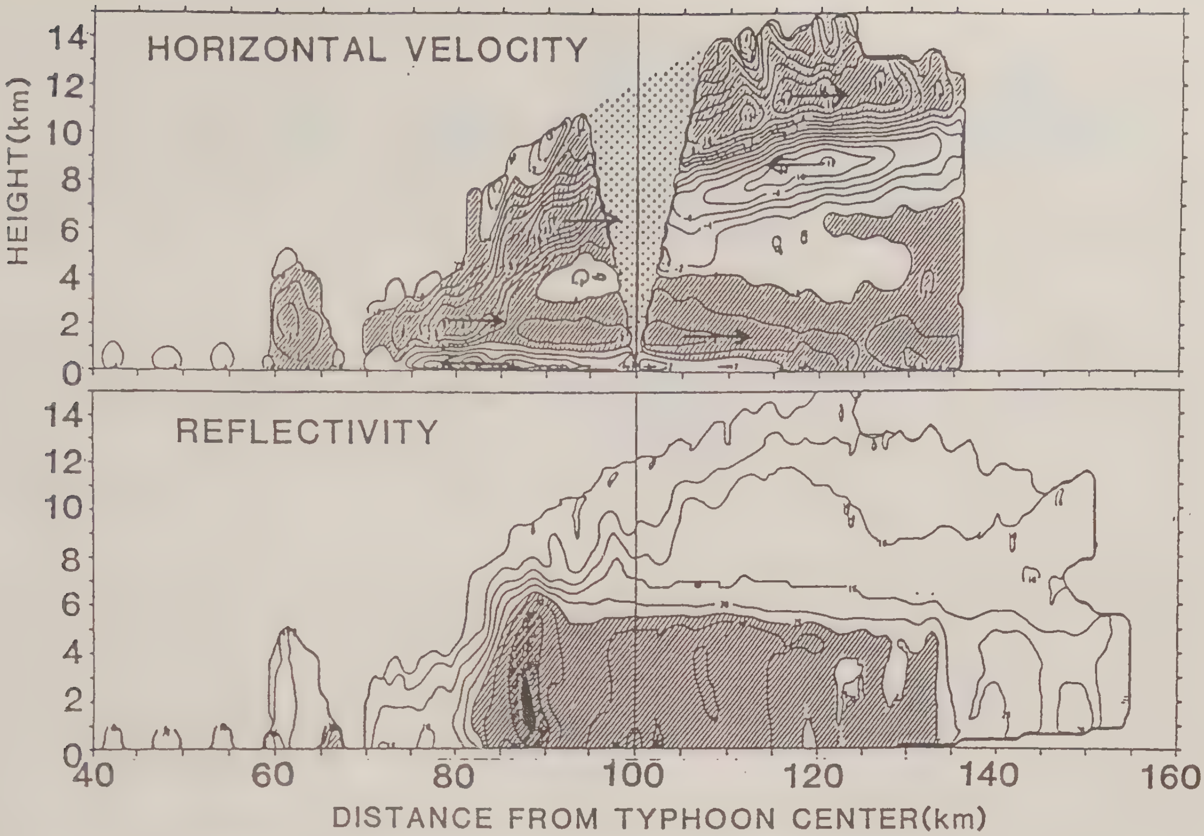


Fig.3 Vertical cross section of eyewall of Typhoon 9015 at 0931JST August 30, 1990. The contour intervals are 2 m/s for horizontal velocity and 5 dBZ for reflectivity. Rightward flow and reflectivity greater than 25 dBZ are shaded.

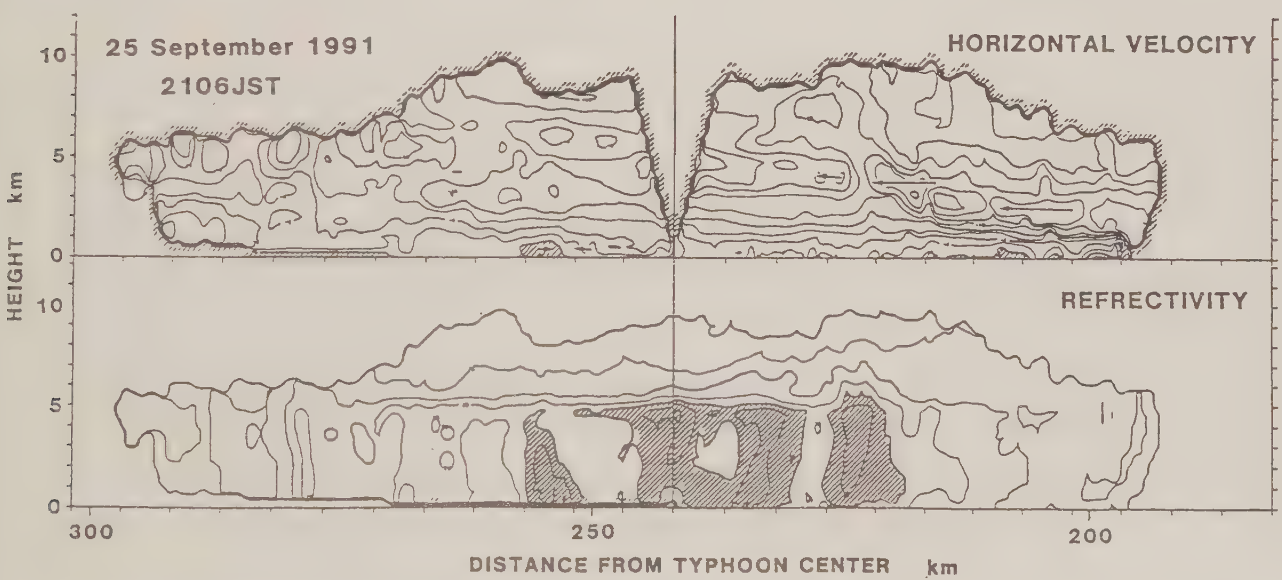


Fig.4 As in Fig.3 except for inner rainbands of Typhoon 9119 at 2106JST September 25, 1991.

(3) Outer rainbands

Since the frictionally induced warm and moist inflow in the lowest layer causes the stratification unstable in the outer portion of typhoons, convective rainbands often form in this portion (Fig.6). Some outer rainbands accompany stratiform precipitation areas on the inner side or on the outer side. In Fig.6 convective areas are seen on the outer side and stratiform areas are seen on the

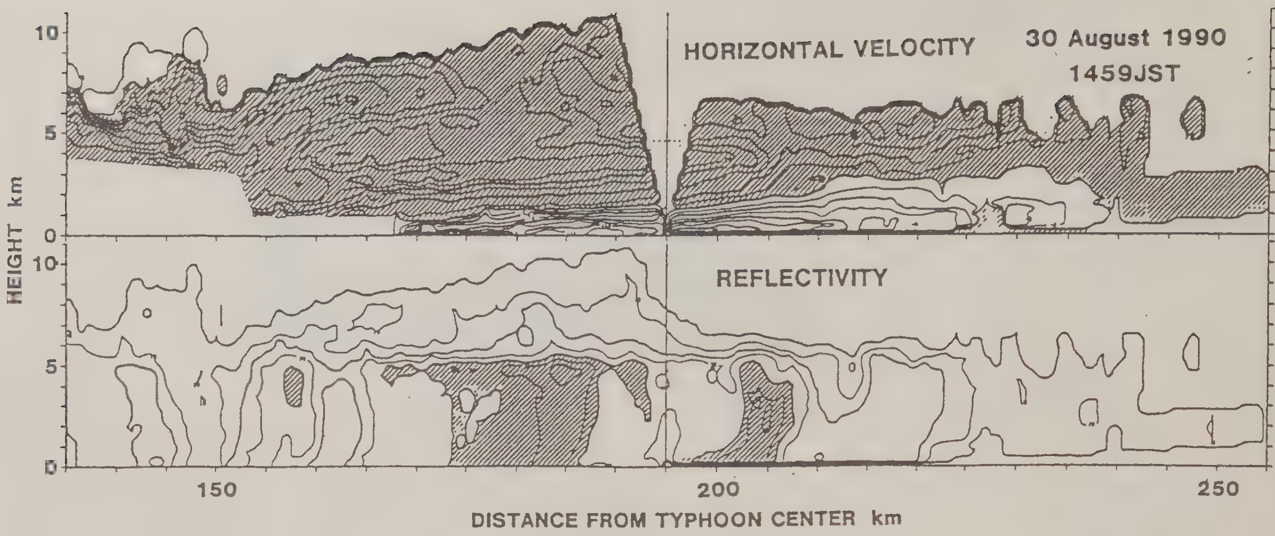


Fig.5 As in Fig.3 except for inner rainbands of Typhoon 9015 at 1459JST August 30, 1990.

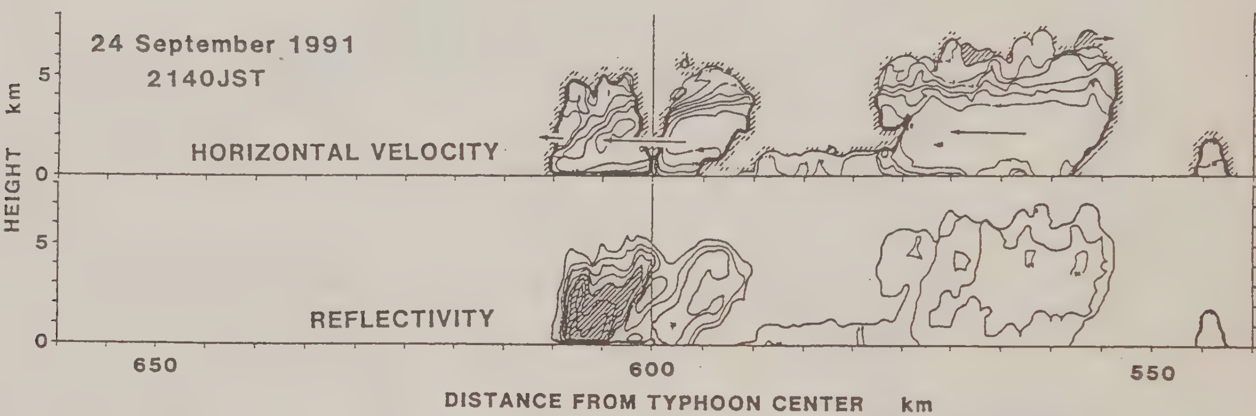


Fig.6 As in Fig.3 except for outer rainbands of Typhoon 9119 at 2140JST September 24, 1991.

inner side. The horizontal velocity in the outer rainband shows that the convective echo formed in the convergence area near the surface between the outer low-level air and inner air originating from the 1-3-km layer. In the stratiform precipitation area on the inner side, horizontal velocity was fairly uniform in the horizontal direction. During the passage of this rainband temperature decrease of about 3 °C was observed. The colder air on the inner side seems to be formed mainly by the evaporation of precipitation in the rainband. Such structure is also seen in other typhoons.

3.2 Cloud clusters during the Baiu season in 1992

(1) Large-scale environment of the cloud clusters associated with the Baiu front

Large-scale situation of the Baiu season is examined for the Okinawa area in 1992. During this Baiu season, precipitation over several tens mm/day were frequently observed in the islands of Okinawa, Miyako and Ishigaki. Total rainfall amount in the island of Miyako was 519mm, which was slightly larger than the climate mean of 410mm.

Period mean equivalent black body temperature (TBB) distribution and large-scale circulation during the Baiu season are examined. A cloud zone originating from southern China lay along the

Okinawa area from west-southwest to east-northeast. Corresponding to this cloud zone, southwesterly flow from Southeast Asia and southerly or southeasterly flow from the subtropical anticyclonic circulation over the northwestern Pacific were confluent around the Okinawa area.

Variation of the Baiu cloud zone is investigated using time-latitude cross sections of TBB and GANAL data (Fig.7). The Baiu cloud zone roughly corresponded to low-level (850hPa) positive vorticity area and sharp latitudinal gradient zone of equivalent potential temperature (θ e).

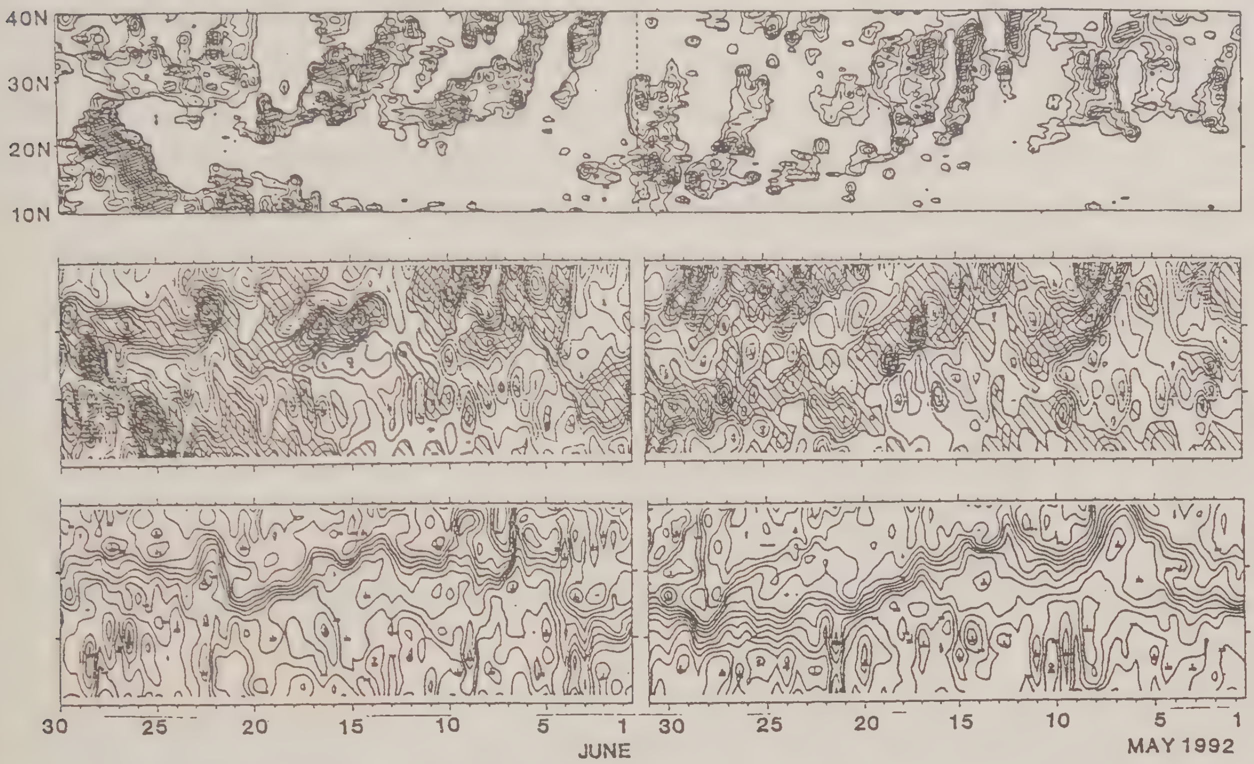


Fig.7 Latitude-time cross section along 125°E of (a)TBB, (b)vorticity at 850hPa and (c) θ e at 850 hPa. The contour interval of TBB is 10 °C. TBB lower than -30 °C and positive vorticity are shaded.

(2) Structures of cloud clusters around the Baiu front

Twelve cases of mesoscale precipitation systems (MPSs) were observed by Doppler radars. If we define a cloud cluster as an area of clouds with the cloud top above the 400hPa level and with horizontal extent more than 7,500km², there were seven cases of cloud clusters. Most convective areas in the cloud clusters were linear in shape and some banded convective areas were also found. These cloud clusters show various flow and precipitation structures. Structures of a stationary cloud cluster and two cold-frontal cloud clusters are described in the following subsections.

(3) Structure of convective clouds in a stationary cloud cluster

This cloud cluster occurred on June 10 and caused the heaviest precipitation in the island of Miyako during the Baiu season. In this case, large-scale low-level convergence was not observed and warm southerly wind was remarkable around the cluster. The cloud cluster had triangle-like shape (so-called "tapering cloud"). Several MPSs evolved in the cluster. They first formed at the western edge of the cloud cluster, moved eastward and then decayed. This process repeated several times and the whole cloud area seemed to be stationary. Total rain of 170mm fell in the island of Miyako

between 0830JST and 2300JST and it was brought by three MPSs. The precipitation was characterized by several peaks due to convective rain with intervals of 30 to 40 minutes in the former two MPSs and one strong peak surrounded by stratiform precipitation in the third MPS.

These MPSs were mainly composed of linear convective areas which were formed by the strong surface convergence between southerly wind in the front and westerly or northwesterly wind in the rear. The motions of these three MPSs were 120°, 6.1m/s; 125°, 6.9m/s; 80°, 11.2m/s, respectively. The former two MPSs show similar movement but the third one is different and faster than the others are. While the former two MPSs consisted of several sub-systems, one steady convective band was maintained in the third MPS. Figure 8 shows the system-relative horizontal flow in the panel parallel to the movement of each MPS derived by VAD analysis. In these figures, low-level convergence is prominent in all cases. Meanwhile, the middle-level flow is different between the former two MPSs and the third one. In the former two MPSs middle-level flow entered from the front of the system and passed through it to the rear. Middle-level inflow from the front was blocked by rear inflow in the third MPS to form a deep convergence layer up to 8km. This deep convergence maintained one quasi-steady convective band. On the contrary, in the former two MPSs a convective cloud which developed at low-level convergence area moved rearward according to the middle-level front-to-rear flow. After the convective cloud is moved out to the rear, next convective cloud is formed at the low-level convergence area. This repeated formation and translation of convective clouds can probably explain the precipitation peaks with interval of 30 to 40 minutes in the former two MPSs.

(4) Structure of convective clouds in cold-frontal cloud clusters

Two cloud clusters formed in cold-frontal zones on June 7 and on June 17. In these cloud

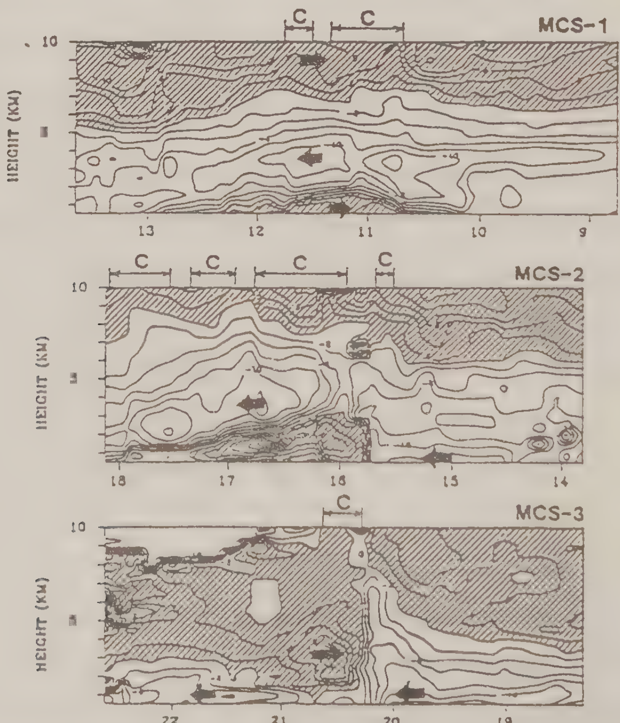


Fig.8 Time-height cross sections of system-relative flow along each MCS movement on June 10, 1992. The contour intervals are 2 m/s. Rear-to-front flow is shaded. Letter "C" in the upper part of each panel indicates convective part.

clusters repeated evolution of MPSs was not remarkable. The MPSs were nearly two-dimensional. Vorticity fields were fairly uniform along the front in both cases.

The MPS observed on June 7 around the island of Miyako occurred within a dissipating cloud cluster associated with the cold front. The cloud cluster corresponding to the MPS was not large. The MPS was composed of active convective areas in the front, somewhat cellular precipitation areas with moderate intensity and stratiform precipitation areas with bright band in the rear (Fig.9). Although the MPS contained stratiform precipitation areas, their extent was very limited. The horizontal scale of cellular precipitation agrees with that of convection. This cellular precipitation was the remnant of convective cells formed in the front. In the MPS a descending rear-to-front flow at middle levels (4-6km) was observed on the rear side of the convective area.

In contrast, the MPS observed around the island of Miyako on June 18 occurred in an extensive cloud cluster which was on the southern edge of a remarkable frontal zone. The MPS also

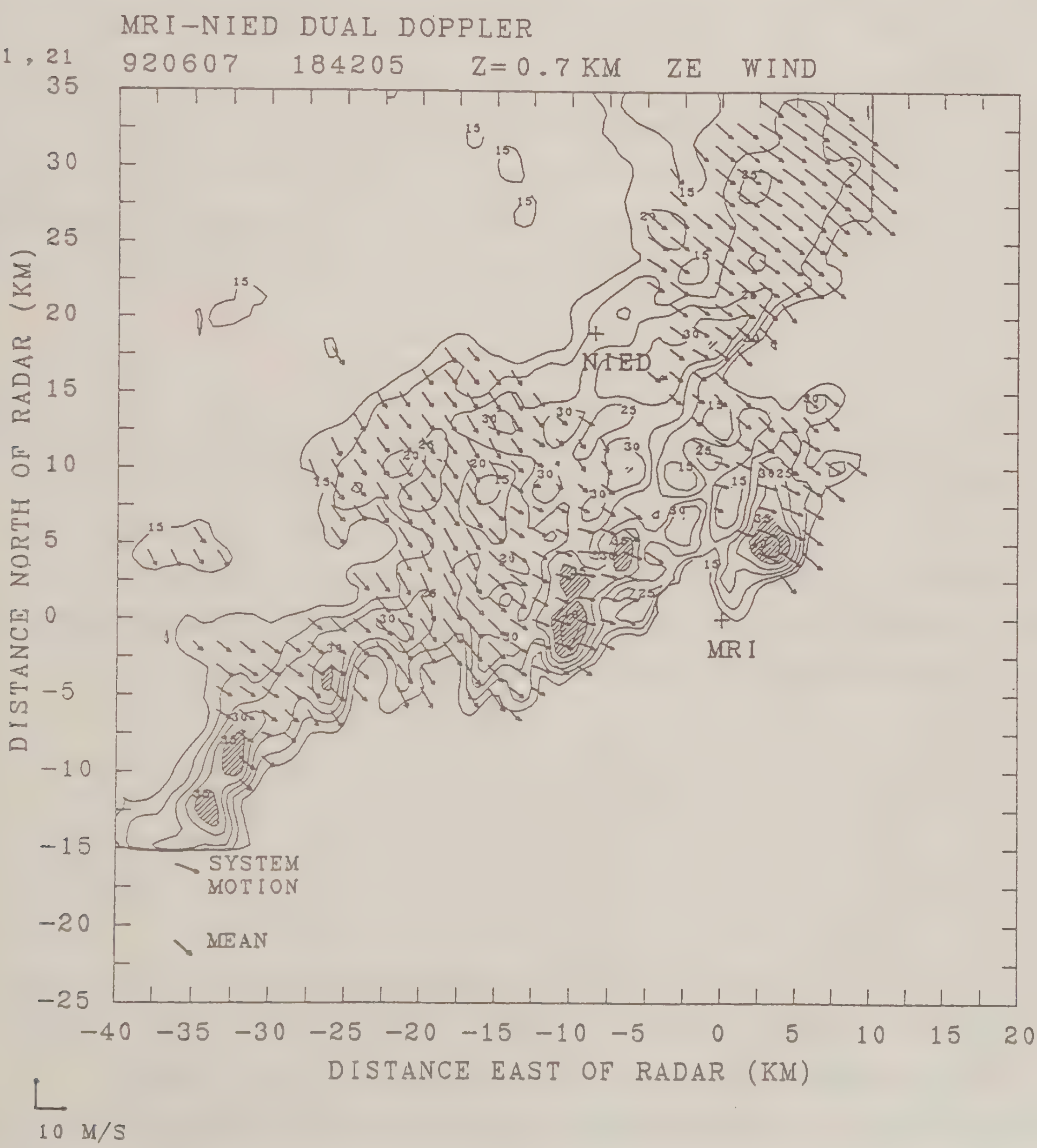


Fig.9 Reflectivity and horizontal velocity fields at the 0.7-km level at 1842 JST June 7, 1992. The contour interval of reflectivity is 5 dBZ and reflectivity higher than 35 dBZ is shaded.

contained active convection on the leading edge and cellular precipitation areas on the rear side. Few stratiform precipitation areas were observed. The rear cellular precipitation areas were not the remnant of convective cells in the front, because the convective cells developed and disappeared near the leading edge in this case. Precipitation intensity tends to be weaker with the distance from the leading edge. In this case, rear-to-front flow was observed at low levels (1-2km).

4. Discussion

It was shown that mesoscale precipitation systems in typhoons have similar structure when their locations relative to the storm center are similar. Structure and mechanisms of eyewalls have been investigated observationally and theoretically (e.g. Jorgensen, 1984 a,b; Shapiro and Willoughby, 1982) and our results are consistent with previous studies. The main mechanisms of outer rainbands seem to be destabilization of the stratification due to the warm air inflow in the lowest layer and lifting of the warm air over the cold air near the surface which is formed by preceding convection. In contrast, mechanisms of inner rainbands, especially those with middle-level convergence and those without remarkable convergence, still remain unclear. It is necessary to study the mechanisms of inner rainbands further through observations and numerical simulations.

The environment of mesoscale precipitation systems in cloud clusters in the Baiu season in 1992 was various and the MPSs show different structures even in the practically same environment (e.g. MPSs on June 10). We need to study further what kind of MPS is predominant for typical Baiu environments.

5. References

Jorgensen, D.P., 1984a: Mesoscale and convective-scale characteristics of mature hurricanes. Part I: General observations by research aircraft. J. Atmos. Sci., 41, 1268-1285.

__________, 1984b: Mesoscale and convective-scale characteristics of mature hurricanes. Part II: Inner core structure of Hurricane Allen (1980). J. Atmos. Sci., 41, 1287-1311.

Shapiro, S.J., and H.E. Willoughby, 1982: The response of balanced hurricanes to local sources of heat and momentum. J. Atmos. Sci., 39, 378-394.

6. Publication

① Journal with referee

None

② Others

1) Domestic (papers)

Sakakibara, H. et al., Observation of structure of convective clouds in large-scale cloud systems. Japanese Experiment on Asian Monsoon (JEXAM) Annual Report, Research and Development Bureau, Science and Technology Agency, 1991-1998 (8 reports)

Sakakibara, H., Structure of convective clouds in cloud clusters around southwestern Japan. Study of Asian Monsoon in Japan and China, Edited by M.Murakami and Ding Yihui, 92-110, 1992.

Sakakibara, H. et al., Observation of structure of convective clouds in large-scale cloud systems,

Research and Development Bureau, Science and Technology Agency, Recent Progress in Studies of Asian Monsoon Mechanism, 147-156, 1999.

2) International (papers)

Ishihara, M. et al., Doppler radar analysis of a typhoon eyewall. Preprints of 25th International Conference on Radar Meteorology, American Meteorological Society, 702-705, 1991.

Akaeda, K. and S. Nakai, Two types of organized convective system observed in subtropical cloud cluster. Preprints of 27th Conference on Radar Meteorology, American Meteorological Society, 383-385, 1995.

Yoshizaki, M., H.Sakakibara and members of MRI-TREX, Research activities of Meteorological Research Institute (MRI) on Torrential Rain Experiment (TREX;1996). Proceedings of International Symposium on Meso-scale Water Cycle and Heavy Rainfall in East Asia. Nagoya University, 135-138, 1998.

Bessho, K. et al., Activities of the Baiu front in the TREX period analyzed by using GANAL and GMS data. Proceedings of International Symposium on Meso-scale Water Cycle and Heavy Rainfall in East Asia. Nagoya University, 32-35, 1998.

7. International Cooperation

None

要旨

大規模雲域(クラウドクラスター)はアジアモンスーン領域内で降水をもたらし熱と水蒸気を上方に輸送するので重要である。クラウドクラスター内で降水をもたらし、熱と水蒸気を輸送する対流雲の構造を明らかにするため、気象研究所と防災科学技術研究所は1990－92年に沖縄県宮古島でドップラーレーダーと高層気象の観測を行った。台風と梅雨期のクラウドクラスターが観測された。

台風は眼の壁雲、内側降雨帯、外側降雨帯に分類されるメソ降水システムからできている。メソ降水システムは台風ごとに外見が異なるにも関わらず、気流と降水の構造に固有の特徴があった。眼の壁雲には外側に傾く上昇流と対流雲がある。内側降雨帯は気流と降水の構造に基づきさらに (a)地表近くに収束のある対流雲、(b)中層に収束のある対流雲、(c)層状性の降雨帯の3種類に分けられる。内側降雨帯は層状性降水域でしばしば観測される。外側降雨帯には地表近くに顕著な収束があり、対流雲を含む。

1992年梅雨前線に伴うクラウドクラスターの環境、時間変化、構造を調べた。梅雨期の雲帯は下層の正渦度域および相当温位(θ e)の傾度の大きいところにおおよそ対応していた。二つのタイプのクラウドクラスターを調べた。梅雨前線から離れたところに発生した停滞性クラウドクラスターはメソ降水システムが繰り返し発生することにより維持されていた。それぞれのメソ降水システムはクラウドクラスターの西端で発生し、東に移動し、そして消滅した。3個のメソ降水システムが宮古島で観測された。初めの2個のメソ降水システムでは中層の流れがシステムの前方から入り、後方に通り抜けた。対流雲は下層収束域で繰り返し発生、発達し、中層の前方から後方への流れに乗って後方に移動した。3番目のメソ降水システムでは前方からの中層の流入は後方からの流れにせき止められ、高度8kmに達する深い収束域ができた。この深い収束により1本の準定常な対流性降雨帯が維持された。寒冷前線帯では二つのクラウドクラスターが発生した。これらのクラウドクラスターではメソ降水システムの繰り返し発生は見られなかった。

I. Observation and analysis on the process of the atmosphere-ocean-land interactions
大気・海洋・陸域間相互作用の諸過程に関する観測・解析研究

1. Observation and analysis on the process in the atmosphere
大気における諸過程に関する観測・解析研究

(3) Analysis on the evolution of convective cloud systems
モンスーン域対流雲の維持過程と水収支に関する研究

Advanced Measurement and Analysis Technology Division
National Research Institute for Earth Science and Disaster Prevention (NIED)
Science and Technology Agency
Sento Nakai
科学技術庁防災科学技術研究所
先端解析技術研究部
中井　専人

Abstract

Baiu frontal zone over the East China sea and the northwestern Pacific is one of the regions that generate many convective cloud systems. They play an important role on the water cycle of Baiu front. The activity of Baiu front is closely related to the global Monsoon circulation. So, it is important to clarify the water cycle of the Baiu frontal zone focusing on the evolution of convective cloud systems.

Investigations on the evolution and the maintenance mechanism of MCSs were conducted as a part of JEXAM project. A cloud cluster and constituent MCSs on 10 June 1992 were analyzed using the special observation data, GMS-4 WEFAX H-image (IR) and SSM/I data. On the radar data processing, an attenuation correction method was developed introducing convective/stratiform area definition.

Band-shaped area of concentrated cloud water (CCW area) suggested that orographic convergence downwind of Taiwan increased column cloud water and favored the generation of cloud clusters. The cloud cluster coexisted with CCW area except the eastern edge where upper-tropospheric cloud shield extended to the downshear direction. In a smaller scale, however, the locations of T_{BB} cold cores and column cloud water maxima were not coexisted. It was attributed to the evolution of MCSs and ice scattering. MCSs were observed by radars below upper-level cloud shields of cloud clusters. An MCS had a convective line, and stratiform precipitation regions and weak-echo zones on both side of the convective line. The cloud shields were considered to be important for the formation of stratiform precipitation. The mesoscale circulation on the rear side was similar to that observed in typical squall lines. The rear-side weak-echo zone possibly had the same maintenance mechanism as seen in the 'transition zone' of a typical squall line. The maintenance mechanism of front-side weak-echo zone is not clear. Further case studies and statistical investigations using radar and satellite data are necessary for correct understanding of the structure and evolution of MCSs in Baiu cloud zone.

1. Objectives

The activity of Baiu front closely related to the global Monsoon circulation (*e.g.*, Kato, 1993). It typically appears as an elongated cloud zone including cloud clusters. The cloud clusters are usually composed of one to a few mesoscale convective systems (MCSs). MCSs play an important role on water cycle of Baiu frontal zone, because they have long-lived organized convections with a lot of precipitation, which are maintained by mesoscale circulation (Akaeda et al., 1991). So far, many case studies revealed the structures and evolution processes of the MCSs in relation to the environmental conditions using synoptic charts and rawinsonde data (*e.g.*, Ninomiya et al., 1988; Wang et al., 1990; Akaeda et al., 1991; Iwasaki and Takeda, 1993). Recently, satellite microwave data made environmental conditions of precipitating clouds to be discussed based on high-resolution water substance distributions (Aonashi and Shibata, 1996; Aonashi et al., 1996). It is expected that combining the microwave data with radar and conventional meteorological data gives comprehensive description of MCS evolution processes.

Investigations of the evolution of MCSs were conducted as a part of JEXAM project. Convective activities characterizing the Asian Monsoon is the sum of the effect of precipitating cloud systems including MCSs. An MCS is smaller in scale than other phenomena investigated in JEXAM project, and is an elementary process of the Asian Monsoon. We intended to contribute to physical understanding of the Asian Monsoon activities through analyses of MCSs.

2. Methods

Cooperative observations on the structure of convective clouds were made in June 1992 by Meteorological Research Institute (MRI) and National Research Institute for Earth Science and Disaster Prevention (NIED). Portable X-band Doppler radars were placed at Miyako Island, and synchronized three-dimensional observations were done for dual-Doppler analyses. Radar coverage area was approximately an oval shape with a major axis of 150 km and a minor axis of 130 km (Fig. 1). Each of the dual-Doppler lobes had a diameter of about 40 km. The length of the baseline was about 21 km. RHI and vertical incidence data were also obtained by NIED Doppler radar. Omega sonde observations were conducted by MRI. Observation period was divided into two, Baiu observation period (from May 25 to Jun 20) and Typhoon observation period (from August 21 to September 23). The whole observation schedule of NIED was shown in Table 1. Observations were done when precipitating cloud systems appeared. Amount of observation data of NIED Doppler radar reached 51 volumes of 6250 BPI, 2400 ft magnetic tapes. Observed phenomena includes various types of precipitation in Asian Monsoon region, such as isolated precipitation, severe convective precipitation with echo top at a height of 15 km, very shallow precipitation.

We analyzed the structure and the wind field of MCSs observed on 10 June 1992 using single Doppler radar data and satellite data. Original Doppler radar data were converted to two- and three-dimensional Cartesian grid data. Equivalent reflectivity factor (Ze) and radial velocity fields are used for the analysis of structures of MCSs. Attenuation of radar beam was corrected using the method described in Nakai (1997). Attenuation rate K was defined, in a conventional manner, for one-way attenuation as $K=a\ Ze^{b}$ (dB/km). We fixed b at 0.755 following Kozu(1991)'s formula using the famous Marshall-Palmer raindrop-size distribution, and derived a for 'convective' rain (a_c) and for 'stratiform' rain (a_s). The 'convective' rain area was defined as the area that the reflectivity gradient was more than 2 dB/km, and the rest was defined as 'stratiform' rain area. The best pair of a_c and a_s was $a_c=2.3\times10^{-4}$ and $a_s=0.7\times10^{-4}$, which minimize Ze difference of the two radars averaged for 95 synchronized volume scans on 10 June.

In addition to the cooperative observation data, we used GMS-4 WEFAX H-image (IR) and SSM/I data (antenna temperature data and retrieved geophysical data distributed from Remote Sensing Systems). SSM/I precipitable water and column cloud water were derived using algorithm by Shibata (1994). Spatial resolution and coverage significantly differ among these data (Table 2). Radar data with high time and spatial resolutions are suitable for the analysis of meso-β and meso-γ scale structures of MCSs. Satellite microwave radiometer data can be used for the description of meso-α scale structure and environment around MCSs. Hourly GMS data is indispensable to know the evolution of cloud systems. Data from different sources were mapped on a common coordinate system for comparison as much as possible.

Table 1 Observation schedule of NIED in 1992.

PREPARATION		
Apr.	15(Wed.)-17(Fri.)	location hunting
May.		machine maintenance, shipping arrangement
May.	15(Fri.)	shipping of facilities
BAIU OBSERVATION PERIOD		
May.	22(Fri.)	setting up of radar and observation site
	23(Sat.)-24(Sun.)	facility tuning
	25(Mon.)	
	|	observation
Jun.	20(Sat.)	
BREAK		
Jun.	21(Sun.)	
	|	break
Aug.	20(Thu.)	
TYPHOON OBSERVATION PERIOD		
Aug.	21(Fri.)	
	|	observation (including standby time)
Sep.	23(Wed.)	
Sep.	24(Thu.)-25(Fri.)	dismantlement of observation site
Sep.	26(Sat.)	shipping of facilities at Miyako
Oct.	3(Sat.)	arrival of facilities

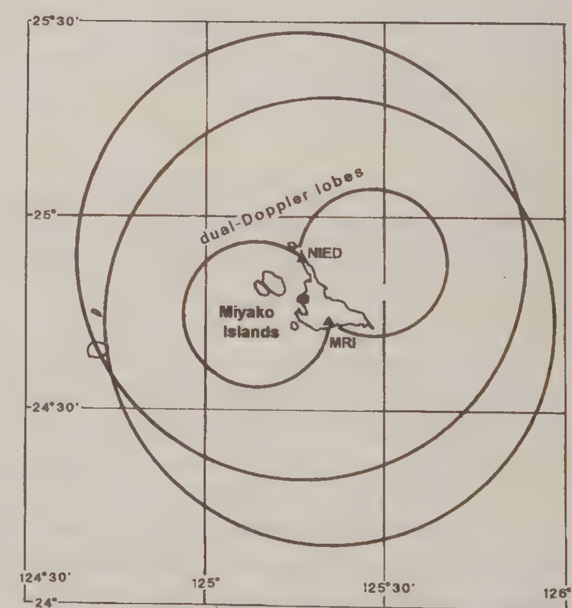


Fig. 1 The Doppler radar observation sites (MRI, NIED) and the radar coverage.

Table 2 Resolution and coverage of the data used for analyses.

data	X-band Doppler radar	SSM/I	GMS WEFAX IR
time resolution	520 seconds	0〜2 times per day	hourly
spacial resolution	0.25 km	about 25 km	5-8 km
coverage	128 km in diameter	swath width of about 1400km	about 4500 km square

3. Results

3-1. water substance distribution derived from satellite data

A cloud cluster composed of three MCSs passed over Miyako Islands on 10 June 1992. Time series of upper-level cloud field indicated that the cloud cluster was nearly stationary and characterized by low black-body temperature (T_{BB}) and large T_{BB} gradient at the western edge of the cloud area. This was the result of repeated formation at the western edge and following eastward propagation of MCSs (Akaeda and Nakai, 1995).

At 1739 JST, cold cores (T_{BB}< -70 °C) were seen around (24 °N, 124 °E), where the most active convection within the cloud cluster was suggested (Fig. 2). Upper-level solid cloud mass extended to the west-southwest of the cold cores. Simultaneously observed SSM/I column cloud water distribution (Fig. 3) indicates that the cold cores located within the area where column cloud water was more than 0.5 mm. However, the cold cores did not coexist with the maximum of column cloud water. Column cloud water was concentrated to more than 0.3 mm in a band-shaped area (hereafter referred to as CCW area). CCW area extended west-southwesterly toward the west end of the cloud cluster, reached to the east coast of Taiwan. It is inferred that orographic convergence downwind of Taiwan (Akaeda and Sakakibara, 1996) increased column cloud water and favored the generation of convective clouds. SSM/I precipitable water (Fig. 4a) was more than 50 mm around cloud cluster, which was considered as the condition necessary for the development of cloud clusters (Nakai and Kawamura, 1998). To the east of 125 °E, upper-level cloud and CCW area did not necessarily coexist. T_{BB} was higher in eastern half of the cloud cluster and extended nearly eastward, that is, the direction of wind shear. CCW area extended to the northeast out of upper-level cloud shield of the cloud cluster. Column liquid water, which is the sum of column cloud water and column rainwater, is shown in Fig. 4b. The ratio of column rainwater to column liquid water varied 0.67 in weak rain to 0.36 in strong rain. The reason of this difference is not clear because water substances may contain some errors under upper-level cloud shield of the cloud cluster. Further examinations on the data and analysis method are necessary for quantitative analyses.

3-2. Precipitation and wind field derived from satellite and radar data

Precipitation on 10 June 1992 was brought by several MCSs. Three of them were observed by the Doppler radars. It was inferred from comparisons of radar rainfall pattern and satellite cloud images that MCSs existed below upper-level cloud shields of cloud clusters.

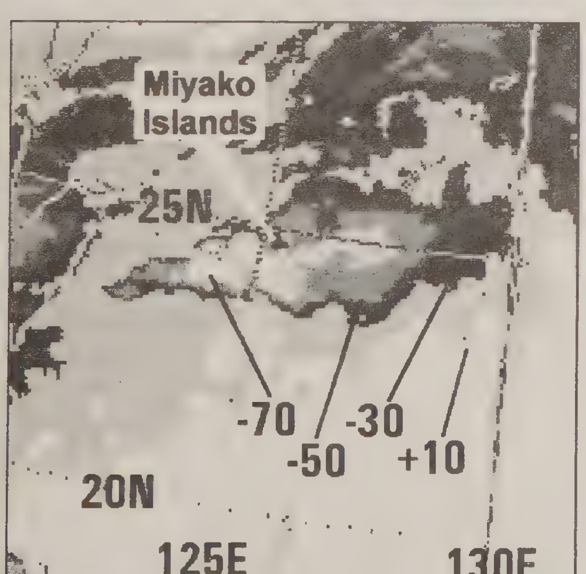


Fig. 2 GMS-4 IR T_{BB} distribution in °C at 1739 JST.

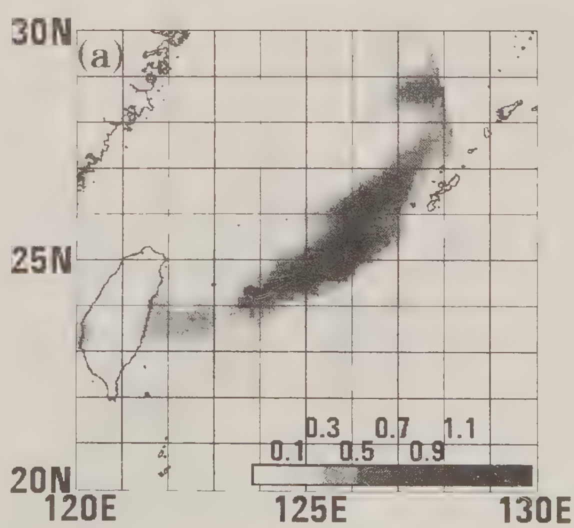


Fig. 3 Column cloud water in mm derived from SSM/I by Wentz (1994) at 1744 JST.

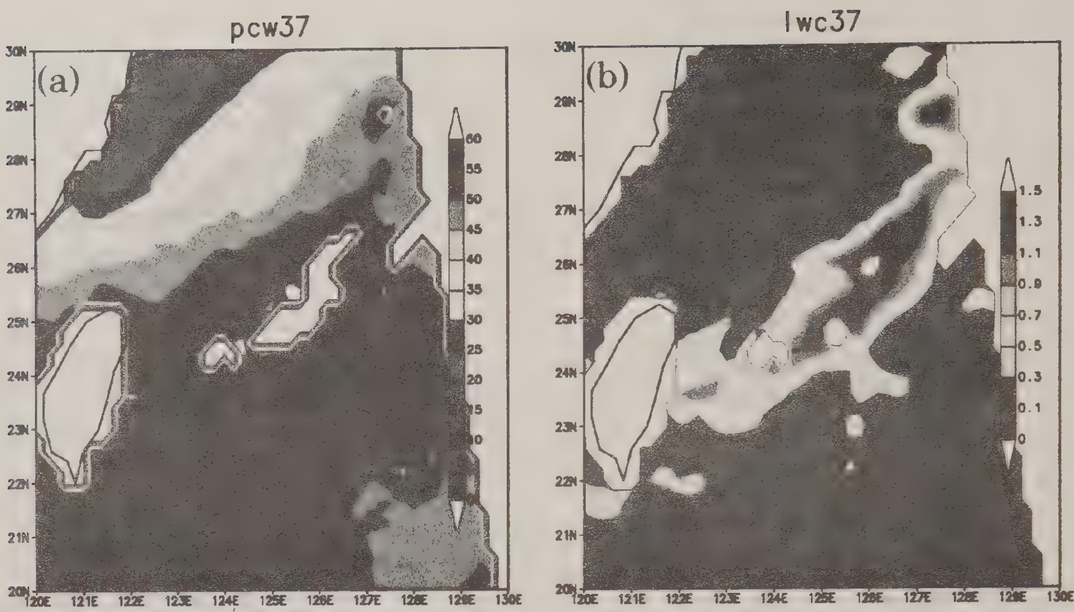


Fig. 4 Water substance distribution in the same area as in Fig. 6 derived from SSM/I by Shibata (1994) at 1744 JST: (a) precipitable water in mm, (b) column liquid water in mm.

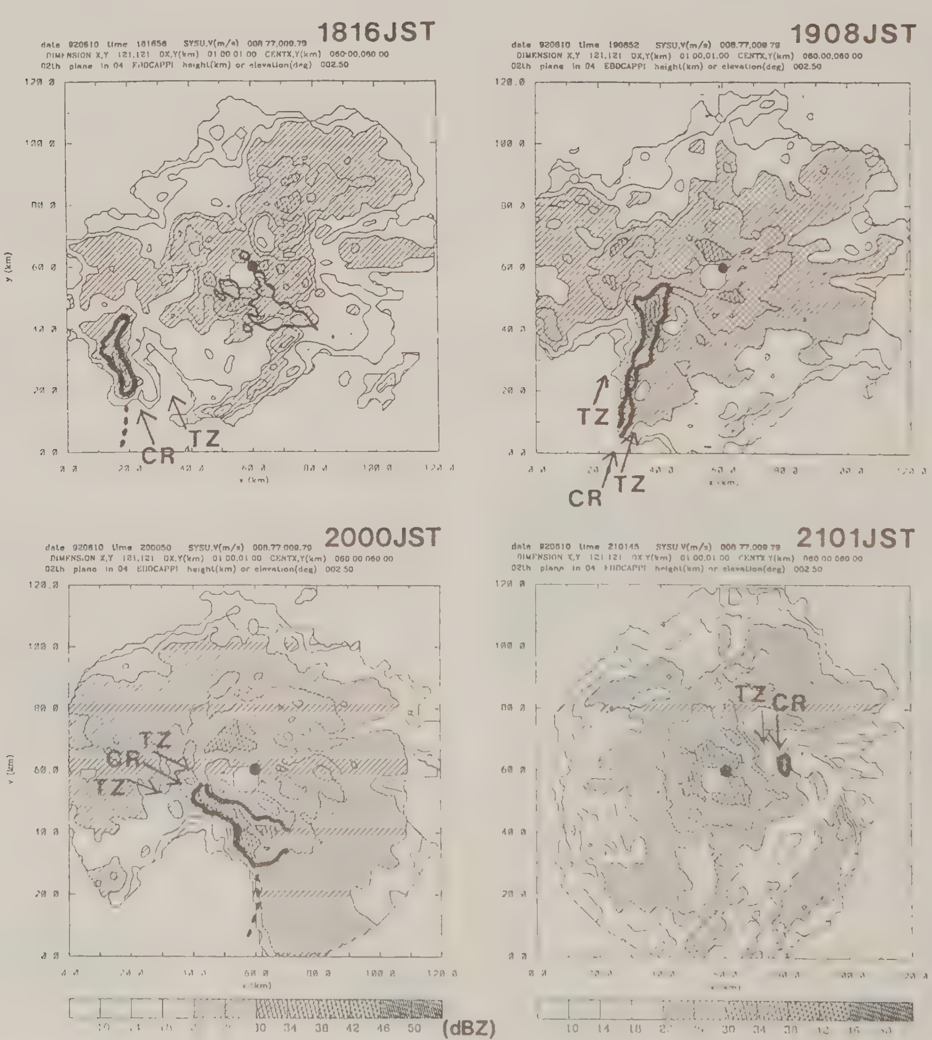


Fig. 5 Ze fields at a height of 2.5 km. The radar (large dot) was at the center of each panel and the maximum detectable range was 64 km. CR: convective line. TZ: weak echo zone. CR location is emphasized by thick contour line of 26 dBZ.

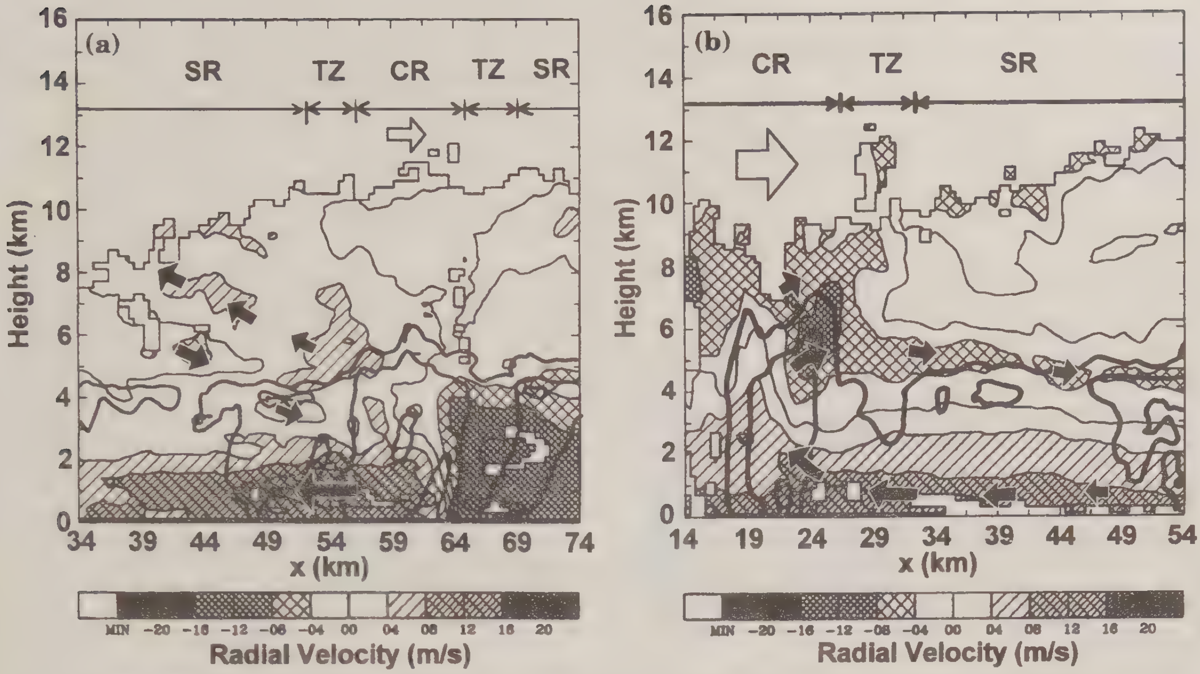


Fig. 6 Ze (thick lines) and radial velocity (thin lines and shading) fields on a vertical section in 226° - 46° direction around a convective line observed using NIED Doppler radar (located at x=64 km) at (a) 2025 JST and (b) 1841 JST. The horizontal velocity is relative to the mean motion of the convection cells. Positive velocity indicates rightward motion in the figure (from 226° to 46°). Ze contour lines indicate 18, 26 and 34 dBZ. CR: convective line. TZ: weak echo zone. SR: stratiform precipitation region. White and black arrows schematically indicate the motion of convective line and convective-line relative wind, respectively.

MCS appeared on 18-22 JST 10 June 1992 had a convective line surrounded by stratiform precipitation through the period it was observed by NIED Doppler radar. Figure 5 shows the reflectivity field within almost full radar coverage at a height of 2.5 km. A convective line (CR) appeared at the southwest edge of the radar coverage about 18 JST, and after moving toward the radar, disappeared about 21 JST to the east of the radar. Mesoscale circulation rearward the convective line persisted until 22 JST. Weak-echo zones (TZ) existed on both sides of the convective line.

Ze and the convective-line relative radial velocity fields on a vertical plane at 1841 JST are shown in Fig. 6b. The convective line was at x=21 km, and the front-side stratiform precipitation extended several tens of kilometers wide. The wind blew toward the convective line at levels below 3 km, while it blew from the convective region at levels between 3 km and 6 km through the stratiform precipitation region. On a vertical section at 2025 JST, the convective line (at x=60 km) and the rear-side stratiform precipitation region extending several tens of kilometers wide were seen (Fig. 6a). In the rear-side stratiform region at x<52 km, the wind blew from the convective region at levels less than 2 km. At levels more than 3 km, a pair of rear inflow and front to rear outflow was seen, which had the similar configuration to that seen in squall line with trailing stratiform precipitation. This suggests that the flow pattern is the manifestation of a mesoscale circulation that closely related to the activity of the convective line, that is, the ice particles generated in the convective line entrained to the rear-side stratiform precipitation region in the upper levels.

4. Discussions

The precipitating cloud system described in the previous section was a cloud cluster embedded in Baiu cloud zone. The cloud clusters were defined by T_{BB}= -30 °C (Nakai and Kawamura, 1998) with cold T_{BB} core of less than -60 °C. A cloud cluster was composed of MCSs. The cold core indicates strong convection, and upper-level cloud area of the cloud cluster extending to the east of the cold core is considered as weakened old convection and the resulting anvil cloud. Isolated convective precipitation was seen outside cloud clusters. Stratiform precipitation spread mainly below upper-tropospheric cloud shield of cloud clusters. It is suggested that the cloud shield was important for the formation of stratiform precipitation.

Around the cold cores at (24 °N, 124 °E) in the analyzed cloud cluster (Fig. 2), column liquid water (Fig. 4b) was smaller than that in the north edge of the cloud cluster. The dislocation of the cold cores and column liquid water maximum can be attributed to the following two reasons. One is the evolution of MCSs included in the cloud cluster. Young MCS contain strong updrafts those make the cloud top at the highest level in the troposphere. As the MCS evolves, the updraft weakens and larger precipitation particles may be formed. So, an older MCS with higher cloud-top T_{BB} can show large column liquid water content. The other is an effect of scattering by ice particles. An MCS with

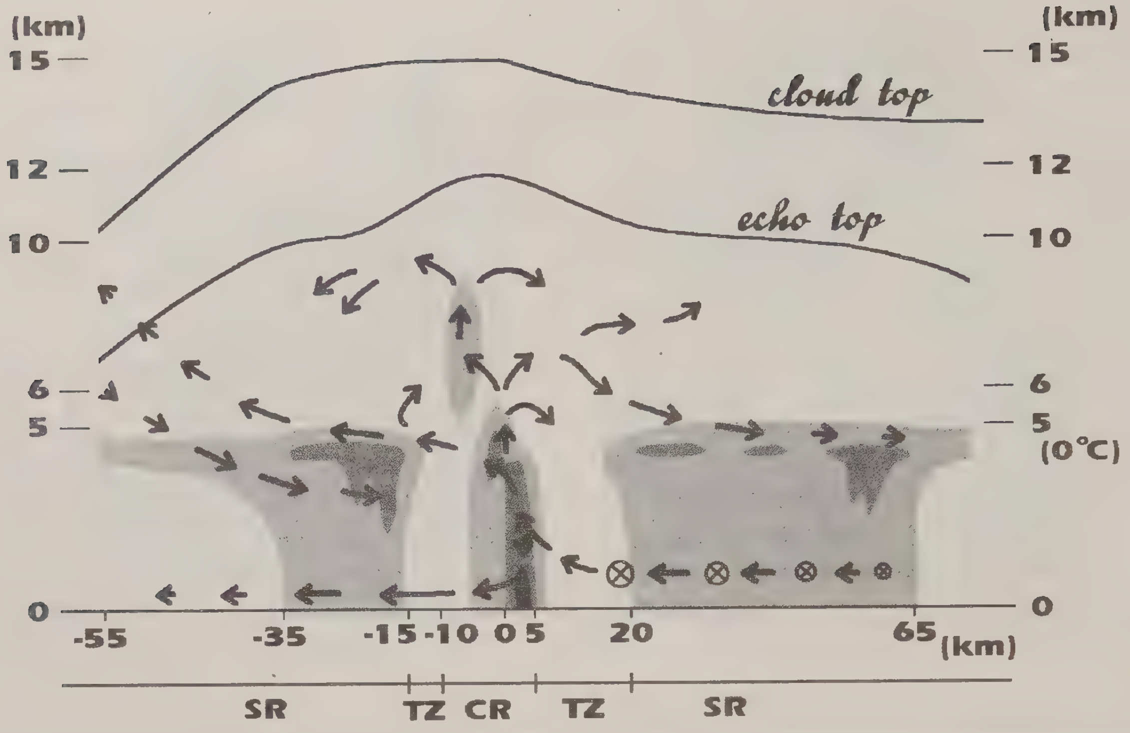


Fig. 7 Schematic illustration of the MCS observed during 18-22 JST on 10 June 1992. Distance from the center of convective line is shown in abscissa. CR: convective line, TZ: transition zone, SR: stratiform precipitation region. Ze is indicated by graded shading. Solid arrows are flows relative to the convective line. Circled Xs indicate the wind blowing into the figure.

vigorous convection may yield a dense ice cloud, which causes strong scattering. The ice scattering decreases microwave brightness temperature and leads to apparent low liquid water content, which causes error in the analysis of water cycle of the cloud system.

Doppler radar data analysis showed that an MCS had weak-echo zones and stratiform precipitation regions on both sides of a convective line. The convective line was 10-20 km wide, and moved slowly in 10-15 m/s. The wind blew into the convective line on the front side in the lowest level and diverged on both sides above the melting level. The outflow above the melting level èxtended to the stratiform precipitation region. The inflow and outflow formed a mesoscale circulation extending in the entire MCS about 120 km wide (Fig. 7). Ishihara et al. (1992) analyzed a squall line appeared on 20 May 1987 in the area near Miyako Islands, and reported that it had stratiform precipitation regions on both side of the convective line as described in this report. It is different from typical squall lines reported in north America and in the Tropics, which have stratiform precipitation on the rear side only. This feature may be characteristics of MCSs in this region.

A weak echo zone of a squall line between the convective line and the stratiform region is characterized by downdraft throughout the troposphere and called 'transition zone' (Biggerstaff and Houze, 1993). The transition zone is formed on the rear side closely related to the activity of the convective line. Squall lines reported by Ishihara et al. (1992) also had one transition zone on the rear side. The MCS analyzed in this report had weak-echo regions on both sides of the convective lines, and the mesoscale circulation on the rear side was similar to that observed in typical squall lines. It is inferred that the weak-echo zone formed on the rear side had the same maintenance mechanism as seen in the 'transition zone'. The front-side weak-echo zone has not been reported so far. Weak echo intensity suggests the existence of a deep downdraft region, however, the mechanism of the formation of the front-side weak echo zone is a problem to be solved.

The structure and evolution processes of MCSs may differ by location and stage of the Baiu front, and of the Asian Monsoon. An interesting and important problem related to the water cycle and intraseasonal change of the Baiu front is the difference of structure and evolution mechanisms between MCSs observed in this investigation and those in the well investigated later stage of Baiu front around Kyushu. Further case studies and statistical investigations using radar and satellite data are necessary for correct understanding of the structure and evolution of MCSs in Baiu cloud zone.

Satellite microwave data analysis is hopeful to clarify the distribution of water substance in Baiu frontal zone including MCSs. However, the relation between the precipitation rate and microwave brightness temperature is nonlinear and dependent on the distribution of the size and phase of precipitation particles. The knowledge on the

structure of MCSs. for example. types of precipitation, the height of melting level. inhomogeneity of the precipitation rate within the footprint of the satellite microwave radiometer. are important parameters. Estimation of these parameters is also an important remaining problem.

Acknowledgments. The author is grateful to the staff members of Miyakojima Local Meteorological Observatory for their kind support of our observations.

5. References

Aonashi. K. and A. Shibata. 1996: The impact of assimilating SSM/I precipitable water and rain flag data on humidity analysis and short-term precipitation forecasts. J. Meteor. Soc. Japan, 74. 77-99.

Aonashi. K.. A. Shibata and G. Liu. 1996: An over-ocean precipitation retrieval using SSM/I multichannel brightness temperatures. J. Meteor. Soc. Japan, 74, 617-637.

Akaeda. K.. T. Yokoyama. A. Tabata. M. Ishihara and H. Sakakibara. 1991: Evolution of the kinematic structure within a meso- β -scale convective system in the growing and mature stages. Mon. Wea. Rev. 119, 2664-2676.

Akaeda. K. and S. Nakai. 1995: Two types of organized convective system observed in subtropical cloud cluster. Preprints of 27th Conference on Radar Meteorology. 9-13 October 1995. Vail. Colorado. 383-385.

Akaeda. K. and H. Sakakibara. 1996: Heavy rain brought by 'tapering cloud'. Proceedings of Workshop on Formation Process of Heavy Rain System, 28 July 1995, Nagoya, 55-67.

Biggerstaff. M. I. and R. A. Houze. Jr.. 1993: Kinematics and microphysics of the transition zone of the 10-11 June 1985 squall line. J. Atmos. Sci., 50, 3091-3110.

Ishihara. M.. A. Tabata. K. Akaeda. T. Yokoyama and H. Sakakibara, 1992: The structure of a subtropical squall line observed with a Doppler radar (Japanese). Tenki, 39, 727-743.

Iwasaki. H. and T. Takeda. 1993: Structure and behavior of mesoscale cloud clusters traveling over the Baiu-frontal zone. J. Meteor. Soc. Japan, 71, 733-747.

Kato. K. 1993: The processes of the seasonal transition of Baiu front in East Asia: The effect of Indian Monsoon and the semiarid region around China (Japanese). Kaiyo Monthly, extra issue No.5. 96-101.

Kozu. T.. 1991: Estimation of raindrop size distribution from space-borne radar measurements. Ph. D. dissertation, Kyoto University, 196pp.

Nakai. S.. 1997: Analysis on the evolution of convective cloud systems. Japanese experiment on Asian Monsoon (JEXAM): Annual report (April 1996 - March 1997). Research and Development Bureau. STA. Japan. I-1-(3).

Nakai. S. and R. Kawamura. 1998: Prevailing scale of cloud clusters appeared in Baiu cloud zone: June 1992 case. Extended papers. International Symposium: Meso-scale Water Cycle and Heavy Rainfall in East Asia, February 2-4, 1998, Nagoya.

Ninomiya. K.. T. Akiyama and M. Ikawa. 1988: Evolution and fine structure of a long-lived meso- α -scale convective system in Baiu frontal zone. Part I: Evolution and meso- β -scale characteristics. J. Meteor. Soc. Japan, 66, 331-350.

Shibata. A.. 1994: Determination of water vapor and liquid water content by an iterative method. Meteorol. Atmos. Phys., 54, 173-181.

Wang, T. C.. Y. J. Lin. R. W. Pasken and H. Shen. 1990: Characteristics of a Subtropical Squall Line Determined from TAMEX Dual-Doppler Data. Part I: Kinematic Structure. J. Atmos. Sci.. 47. 2357-2381.

Wentz. F. J., 1994: User's Manual SSM/I-2 geophysical tapes. RSS Technical Report 070194. Remote Sensing Systems, Santa Rosa, CA 95404, USA, 20pp.

6. Publications

[1] Journals

1) Japanese (1)

Nakai. S. and R. Kawamura. 1998: Characteristics of cloud clusters appeared around the Baiu front: Prevailing scale of organized convection and environmental condition (Japanese). Tenki. 45. 895-905.

[2] Others

1) Japanese (4)

Nakai. 1992: On observations and analyses using NIED Doppler radar (Japanese). Symposium "New Observation Systems" databook, May 1992, Meteorological Society of Japan.

Nakai. S., 1995: On the analysis method of the Doppler-radar data and the examples of its application: VAD analysis (Japanese). Bosai Kagaku Gijutsu, No. 73, 67-72.

Nakai. S., 1995: Extraction of characteristic mesoscale wind fields by VAD analysis (Japanese with English abstract). Rep. Natl. Res. Inst. Earth Sci. Disast. Prev., No. 55, 9-23.

Nakai, S., 1995: Heavy precipitation and wind field below anvil of a cloud cluster (Japanese). News Natl. Res.

Inst. Earth Sci. Disast. Prev., No. 102, 1-4.

2) English (1)

Nakai. S. and R. Kawamura. 1998: Prevailing scale of cloud clusters appeared in Baiu cloud zone: June 1992 case. Extended papers, International Symposium: Meso-scale Water Cycle and Heavy Rainfall in East Asia, February 2-4, 1998, Nagoya.

和文アブストラクト

東シナ海から北西太平洋にかけて現れる梅雨前線帯では多くの対流性雲システムが形成される。それらの雲システムはモンスーン循環と密接に関連した梅雨前線帯の水循環に重要な役割を果たしている。従って、対流性雲システムの発達に焦点を当てて梅雨前線帯の水循環を解明することは、モンスーン機構の解明にとって重要なことのひとつである。

東シナ海上のモンスーン域対流雲(mesoscale convective system)とそれを含むクラウド・クラスターについて、ドップラーレーダー等の特別観測データ、GMS-4 WEFAX H-image(IR)、SSM/Iデータを併用した解析により、その構造と維持機構を調査した。ドップラーレーダーデータ処理に関しては、対流／層状の判別を取り入れた減衰補正法を開発した。

台湾の風下に地形性収束によると思われる雲水極大軸が存在し、クラウド・クラスターの発生に有利に働いていたと思われる。クラウド・クラスターはシアー風下にかなとこ雲が広がった領域を除き、雲水極大軸と同じ場所に存在した。しかし、さらに小さいスケールでは、T_{BB}極小域と積算雲水量極大域は一致しなかった。これは対流雲の発達過程と氷の散乱にによる雲水量の過小評価に帰着する。レーダーで観測された対流雲はクラウド・クラスターの実体であった。対流雲は対流域、及びその両側に存在する層状域と弱エコー域から構成されており、層状域の形成にはかなとこ雲の存在が重要であったと考えられる。対流域後方のメソスケール循環は典型的なスコールラインのものと似ており、その循環や弱エコー域の維持機構もスコールライン同様と思われる。対流域前方の層状域と弱エコー域の維持機構ははっきりしない。レーダーと衛星のデータを用いた事例解析と統計とが必要である。

I. 大気・海洋・陸域間相互作用の諸過程に関する観測・解析研究

Observation and Analysis on the Process of the Atmosphere-Ocean-Land Interactions

2. 海洋における諸過程に関する観測・解析研究

Observation and Analysis on the Process over the Ocean

(1) 表層水温に関する観測研究

Observation on Sub-Surface Temperature by Voluntary Ships

水産庁 遠洋水産研究所

水野 恵介*, 渡辺 朝生, 岡崎 誠, 稲掛 伝三

National Research Institute of Far Seas Fisheries, Fisheries Agency

K. Mizuno*, T. Watanabe, M. Okazaki and D. Inagake

(Abstract)

Large-scale upper layer thermal field and circulation of the Indian Ocean was described and discussed their variability relation to wave phenomena and ENSO cycle. Data sets of SST, depth/temperature and depth/temperature/salinity were constructed using observation data by fisheries research vessels supervised by Fisheries Agency and data sets of COADS, JODC, NOCD and INODC.

Seasonal variability was dominant for SST in the entire Indian Ocean, but semi-annual variability also observed in the north of 20°S of the ocean. 1st mode of EOF, which is that the entire Indian Ocean anomalous SST changed simultaneously, was highly correlated to ENSO signal temporally with 3 months time lag.

Zonal movements of warm water were observed remarkably along the equator and in its northern area by maps of upper layer thickness (ULT). Coastal upwelling and typical temperature front were found along the south coast of Java to Timor from August to September, and warm water transported by the Indonesian throughflow (ITF) spread westward from July to October.

The equatorial jet transported warm water to the eastern Indian Ocean and warm water pool appeared in the offshore area of Sumatra in the inter-monsoon periods. This warm water spread westward after the periods. The structure of the equatorial jet could be clearly obtained by R/V *Shoyo Maru* during inter-monsoon period in November 1995. The jet was confined to shallow depths (about 100m), and the width was estimated to be approximately 400km (2S-2N). Eastward mass transport was large (20sv).

The time-longitude sections of UTL and dynamic height anomalies along different latitudes were enables to bring out the annual and semi-annual signals of circulation. The semi-annual signal of the Kelvin wave, which corresponded with the equatorial jet, was clearly identified at the equator. Away from the equator the westward propagating Rossby wave signal was obtained and was very strong along 4° N and S. Along 12°S an annual signal of westward propagating Rossby wave generating from the Indonesian throughflow (ITF) region was distinguished. The phase speed of the Rossby wave obtained at 12°S was less than 0.2m/s, whereas 0.4m/s speed was found at 4°N and S. The equatorial Kelvin wave was propagating at a greater speed of about 1 m/s.

Interannual signal related to ENSO was found in the fluctuation of 100m temperature anomaly in the ITF area. In El Nino/La Nina years, negative/positive anomalies tended to appear

---

* Present office: Fisheries Agency

with 3-4 months time lag, in contrasted with the EOF 1st mode of SST, which was found positive/negative anomalies in El Nino/La Nina years.

1. Objectives

Large scale upper layer thermal field of the ocean is important for the mechanism of the Asia Monsoon as a major boundary condition which plays as a sink/source of heat of the atmosphere. Since the upper layer of the ocean is not quiet and stable, heat storage of oceanic upper layer and its transport by oceanic current, which make net oceanic heat gain, play an important role for the heat exchange between atmosphere and ocean. So, we extended the observation area in the Indian Ocean by fisheries research vessels (fisheries experimental stations and fisheries high schools of several prefectural governments) and tried to make clear the circulation and temperature distributions in the Indian Ocean using these data and COADAS, JODC, NODC data.

2. Method

2-1. Observations by research vessels of several prefectural governments

Observation on sub-surface temperature in the Indian Ocean has been conducted over the past 30 years by fisheries research vessels (Fisheries Experimental Stations and fisheries high schools of several prefectural governments) under the supervision of the Fisheries Agency. Based upon these data, with additional data sources, a data set of sub-surface temperature for period 1967 through 1988 covering the area 40 ° S-20 ° N and 50° E-130 ° E bas been constructed. From 1989 to 1998 in this project (JEXAM), number of data observed by these research vessels and voluntary observation ships became over 4,870 stations (Fig.1), which involved the observations in the high density XBT line, CLIVER/WOCE IX-6.

Making clear the oceanographic structure and the circulation in the Indian Ocean, we merged these observation data and NODC and INODC data set to a single data set, and drew annual and monthly and/or bimonthly maps of surface temperature, 100 m temperature, dynamic height and upper layer thickness (ULT).

2-2. Surface temperature analysis

COADS monthly SST data (2 ° ×2 ° latitude/longitude) was analyzed to investigate annual and interannual variability of SST in the Indian Ocean (40 ° S–20 ° N and 40 ° E－130 ° E) for the period of 1970-1984. COADS data set involves anomaly data set calculated using the data from 1850 to 1979 by Reynolds (1982). But, these data has long term trend because of the changing of the measurement technique in these years. So, we calculated monthly long-term mean and anomaly of SST using the temperature data from 1970 to 1984.

2-3. Data set for upper layer thickness (UTL)

To investigate annual cycle of UTL (represented by 20℃ isotherm depth) in the Indian Ocean (35 ° S–30 ° N and 40 ° E–125 ° E), historical temperature/depth data set was conducted by merging our data observed by aforesaid research vessels in 1966 to 1989 and NODC data from 1906 to 1990. These data are checked by a quality control system (Mizuno and Watanabe, 1994). 9.5% of the data was rejected from the data set, and 123,646 temperature profiles became available.

We calculated the 20℃ isotherm depth in each station and distributed these depth data in every 1 ° ×1 ° latitude/longitude grid. And then, monthly mean 20℃ isotherm depth were calculated in a elliptic area (the minor axis is 2 ° in latitude and the major axis is 5 ° in longitude) around each grid, provided that the mean depth was rejected when the number of data in the

elliptic area was less than three.

2-4. Observations by Research vessel of Fisheries Agency

Hydrographic observations were conducted in the tropical Indian Ocean by using *Shoyo Maru* (Fisheries Agency research vessel; 1362 gloss ton) from November to December 1995. We conducted observations along the equator and 64° E to obtain zonal and meridional structures of the equatorial jet. At each CTD station, a CTD sensor (Sea Bird Instrument Co. model 911 plus) with Rosset sampler (12 Niskin bottle array) was lowered down to 3000m. Measured salinity and dissolved oxygen by CTD were corrected by comparing with the laboratory measurements of sampled sea water. Additionally, XCTD was dropped midway of the CTD stations in the ITF area. Currents were directly measured by Acoustic Doppler Current Profiler (ADCP; RD instrument Co.) during all steaming time. Although five minutes ensemble mean of 1 second pinging interval surface to 500m for every 16m bin were taken.

3. Results and Discussions

3-1. Surface temperature distribution and its variability

Semi-annual variability is dominant in the area from northeast coast of Africa to the coast of India, and also weaker semi-annual signal was found in the vicinity of Indonesia to Australia (Mizuno and Yukinawa, 1991).

Interannual variability of anomalous SST was analyzed by empirical orthogonal function (EOF) shown in Fig.2. It was revealed that the most important variability (1^{st} mode of EOF, 24% of total interannual RMS was explained) is highly correlated to ENSO signal temporally with 3 months time lag (Fig. 3). In this mode, the entire Indian Ocean anomalous SST changed simultaneously.

3-2. Distribution of upper layer thickness and its variability

Fig.4 showed maps of the monthly long-term mean of upper layer thickness (ULT : represented by 20℃ isotherm depth). Thin ULT, which corresponds to the ECC (Equatorial Counter Current) trough, exists zonally along approximately 7° S line in the west Indian Ocean. Northern and southern edge of this trough are ECC and SEC (South Equatorial Current), respectively. This trough has annual variability typically. Thickness of warm water increases from January (ULT=60m) to March (ULT=90m), and it grows stronger and spreads almost all over the trough in May. In July the trough spreads eastward but begins to get weaker in September. However, it grows stronger again in November.

Corresponding to a development of ITF, the strong temperature front is observed in the ITF area from May to November, especially in September with coastal upwelling along the south coast of Java to Timor. This front lies along 10° S from north of Australia (125° E) to approximately 90° E and extends to the front of SEC.

Semi-annual variability is observed west of Sumatra. ULT is approximately 110m in January to March, but it increases rapidly in May to over 140m. After it reduces to 110～120m in September, it increases again to over 130m. This variability is corresponded to the equatorial jet caused by west wind in May and November (inter-monsoon period) which transports warm water eastward and build up a warm pool west off Sumatra. Corresponding to the warm pool formation, the ECC trough grows stronger, which means that the upper layer water in ECC is cut off and becomes the origin of the warm pool.

ULT in Arabian Sea becomes thin along the coast of Somalia and Arabia Peninsula from July,

which indicates that a coastal upwelling occurs. In the offshore area (the center of the Arabian Sea) thick warm water is formed, and the strong temperature front exists between these cold and warm area. This condition is also found out in September, and remains in November. It is considered that this front is generated by the Somali jet. And it suggests that the onshore and offshore sides of the jet become divergence and convergence areas of the Ekman transport, respectively.

From the Andaman Sea to the coastal area east of Indo warm water exists in May and November, which is same period of the warm pool development. It suggests that warm water moves northward along the coast by the coastal Kelvin wave dynamics.

3-3. Wave phenomenon in the Indian Ocean

The ULT maps (Fig. 4) suggest the presence of short period wave like disturbances in the tropical circulation. In order to bring out the nature of these signals, time-longitude section of ULT anomaly (monthly−annual) along equator and 4°N are prepared in Fig. 5. Also, Mizuno *et al.* (1995) showed time-longitude sections of dynamic anomaly along equator and different latitudes.

At the equator the anomaly distribution depicts the eastward propagating waves in the pre-monsoon and post-monsoon periods. The first signal generated at the western coast in March is propagating to the east in a greater speed and reaches at the eastern coast by May to June. The next wave is originating in September and takes about the same time to arrive at the west.

Away from the equator along 4°N, very strong westward propagating biannual signals are observed. The first signal is initiating in the eastern side during May and it takes about three months time to reach the west. The next signal is originating in November. The signals are also observed in 4°S, but much stronger in the Northern Hemisphere compared to the Southern Hemisphere (Mizuno *et al.*, 1995).

The phase speed of the wave propagation is determined from the figures by estimating the slant of wave pattern. The Kelvin wave at the equator propagates at greater speed of about 1 m/s. The Rossby wave speed at 4 degrees latitude is about 0.4 m/s and the speed is decreasing as the latitude increases. The phase speed of annual Rossby wave obtained is less than 0.2 m/s along 12°S (time-longitude section of dynamic anomaly). The phase speed of the wave propagation determined from the figures are to be consistent with the earlier estimations.

Reverdin and Luyten (1986) examined near equatorial meanders beginning in August - September and westward propagation of 40±15 cm/s. Chang and Philander (1989) analyzed the effect of mean currents with weak latitudinal shear on Rossby wave. They found that the presence of the baroclinic mean currents can modify the characteristics of wave propagation significantly, and a westward current can cause the speed of the long Rossby waves to decrease with decreasing latitude.

3-4. Observation of the Equatorial jet

Along the route of *Shoyo Maru* in November of 1995, westerly winds were predominant especially in the eastern part with the speed of over 10m/s which is much larger than COADS climatology for November.

Surface currents on the equator were strong eastward flow greater than 2-3 knots (Fig. 6 upper panel). The current was strong in the central part but was small in both ends. In the eastern part directions of the current vector fluctuated, indicating eddies on the equator.

The thermal field along the equator (Fig. 6 lower panel) shows surface thermostad is deeper in the eastern part than the west. Thermocline is also deeper in the east. But in the central part,

downstream of Maldives islands (73 ° E), the thermocline clearly undulated. It shows the current structure is well affected by bottom topography.

Vertical sections across the equator (along 64 ° E : Fig. 7 upper panel) shows that thermostad (28℃) is in the vicinity of the equator. Isobaric height is also estimated (Fig. 7 middle panel) in the same manner as the previous one. Sea surface (0db) shows small peak at the equator. The down slopes to both sides of the equator generate meridional pressure gradient which balances the equatorial jet as geostrophic flow. This small pressure gradient can generate fast current (the equatorial jet) because of small Colioli's parameter near the equator.

The vertical section (Fig. 7 lower panel) shows the cross stream structure of the jet clearly. This flow is confined to upper 100m or less. Northern limit of the jet is 2 ° N, but the southern one is not clear because it is joined to ECC. Judging from high speed core the southern limit of the jet is 2-3 ° S. Mass transport of this jet is calculated to be 20Sv.

The jet is confined to shallow depths, and the width is estimated to be approximately 400km (2 ° S-2 ° N). Eastward mass transport is large (comparable to the Kuroshio). On the other hand, the zonal temperature difference is so faint, that the zonal heat transport may be small. However, the jet is a duct which transports warm water to the east twice a year (May-June, October-November). It generates thick warm pool off Sumatra. The warm water has also dynamical impacts to wide areas (Yamagata *et al.*, 1996). The results obtained here will be useful to verify ocean models which reproduces the equatorial jet.

3-5. Relation between ENSO and the Indonesian throughflow

Fig. 8 upper panel shows bimonthly normalized 100m temperature (T100) anomaly along 115 ° E and SOI. In the El Nino periods in 1972-73, 1976-77 and 1982-83 not only SOI but also T100 anomaly is negative with a time lag of a few months. Fig. 8 lower panel shows lag-correlation between T100 anomaly and SOI. SOI leads T100 anomaly by 3～4 months (lag-2× bimonthly), indicating negative/positive anomalies in the Pacific Ocean in El Nino/La Nina periods propagate to the area by the perturbation in ITF, probably coastal Kelvin wave in the Indonesian archipelago and Rossby wave after it enters the Indian Ocean. Instead of this variability in T100 anomaly, the SST variability (1^{st} mode of EOF), which changes the entire Indian Ocean simultaneously, indicated positive/negative anomalies in El Nino/La Nina periods with 3 months time lag (Fig. 3). This anti-phase between T100 and SST to SOI is interest in the relation between the variability of the Indian Ocean and ENSO cycle, which suggests that important roles for heat budget are not only atmospheric variability but also water transport, which we have to investigate in future studies.

5. References

1) K. Mizuno and T. Watanabe; JEXAM annual report (FY1993), pp15-24, 1994.
2) K. Mizuno and T. Watanabe; JEXAM annual report (FY1995), pp45-54, 1996.
3) K. Mizuno, B. Peter and T. Watanabe; JEXAM annual report (FY1994), pp12-22, 1995.
4) K. Mizuno and M. Yukinawa; JEXAM annual report (FY1990), pp15-44, 1991.
5) G. Reverdin and J. Luyten; J. Phys. Oceanog. **16**, pp1088-1100, 1986.
6) R. W. Reynolds; NOAA Tech. Rep. NWS., **31**, 35pp, 1982.
7) T. Yamagata, K. Mizuno and Y. Masumoto; J.G.R, **101**(C5), 12465-12473, 1996.

6. Publications

① Publications to a scientific society

1) International (4 papers)

K. Mizuno, T. Watanabe; Preliminary results of in-situ XCTD/CTD comparison test. Journal of Oceanography, 54(4), pp373-380, 1998.

T. Yamagata, K. Mizuno and Y. Masumoto; Seasonal variations in the equatorial Indian Ocean and their impact on the Lombok throughflow. J. G. R., 101(C5), pp12465-12473, 1996.

K. Mizuno; Variability of thermal and velocity field in the vicinity of North Australian Basin with Regard to the Indonesian Throughflow. Proceeding of international workshop on the Trhoughflow studies in and around Indonesia Waters. BPPT, 363-379. (1995)

P. Benny and K. Mizuno; Annual cycles of steric height in the Indian Ocean estimated from the thermal field. Deep-Sea Res, submitted.

② Other publications

1) In Japan (5 papers)

K. Mizuno and T. Watanabe; Seasonal vertical temperature profile in the Indian Ocean. Bull. National Res. Inst. Far Seas. Fish S-series 22, 102pp.1991.

NRIFSF, MSA and MA; Surface Currents and upper ocean thermal structure in the Indian ocean. JEXAM Atlas. STA, 55pp. (1994)

水野恵介；大洋規模の海況解析と最適内挿法，海の研究，4,(3),pp187-208, 1995.

水野恵介，渡邊朝生，岡崎誠; XCTD の開発とその利用，月刊海洋，号外 9，204-209, 1996.

水野恵介；季節変動から 10 年規模の大気・海洋変動に関する今後の研究課題 －第 2 章モンスーンと海洋変動，海洋熱循環研究会，12-21, 1996.

2) International (3 papers)

S. Godfrey *et al.*; The role of the Indian Ocean in the global climate system, Recommendations regarding the global ocean observing system, OOSDP background paper No.6, 89pp, 1995.

T. Watanabe; Interannual variation of upper ocean in the western North Pacific and its relationship to East Asian wintertime monsoon, Proceedings of the international workshop on the climate system of monsoon Asia, pp288-290, 1996.

K. Mizuno; Observation of the Indian Ocean — Equatorial Jet —. Proceedings of international workshop on ocean climate variations from seasons to decades with special emphasis on Pacific Ocean buoy network, pp149-156, 1996.

7. International Cooperation

None

要旨

水産関係の官庁船や漁船に表層水温観測を依頼し、インド洋の国際的な広域海洋観測網の確立に貢献した。また、表層塩分資料収集のため XCTD を実用化した。

上記で選られた資料と既往資料を併せたデータベースを作成して表層水温の変動特性を調べた。表面水温は、ほぼ全域が ENSO と同位相で変化する経年変動パターンが卓越することを見出した。表層暖水の厚みの変化は特に東部インド洋で ENSO の影響が顕著であった。

表層水温の季節変動は赤道ジェットとその反射による変動が特に熱帯海域で卓越し、その影響は広い範囲にわたることを見出した。さらに、調査船により赤道ジェットの詳細な構造や流量を把握した。

インド洋の熱収支に重要と思われる太平洋からの海水の流入を漁具の漂移の資料から調べ、表層の流量の季節変化（7・8月に最大；15SV）と ENSO との逆位相の経年変化傾向を明らかにした。

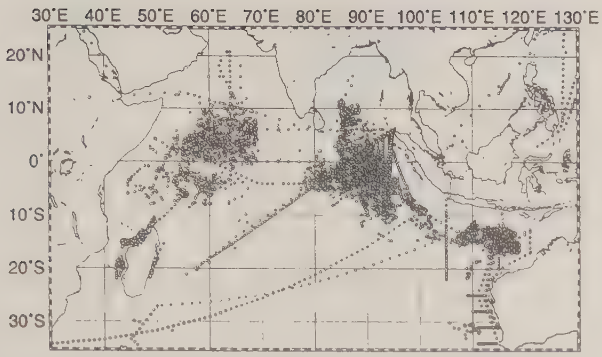


Fig. 1. Station plot in the Indian Ocean observed by research vessels and voluntary observation ships under the supervision of the Fisheries Agency (4,870 stations during 1989-1998).

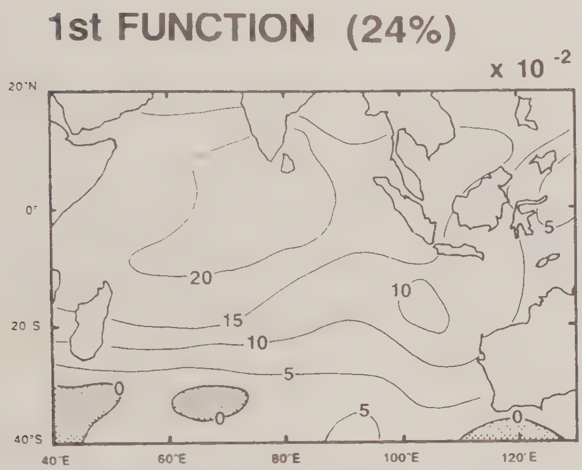


Fig. 2. EOF (empirical orthogonal function) of anomalous sea surface temperature in the Indian Ocean using COADS data during 1970 – 1984.

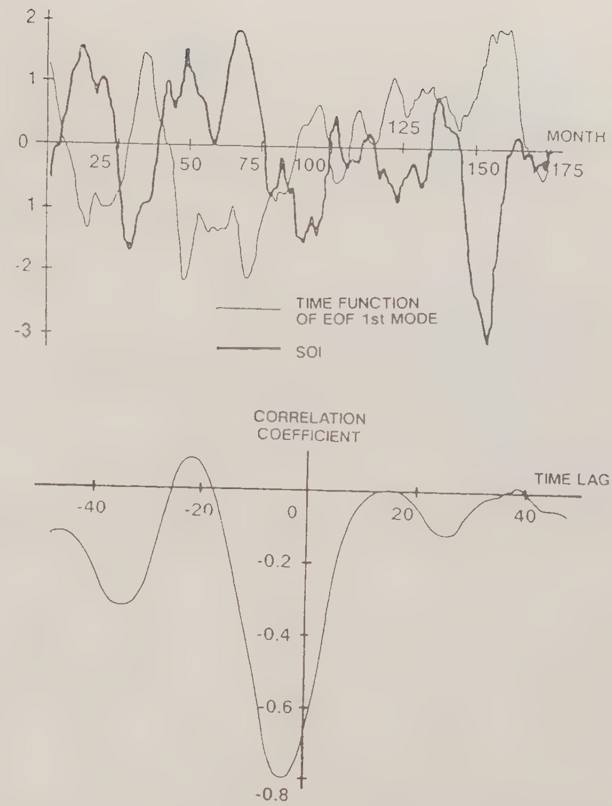


Fig. 3. Upper panel: Southern Oscillation Index (SOI: thick line) and normalized amplitude function of the 1st mode of EOF (thin line). Both time series are smoothed by 5-month running mean.

Lower panel: Lagged correlation function between the two.

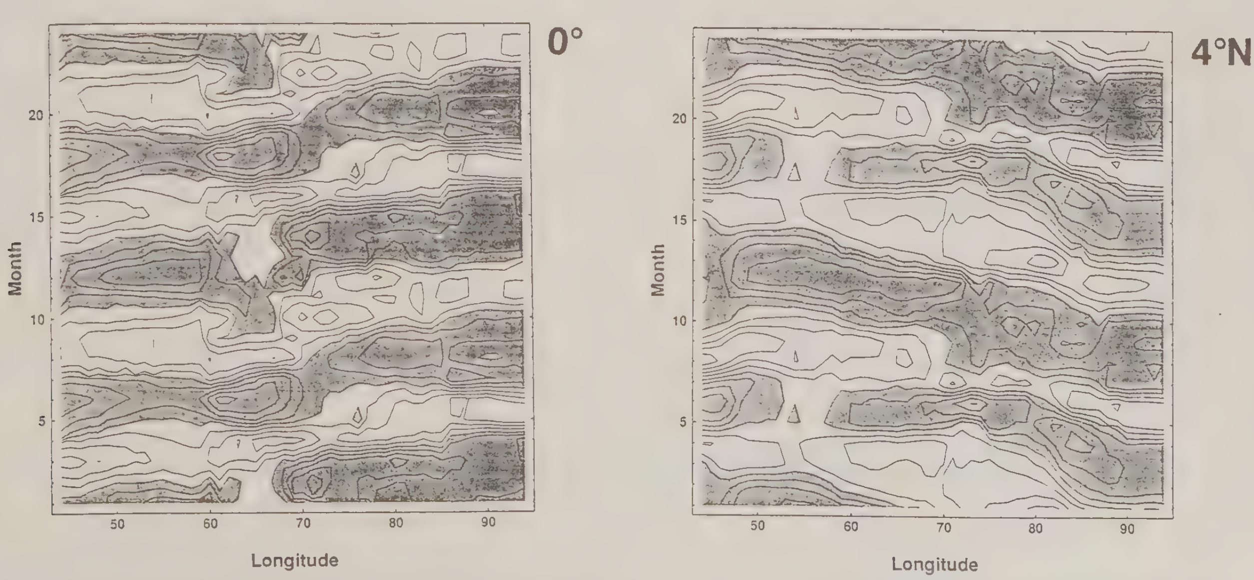


Fig. 5. Time-longitude section of 20℃ isotherm depth anomaly from the climatological mean value at equator (left) and 4°N (right). Contour interval is 10 cm. Negative anomalies are shaded.

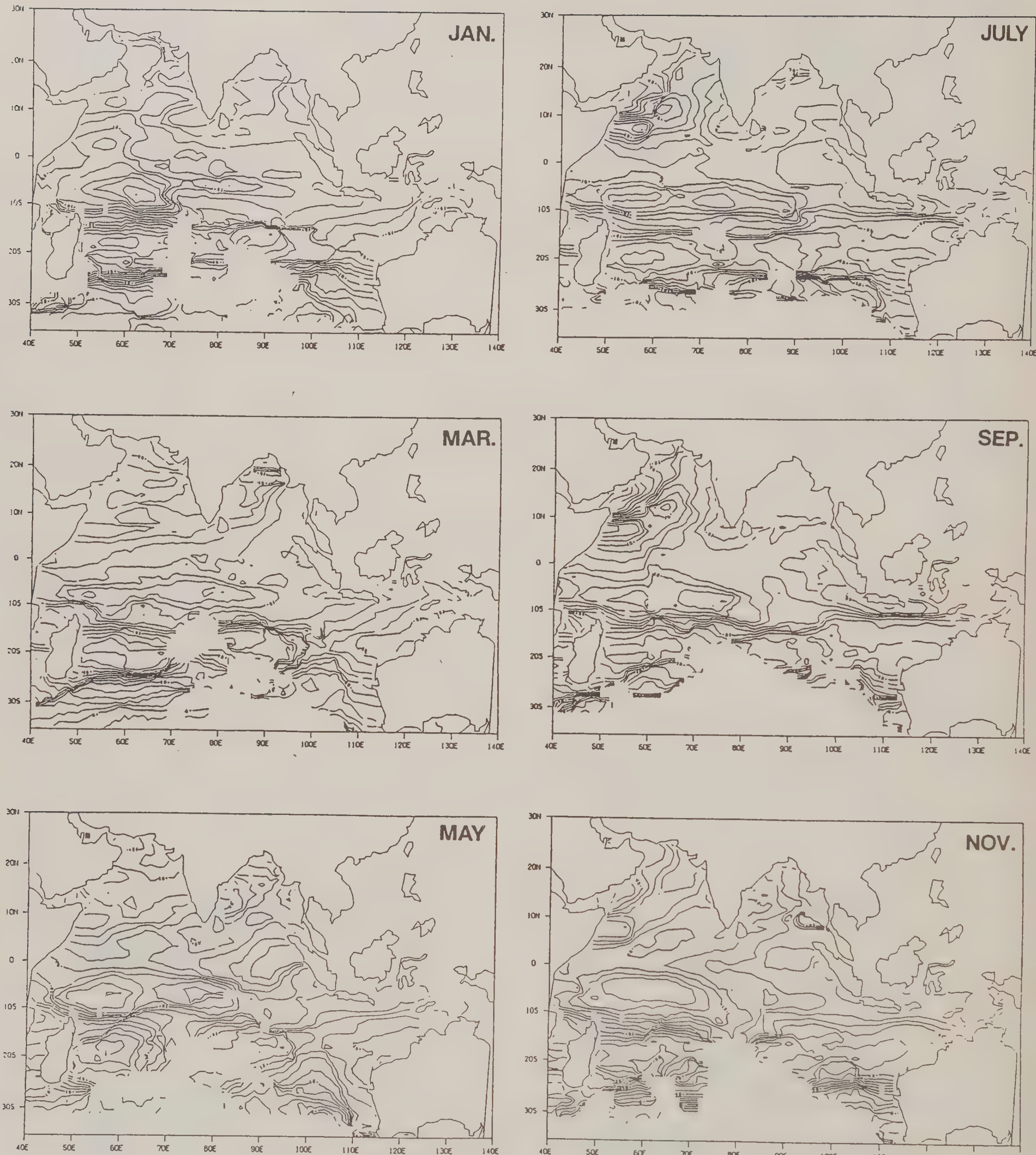


Fig. 4. Monthly long-term mean of upper layer thickness (20℃ isotherm depth).

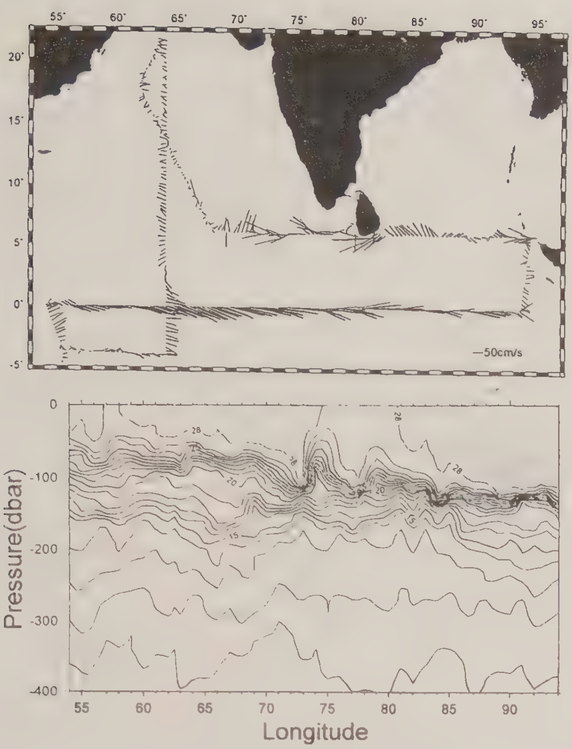


Fig. 6. Upper panel: Surface layer current vector measured by ADCP. Actual depth is 20-36m which is the first bin of ADCP measurement.

Lower panel: Vertical temperature section along the equator. Warm water higher than 28℃ is shaded.

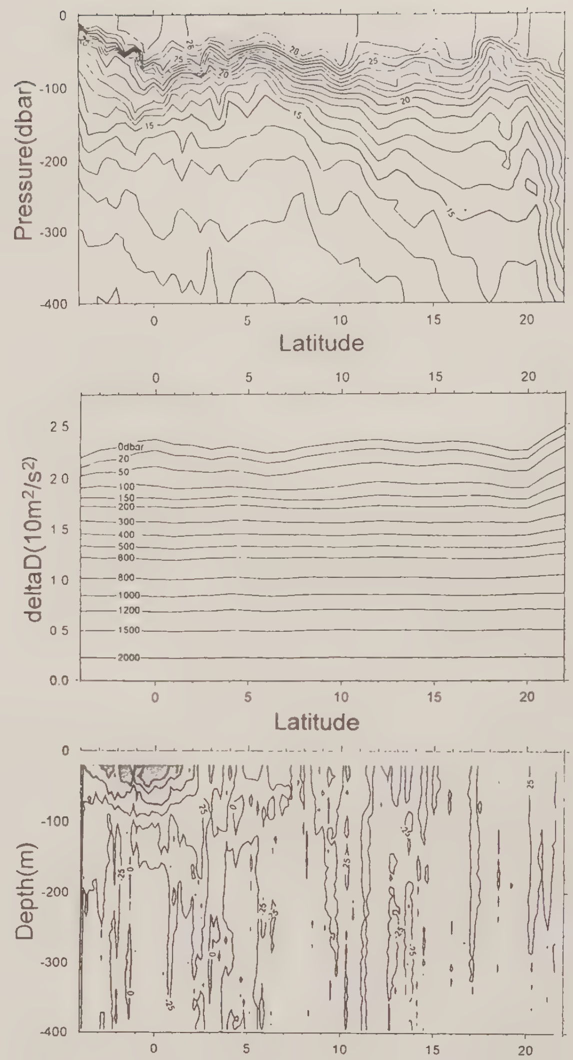


Fig. 7. Upper panel: Vertical temperature section along the equator. Warm water higher than 28℃ is shaded.

Middle panel: Anomaly of dynamic depth of isobaric surface (reference level is 2500db).

Lower panel: Vertical section of zonal component of ocean current. Positive (eastward) values are shaded. Contour interval is 25cm/s.

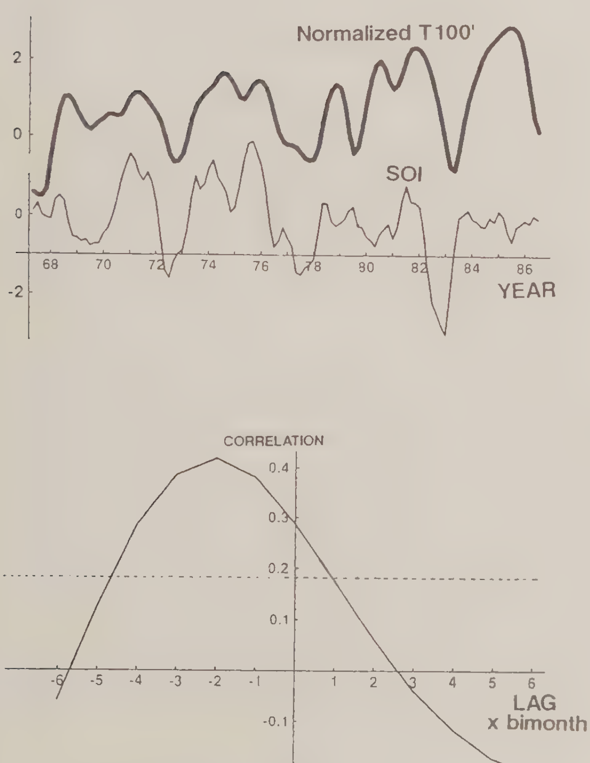


Fig. 8. Upper panel: Bimonthly normalized 100m temperature anomaly along 115° E (thick line) and SOI (thin line).

Lower panel: Lag-correlation between the two. Negative lag denotes SOI leads the anomalous of 100m temperature. The horizontal dashed line indicates 95% confidence limit.

Ⅰ. 大気・海洋・陸域間相互作用の諸過程に関する観測・解析研究

Observation and analysis on the process of the atmosphere-ocean-land interactions

2. 海洋における諸過程に関する観測・解析研究

Observation and analysis on the process over the ocean

(1) 表層水温に関する観測研究

Observation on Subsurface Temperature by Voluntary Ships

気象庁 気候・海洋気象部

佐伯 理郎、網野 正明、吉田 隆、安藤 正、野崎 太、
森 真理子、石川 孝一、三河 哲也、水野 孝則、
吉川 郁夫、石川 一郎、麻生 正、二階堂義信

Climate and Marine Department,
Japan Meteorological Agency

Masaro Saiki, Masaaki Amino, Takashi Yoshida, Tadashi Ando, Futoshi Nozaki,
Mairiko Mori, Koichi Ishikawa, Tetsuya Mikawa, Takanori Mizuno,
Ikuo Yoshikawa, Ichiro Ishikawa, Tadashi Asoh and Yoshinobu Nikaidou

(Abstract)

We have conducted observations on subsurface temperature in the Indian Ocean by voluntary observing ships ("Kashimasan-Maru" and "Delmas Tourville") for ten years since 1989 and obtained more than 3800 subsurface observations along their cruise tracks ("Kashimasan-Maru: from the Strait of Malacca to the Persian Gulf, "Delmas Tourville: from the Strait of Malacca to the Cape of Good Hope).

In the first half of this study (1989 to 1994), we directly analyzed space-time variations of subsurface temperature in the sections of the Indian Ocean along the cruise tracks and found conspicuous differences in structure of subsurface temperature over the Arabian Sea and the Bay of Bengal between the Northeast Monsoon season and the Southwest Monsoon season. We also discovered significant vertical temperature inversions in the subsurface water around the northwestern Arabian Sean and the Gulf of Oman. Judging from their static stability and the frequency distribution of the inversions calculated from historical records of subsurface temperature over the Arabian Sea, we inferred that warm and saline waters originated in the Persian Gulf drained out with sinking in the Arabian Sea.

In the beginning of 1995, Japan Meteorological Agency commenced the operational use of the Ocean Data Assimilation System, which produced spatially uniform and physically consistent data in the subsurface to assimilate subsurface temperature data observed by ships. In the latter half of this study (1995 to 1998), we mainly analyzed the assimilated data and studied seasonal and interannual variations of the subsurface temperature over the Indian Ocean with focusing on the relationship to El Niño-Southern Oscillation.

As for the seasonal variation of subsurface temperature in the equatorial Indian Ocean, the assimilated data clearly showed the east-west difference that the annual variation was dominant in the eastern Indian Ocean while the semiannual variation in the western Indian Ocean. On the other hand, the interannual variation of subsurface temperature in the Indian Ocean was examined by performing the empirical orthogonal function analysis of the ocean heat content anomaly over the Indian Ocean. The first mode of the empirical orthogonal function, which showed an east-west dipole pattern in the Indian Ocean, had significant correlation to Monsoon low-level wind and El Niño phenomena.

A strong El Niño event occurred in boreal spring 1997 and ceased in boreal summer 1998. The El Niño event had great impacts on the subsurface in the equatorial Indian Ocean through the wind stress above there. In the mature phase of the El Niño event from the end of 1997 to the beginning of 1998, the

thermocline in the equatorial Indian Ocean slanted to the reverse direction of normal. The sea surface temperature in the equatorial Indian Ocean was 0.5°C to 1.5°C higher than normal during the first half of 1998. Examining the ocean assimilation data in the Indian Ocean, we found that the phenomenon was caused by the passage of warm Kelvin waves in the equatorial Indian Ocean, which had been generated by the wind stress anomaly over the Indian Ocean due to the El Niño event like the delayed action oscillator theory.

1. Objectives

The Asian Monsoon over the Indian Ocean and the seas around Southeast Asia is considered to be related to El Niño-Southern Oscillation (ENSO) events which affect the global climate, through the interaction between the ocean and the atmosphere in the Indonesian region (Barnett 1983, Nicholls 1984). Recently, further understanding of the physical structure of the ocean in these regions, and clearer elucidation of the relation between the Asian Monsoon and ENSO have been required. However, the oceanographic data in these regions are too sparse to fully understand the physical structure of the ocean.

In this study, Japan Meteorological Agency (JMA) has conducted the subsurface temperature observation with expendable bathythermograph (XBT) in the Indian Ocean where oceanographic data are too poor, by voluntary observing ships (VOS), a crude oil tanker "Kashimasan-Maru" cruising between Japan and the Persian Gulf since October 1990 and a cargo carrier "Delmas Tourville" between Japan and the Cape of Good Hope for five years since 1990 (Fig.1). The subsurface temperature data observed by the ships have been distributed to national meteorological/oceanographical services throughout the world via the Global Telecommunication System (GTS) of the World Meteorological Organization (WMO). XBT data collected via GTS including those from the ships were used to investigate annual variation of subsurface waters in this region.

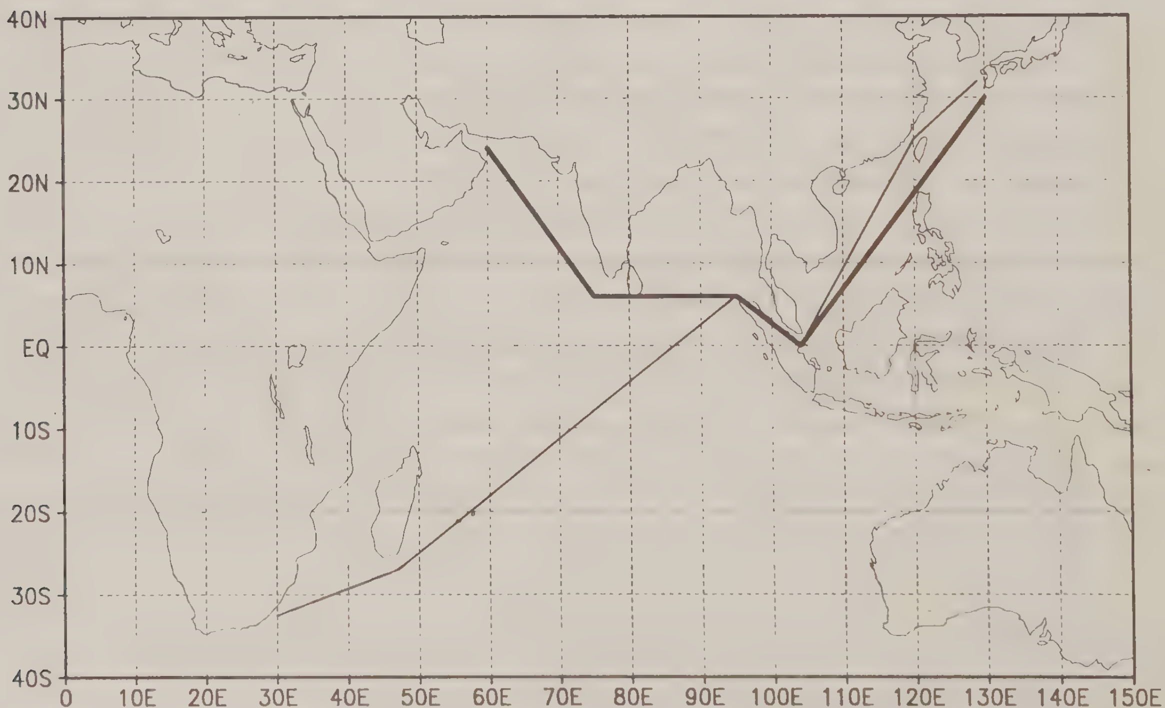


図1 委託商船の航路。太線は「鹿島山丸」、細線は「Delmas Tourville」
Fig.1 Cruise tracks of "Kashimasan-Maru" (thick line) and "Delmas Tourville" (thin line)

2. Methods

In the first half of this study (1989 to 1994), subsurface temperatures in the Indian Ocean and the South China Sea were observed by "Kashimasan-Maru" and "Delmas Tourville (renamed from "C. R. Point-Noire" in May 1991) under cooperation between JMA and Office de Recherche Scientifique et Technique d'Outre-Mer (ORSTM) in France. During this period, we obtained 1181 subsurface observations by "Kashimasan-Maru" which made 50-day round trips between Japan and the Persian Gulf and 490 subsurface observations by "Delmas Tourville" which made 4-month round trips between Japan and the Cape of Good Hope. The subsurface temperature data were used for analyzing seasonal and annual variations of subsurface waters in the Indian Ocean along the cruise tracks with historical temperature and salinity data in the Arabian Sea and its adjacent seas since 1940.

Although the spatial density of the subsurface temperature observations is rather high along the regular sea routes, observations over the other regions in the Indian Ocean are very sparsely distributed both in time and space. Thus, it is very difficult to understand the time-serial three-dimensional structure of the ocean only from the observed data. In order to overcome the difficulty, JMA had developed the Ocean Data Assimilation System (ODAS) (Kimoto et al. 1997) and commenced its operational use at the beginning of 1995 to assimilate subsurface temperature data collected via GTS including XBT data observed by "Kashimasan-Maru" and "Delmas Tourville". As the ODAS enabled us to get spatially uniform and physically consistent data (temperature and current) in the subsurface on every pentad since April 1986, we studied three-dimensional features of seasonal and annual variations in the subsurface of the Indian Ocean in parallel with the former analyses of subsurface waters along the cruise tracks during the latter half of this study (1995 to 1999). In the spring of 1997, an El Niño phenomenon occurred and it developed as much as the El Niño event in 1982/83. Therefore, we analyzed changes of the subsurface temperature in the Indian Ocean since 1997 by making use of the ODAS data to clarify impacts of the El Niño phenomenon on the Indian Ocean.

3. Results

(1) Observations of subsurface temperature by the voluntary observing ships and observed profiles of subsurface temperature in the Indian Ocean along their cruise tracks

Subsurface temperature observations with XBT have been performed six hourly (at intervals of 200km) by the voluntary observing ships ("Kashimasan-Maru" and "Delmas Tourville") along their cruise tracks (Fig.1). As "Kashimasan-Maru" usually made seven round trips in a year, we obtained fourteen sections of subsurface temperature every year. The total number of its observations amounted to 3,396 by March 1999, including its intensive observations between the Strait of Malacca and Sri Lanka since 1995. On the other hand, "Delmas Tourville" made 490 observations though its observations were finished on April 1994. These observations, which offered most of the subsurface temperature data over the Indian Ocean, greatly contributed to elucidation of the structures in the subsurface waters over the Indian Ocean by distributing the observed data to meteorological centers, oceanographic centers and scientific communities in the world.

Fig.2 and Fig.3 show vertical sections of the subsurface temperature along the cruise tracks of "Delmas Tourville" and "Kashimasan-Maru", respectively. In Fig.2, we can see seasonal variations of surface warm water more than 28°C in the tropical Indian Ocean that it expanded southward during the Northeast Monsoon season and vice versa (the cruise track of "Delmas Tourville" crosses the equator from the northeast to the southwest). In Fig.3a, we can find an anticyclonic circulation in the Arabian Sea and the thermocline steeply slanted to the east in the sea south of the Bay of Bengal during the Southwest Monsoon season. On the contrary, the anticyclonic circulation disappeared and the thermocline became level during the Northeast Monsoon season (Fig.3b).

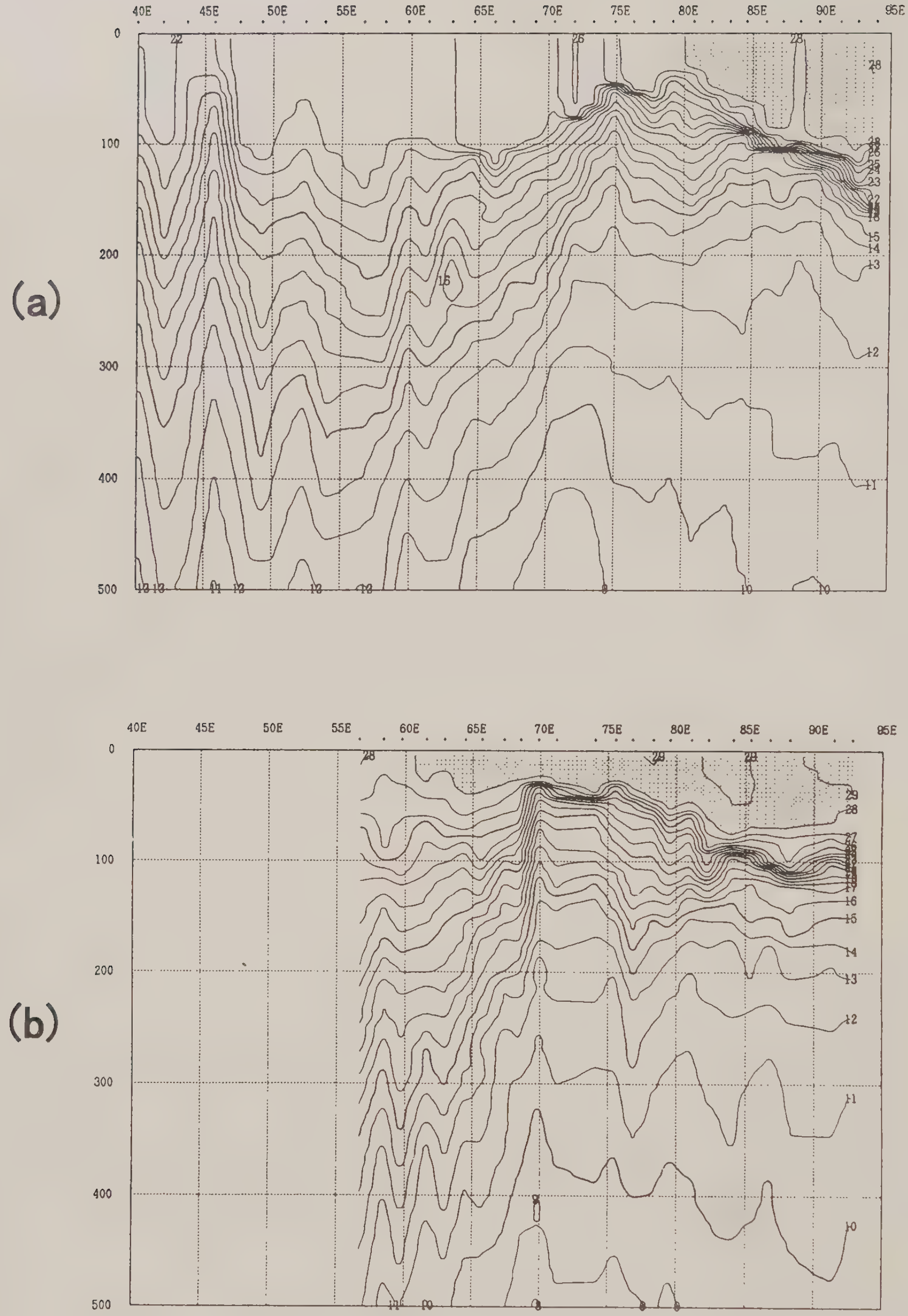
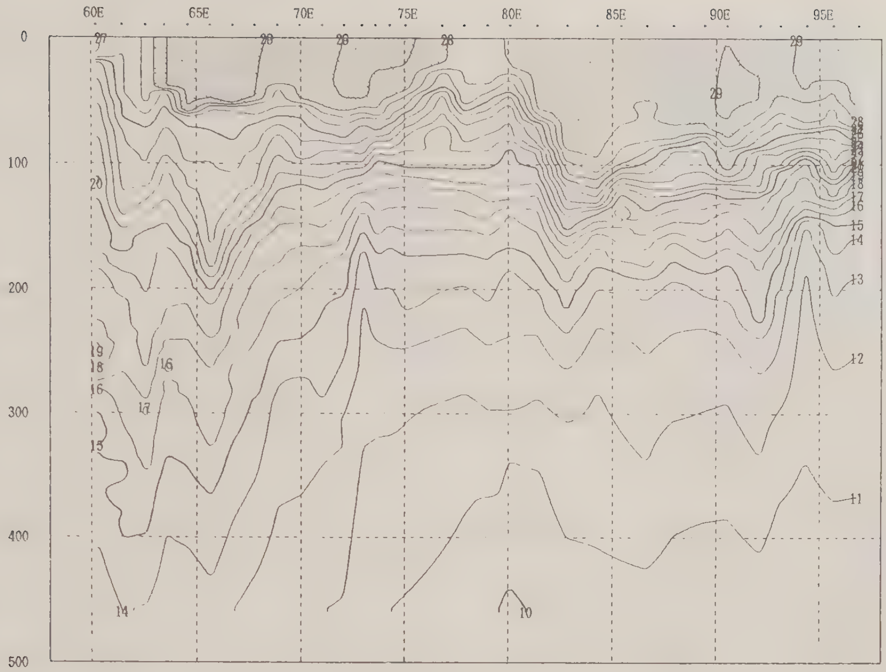


図2.「Delmas Tourville」の航路に沿った表層水温断面図
横軸は経度、縦軸は深度、等値線の間隔は1℃、陰影部は28℃以上の領域。
(a) 1990 年 8 月、(b) 1991 年 2 月
Fig.2 Vertical sections of subsurface temperature along the cruise track of “Delmas Tourville”
The abscissa and the ordinate are longitude and depth, respectively. The contour interval is 1°C. Regions more than 28°C are shaded. (a) August 1990, (b) February 1991

(a)



(b)

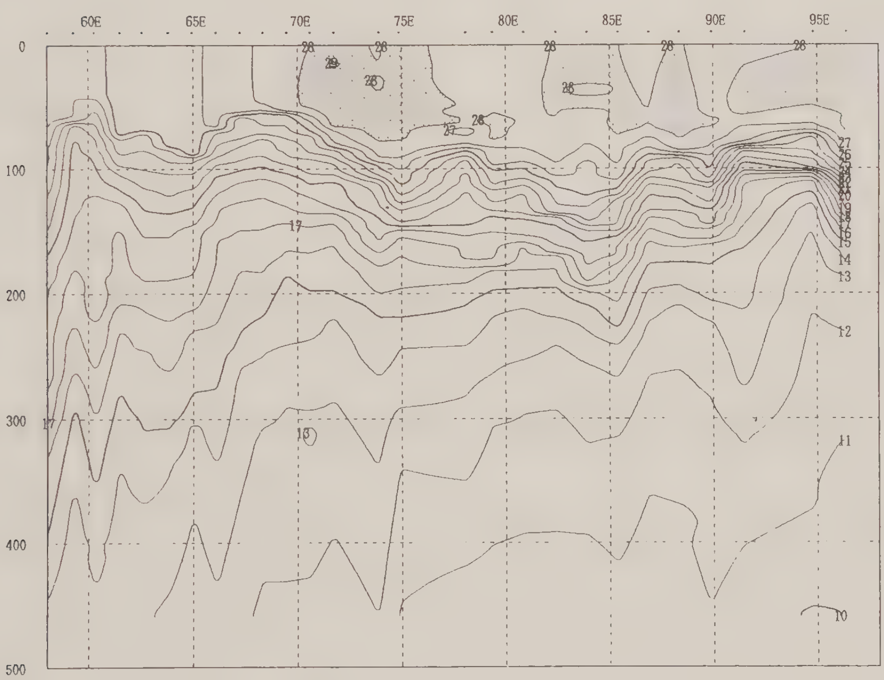


図3.「鹿島山丸」の航路に沿った表層水温断面図
横軸は経度、縦軸は深度、等値線の間隔は1℃、陰影部は28℃以上の領域。
(a) 1996年7月、(b) 1996年1月
Fig.3 Vertical sections of subsurface temperature along the cruise track of "Kashimasan-Maru"
The abscissa and the ordinate are longitude and depth, respectively. The contour interval is 1°C. Regions more than 28°C are shaded. (a) July 1996, (b) January 1996

(2) *Warm and saline waters draining from the Persian Gulf into the Arabian Sea*

We found significant vertical temperature inversions (>=1°C) in the subsurface water at depths of 150m to 400m around the northwestern Arabian Sea and the Gulf of Oman in more than ten cases of the 1181 subsurface temperature data observed by "Kashimasan Maru" from October 1990 to April 1994 (Fig.4). We thought that the inversions corresponded to warm and saline waters which originated in the Persian Gulf and drained through the Gulf of Oman into the Arabian Sea, judging from the facts that they were stably stratified and salinity inversions were found in the historical temperature data over the Arabian Sea and its adjacent seas (Ando, 1992). We also found the tendency that the inversions in the gulfs became deeper toward the Arabian Sea, therefore, we thought the warm and saline waters to drain out with sinking in the Arabian Sea. Fig.5 shows the frequency distribution of the temperature inversions over the Arabian Sea and its adjacent seas based on the historical temperature data and observations of "Kashimasan Maru" (the total number of data : 61,564). As the high frequencies are distributed from the Persian Gulf to the Gulf of Oman and from the Red Sea to the Gulf of Aden, we guessed that the warm and saline waters originated in the Persian Gulf and the Red Sea diffused southwestward along the Arabian Peninsula and Somalia and southeastward along the west coast of India.

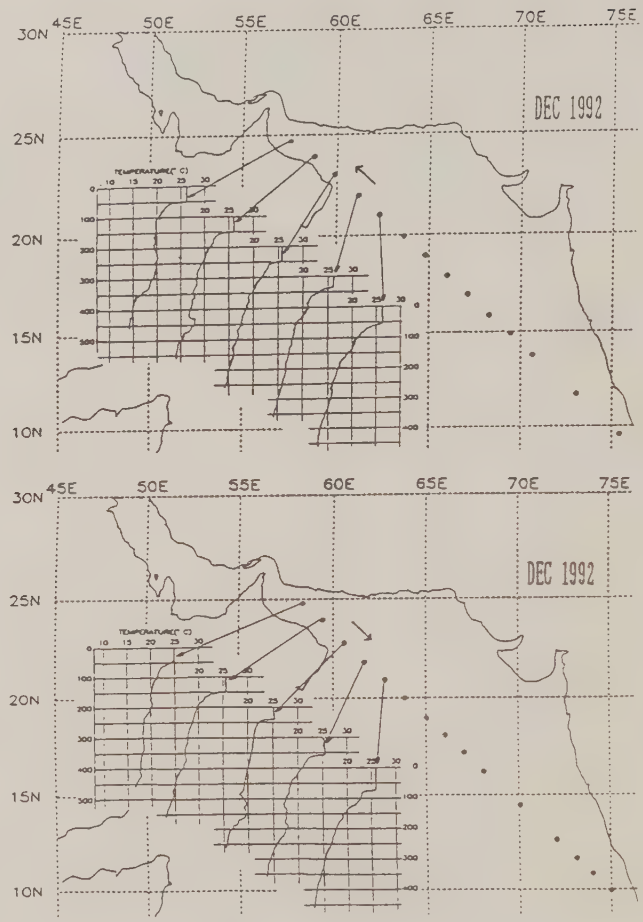


図4.「鹿島山丸」によってオマーン湾沖で観測された水温逆転
（1992 年 12 月）

Fig.4 Vertical temperature inversions observed by "Kashimasan-Maru" off the Gulf of Oman

(3) Analyses of subsurface temperature in the Indian Ocean by means of the ocean data assimilation system (ODAS)

(3-1) Seasonal variations of subsurface temperature

Fig.6 shows a time-longitude section of the normal depth of 20°C isotherm (D20) along the equator in the Indian Ocean, and Fig.7 the monthly mean normal depths of 20°C over the Indian Ocean. The normal values were calculated by averaging D20 for 8 or 9 years (Fig.6 : 1987-1994, Fig.7 : 1987-1995), so these figures display seasonal variations of the climatological D20 in the Indian Ocean.

In Fig.6 we can find conspicuous differences in the seasonal variations of D20 between the eastern Indian Ocean and the western Indian Ocean along the equator. D20 in the eastern Indian Ocean east of 80°E varies with great amplitude. It becomes more than 140m at its maximum in June when the Northeast Monsoon shifts to the Southwest Monsoon. It also becomes more than 120m at its second maximum in October/November when the Southwest Monsoon shifts to the Northeast Monsoon. These phenomena are due to accumulation of surface warm waters driven by strong eastward jet flow along the equator appearing in the transition periods of Monsoons (Wyrtki, 1973). On the other hand, it becomes less than 90m at its minimum in February/March during the Northeast Monsoon period, when D20 in the equatorial Indian Ocean increases westward along the equator. The local minimum of D20 in the equatorial eastern Indian Ocean can be also found in September during the Southwest Monsoon season.

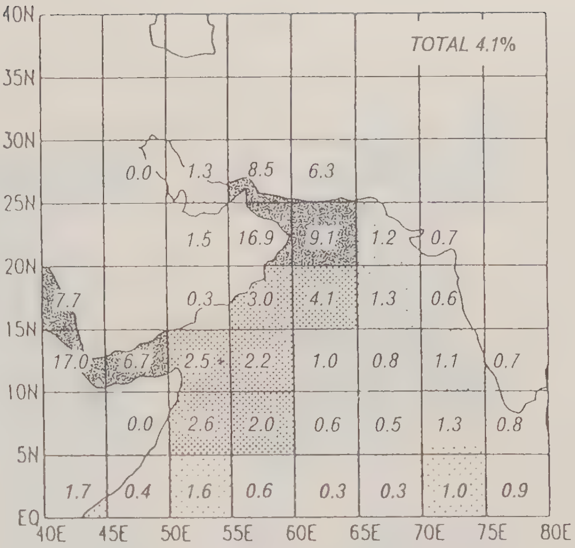


図5. 水温逆転構造を持つ水温観測データの頻度分布
Fig.5 Frequency distribution of observed vertical temperature inversions

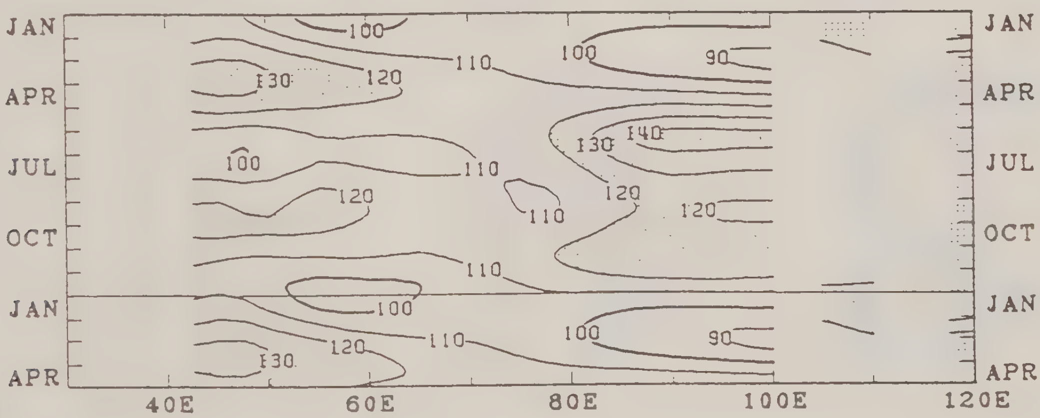


図6. インド洋の赤道に沿った20℃深度平年値時間－経度断面図
等値線の間隔は10m、平年値は1987～1994年の8年間の平均値
Fig.6 A time-longitude section of the normal depth of 20°C isotherm along the equator in the Indian Ocean
The contour interval is 10m. The normal is the averaged depth for 8 years since 1987.

D20 in the western Indian Ocean shows clear semiannual variations in contrast with that in the eastern Indian Ocean. The semiannual variations also can be found in sea surface temperature (SST) along the equatorial Indian Ocean west of 60°E, but it lags by one or two months behind D20. On the contrary, there are no semiannual variations in surface wind over the same region.

In Fig.7 we can find clear differences of the seasonal variations of D20 between the southern part of the Indian Ocean and the other part. The seasonal variation signal is week in the southern part of the Indian Ocean. D20 is more than 150m from Madagascar to Australia between 15°S and 25°S, while it is less than 100m between 5°S and 10°S throughout the year. On the other hand, D20 shows strong seasonal variations



図7. インド洋における20℃深度の月別平年値
等値線の間隔は10m。平年値は1987～1995年の9年間の平均値
Fig.7 Normals of monthly mean depth of 20°C isotherm depth in the Indian Ocean
The contour interval is 10m. The normal is the averaged depth for 9 years since 1987.

over the Indian Ocean around the equator and in the Northern Hemisphere.

(3-2) Interannual variations of subsurface temperature in the Indian Ocean

We performed the empirical orthogonal function (EOF) analyses of the ocean heat content (OHC) anomaly from ODAS to investigate interannual variations of the subsurface thermal structure in the Indian Ocean. The domain for the EOF analyses is between 20°N and 20°S, from 40°E to 120°E with 2.5°×2.5° grids in longitude and latitude. The period for the analyses is ten years from 1987 to 1996.

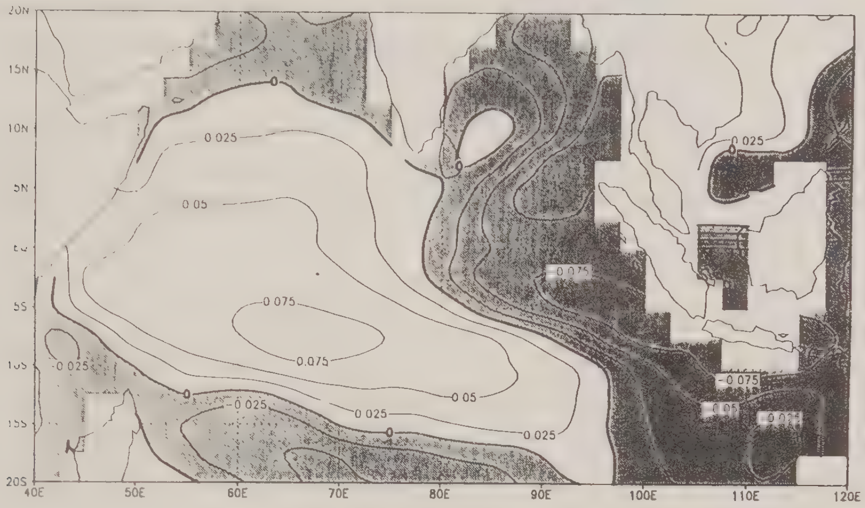


図8. 海洋データ同化システム(ODAS)による OHC 平年偏差の EOF 第1モードのパターン
解析期間は1987～1996年の 10 年間。陰影部は負の領域をあらわす。
Fig.8 The spatial pattern of the first EOF mode for OHC anomaly derived from ODAS
The period for analysis is 10 years from 1987 to 1996. Negative regions are shaded.

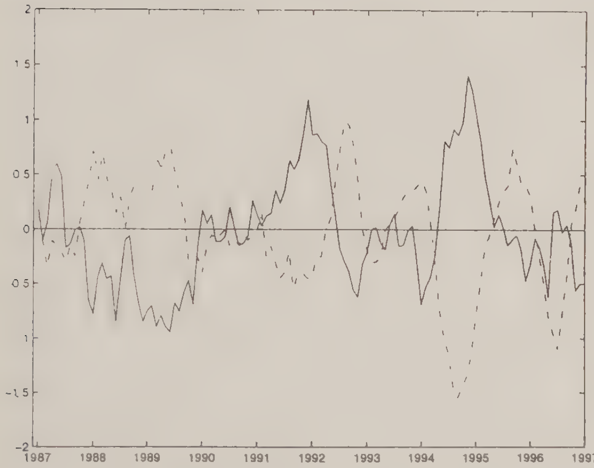


図9. OHC 平年偏差 EOF 第1モード(実線)とモンスーン風指数(一点鎖線)の時系列
Fig.9 Time sequences of the first EOF mode of OHC anomaly (solid line) and the Monsoon wind index (dot-and-dash line)

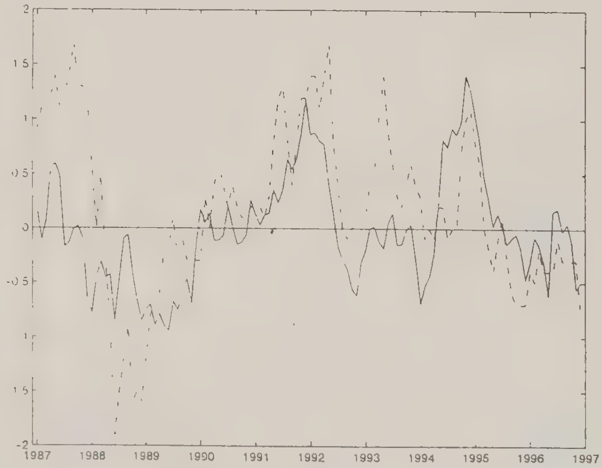


図 10. OHC 平年偏差 EOF 第1モード(実線)と B 海域海面水温偏差(破線)の時系列
Fig.10 Time sequences of the first EOF mode of OHC anomaly (solid line) and the monthly mean SST anomaly for Region B (dashed line)

The spatial pattern of the first EOF mode is shown in Fig.8. The spatial pattern displays a positive load around 5°S to 10°S in the western equatorial Indian Ocean and a negative load off Sumatra Island in the

equatorial Indian Ocean, explaining 17.6% of the total variance. In order to make clear the relationship between the first EOF mode and Monsoon wind strength, we show in Fig.9 the time sequences of the EOF score and Monsoon wind index, which is defined as the monthly mean zonal component of wind stress anomalies averaged over the central equatorial Indian Ocean (between 5°N and 5°S from 70°E to 90°E). We can find high negative correlation (-0.77) between the EOF score and the Monsoon wind index with 2-month lag of the former behind the latter. This fact implies that the OHC over the Indian Ocean is considerably affected by the Asian Monsoon wind. Fig.10 shows the time sequences of the EOF score and monthly mean SST anomaly for Region B (between 4°N and 4°S from 150°W to 90°W; almost the same as NINO.3), which is used as an index of ENSO signals. The two quantities vary in phase and the simultaneous correlation between them is significant (0.56). This suggests the close connection between the subsurface thermal structure in the Indian Ocean and ENSO.

In the spatial pattern of the second EOF mode, there are a negative load around 10°S, 60°E and a positive load around 10°N in the western tropical Indian Ocean. The similarity of the pattern to the annual mean D20 in the western Indian Ocean suggests the relationship between the second EOF and the Southern Equatorial Current in the Indian Ocean.

(4) Impacts of the 1997/98 El Niño event on the subsurface temperature in the Indian Ocean

SST anomalies over the eastern equatorial Pacific rapidly increased during boreal spring and summer in 1997 accompanied with weakening of the trade winds, and an El Niño event occurred after an interval of four years. In November 1997 the SST anomaly for Region B reached +3.6°C at the maximum, that is the greatest record since 1949. The El Niño event had great impacts not only on climate in the world but also on the subsurface in the Indian Ocean.

Fig.11a and 11b show time-longitude sections of zonal wind stress and zonal wind stress anomaly along the equator over the Indian Ocean during 1996 and 1997, respectively. The wind stress was calculated by the JMA four-dimensional atmospheric data assimilation system and was used to drive the ODAS. It can be easily seen in Fig.11b that strong easterly wind stress anomalies were dominant over the tropical Indian Ocean east of 60°E since March 1997. Usually, westerly wind is observed in the lower troposphere over the tropical Indian Ocean around 80°E during the Southwest Monsoon period including its transition period. On the contrary, easterly wind was prevailing throughout 1997, even in the Southwest Monsoon period except for May (Fig. 11a). Active convection regions, which are usually observed around the Maritime Continent, were moved to the date line by the strong El Niño event, and lower tropospheric wind became strongly divergent over the Maritime Continent. That can be thought as the cause of the easterly wind over the equatorial Indian Ocean. It is the first event in the ODAS data since 1986 that easterly wind was observed in the Southwest Monsoon period.

The changes of lower tropospheric wind over the Indian Ocean caused by the El Niño event had the following impacts on the structure of subsurface temperature in the equatorial Indian Ocean. Fig.12 shows a time-longitude section of OHC anomaly along the equator. There had been positive anomalies in the eastern Indian Ocean and negative ones in the western Indian Ocean before April 1997 when the El Niño event occurred. After then, the anomaly distribution was completely reversed and this lasted during 1997. Especially, large negative (< -3°C) anomalies east of 90°E were found in July and November to December 1997, and positive anomalies more than +1°C west of 70°E since November 1997. We find in the ODAS data since 1986 neither negative anomalies less than -3°C in the eastern Indian Ocean nor positive ones more than +1°C in the western Indian Ocean except in this case.

Fig.13 shows depth-longitude sections of subsurface temperature along the equatorial Indian Ocean. In the climatological temperature shown by Fig.13a, the thermocline slants to the east and warm water (>28°C) is accumulated between the sea surface and 30-40m depth in the east. In December 1997, while the

warm water almost disappeared in the east, it was accumulated in the west. The thermocline slanted to the reverse direction (west) of that in the climatological condition.

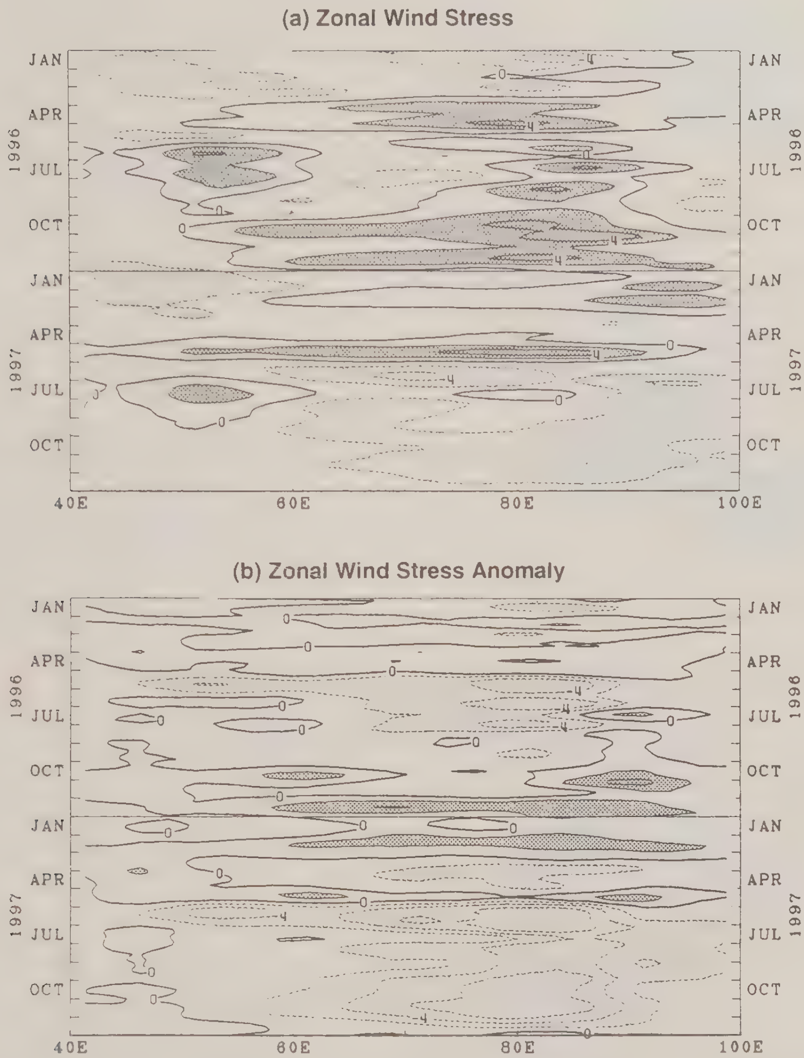


図 11. 1996～1997 年におけるインド洋の赤道に沿った風応力東西成分とその平年偏差の時間－経度断面図
等値線の間隔は 0.02N/m^2。(a) 風応力東西成分、(b) 風応力東西成分平年偏差。
Fig.11 Time-longitude sections of zonal wind stress and zonal wind stress anomaly along the equator over the Indian Ocean during 1996 and 1997.
The contour interval is 0.02N/m^2. (a) zonal wind stress, (b) zonal wind stress anomaly.

The El Niño event entered upon the decaying phase and ceased in the boreal summer of 1997. During the latter half of the El Niño event, SSTs over the equatorial Indian Ocean were 0.5°C to 1.5°C higher than normal (Fig.14). Warmings of SST over the equatorial Indian Ocean were usually observed during the decaying phase of El Niño events, but the warming in this case was exceptionally strong. In order to investigate the cause of this warming, we analyzed wind stress, OHC and energy flux into the surface over the Indian Ocean. The wind stress and OHC were from ODAS, and the energy flux was calculated from the climate data assimilation system (CDAS) data of National Centers for Environmental Prediction (NCEP/NOAA).

Fig.15 shows anomalies of OHC and the surface current velocity over the Indian Ocean (Fig.15a : 25OCT97, Fig.15b : 24NOV97, Fig.15c : 23JAN98). As described above, there were strong easterly wind

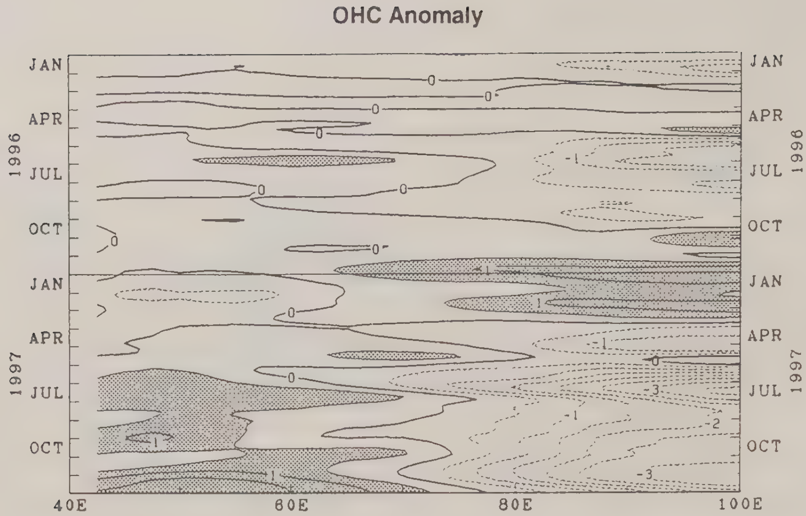


図 12. 1996〜1997 年におけるインド洋の赤道に沿った OHC 平年偏差の時間－経度断面図
等値線の間隔は 0.5℃。
Fig.12 Time-longitude sections of OHC anomaly along the equator over the Indian Ocean during 1996 and 1997. The contour interval is 0.5°C.

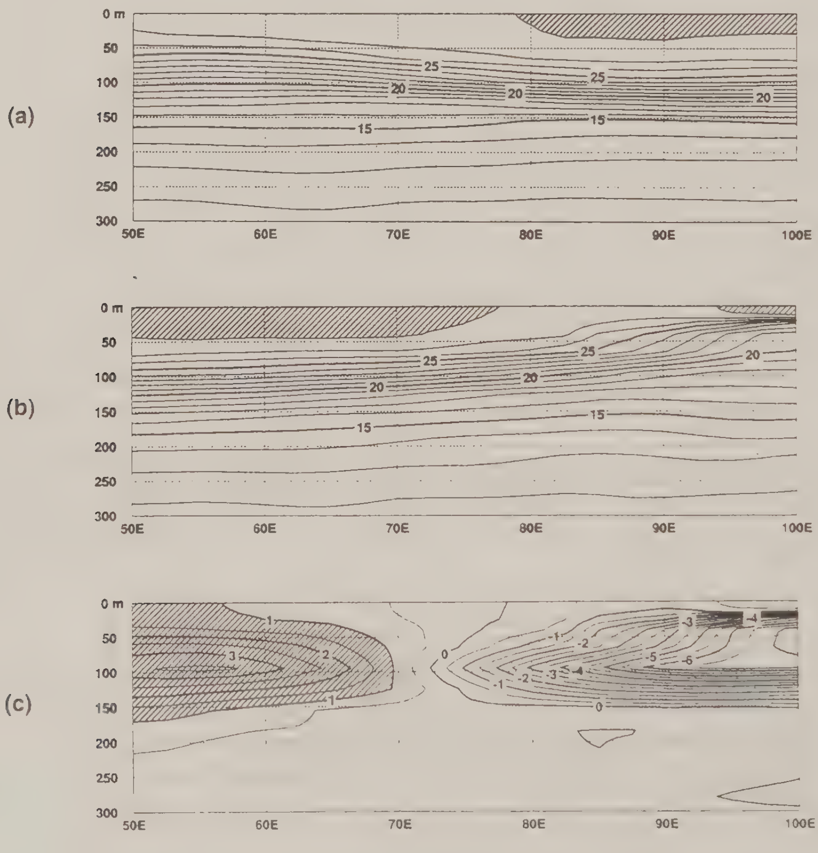


図 13. インド洋の赤道に沿った月平均表層水温とその平年偏差の深度－経度断面図
(a) 12 月の平年値、(b) 1997 年 12 月、(c) 1997 年 12 月の平年偏差
Fig.13 Depth-longitude sections of subsurface temperature and its anomaly along the equator in the Indian Ocean
(a) normal temperature in December, (b) temperature in December 1997,
(c) temperature anomaly in December 1997.

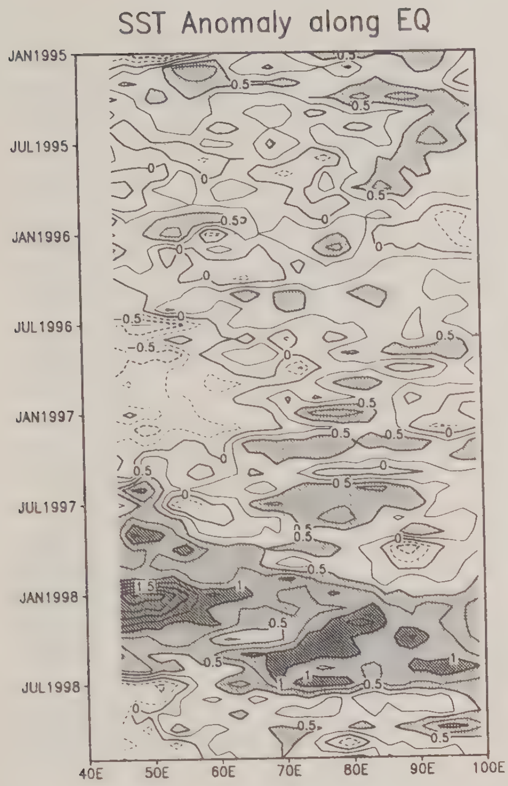


図 14. インド洋の赤道に沿った海面水温偏差
時間－経度断面図　等値線の間隔は 0.25℃
Fig.14 A time-longitude section of SST anomaly along the equator in the Indian Ocean. The contour interval is 0.25°C

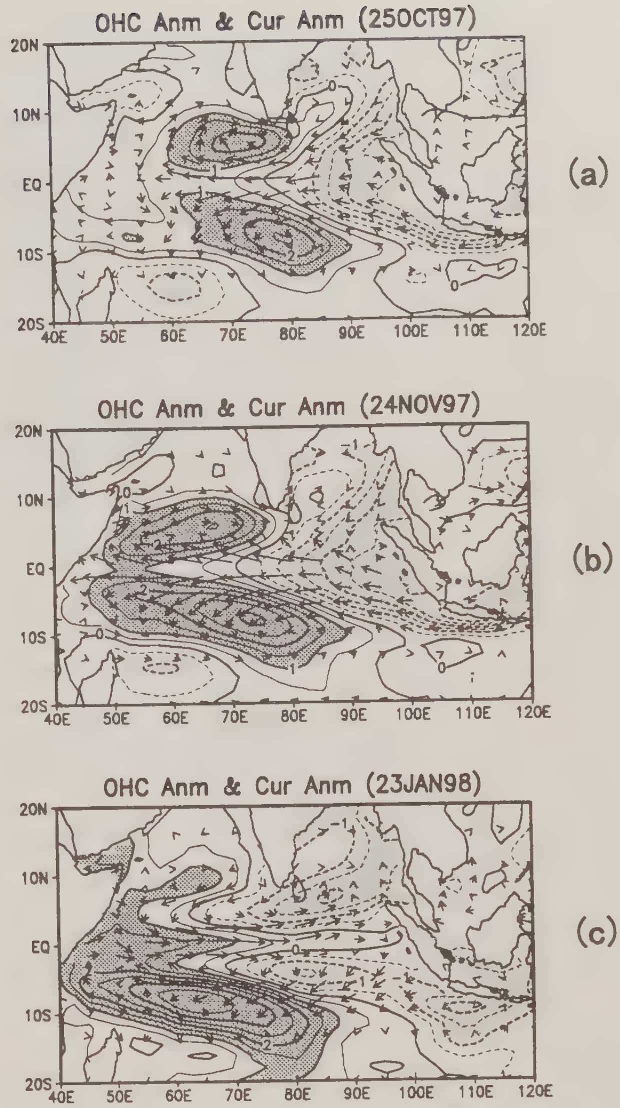


図 15. ODAS によるインド洋の OHC 偏差と海面流速偏差　等値線の間隔は 0.5℃、(a) 1997 年 10 月 25 日、(b) 1997 年 11 月 24 日、(c) 1998 年 1 月 23 日
Fig.15 OHC anomaly and surface current anomaly in the Indian Ocean by ODAS. The contour interval is 0.5°C. (a) 25OCT1997, (b)24NOV1997, (c) 23JAN1998

stress anomalies along the equatorial Indian Ocean during the latter half of 1997. The easterly wind anomaly concentrated on the equator not only made the thermocline shallow in the eastern Indian Ocean but also generated a pair of anticyclonic vortices which can be seen as positive OHC anomalies straddling the equator in the Indian Ocean (Fig.15a,b). The vortices migrated westward as warm Rossby wave packets and reached the east coast of Africa at the beginning of 1998. The Rossby wave packets were reflected at the African coast to be converted into an equatorial Kelvin wave, which can be seen as strong eastward current anomalies in the equatorial Indian Ocean (Fig.15c). As the equatorial Kelvin wave was accompanied with the warm waters, its eastward propagation can be clearly seen in the time-longitude section of OHC anomaly along the equator from January to March in 1998 (Fig.16). The westward propagation of Rossby waves followed by the eastward propagation of equatorial Kelvin wave was very similar to the delayed action oscillator theory (Schopf and Suarez, 1988) explaining ENSO.

Fig.17 shows a time-longitude section of the total energy flux (total downward radiative flux – total upward radiative flux – sensible heat flux – latent heat flux) anomaly into the surface along the equator. Comparing Fig.14 and Fig.17, we can find that the warming of the equatorial Indian Ocean during the first

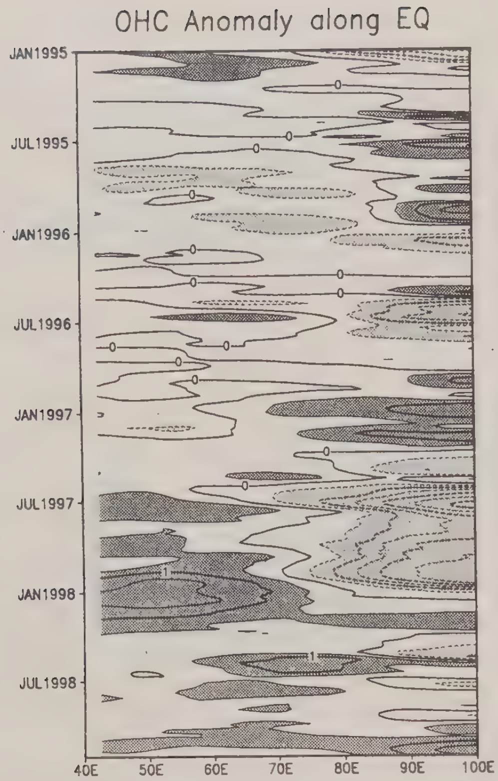


図 16. インド洋の赤道に沿った OHC 偏差
時間－経度断面図　等値線の間隔は 0.5℃
Fig.16 A time-longitude section of OHC anomaly along the equator in the Indian Ocean. The contour interval is 0.5°C.

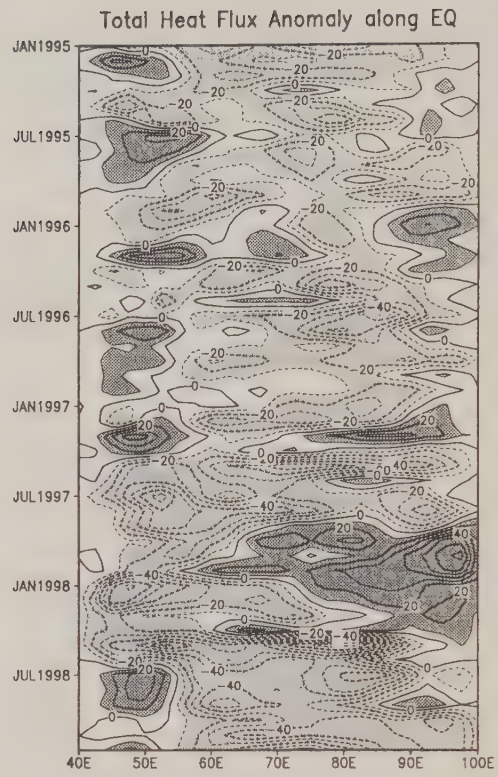


図 17. インド洋の赤道に沿った地表面入射全エネルギーフラックス平年偏差時間－経度断面図　等値線の間隔は 10W/m²
Fig.17 A time-longitude section of total energy flux anomaly into the surface along the equator in the Indian Ocean. The contour interval is $10W/m^2$.

half of 1998 corresponds rather to the negative flux anomaly than to the positive flux anomaly. We can also find the good agreement between the beginning of SST warming and the eastward propagation of warm Kelvin wave in Fig.14 and Fig.16. Therefore, we tentatively conclude from these facts that the SST warming in the equatorial Indian Ocean was caused not by thermal effects (e.g. variations of solar energy flux, evapolation, etc.) but the dynamical effect (i.e. the propagation of warm Kelvin wave accompanied with the increment of the mixed layer depth in the equatorial Indian Ocean).

4. Discussions

We have analyzed the subsurface temperature data in the Indian Ocean observed by VOS directly and ODAS data in which the subsurface data were assimilated. We could acquire a lot of information about the seasonal and interannual variations of subsurface temperature in the Indian Ocean through the analyses. Especially, ODAS was a very powerful tool for this study and made very clear the differences in subsurface temperature structure between the Indian Ocean and Pacific Ocean.

We experienced El Niño events three times during the period of the study. From the experiences, we could estimate impacts of El Niño phenomena on the subsurface temperature structure in the Indian Ocean and found that the El Niño phenomena were the primary factor as to interannual variations of the subsurface temperature in the tropical Indian Ocean.

Generally speaking, the Asian Monsoon is a seasonal phenomenon driven by the thermal contrast between the Asian Continent and the Indian Ocean. As the thermal condition of land surface is affected very

much by the soil moisture and the snow mass, the Indian Ocean could have indirect influence on the Asian Monsoon as a moisture supplier to the Asian Continent. We have studied impacts of the Asian Monsoon on the Indian Ocean so far, but we should also study interactions between the Indian Ocean and the Asian Continent through the hydrological processes to elucidate the mechanism of the Asian Monsoon variations.

5. References

Ando, T., 1992: Observation on Subsurface Temperature by Voluntary Merchant Ships in the Indian Ocean. *International Symposium on Asian Monsoon. September, 1992, Tsukuba.*

Barnett, T. P., 1983: Interaction of the Monsoon and Pacific Trade Wind System at Interannual Time Scales. Part I : The equatorial Zone. *Mon. Wea. Rev.*, **111**, 756-773.

Kimoto M., I. Yoshikawa and M. Ishii, 1997: An Ocean Data Assimilation System for Climate Monitoring. *J. Met. Soc. Japan.*, **75**, 471-487.

Nicholls, N., 1984: The Southern Oscillation and Indonesian Sea Surface Temperature. *Mon. Wea. Rev.*, **112**, 424-432.

Schopf, P.S. and M.J. Suarez, 1988: Vacillations in a coupled ocean-atmosphere model, *J. Atmos. Sci.*, **45**, 549-566.

Wyrtki, K., 1971: An Equatorial Jet in the Indian Ocean. *Science*, **181**, 262-264.

6. Publications

Ando, T., 1992: Observation on Subsurface Temperature by Voluntary Merchant Ships in the Indian Ocean. *International Symposium on Asian Monsoon. September, 1992, Tsukuba.*

Mikawa, T. and T. Mizuno, 1996: Seasonal Variation of the Subsurface Thermal Structure in the Indian Ocean in the Ocean Data Assimilation System of JMA. *Proceedings of the International Workshop on the Climate System of Monsoon Asia.*, 306-308.

Nikaidou, Y., 1999: Observation of Subsurface Water in the Indian Ocean by Ship-Of-Opportunity and its Analysis. (in Japanese) 測候時報, 第 66 巻特別号, S113-S121.

7. International Cooperation

None

(要旨)

本研究では、1989 年から 10 年間、インド洋において委託観測船(「鹿島山丸」と「Delmas Tourville」)による表層水温観測を行い、その航路(「鹿島山丸」:マラッカ海峡－ペルシャ湾間、「Delmas Tourville」:マラッカ海峡－喜望峰間)に沿って 3800 個以上の表層水温観測データを得た。

本研究期間の前半(1989～1994 年)では、航路に沿ったインド洋の表層水温断面の時間－空間変動を直接解析し、アラビア海やベンガル湾では北東モンスーン期と南西モンスーン期で表層水温の構造に明瞭な違いが見られることを発見した。また、アラビア海北西部やオマーン湾の表層水中に明瞭な鉛直方向の温度逆転を発見したが、それが安定であることや、アラビア海における過去の表層水温観測データに基づいて求めた水温逆転出現の頻度分布から判断して、これはペルシャ湾で形成された高温・高塩分水が沈降しながらアラビア海へ流出している現れであると判断した。

1995 年初頭に気象庁では海洋データ同化システムの業務運用を開始したが、このシステムは船舶によって観測された表層水温データを同化して、空間的に均質で物理的につじつまのあった海洋表層中の物理データを作成するものである。本研究期間の後半(1995～1998 年)では、エルニーニョ南方振動との関係に注目しながら、主に同化データを解析しインド洋表層水温の季節変化や年々変動を研究した。

赤道インド洋における表層水温の季節変化に関しては、東部で一年周期の変化が卓越しているのに対し、西部では半年周期の変化が卓越しているという東西間の違いが、同化データから明瞭に見られた。

一方、インド洋における表層水温の年々変動は海洋貯熱量平年偏差を経験直交関数解析することによって調べた。経験直交関数の第一モードは、インド洋で東西方向の双極子パターンとして現れているが、モンスーンの下層風やエルニーニョ現象とかなり高い相関が見られた。

強いエルニーニョ現象が 1997 年北半球の春に発生し、1998 年北半球の夏に終息した。このエルニーニョ現象は風の応力を通じて赤道インド洋の表層に大きな影響を与えた。1997 年の終わりから 1998 年始めにかけてのエルニーニョ現象成熟期には、赤道インド洋の水温躍層の傾きが平年の状態とは逆の方向に傾いた。さらに、赤道インド洋の海面水温は 1998 年の前半、平年より 0.5～1.5℃高くなった。インド洋における海洋同化データを調査したところ、この海面水温が高くなった現象は赤道インド洋を暖水ケルビン波が通過したためであり、またこの暖水ケルビン波はエルニーニョ現象によって引き起こされたインド洋上での風応力偏差によって、遅延振動子理論に似たメカニズムで発生したことなどがわかった。

I．大気・海洋・陸域間相互作用の諸過程に関する観測・解析研究

Observation and Analysis on the Process of the Atmosphere-Ocean-Land Interactions

2．海洋における諸過程に関する観測・解析研究

Observation and Analysis on the Process over the Ocean

(2) 海流循環に関する観測研究

Observation on Oceanic Currents with Drifting Buoys

海上保安庁水路部

寄高博行、道田　豊、木下秀樹、林王弘道

Hydrographic Department, Maritime Safety Agency

Hiroyuki Yoritaka, Yutaka Michida, Hideki Kinoshita and Hiromichi Rinnou

(Abstract)

The purpose of this study is to elucidate the ocean circulation including its temporal (annual, interannual) and spatial variation in the Indian Ocean, particularly in the tropical region. For this purpose, Lagrangian observation of the surface currents has been carried out with satellite-tracked ARGOS drifters since 1990.

Bimonthly climatology of surface current field in the tropical Indian Ocean was generated from tracks of surface drifters in JEXAM programme together with tracks of ones in SVP (Surface Velocity Programme). New climatology showed some differences from existing one by ship drift data, for example, in developing season and velocity of eastward equatorial jet.

Surface currents in the Indo-Pacific throughflow area flowing from the Indian Ocean toward the Indonesian Seas in boreal winter, to the opposite direction to other seasons, are traced with the drifters deployed in the region south of the Indonesian Archipelago in 1993. In particular, northward flows in Lombok Strait in boreal winter that has been presented by a numerical model is clearly displayed by a drifter which drifted from the Indian Ocean to Flores Sea through Lombok Strait in December 1993.

1. Introduction

Interannual variation of the Asian Monsoon, which has big influence upon the climatological variabilities in the region of south east Asia, may play an important role in the global climate change through the atmospheric general circulation. Some of previous studies have suggested that the Asian Monsoon would cause changes in the oceanographic condition in the western tropical Pacific and should have close relationship with ENSO events. As a successful example of oceanographic research related to climate change, TOGA (Tropical Ocean and Global Atmosphere), whose major field was the tropical Pacific, provided so much knowledge on ENSO mechanism. In the Indian Ocean, on the other hand, there have been very few oceanographic data available in comparison with other oceans.

Sixty-four surface drifters were deployed by the end of FY1998 in the Indian Ocean and tracked with ARGOS system within this research programme, Japanese EXperiment on Asian

Monsoon (JEXAM) to illustrate the surface current system of the tropical Indian Ocean and the Seas adjacent to Indonesia, which is very interesting issue for oceanographers from the view points of, for examples, mass/heat/salt exchange between the Pacific Ocean and the Indian Ocean, or air-sea interactions there.

A schematic representation of the Indian Ocean currents and their seasonal changes has been proposed by Molinari et al. (1990), who have presented a monthly climatology of surface currents by analyzing historical drifter data. To investigate their results and to complement their study, trajectories of the drifters, which are uniformly designed according to the recommendation of WOCE/TOGA SVP (Surface Velocity Programme), have been analyzed in this study.

2. Methods

Four to twelve drifters have been deployed in the Indian Ocean every year since 1990, the commencements of JEXAM programme (Figure 1). The drifters are designed according to the WOCE/TOGA SVP standard. A holey sock drogue of 8.6 m in length whose drag center is at 15 m below the sea surface is attached to the surface float that contains a processing unit for sensor data (sea surface temperature, on/off of the drogue and battery voltage) and a transmitter for ARGOS system. There is also a small subsurface float, which would reduce the tension of the tether between the surface float and the drogue (cf. Michida and Ishii, 1993; Michida and Yoritaka, 1995).

Bimonthly climatology of surface current field in the tropical Indian Ocean was generated from tracks of surface drifters in SVP (Surface Velocity Programme) including tracks of surface drifters in JEXAM programme. Positions of drifters deployed from 1990 to 1996 were converted to daily mean positions and velocity, and then vector mean were calculated for each mesh (2 degrees x 2 degrees), for each two months (Jan. and Feb., Mar. and Apr., ...).

Five drifters were deployed south off Java Island and one in Makassar Strait in December 1993, to see the currents in the area of Indo-Pacific throughflow. And six drifters were deployed south off Java Island on November 1997, to examine seasonal and interannual variation of Indo-Pacific throughflow. These drifters were released by Kagoshima University from the training vessel 'Kagoshima-maru'.

3. Results

New climatology of surface current field in the tropical Indian Ocean showed some differences from existing one by ship drift data, for example, in developing season (April, November-December) and velocity (over 100 cm/s) of eastward equatorial jet (Figure 2).

Five drifters were deployed south of Java Island in 1993, and four of them were conveyed by the ocean current toward Indonesian Seas from the Indian Ocean. This result should be of interest to oceanographers as an important observational fact that would tell us the seasonal change of the surface current in the region (Michida and Yoritaka, 1996). Tracks of the drifters deployed in 1993 are given in Figure 3, and those deployed in 1991 are also shown in

Figure 3, to see the seasonal difference of the current. The drifters for 1991 were released in boreal spring (May) and drifted west or southwest in boreal summer, except for one that was driven ashore at the south coast of Java in August or September. The drifters for 1993, on the other hand, released in boreal autumn (November) were drifted east or northeast, though the release points were close to those for 1991.

Masumoto and Yamagata (1993) have carried out numerical experiments on the mechanism of the seasonal variations of the Indo-pacific throughflow and made investigation into the current structure in the seas adjacent to Indonesia. They mainly discuss about the seasonal change of the volume transport in some channels. We compare the drifter tracks with the numerically simulated current by Masumoto and Yamagata (1993) to examine the current field.

The annual cycle of numerically simulated surface current field at a depth of 5m presented by Masumoto and Yamagata (1993) is shown in Figure 4. Seasonal contrast in the surface current can be easily seen in Figure 4. In the area where our drifters were tracked, there can be also found big seasonal differences. In Lombok Strait, in particular, there are northward flows simulated in February, while stronger southward flows are simulated in other seasons. It is pointed out for the currents west of 110E that the currents are generally weak in February though the current directions are not very different from those in other seasons. As for the currents east of 110E, it is suggested as a remarkable seasonal change that they have northward components in February and southward in other seasons.

A time series of daily drifting velocity of a buoy, which drifted through Lombok Strait, is shown in Figure 5. The drifter was at about 150 km south of Java Island in early December 1993, after deployment in November. Then it was drifted along the south coast of Java with a speed of 50-90 cm/s in an eastward current. The northward velocity in Lombok Strait was over 130 cm/s as seen in Figure 5, showing a strong current in the strait. After passing the strait, it was further drifted eastward in Flores Sea and Banda Sea with a speed of about 50 cm/s, sometimes over 100 cm/s, from January to March, 1994.

The tracks of six drifters deployed south off Java Island on November 1997 are shown in Figure 3. They were released at almost same area and in same season as ones deployed in 1993. However, the drifters deployed in 1997 described westward flow with anti-cyclonic eddy same as tracks on boreal summer of 1991. After the drifters flowed into open ocean, they drifted westward on South Equatorial Current with the drifting velocity 20 cm/s.

4. Discussions

From climatology of surface current field by drifters deployed for seven years, difference was shown in eastward equatorial jet from description by ship drift data. In existing climatology, equatorial jet was developed on May and October-November, and its maximum velocity was 80 cm/s (cf. Reverdin, 1987; Hastenrath and Greischar, 1991). In new climatology, equatorial jet was developed on April and November-December, and its maximum velocity was over 100 cm/s for bimonthly mean same as the results only for drifters in JEXAM (Yoritaka et al.,

1997). It is possible for two reason, one is climatological change in this decade, the other is over-smoothing in generation from ship drift data to reduce its error, and selective sampling of equatorial jet by drifters due to Ekman convergence near the equator.

Figure 6 shows difference between the eastern and central Indian Ocean in sea surface height anomaly from TOPEX/POSEIDON altimeter data on the equator, and daily mean eastward velocity for the drifters near the equator. Only for 1994, the lower surface appeared in the eastern part and equatorial jet was not developed in boreal fall due to weak westerly wind. For clarifying the mechanism of interaction between atmosphere and ocean, seasonal and interannual variation should be investigated in the key area for heat transport.

With comparison between the surface current system in the area of Indo-Pacific throughflow derived from drifters experiments and that numerically simulated by Masumoto and Yamagata (1993), we would conclude that the numerical model has well simulated the surface currents there including seasonal variations, as far as in qualitative words. In some quantitative comparison, we could also suggest that the stronger eastward flows in Java Sea and Flores Sea appeared in February in the numerical model (Figure 4) should agree with the trajectories of the drifter which passed Lombok Strait northward and had a eastward drifting speed of about 50 cm/s to 100 cm/s.

To examine the sea level difference between the Pacific and the Indian Ocean which will drive the currents in the Indonesian Seas, the mean sea levels observed by a satellite altimeter on TOPEX/POSEIDON are calculated for the area shown in Figure 7, two box areas of ten-degrees square are selected as representatives for both oceans. After the standard procedures of correction for TOPEX/POSEIDON data, for examples, correction for atmosphere, ionosphere, earth/ocean tides and so on; the time series of averaged sea level for each box area and difference between the two areas are obtained as shown in Figure 8. As a good assumption, we do not take the spatial fluctuation of the geoid into account in the above calculation, because the fluctuations of the ground tracks of the satellite are small enough. And, of course, the temporal fluctuation of the geoid should be negligible in such an analysis for 1 or 2 years. It is suggested from Figure 8 that the sea level in the Pacific Ocean was lower relative to the Indian during the period when the drifter experiment has been carried out in 1993 to 1994, although a trend of sea level rising can be observed in the series for both oceans for which the reason is not clear. The lower sea level in the Pacific in boreal winter may be a coincident phenomenon with the reversal in the surface current in the Indonesian Seas. Masumoto and Yamagata (1993) have numerically shown that the depth-integrated volume transport through Lombok Strait always flows out from the Pacific but the flow in the surface layer changes its direction by seasons. The reversal of the surface current in the region, which will transport much heat because of its high temperature, should affect not little on the inter-ocean heat transport, even if the volume transport always comes from the Pacific toward the Indian Ocean.

The drifters deployed south of Java Island in 1997 described westward flow with anti-cyclonic eddy same as tracks on boreal summer of 1991. Strong contrast between the tracks in 1997-1998 and the tracks in same season (boreal winter) of 1993-1994 indicated different in

seasonal variation of surface currents between eastern area and western area of 110E, and interannual variation of surface currents in Indo-Pacific throughflow area. While climatology of current field in this area was simulated with numerical model by Masumoto and Yamagata (1993), interannual variation should be monitored for evaluation of heat/salt exchange between Indian Ocean and Pacific Ocean.

Acknowledgments

We thank the training vessels of Kagoshima University, the research vessel Hakuho-maru of Ocean Reserach Institute of the University of Tokyo, the research vessel Shoyo-maru of Fisheries Agency, the training vessel Watatori-maru of Sakai Fisheries High School and the training vessel Oyama of Toyama prefecture for cooperation in deploying the drifters in the Indian Ocean.

5. References

1) R. L. Molinari, D. Olson and G. Reverdin; J. Geophys. Res., 95, pp7217-7238, 1990.
2) Y. Michida and H. Ishii; Kaiyo monthly, extra 4, pp115-122, 1993 (in Japanese).
3) Y. Michida and H. Yoritaka; J. Japan Soc. Mar. Surv. Tech., 7(2), pp21-28, 1995.
4) Y. Michida and H. Yoritaka; J. Geophys. Res., 101, pp12475-12482, 1996.
5) Y. Masumoto and T. Yamagata; J. Geophys. Res., 98, pp12501-12509, 1993.
6) G. Reverdin; J. Phys. Oceanogr., 17, pp903-927, 1987.
7) S. Hastenrath and L. Greischar; J. Geophys. Res., 96, pp12619-12633, 1991.
8) H. Yoritaka, Y. Michida and H. Kinoshita; Annual Report of JEXAM for FY1996, pp57-63, 1997.

6. Publications

Scientific Journals (5)

Y. Michida and H. Ishii, Observation of ocean circulation with surface drifters, Kaiyo monthly, extra 4, pp115-122, 1993.

Y. Michida and H. Yoritaka, Survivability of the surface drifters deployed by Hydrographic Department of Japan for the period from 1988 to 1993, J. Japan Soc. Mar. Surv. Tech., 7(2), pp21-28, 1995.

Y. Michida and H. Yoritaka, Surface currents in the areas of Indo-Pacific throughflow and tropical Indian Ocean observed with surface drifters, J. Geophys. Res., 101, pp12475-12482, 1996.

Y. Michida and H. Yoritaka, A Comparison between the Tracks of Surface Drifters and Sea Levels Derived from Satellite Altimetry in the Seas of Adjacent to Indonesia, Proceedings of International Workshop on the Throughflow Studies in and around Indonesian Waters, pp177-183, 1996.

H. Yoritaka, The Circulation in the Indian Ocean, Lectures on Technology in Hydrography, 11, pp85-91, 1998.

Reports (12)

H. Ishii and A. Ito, Annual Report of JEXAM for FY1989, pp27-31, 1990.

H. Ishii, H. Yoritaka and A. Ito, Annual Report of JEXAM for FY1990, 1991.

H. Ishii, Y. Michida and H. Yoritaka, Annual Report of JEXAM for FY1991, pp37-42, 1992.

Surface Currents and Upper Ocean Thermal Structure in the Indian Ocean, 1994 (small atlas).

H. Yoritaka, Y. Michida and S. Wakamatsu, Annual Report of JEXAM for FY1992, pp45-49, 1994.

Y. Michida and H. Yoritaka, Annual Report of JEXAM for FY1993, pp33-39, 1994.

Y. Michida and H. Kinoshita, Annual Report of JEXAM for FY1994, pp73-80, 1995.

Y. Michida et al., Pacific/Indian Ocean Throughflow, WESTPAC Information, 4, pp4, 1996.

Y. Michida and H. Yoritaka, Surface Currents in the Area of Indo-Pacific Throughflow and Tropical Indian Ocean Observed with Surface Drifters, International WOCE newsletter, 22, pp38-41, 1996.

Y. Michida and H. Kinoshita, Annual Report of JEXAM for FY1995, pp67-74, 1996.

H. Yoritaka, Y. Michida and H. Kinoshita, Annual Report of JEXAM for FY1996, pp57-63, 1997.

H. Yoritaka, H. Kinoshita and H. Rinnou, Annual Report of JEXAM for FY1997, pp61-68, 1998.

H. Yoritaka, Y. Michida and H. Kinoshita, Recent Progress in Studies of Asian Monsoon, pp237-246, 1999.

7. International Cooperation

The deployments of drifters in JEXAM Programme have been contributing to WOCE/TOGA Surface Velocity Programme for re-description of ocean surface circulation.

（和文アブストラクト）

アジアモンスーンの変動に大きな影響を及ぼすインド洋、特にインド洋熱帯域の海流循環の実態とその時間空間的な変動を解明するため、海上保安庁水路部は「アジアモンスーン機構に関する研究（JEXAM）」の一環として、1989 年以来表面漂流ブイを放流して海流の追跡観測を行った。

「アジアモンスーン機構に関する研究（JEXAM）」における表層漂流ブイの観測結果に、国際プロジェクトである表層海流計画（SVP）における観測結果を併せて、インド洋熱帯域における 2 か月毎の平均表層海流場を作成した。これまでの偏流データによる気候値と比較して、東向き赤道ジェットの発達期、流速等の相違が抽出された。

インドネシア通過流の海域の表層の流れは、北半球の冬季には他の季節と異なり、インド洋から太平洋側に向かって流れることが、1993 年にジャワ島南方で放流したブイによって確認された。特に、ロンボク海峡の強い北向きの流れが北半球の冬季に現われることが数値実験によって示されていたが、この流れも漂流ブイによって存在が確認された。

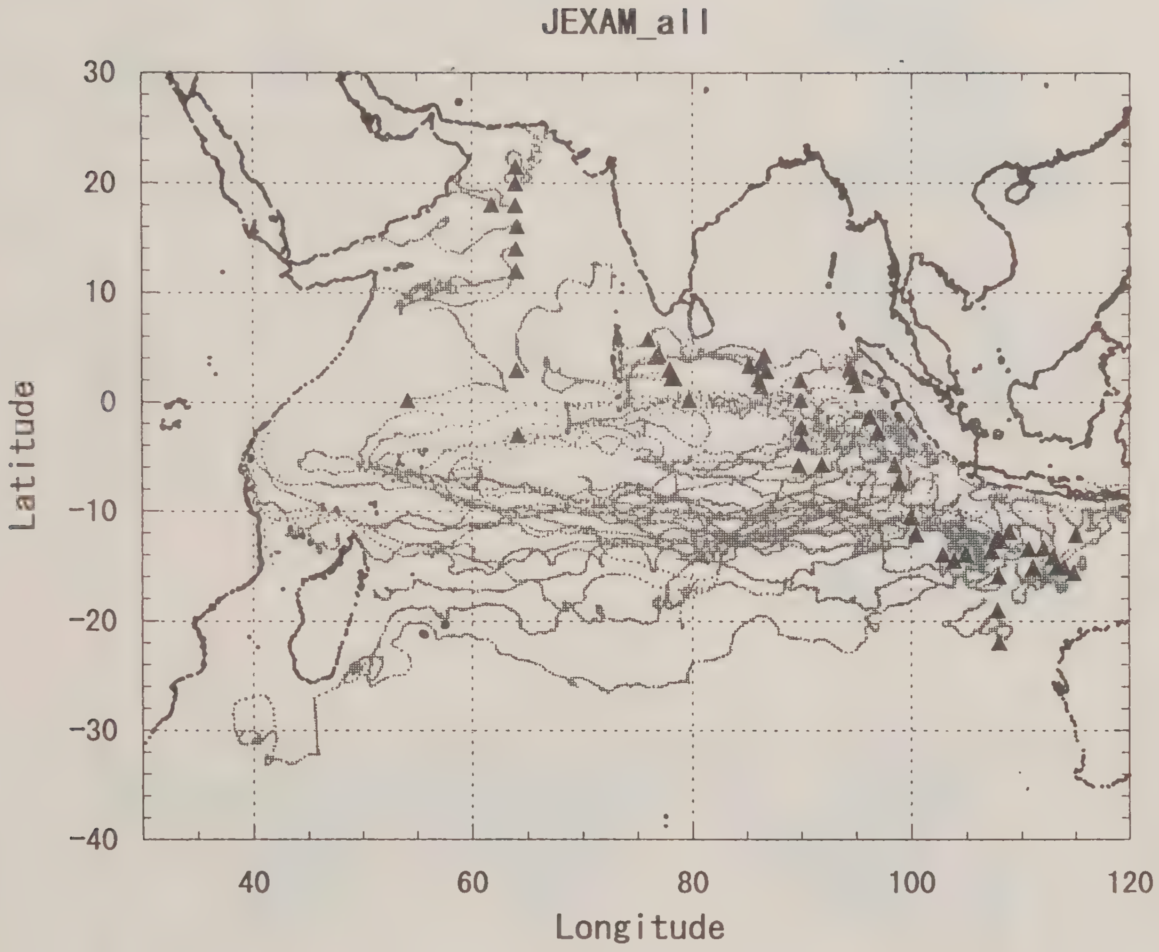
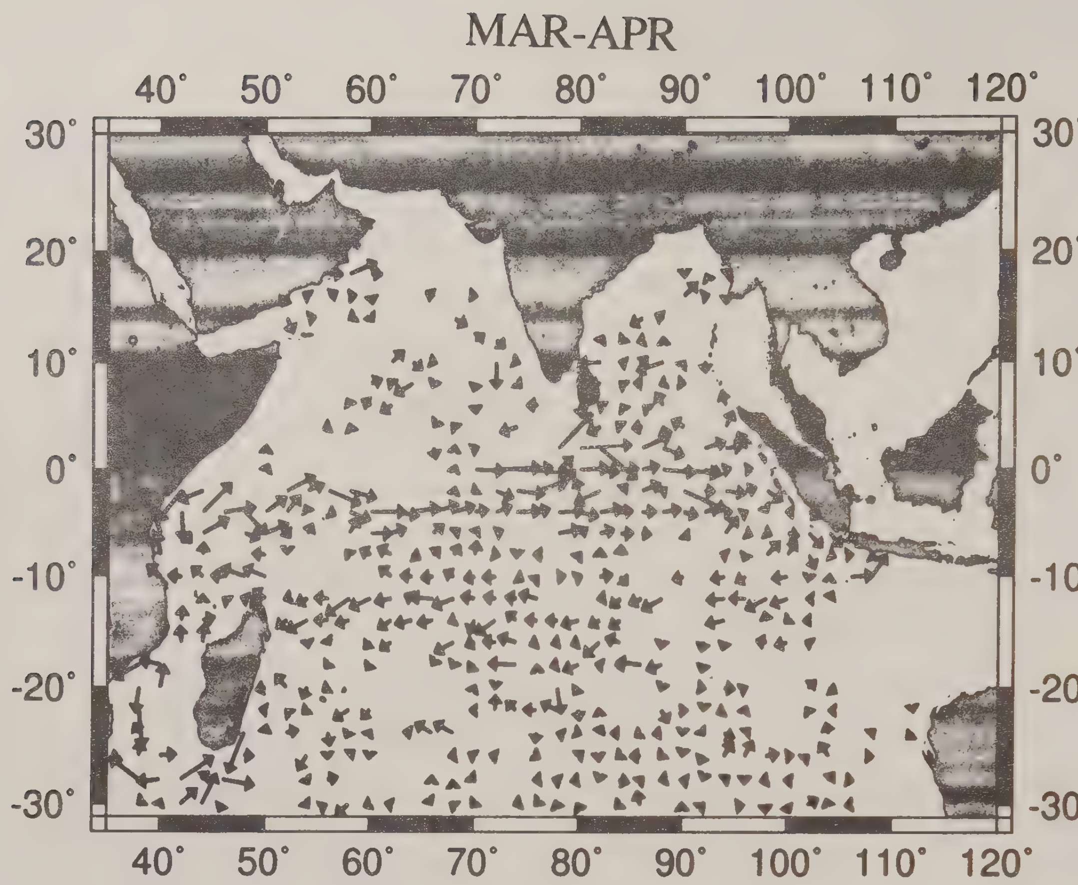


Figure 1. All tracks of the drifters deployed in JEXAM since 1990. Solid triangles mark the deployment location.



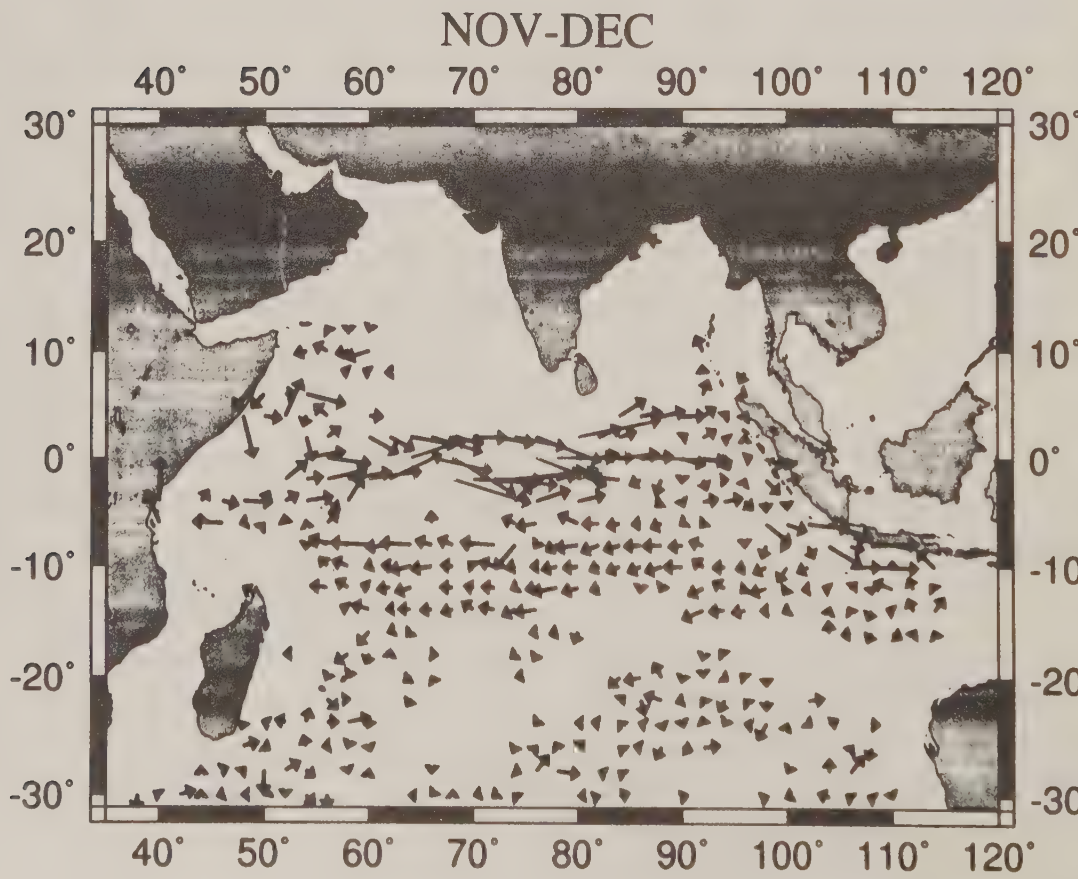


Figure 2. Grid averaged surface current field computed from drifter data for 2 degrees x 2 degrees bins for March-April (upper panel), November-December (lower panel).

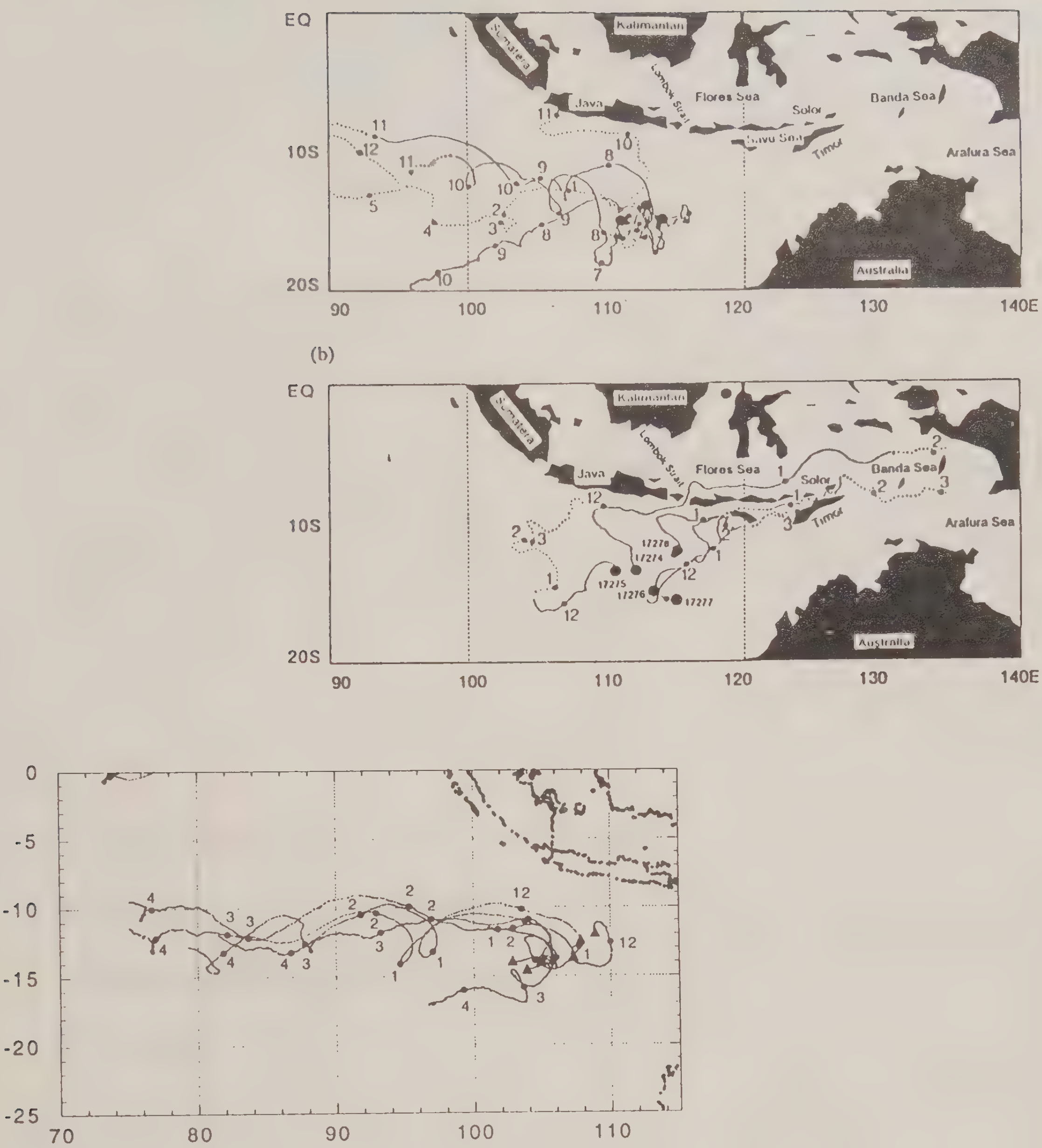


Figure 3. Tracks of the drifters deployed off Java Island on May 1991 (upper Panel), November 1993 (center panel) and November 1997 (lower panel) for drogued (solid lines) and undrogued (dotted lines) segments. Large solid circles and solid triangles mark the deployment location. Small solid circles mark the locations on the first day of every month, with the month number (January is 1, February is 2,...).

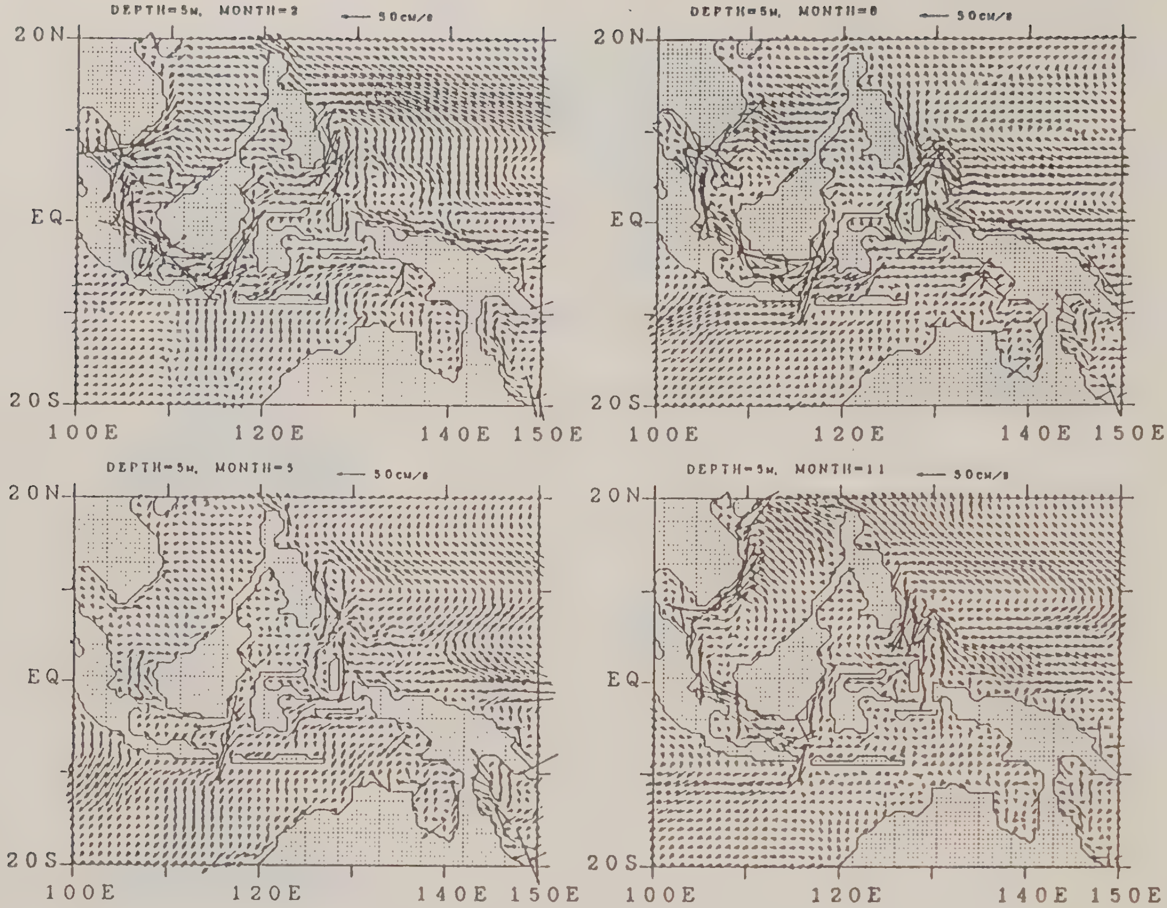


Figure 4. Annual cycle of numerically simulated surface current field at a depth of 5m in the Indonesian Seas (after Masumoto and Yamagata[1993]).

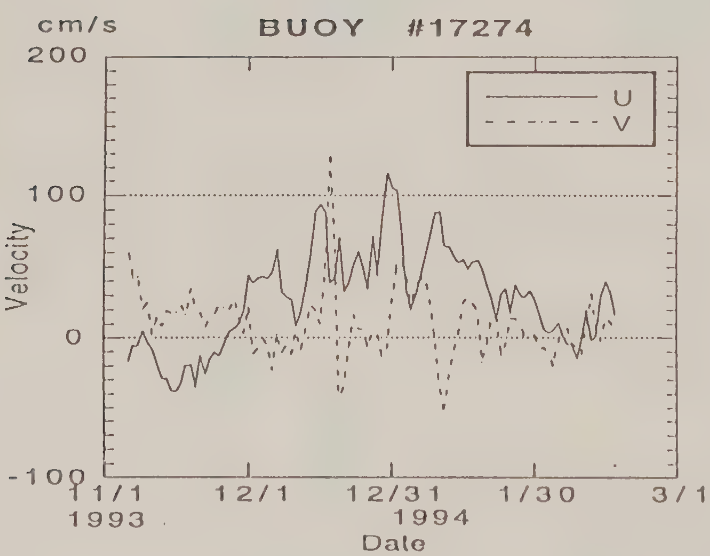


Figure 5. Time series of daily drifting velocities for drifter #17274, which drifted into Flores Sea north through Lombok Strait.

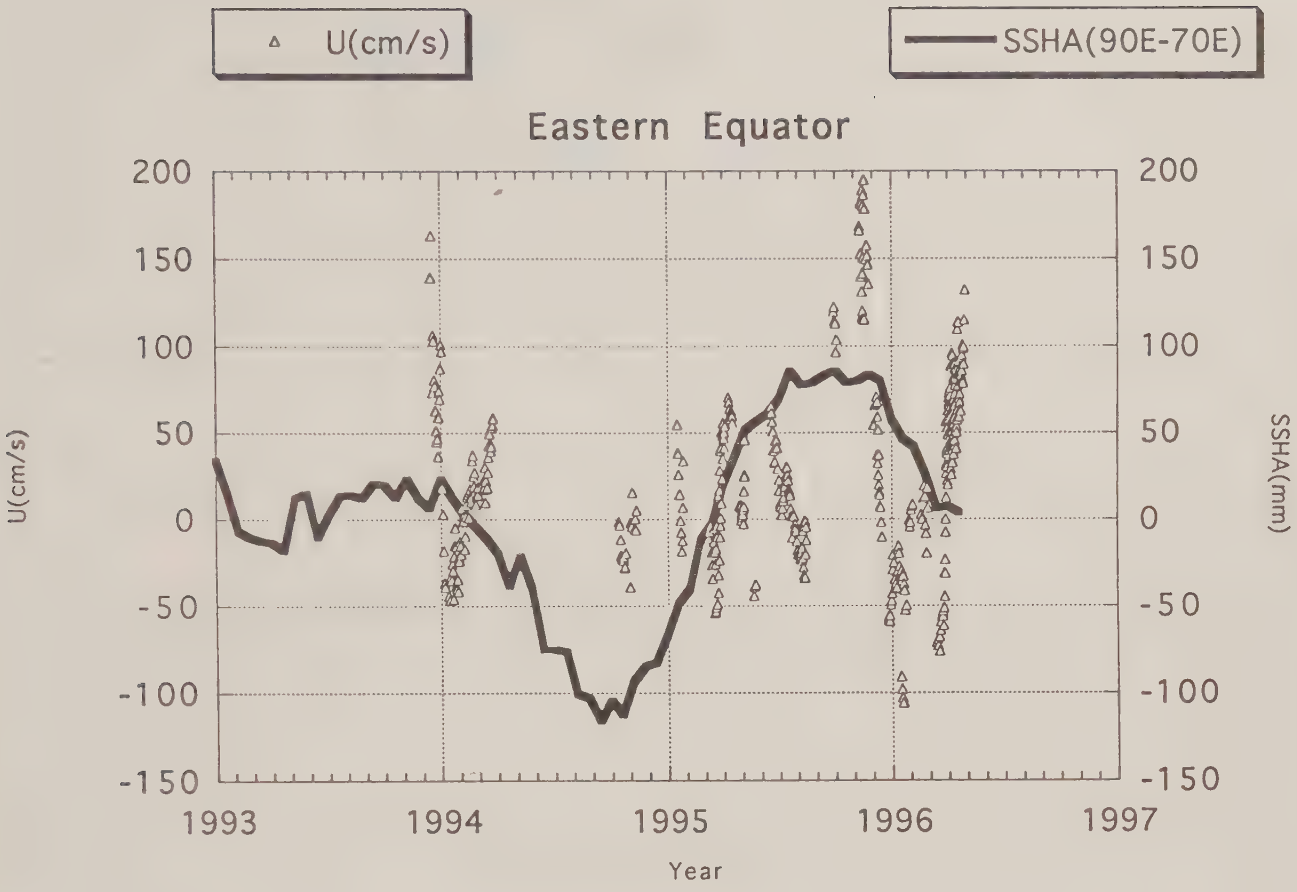


Figure 6. Difference between the eastern and central Indian Ocean (90E-70E) in sea surface height anomaly from TOPEX/POSEIDON altimeter data on the equator (solid line), and daily mean eastward velocity for drifters near the equator (open triangles).

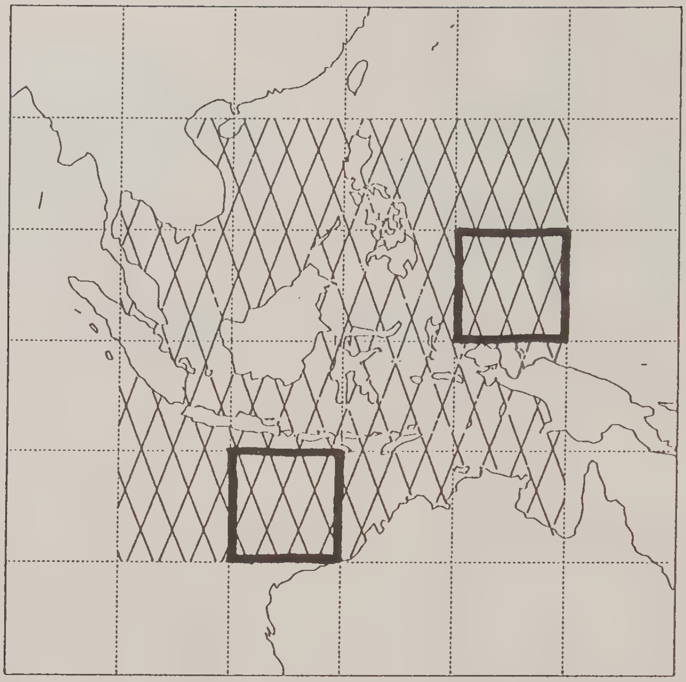


Figure 7. Available data points for TOPEX/POSEIDON satellite altimeter for a cycle in the area of Indonesian Seas. Solid squares indicate two ten-degrees boxes for which mean sea levels are calculated.

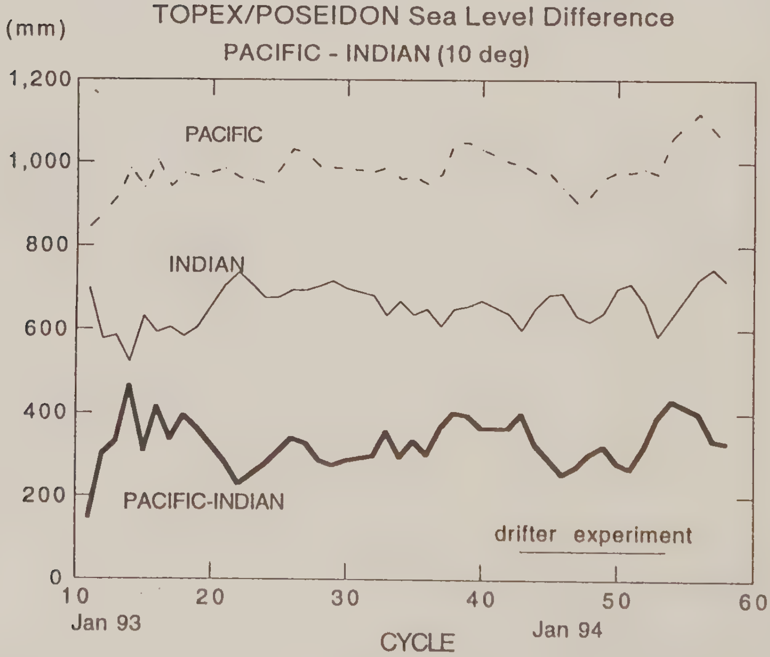


Figure 8. Time series of averaged sea level for each box area shown in Figure 7 and difference between the two areas, i.e. between the Pacific and Indian Ocean, calculated from TOPEX/POSEIDON data.

Ⅰ. 大気・海洋・陸域間相互作用の諸過程に関する観測・解析研究

Observation and Analysis on the Process of the Atmosphere-Ocean-Land Interactions

2. 海洋における諸過程に関する観測・解析研究

Observation and Analysis on the Process over the Ocean

(3) 海洋データの標準化及び海洋データ交換の推進

. Promoting the standardization and exchange of oceanographic data

海上保安庁水路部海洋情報課
Oceanographic Data and Information Division,
Hydrographic Department, Maritime Safety Agency
(日本海洋データセンター)
(Japan Oceanographic Data Center)
高芝利博、三宅武治
Toshihiro Takashiba , Takeharu Miyake

(Abstract)

A project entitled 'Observations on the Ocean' is being conducted as part of the Japanese Experiment on Asian Monsoon (JEXAM). The Japan Oceanographic Data Center (JODC) conducts research and development work through studies on the following four main items. The aim of the studies is to prepare data of the highest quality to be supplied to the researchers in this project. In order to also collect and provide other information related to JEXAM program we have studied and developed on the basis of following four items.

(1) Creation of a data management system and a database system.

Management system to standardize the oceanographic data collected in the subprogram 'Observation on the Ocean' to the form which researchers can use, and register them to its database.

(2) Collection of information related to oceanographic surveys and their data in various countries.

Collection of information regarding oceanographic surveys that have been conducted by various countries on the Indian Ocean and the seas around South- East Asia.

Moreover, rescue activities of historical data that were collected by the countries which carried out oceanographic surveys.

(3) Creation of a data and information network system.

Development of a data and information network system by combining the above-mentioned database with the Internet. This will realize the smooth and rapid distribution of information and data of this project, so that they can be shared by researchers both at home and abroad. It will also improve the exchange of information related to the current project between the various countries concerned.

With regard to (1) and (3) above, a data management system and a data and information network system, both of which have forms suitable for fulfilling the desired

purposes, have already been created. With regard to (2), we succeeded in collecting information related to the oceanographic surveys in the project regions, directory of historical data, and oceanographic data obtained outside of this project. In short, a considerable amount of data was collected.

(4) Preparation of a comprehensive data set

The putting together of a data set based on the oceanographic data collected in (1) and (2) above, and the provision of this data set to persons concerned with the project so that the data may be utilized effectively.

Moreover, the inclusion in the data set of things like graphics display programs, meaning that the observation data can be examined visually, thus reducing the burden on researchers.

1.Objectives

First aim of this research was to create data of the finest quality and to then provide them to researchers involved with the Japanese Experiment on Asian Monsoon (JEXAM) and investigative research related to the Indian Ocean, so that such research can be carried out smoothly and effectively. Second aim was to construct systems that would enable the processing and exchange of data as groundwork for the project.

2. Methods

(1) Standardization of data and the creation of a database system.

A data management system was built for handling observation data that have been obtained from the 'Observations on the Ocean', which is a sub-theme of JEXAM.

Such data includes the sea surface temperature, ocean currents and trajectories of drifting buoys.

The data management system involves a unified series of processes from converting the format of the data, through processing and standardizing the data (considering things such as quality control), to storing this processed data in the form of a database. It was aimed, through the creation of this system, to make it easier for researchers involved in the project to share the data.

(2) Collection of information related to oceanographic surveys conducted in various countries, along with other oceanographic data.

The main region targeted in the 'Observations on the Ocean' project is the Indian Ocean and surrounding sea areas. However, few oceanographic surveys are carried out in this region and, moreover, there are insufficient systems to assemble and manage the data in the countries in the region. Because of this, JODC has been able to obtain extremely little information regarding the data compared with other oceans, and so there is insufficient basic data to be used by the researchers in the current project. Nevertheless, as much information as possible are collected on the few oceanographic surveys that have been conducted by various countries in the region.

Furthermore, along with the above, historical data held by the various countries will be found out and assembled. Such data are important to detect long-term climatic changes, and will also be useful when sorting out the oceanographic data obtained by this project according to its quality.

(3) Construction of a data and information network system.

An environment in which information can be processed smoothly and rapidly will be provided through a data and information network system which is constructed to connect the oceanographic data centers (or equivalent organization) in each country. The aims of this are to make it easier to gain the cooperation of each of the related countries and to promote the procurement of information related to the oceanographic surveys in (2) above.

Moreover, along with this, a system will be created to enable the smooth and timely exchange between researchers of information on plans of surveys related to various types of research or results of such surveys. In this way, it is aimed to build a unified system for the exchange of oceanographic data that covers both Japan and foreign countries.

(4) Preparation of a comprehensive data set

A data set will be prepared based on the oceanographic data (on water temperature, ocean currents etc.) obtained during this project and data sets put together by oceanographic data centers etc. in other countries, the aim being to enable research organizations participating in the project to utilize the data effectively.

Along with the collected data, graphics display programs will also be included with the data set, meaning that the data can be processed statistically and utilized as graphical data.

3. Results

(1) Standardization of data and Creation of a database system

Using the developed system, JODC has processed the following data related to the JEXAM project until FY 1998.

① Japan Meteorological Agency

Data on surface water temperature (XBT) measured at 4170 points by a volunteer ship between February 1990 and January 1998 are received and processed.

A map of the observation points is shown in Figure 1.

② National Research Institute of Far Sea Fisheries

Data on surface water temperature (XBT,DBT,CTD) measured at 7160 points by survey ship and volunteer ships between 1989 and 1997, are received and processed.

A map of the observation points by research vessel 'Shoyomaru' is shown in Figure 2.

③ Hydrographic Department, Maritime Safety Agency

Data on 48 drifting buoys using ARGOS system between 1990 and 1996 are received and processed.

Drifting trajectories of the buoys are shown in Figure 3.

The database for drifting buoys was established in 1996. The identification number of

each buoy, its longitude and latitude, and date of observation are all recorded in the system.

This means that it is possible to extract required data, display catalogues that show things like the observation region for each buoy, and draw a map showing the trajectories of selected buoys.

(2) Collection of the information related to oceanographic surveys conducted in various countries, along with other oceanographic data.

① The 'International Workshop on Oceanographic Data Management' was held in November 1992 and discussed with specialists in charge of oceanographic data management from India , Indonesia, Republic of Korea, Thailand, Vietnam, Malaysia and Japan, in particular, how to improve data management activities in neighboring Asian countries. At the same time, Oceanographic surveys was carried out as the state of affairs by India and Indonesia. Both countries are closely related with the ocean regions that are the target of the JEXAM surveys.

As result of the above, it became clear that the Indian National Oceanographic Data Center(INODC) was holding a valuable data source that covered the northern part of the Indian Ocean, for which there had previously been no data available for the JEXAM community. JODC held negotiation with INODC regarding the international exchange of data. And it was ultimately agreed that only information on an inventory of physical data on the ocean would be exchanged.

Tables 1~3 show the situation regarding surveys on the Indian Ocean.

(Note that Indonesia is conducting or planning a number of projects in the Indian Ocean in collaboration with survey and research organization in other countries. JODC therefore expects to be able to obtain more data on the Indian Ocean in the future.)

② The deputy director of INODC was invited to Japan in October 1993. Opinions were exchanged on a cooperative relationship involving the exchange of data between the data centers in the two countries. Moreover, one of the JODC staff was dispatched to INODC in March 1997, again with the aim of promoting exchange of oceanographic data between the two countries.

As a result of the above, it has been confirmed that INODC is collecting and managing in a unified way both oceanographic data collected at 11 observing stations along the Indian coast and data collected by domestic organizations (including neighboring countries). It has also been confirmed that a network system is being developed at INODC and that, using this, Japan and India will be able to start online information exchange in close cooperation in the near future.

③ In August 1993, JODC received Indian oceanographic data at 650 serial stations (1976~1988) through US-NODC. The data are those submitted from INODC to US-NODC(which is World Data Center A for Oceanography (WDC-A)).

Figure 4 shows a map that shows the measuring points for the data.

④ In October 1993, JODC received the location data of 1654 drifters from the Marine

Environmental Data Service (MEDS) of Canada which also acts as the Responsible National Oceanographic Data Center for Drifting Buoys. The data contain drifting buoys in the Indian Ocean as well as the Pacific Ocean.

Figure 5 shows trajectories of these drifting buoys.

⑤ In March 1994, JODC participated in the second workshop of 'The Global Oceanographic Data Archaeology and Rescue Project(GODAR)' held in Tianjin, China. (GODAR is promoted by the Intergovernmental Oceanographic Commission(IOC).) Information was collected regarding historical oceanographic data on all of the world's oceans, including the regions targeted in the current project. (As an example, in Russia 450,000 points of MBT data on all the world's oceans, along with 800,000 serial stations data, all of which had been recorded in handwritten format, were digitized.)

Figure 6 shows the results of digitizing data related to the oceanic regions that were collected during the GODAR project.

⑥ In August 1994, JODC received from NASA's Jet Propulsion Laboratory oceanographic data set for 1985-1990 in the Indian Ocean. This data set had been obtained as part of the Tropical Ocean Global Atmosphere Program(TOGA), an international research project.

Table 4 shows a description of the type of data in this data set.

⑦ In December 1994, JODC received the 'World Ocean Atlas 1994' data set from WDC-A.

This is a revised version of 'Levitus data set'. It was compiled using data that WDC-A had received up to Spring 1993. This data set includes worldwide statistics on water temperature, salinity and nutrients on 1° bins, as well as the data for which quality control had been performed.

Tables 5 and 6 show results of processing statistics in the data set, along with information on the number of measurement points.

⑧ Moreover, through the above-mentioned work, a network system that links JODC with National Oceanographic Data Centers in other countries (or the equivalent organization in countries without NODC) was built for purpose of exchanging oceanographic information and data related to the Indian Ocean and South- East Asia.

⑨ In October 1998, JODC received from the US-NODC the 'World Ocean Database' published in August 1998. This data set was based on the data gathered together in the 'World Ocean Atlas 1994 (WOA94)', and supplemented with meta-data and meteorological data. It also included things like high-resolution CTD data and plankton data received by the promotion of projects like GODAR at US-NODC after WOA94. Table 7 shows the data included in the data set.

⑩ In June 1998, JODC received the WOCE (World Ocean Circulation Experiment) data set from the US-NODC.

This data set included observation data collected from 1990 to 1997, an outline of the data, an inventory list, and information on sources from which other detailed information and data could be obtained.

(3) The creation of a data and information network system

JODC developed JOIDES(the 'JODC Online Information & Data Exchange Service), which was an information exchange system that makes use of telecommunication between computers. It went into operation in FY 1991. The aim of JOIDES was to enable the smooth and timely exchange of observational data and other information related to oceanographic research projects, including JEXAM.

As part of this project, JODC set up an electronic bulletin board system(BBS) to be used exclusively for displaying information related · to the research by the participating researchers in the project, information on meetings related to JEXAM, and reports for such meetings. JODC also provided an E-mail service for the use of JEXAM researchers.

And a network system was added in FY 1992, to be used for exchanging information related to JOIDES with other countries. In this way, JODC has promoted the exchange of information on oceanographic surveys by various countries on the JEXAM ocean regions, together with information on management of oceanographic data.

As the Internet has been widely used in recent days JODC subsequently enabled JOIDES and the Internet to be available. The Internet then became the main tools in distributing information between researchers, and so at the end of 1997 operation of JOIDES was terminated. JOIDES's functions were transferred to the website of J-DOSS (the ' JODC Data Online Service System'), which is an Internet service operated by JODC.

(4) Preparation of a comprehensive data set

A data set was prepared based on the oceanographic data obtained during this project and data sets put together by oceanographic data centers etc. in other countries.

In order that the data set could be viewed not just as raw text but also graphically, the data necessary for providing graphic displays was extracted, and programs were developed to convert this data into standard mesh data.

These graphics display programs make it possible to display the data in the form of both color distribution charts and isopleth charts on a computer screen (UNIX workstation or Windows NT server), thus enabling the data to be utilized effectively.

4. Discussion

At the beginning of this project, JODC developed a system called JOIDES for exchanging data and information. However, as Internet rapidly became popular, JODC also changed the system to Internet. It could be smoothly transferred by the experience of developing JOIDES. JOIDES's functions (for example, the electronic bulletin board system) were also included in the new system. Information technology is being rapidly progressed, and so JODC always makes effort to maintain the systems which will be able to proved data for researchers. We believe that it is important to keep a positive attitude with regard to introducing new technology into our systems in the future.

In this project, the Indian Ocean and the seas around South-East Asia are targeted. In

recent years, the role of the oceans become important in long-term climate change , and so it becomes more important to collect and manage oceanographic data and information on the above- mentioned ocean regions.

In order to clarify the interaction between general oceanic circulation and other climatic factors, it is extremely important to effectively use the data that is obtained for the project to complement data that comes from sources like WOCE and JGOFS. (For this porpose, JODC intends to publish the data of the project as a data set, and to provide online data through the Internet.) In this way, it is hoped to contribute programs that deal with climate change.

It should be noted however that there is little data available on the Indian Ocean that can be used in order to understand climate change and elucidate its mechanisms. We therefore believe that it is important to continue striving to collect oceanographic observation data to the future. At the same time, it is equally important to continue to promote online data exchange making use of the Internet, and to continue providing systems that supply information on surveys and data to researchers.

Moreover, in addition to preparing a data set, we have also developed graphics display programs, which allow data obtained through JEXAM and data collected by oceanographic data centers etc. in other countries to be processed statistically and then utilized visually. The burden on researchers is thus reduced since they can obtain data in a graphical format. We thus anticipate that the number of users of the data will increase, and hope that this will result in a contribution to the elucidation of the mechanisms of the global oceans and the understanding of things like environmental problems.

5. References

IOC: Manual on International Oceanographic Data Exchange,
IOC Manual and Guide 9,1991

Japan Oceanographic Data Center: Manual on International Oceanographic Data Exchange (in Japanese) , JP013-94-1. 82PP, 1994.

6. Publications etc.

(1) Publications

An Oceanographic Data Exchange System that Makes Use of Communication between Computers

Yutaka Michida, Norio Baba

1992, Hydrography Department Technical Report No. 10

The Japan Oceanographic Data Center Database

Yoshio Shimizu

Advanced Marine Science and Technology Society, Summary of the Spring 1995 Lectures

The JODC Oceanographic Data Online Service System (J-DOSS)

Shohei Wakamatsu
Journal of the Japan Society for Marine Surveys and Technology 1997
Vol. 9, No.1
JODC Data Online Service System(J-DOSS)
Tadao Tatsuno
WESTPAC DATA MANAGEMENT GUIDE Revised Edition , 1996
Introduction to JODC on the WWW Server Homepage
1995 JODC news No.51
1997 JODC news No.54
JEXAM Data Set (CD-ROM)
Due to be published in February 1999

(和文アブストラクト)

本研究は、「アジアモンスーン機構解明に関すり研究」(以下 JEXAM という)と、そのサブテーマである「インド洋に関する調査研究」の円滑かつ効果的な実施を図るため、当該研究に携わる研究者に対し、利用可能な最良のデータセット及び調査に係る情報を提供するためのものである。

この目的を達成するために、JEXAM の一研究項目である「海洋に関する観測研究」において取得される水温等の海洋データの標準化を行い、研究者間のデータ相互利用の円滑化を図る。

また、JEXAM の各研究における基礎資料の充実を図るため、インド洋及び周辺海域における既存の海洋データ及び関連情報の収集を行う。さらに、得られたデータにより統計値の信頼度を増すことによってデータ品質管理の精度向上を図る。

一方、これらのデータ管理活動のほかに、情報流通の迅速化を図るため、データの管理状況及び海洋調査計画等に関する情報のオンライン入出力·検索が可能なデータベースを構築した。

さらに、データ·情報提供に関する各国の協力を得やすくするため、各国国立海洋データセンター等と JODC との間に海洋データ·情報交換のためのデータ·情報交換ネットワークシステムを構築した。また、国内から国外まで一環した海洋データ·情報交換のためのシステムを構築し、JEXAM における海洋データの迅速·容易かつ円滑な利用が図れるようになった。さらに、その他の地球環境関係等の各種のプロジェクトにおいても、有効利用に資するものである。

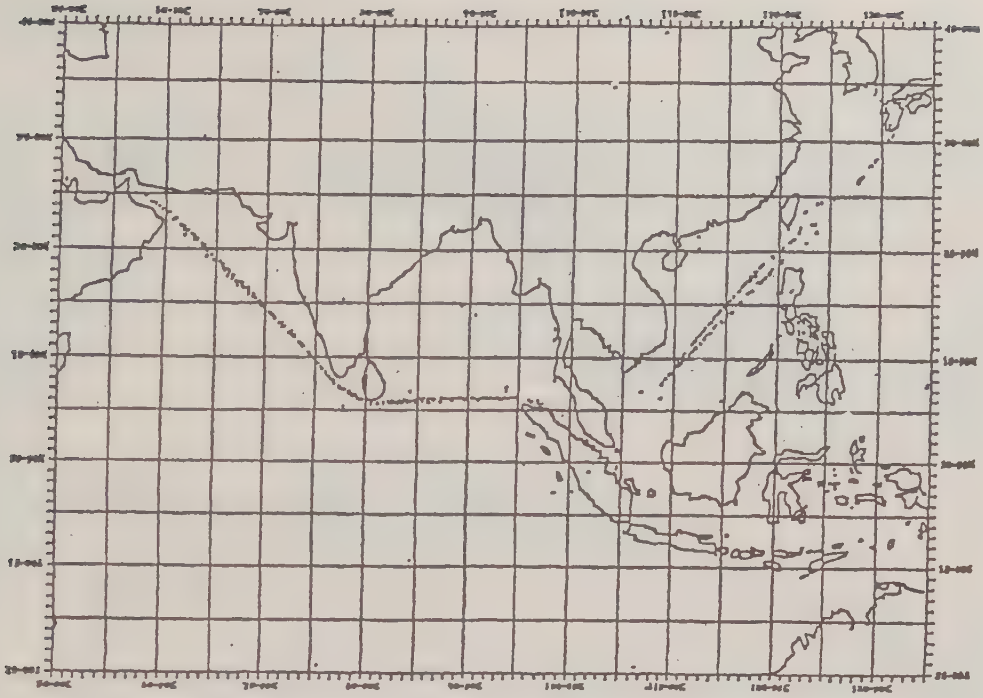


Fig. 1 Observation points for data received from Marine Department ,JMA

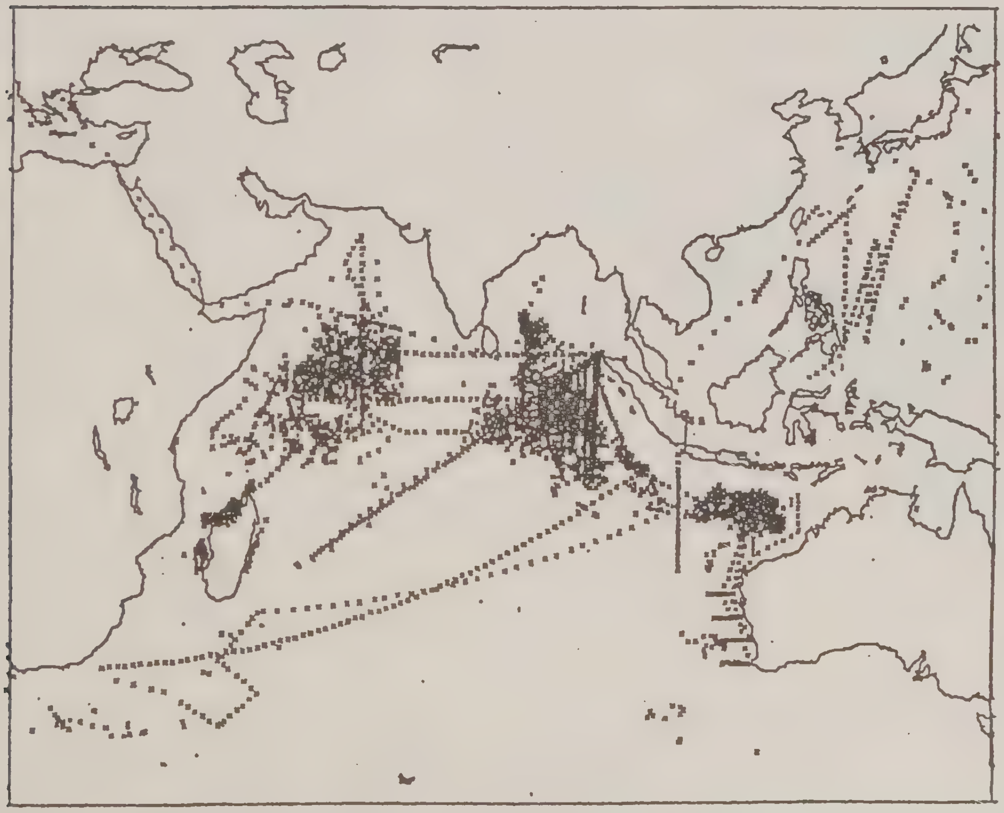


Fig. 2 Observation points for data received by National Research Institute of Far Seas Fisheries

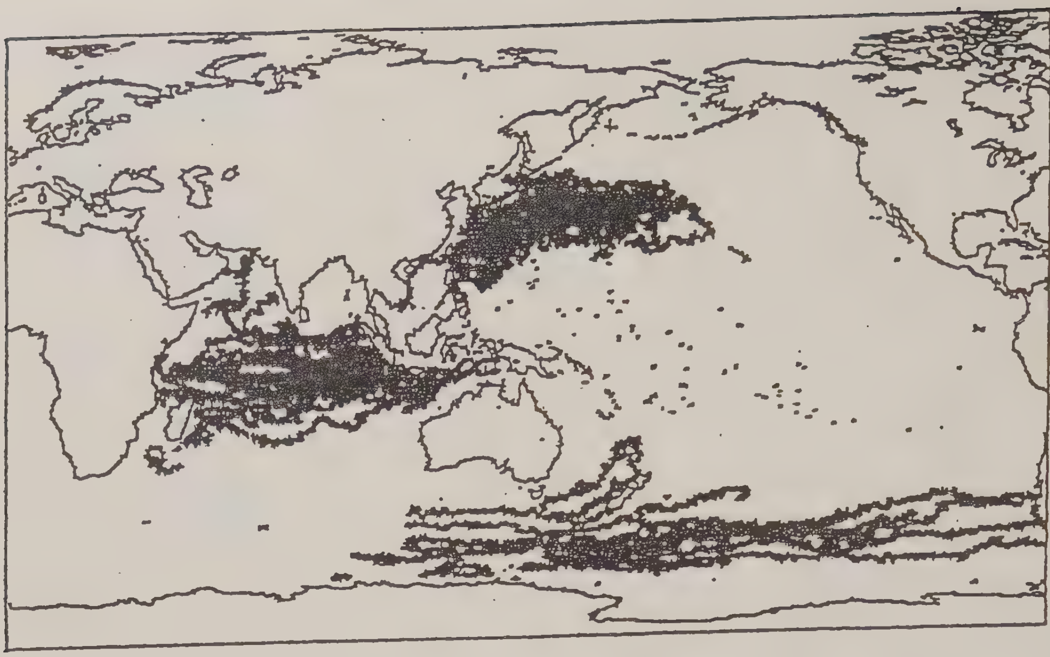


Fig. 3 All trajectories from the drifters deployed from
Hydrographic Department , MSA

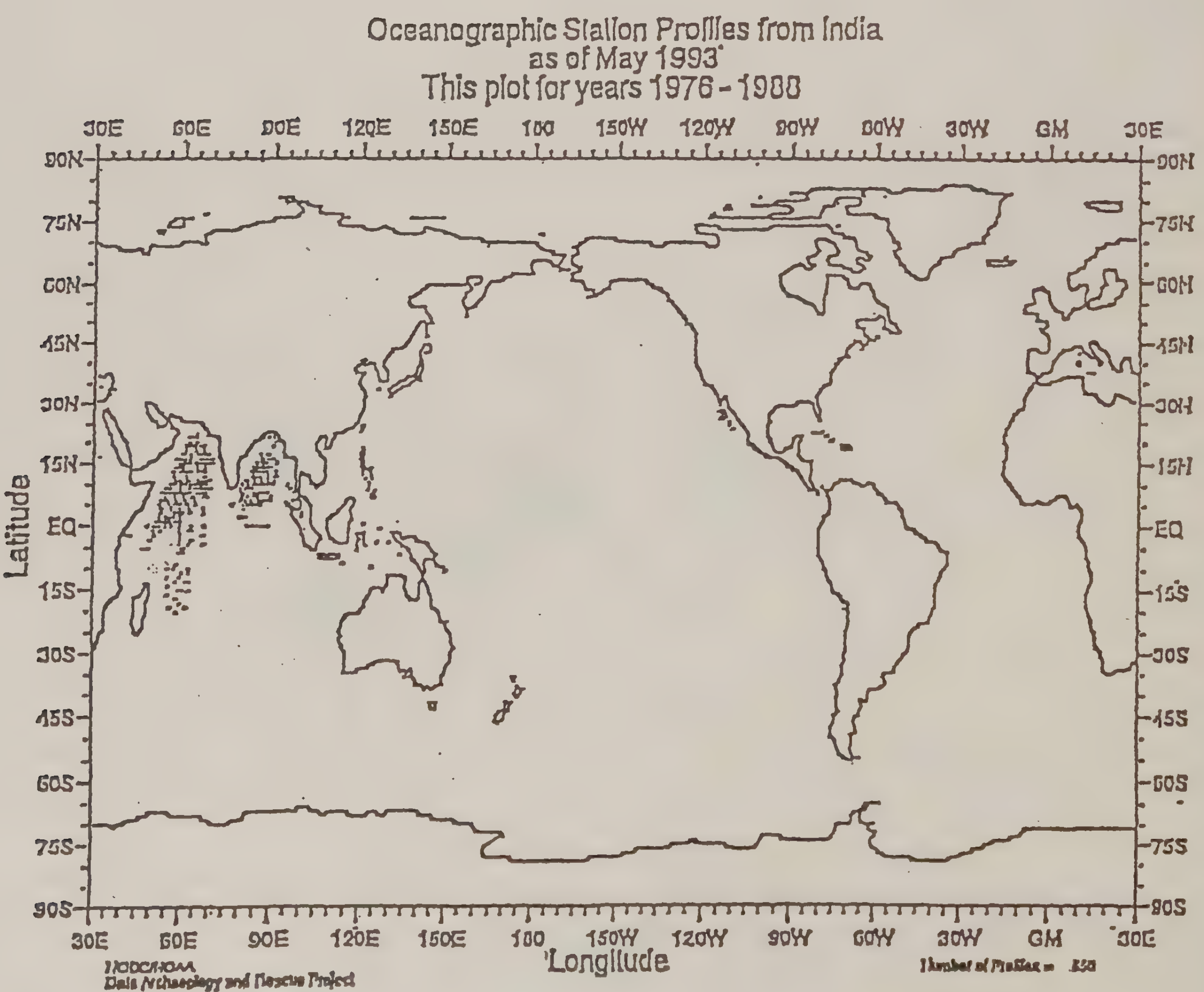


Fig 4 Station data of the India National Oceanographic Data Center

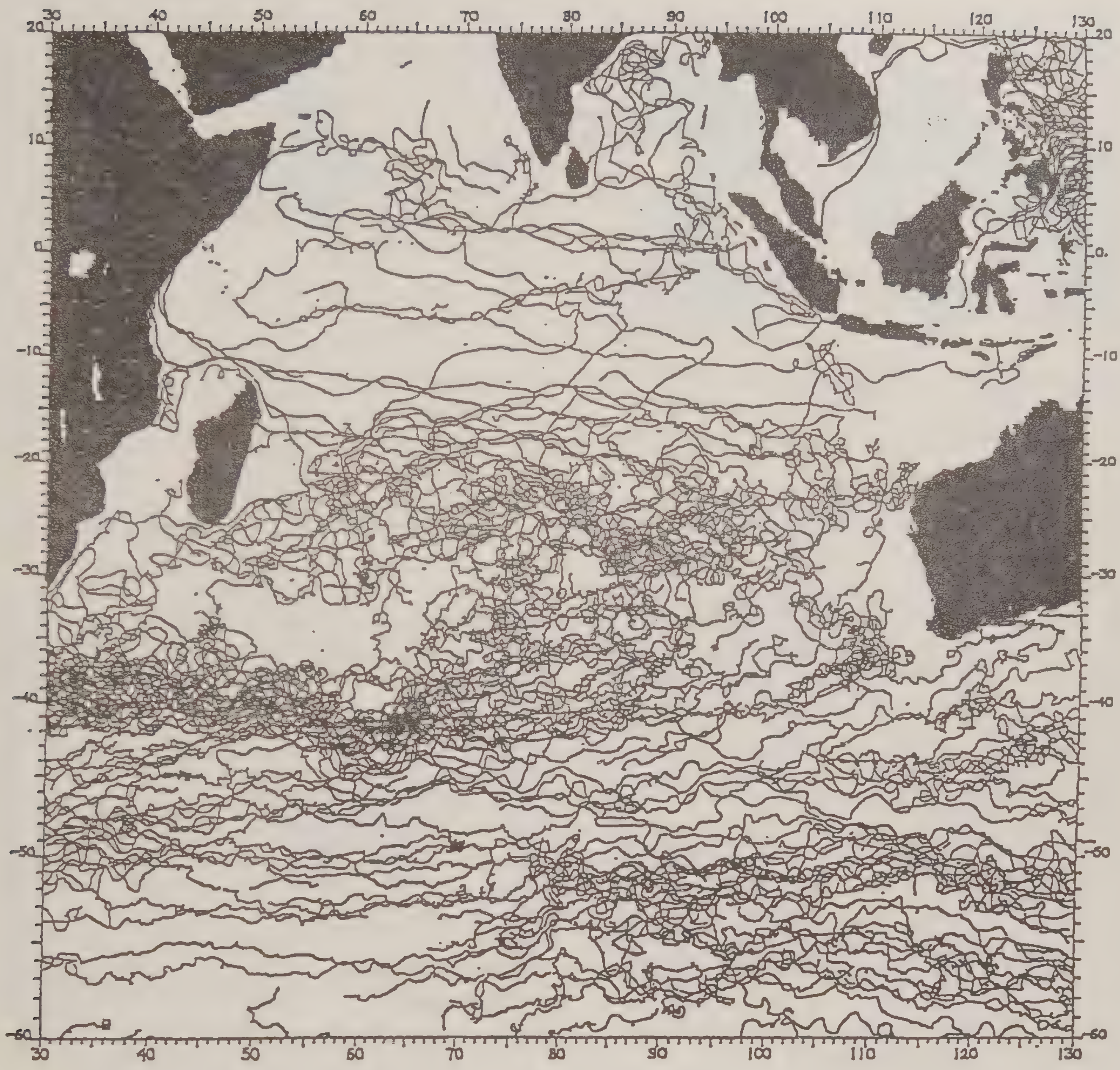
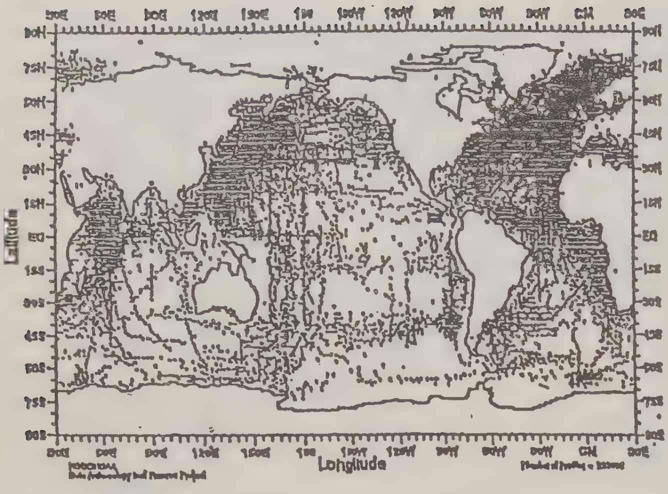
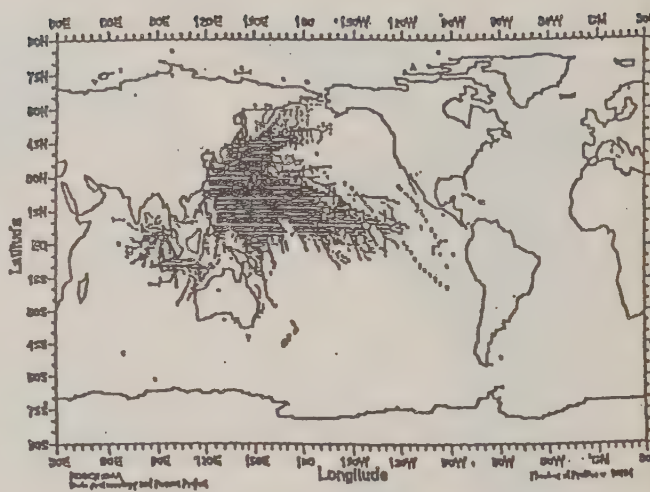


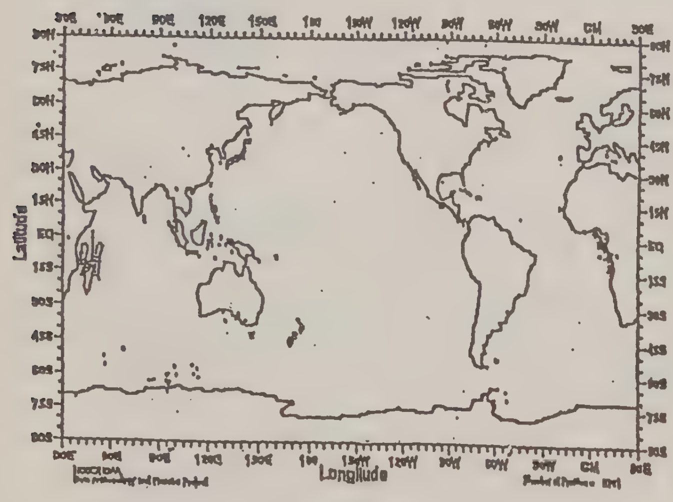
Fig 5 The wake charts of the drifting buoy data in the Indian Ocean (by MEDS)



Mechanical Bathythermographs from Russia
as of May 1993
This plot for years 1941-1988



Mechanical Bathythermographs from Japan
as of May 1993
This plot for years 1965-1985



Mechanical Bathythermographs from Ftance
as of May 1993
This plot for years 1964-1972



Oceanographic Station Profiles from Australla
as of May 1993
This plot for tears 1929-1990

Fig. 6 Major data collected by GODAR project

Table 1 The data possession situations of Indian National Oceanographic Data Center

Category	Kinds of the data	Number
Marine physical data	SD, STD/CTD/DBT, MBT, XBT, Sal., Wave, Current , etc	24,116
Marine chemical data	O2, PO4, NO3, NO2, pH, NH4, Trace metals, etc	13,286
Marine biological data	Chlorophyll, Zooplankton, Benthos, etc	3,640
Geophysical data	Depth, Gravity, Magnetic, etc	125,113

Table 2 The national investigation on the Indian Ocean

Country	Number	%	Country	Number	%	Country	Number	%
USA	105,920	54.6	INDIA	2,454	1.2	MADAGASCAR	982	0.5
AUSTRALIA	23,137	11.9	THAILAND	1,688	0.9	GERMANY	789	0.4
JAPAN	14,894	7.7	NETHERLANDS	1,616	0.8	NEW ZEALAND	650	0.3
RUSSIA	13,820	7.1	CHINA	1,419	0.7	OTHERS	1,827	0.9
ENGLAND	13,711	7.1	SOUTH AFRICA	1,274	0.7	UNKOWN	1,996	1.0
FRANCE	6,940	3.6	INDONESIA	1,036	0.5	Total	194,153	100.0

Table 3 The kinds of the ocean data on the Indian Ocean

Kinds	Number	%	Kinds	Number	%
SD	24,367	12.6	XBT	59,617	30.7
STD	564	0.3	SBT	19,690	10.1
MBT	64,376	33.1	IBT	25,539	13.2
			Total	194,153	100.0

Table 4 Data in TOGA CD-ROM data set

Data Set Name	Providing Institution	Format	Contents
AOML	NOAA Atlantic Oceanographic and Meteorological Laboratory	ASCⅡ	Drifting Buoy data
CAC	NOAA National Meteorological Center (NMC)	ASCⅡ	Sea surface temperature
ECMWF	European Center for Mediumrange Weather Forecasts	ASCⅡ	Numerical model results
FSU	Florida State University	ASCⅡ	Wind pseudo-stress
GEOSAT	NOAA National Ocean Service	ASCⅡ	Sea-surface height
GPCP	NOAA NMC	ASCⅡ	Precipitation estimates
IFREMER	TOGA Subsurface Data Center	ASCⅡ	Subsurface data
ISCCP	NASA Climate Data System	ASCⅡ	Cloud products
LODYC	Universite Pierre et Marie Curie	ASCⅡ	Atlantic model data
MEDS	Marine Environmental Data Service, Canada	ASCⅡ	Drifting buoy
NCAR	National Center for Atmospheric Research	ASCⅡ	CORDA climatologies
ORSTOM	Center ORSTOM de Brest	ASCⅡ	Wind Pseudo-stress
PMEL	NOAA Pacific Marine Environmental Laboratory	ASCⅡ	Moored current and temperature data
UHAWAⅡ	University of Hawaii	ASCⅡ	Sea level
UKMO	United Kingdom Meteorological Office	ASCⅡ	Surface data

Table 5 Types of statistical processing of " The World Ocean Atlas 1994"

Parameter	Anunal	Season	Month
Temperature	*	*	*
Salinity	*	*	*
Dissolved oxygen	*	*	
Apparent Oxygen Utilization	*	*	
Oxygen Saturation	*	*	
Phosphate	*		
Nitrate	*		
Silicate	*		

Table 6 "The World Ocean Atlas 1994"

Data already subjected to quality control

Parameter	Number of profiles
Temperature	4,553,426
Salinity	1,254,771
Oxygen	367.635
Phosphate	184.153
Silicate	110,413
Nitrate	75,403

Table 7 The number of stations in "World Ocean Database 98"

Data type	Number of Profiles
Bottle and low resolution CTD stations	1,373,440
High resolution CTD stations	189,555
MBT and DBT profiles	2,077,200
XBT profiles	1,644,911
Plankton only stations (*1	42,885
Surface only data (*2	131,823

*1 : stations with only plankton and biomass data and no physical/chemical measurements

*2 : includes ship-of-opportunity data

I. Observation and analysis on the process of the atmosphere-ocean-land interactions
大気・海洋・陸域間相互作用の諸過程に関する観測・解析研究

3. Observation and analysis on the process over the land
陸域における諸過程に関する観測研究

(1) Observation on Hydrology over the Tibetan Plateau and Himalayas
チベット・ヒマラヤにおける水文変動に関する観測研究

Shinjo Branch of Snow and Ice Studies,
National Research Institute for Earth Science
and Disaster Prevention,
Science and Technology Agency
Takeshi Sato
防災科学技術研究所
新庄雪氷防災研究支所
科学技術庁
佐藤　威

(Abstract)

In this study, automatic observation sites of snow weight (water equivalent of snow) and frozen ground depth were established at Lhasa, Rikeze and Nagqu in the Tibetan Plateau. The routinely measured data at the meteorological stations in the Tibetan Plateau was also collected. Based on these data, variations of snow cover and frozen ground together with their relation to the Asian Monsoon were analyzed. The results are summarized as follows:

By using the snow weight meter and correcting its output with the ground temperature etc., snow weight (water equivalent of snow) at Nagqu was obtained to be less than 20kg/m^2 from July, 1993 to May, 1998. The density of accumulated snow in this period was in the range of 0.1-0.4g/cm^3, which was calculated from the snow weight values and routinely measured snow depths.

Seasonal variation of the frozen ground was observed with the frozen ground depth meter, which agrees well with the routinely measured one before the midwinter. After that, the difference between them was found, which may be ascribed to the instrumental problems and the disturbances of the temperature field in the ground and of the sensor temperature.

The heat budget analysis of the ground during its freezing stage revealed that the net radiation was positive due to the strong solar radiation and suppresses the frozen ground development. On the contrary, the sum of the turbulent sensible and latent heat fluxes cool the ground in this period.

The frozen ground becomes deep as the altitude increases in the eastern part of the Tibetan Plateau. Frozen ground also forms at Lingzi and Qamdo in spite of these lower elevations. Lingzi and Qamdo are located in the south-eastern part of Tibetan Plateau where the sunshine duration during winter is less than the other parts of the plateau, which leads to the less suppression of the frozen ground development by the solar radiation. Thus the maximum frozen ground depth is not so small at Lingzi and Qamdo in spite of their lower elevations.

Warm and cold winters appeared alternately during the period of 1993-1996. The amount of summer precipitation, which is an index of the monsoon activity in the Tibetan Plateau, varied year by year. In this period, warm winter followed the wet summer with much precipitation and vice versa. The values of the coefficient α, corresponding to the efficiency of the frozen ground development, are different among the meteorological stations. They increase with the precipitation in the preceding summer at Nagqu and Qamdo,

but do not vary with it at Sogxian and Dengqen.

1. Objectives

Snow cover and frozen ground in the Tibetan Plateau have great influence not only on the Asian Monsoon activity but also on the global climate system[1]. In order to understand the mechanism of the Asian Monsoon, seasonal and inter-annual variations of snow cover and frozen ground should be clarified and the quantitative relationship between them and the Asian Monsoon activity should be studied. In this study, automatic observations of snow cover and frozen ground have been carried out since 1993 summer at three sites (Lhasa, Rikeze and Nagqu) in the Tibetan Plateau, as the cooperative study with China Meteorological Administration. The routinely measured data at the meteorological stations in the Tibetan Plateau was also analyzed.

2. Methods

2-1. Snow weight meter

The snow weight meter to measure the weight (water equivalent) of accumulated snow is almost the same as that commonly used in Japan[2] (Fig.1). Four metal wafer units placed on the ground surface are used to support the accumulated snow, in which unti-frozen liquid is filled. The snow on the metal wafer units results in the change of inner pressure within the units, which is detected by the pressure sensor and converted to the snow weight value. The ground temperature just under the metal wafer unit is measured by Pt resistance thermometer. From 96/97 winter, another Pt resistance thermometer was added at Nagqu to measure the temperature near the pressure sensor (hereafter, it is called the box temperature). These data are stored in a data logger every hour.

The snow weight meter used is suitable for the heavy snow cover in relatively warm area, such as Japan. Under such conditions, the temperature at the ground surface under the accumulated snow is almost 0℃ and it is not necessary to consider the temperature dependence of the snow weight meter. In the Tibetan Plateau except for high mountainous area, however, snow cover is not so thick as in the snowy region of Japan and the temperature variation is large. This leads to the necessity of the data correction to obtain reliable snow weight values.

After examining the variations of apparent snow weight, corresponding to the output voltage of the snow weight meter when there is no snow cover, it was found that apparent snow weight has thermal hysteresis. It is impossible to correct the snow weight values taking fully the hysteresis into account. In this study, a regressive relation between the apparent snow weight and three kind of temperatures, that is, air temperature, ground temperature or box temperature, was obtained from the data when there was no snow cover. By using this regressive relation, the snow weight values were corrected.

2-2. Frozen ground depth meter

The frozen ground depth meter (FDM2) consists of the sensor unit and controlling and recording unit installed in a box. The sensor unit is buried in the ground and the box is placed on the ground surface. As shown in Fig.2, the sensor unit of FDM2 is a FRP cylinder, 225cm long and 1.6cm in diameter, in a Silicon rubber tube. Deaired water is filled between the sensor unit and the tube. The thickness of the water around the sensor unit is 1mm. The sensor has 104 electric terminals, separated 2cm from each other, to detect the freezing of deaired water around the terminals by measuring the resistance between the detection terminals and the one common terminal. The scanning is made every two hours and results are stored in an EPROM.

In July, 1995, the frozen ground depth meter was changed from FDM2 to FDM3, whose scanning method and the sensor structure was changed. However, the principle of the measurement is the same. The structure of the FDM3 sensor unit is shown in Fig.3. A soft PVC tube is attached to the board, in which deaired water is filled. One sensor unit has 16 detection terminals in the deaired water at an interval of 2cm.

And seven units are connected to obtain a record from the ground surface to the depth of 2m. The state of the deaired water (water/ice) is detected by scanning every detection terminal.

2-3. Observations

The training of operations of the instruments and data collection was carried out for Chinese scientists in June, 1993 at the Chengdu Meteorological Institute. After that, the instruments were set at three sites (Lhasa, Rikeze, and Nagqu) in the Tibetan Plateau and continuous measurements started in July 1993. These sites are shown in Fig.4 together with the meteorological stations belonging to the Tibet Autonomous Meteorological Bureau. The locations and altitudes of the three sites are summarized in Table 1. At every site, the instruments were installed in the precinct of the meteorological station (Photo 1). The Meteorological Research Institute (MRI) installed the Automatic Weather Station (AWS) for the micrometeorological observations at the same sites. Visual inspection of the instruments has been carried out every month by the staff of the meteorological station. Data collection has been made twice a year in principle using personal computer.

Since significant snow weight was not recorded and the frozen ground did not become deep at Lhasa and Rikeze, the observations at these two sites were stopped in the summer of 1996.

3. Results

3-1. Snow weight and density

The temperature dependence of the snow weight meter is caused by the temperature dependence of the inner pressure of the fluid in the metal wafer units and the temperature drifts of pressure sensor and control circuit. To obtain the temperature dependence of the snow weight meter, the periods without snow cover were selected on referring to the albedo values measured with AWS and the routinely measured snow depth.

Figure 5 shows the time series of the snow depth at Nagqu from July 1993 to May 1998, which was observed routinely at the meteorological station. The snow depth did not exceed 10cm during this period, which was not preferable for the snow weight observation. The snowfall was not frequent and the snow cover did not last for long time, except for the 97/98 winter when serious snow disaster occurred in Tibet.

The method of correcting snow weight values was changed as follows: The relation was represented by the regression line between the daily averaged snow weight meter output and the daily averaged air, ground or box temperature. This correction yields the daily averaged value of the snow weight. The hourly value of the snow weight cannot be corrected due to the thermal hysterisis of the sensor. The snow weight (water equivalent of snow) at Nagqu from July 1993 to May,1998 was less than 20kg/m^2 and the density of accumulated snow was in the range of 0.1-0.4g/cm^3 which was calculated from the snow weight values and routinely measured snow depths.

Figure 6 shows the routinely measured snow depth and daily precipitation (upper) and the daily averaged snow weight after the correction (lower). The open circle in the lower figure is called snow pressure, which is manually obtained in the routine measurement and is the same as the water equivalent of snow. The corrected snow weight sometimes has negative values on the no snow days, which means that the correction is not perfect. However, the error in the snow weight should be within ± 3 kg/m^2. The lower figure shows that the water equivalent of snow obtained by the two methods almost agreed with each other. In February 1995, there were two major snowfalls and the snow cover lasted for about two weeks. The snow weight was 11-14kg/m^2 and the snow density was 0.15-0.2g/cm^3.

Another example is shown in Fig.7, where the upper and the lower figures are the same as in Fig.6 except that the period is from November 1997 to January 1998. Note that the snow weight is the value at 09Z after 12 December, which is corrected with the box temperature at 08Z taking the thermal hysterisis into account. The error in the snow weight should be within ± 4 kg/m^2. Also in this case, the water equivalent of snow obtained by the two methods almost agreed with each other. After the snowfall on 11 December, the snow

weight did not change so much (about 8 kg/m^2) for about one month. The snow density was between 0.2 and 0.3g/cm^3.

3-2. Seasonal variation of frozen ground

Figure 8 shows a seasonal variation of the frozen ground observed with FDM2 at Nagqu in 93/94 winter, where the daily maximum depth during the period from 04Z of the previous day to 02Z is illustrated by the black bar. The local time at Nagqu is GMT+6hours. Except in the midwinter, the soil near the ground surface sometimes melted in the daytime even if the frozen ground was thick.

Some meteorological stations in the Tibet Autonomous Region routinely measure the frozen ground depth. Their instrument is a rubber tube of about 1cm diameter, in which water is filled, and they measure the length of frozen part every morning (00Z). The rubber tube is installed in a protect tube whose inner diameter is 2.6cm. The routine data for the 93/94 winter is shown in Fig.8(b). The seasonal change of the frozen ground at Nagqu in 93/94 winter is as follows: At the beginning of winter, the soil layer near the ground surface froze in the nighttime and melted in the daytime, and the daily maximum frozen ground depth did not increase. At this stage, FDM2 sometimes could not detect a thin frozen ground layer. From the middle of November to the end of January, frozen ground layer grew and the observed data coincided with the routine data. After that, the observation indicates that the frozen ground layer was getting deep until the beginning of March and it attained maximum (158cm). However, the routine data shows that the development continued until the end of March and the maximum depth was 200cm. In spring, the frozen soil melted rapidly from the surface. This comparison shows that the observation agrees well with the routine data before the midwinter but does not after the midwinter.

In Fig.8(a), the daily frozen ground depth sometimes changed stepwise. The frozen ground depth meter scans the resistance between the detection and common terminals by eight paired terminals. The stepwise change may be due to this scanning method. Although the data at Nagqu in 94/95 winter is not shown in the figure, it has a similar tendency as in 93/94 winter.

In July, 1995, the instrument was changed from FDM2 to FDM3, whose scanning method was altered to that by one paired terminals. The example of FDM3 results is shown in Fig.9(a) and the corresponding routine data is shown in Fig.9(b). In case of FDM3, the underestimate of the maximum frozen ground depth and the stepwise change of the frozen ground depth were more serious than the case of FDM2.

The maximum frozen ground depths at Lhasa, Rikeze and Nagqu are summarized in Table 2. At Lhasa, maximum frozen ground depth was 12-15cm in 93/94 to 95/96 winters from the routine measurement, but the frozen ground layer was not detected by FDM2 in 94/95 winter. At Rikeze, the observed values with FDM2 were smaller than the routine data in 93/94 and 94/95 winters. Since the frozen ground layer at these two sites is thin and confined to near the ground surface, the ground temperature distribution around the FDM2 sensor might be different from that around the instrument used in the routine measurement.

The discrepancy between the observed and routine data in the decay stage will be discussed in the following. The ground temperatures at the depths of 80cm and 160cm in 93/94 winter were analyzed, which were measured routinely near the routine frozen ground depth meter. When the frozen ground melted at the depths of 80cm and 160cm, the routine ground temperatures at the corresponding depths were +0.6℃. This means that the temperature in the steel protect tube for the routine frozen ground depth meter was lower than the ground temperature. This may be the one of the reasons why the routinely measured maximum frozen ground depth was greater than the observation and the routinely measured frozen ground layer remained longer than the observation with FDM2.

The profile of the ground temperature is shown in Fig.10 which was routinely measured at Nagqu. The difference in the frozen ground between the observed and routinely measured in the mature to decay stages may partly be due to the fact that the ground temperature between the depths of 40cm and 160cm at these stages was close to 0°C and its vertical gradient was very small. In this situation, small disturbance of the ground and/or

sensor temperature would affect the measurement of frozen ground layer. The deaired water in the sensor unit may be hard to freeze. This is more remarkable for FDM3 with separated units than for FDM2.

3-3. Heat budget of ground during its freezing stage

The heat budget of the ground at Nagqu during the freezing stage was examined. Here, the freezing stage is defined as the 90 days period from the date when the ground temperature attains about 0°C. The routine ground temperature profiles in 93/94 and 94/95 winters were integrated to estimate the heat storage. The heat capacity for each winter was assumed based on the soil moisture observed in the autumn of 1995, amount of precipitation in the preceding summer (July to September) and the measured soil density. The soil should be wetter in 93/94 winter than in 94/95 winter since the amount of summer precipitation was greater in 1993 than in 1994. The latent heat associated with the soil freezing was also estimated with the assumed soil moisture. The net radiation in both winters observed with AWS was averaged over the period and the sum of the turbulent sensible and latent heat fluxes was obtained as the residual. The results are shown in Fig.11. Due to the strong solar radiation and low albedo, the net radiation is positive in both winters, which warms the ground and suppresses the frozen ground development. The ground is cooled only by the sum of the turbulent fluxes, whose magnitudes did not differ much between the two winters. The latent heat of freezing cannot be neglected in the heat budget.

3-4. Altitude dependence of frozen ground depth

The routinely measured frozen ground depth at the eight meteorological stations in the eastern part of Tibetan Plateau was collected (Table 3). In Fig.12, plotted are the maximum frozen ground depth (a) and the accumulated freezing index (b) against the altitude of the station. The definition of the accumulated freezing index will be defined in the next sub-section. The frozen ground becomes deep as the altitude increases in the eastern part of the Tibetan Plateau. Frozen ground also forms at Lingzi and Qamdo in spite of their lower elevations. The increasing tendency of the accumulated freezing index with the altitude is almost the same as that of the maximum frozen ground depth. At Lingzi and Qamdo, whose elevations are low, the index is slightly large. According to the heat budget analysis of the ground during its freezing stage described above, the net radiation is positive and it suppresses the development of the frozen ground. Lingzi and Qamdo are located in the south-eastern part of the Tibetan Plateau and the sunshine duration during winter is less than the other parts of the plateau, which leads to the less suppression of the frozen ground development. Thus the maximum frozen ground depth is not so small at Lingzi and Qamdo in spite of their lower elevations.

3-5. Inter-annual variation of frozen ground depth

It was found from the routine data during the period of 1993-1996 that warm and cold winters appeared alternately (Fig.13(a)). The amount of summer precipitation, which is an index of the monsoon activity in the Tibetan Plateau, varied year by year (Fig.13(b)). In case of 1993-1996, warm winter followed the wet summer with much precipitation and vice versa. The winter meteorological conditions were different from year to year as mentioned above and the development of the frozen ground should be affected by these conditions.

The maximum frozen ground depth D (cm) can roughly be expressed by the following equation[3]:

$$D=\alpha\sqrt{I}, \quad (1)$$

where I (°C·day) is an accumulated freezing index defined by

$$I=\Sigma T. \quad (2)$$

Here, T (°C) is a daily mean ground surface temperature, and the summation is made for only negative values of T. The coefficient α defined by Eq.(1) represents the efficiency of frozen ground development, depending on the soil characteristics such as soil components and soil moisture. The values of α are different among the eight stations, which are listed in Table 3. At Nagqu, α is much larger than 2.0-2.5, which were obtained in Hokkaido, Japan, where the soil would be wetter than Nagqu.

Figure 14 shows the relationship between α at the stations where the maximum frozen ground depth exceeds 40cm and the amount of precipitation during July and August in the preceding summer. They increase with the summer precipitation at Nagqu and Qamdo, but do not vary with it at Sogxian and Dengqen. The soil moisture in winter is considered to be large after wet summer with much precipitation, although the weather conditions in autumn may affect it. The result that α is large under wet soil condition is different from the numerical study[4] showing that the frozen ground does not develop when the soil is wet.

4. Discussions

The snow cover and the frozen ground affect not only the regional but also the global climate system such as the Asian Monsoon through the interactions between the atmosphere and the ground surface. The amount of the accumulated snow is represented by its area, depth and weight (water equivalent). Snow cover area can be estimated by using various remote-sensing techniques. Present study introduced the snow weight meter and could observe the snow weight values, which will be helpful for interpreting the satellite images. In the future, however, the sensitivity of the snow weight meter should be improved for the use in light snow cover area and its temperature dependence should be improved. Present study introduced two types of the frozen ground depth meter. At the present time, both still have some problems for the automatic, continuous and accurate observation of the frozen ground depth. The ground temperature observations at many depths in the ground is a realistic way to obtain the frozen ground depth.

5. References

1) Yasunari, T., A. Kitoh, and T. Tokioka: Local and remote responses to excessive snow mass over Eurasia appearing in the northern spring and summer climate., *Journal of Met. Society of Japan*, 69, 1033-1049, 1991

2) Kimura, T.: Observation of water equivalent of snow cover by metal wafer., *Report of the National Research Center for Disaster Prevention*, 31, 203-217 (in Japanese with English abstract) , 1983

3) Kinosita, S. (ed.): Physics of frozen ground., Morikita Shuppan, 227pp. (in Japanese) , 1982

4) Yamazaki, T., A. Nishida and J. Kondo: Seasonal frost depth of grounds with bare surface, snow cover and vegetation., *Seppyo*, 60, 213-224 (in Japanese with English abstract), 1998

6. Publications

①Scientific Journal

Gong, Y., T. Duan, L. Chen, W. Li, S. Haginoya and T. Sato : Outline of observational study of PRC-JAPAN cooperative program on Asian Monsoon over Tibetan Plateau., *Journal of Chengdu Institute of Meteorology*, 12(No.1), 18-27 (in Chinese), 1997

Zhu, K., J. Wang, T. Duan, L. Chen, W. Li, S. Haginoya and T. Sato : Periodic oscillation analysis of the thermal factors on Tibetan Plateau., *Journal of Chengdu Institute of Meteorology*, 12(No.1), 28-37 (in Chinese), 1997.

Sato, T and T. Kimura. : Observation of hydrology over the Tibetan Plateau and Himalayans., *Recent progress in studies of Asian Monsoon mechanism*, 17-29, 1999

Sato, T. : Snow cover and frozen ground observations in Tibet., (to be submitted), 1999.

7. International cooperation

The observations of the snow weight and frozen ground have been carried out as the cooperative study with China Meteorological Administration. The researcher from the National Research Institute for Earth Science and Disaster Prevention (NIED) visited Tibet in June to July 1998 for the data collection and

maintenance of the instruments. NIED invited three Chinese scientists (Prof. Duan Tingyang from the Chengdu Institute of Meteorology, Dr. Gusang Quji and Dr. Liu Yijun from the Tibet Autonomous Meteorological Bureau) for 5 days in November 1998. During thier stay in Japan, we discussed the results of the observation and analysis. The researcher from NIED visited Beijing in March 1999 to attend the 3rd China-Japan workshop on Asian Monsoon mechanism and the 7th Working Group Meeting.

（要旨）

本研究では積雪重量（相当水量）、凍結深度の自動観測点をチベット高原に３ヶ所（ラサ、シガセ、ナチュ）に設置し、長期間のデータを蓄積するとともに、チベット高原東部にある気象官署のルーチンデータを収集し、積雪、凍土の変動ならびにそれらとアジアモンスーンの関係を解析している。得られた結果は以下の通りである。

ラサ、シガセでは積雪はほとんどなく、ナチュでは年に数回の積雪があるものの、積雪深は10cm程度以下で長続きしない。積雪重量計の温度特性を補正することで観測値の精度を向上させたが、ナチュにおける積雪重量は観測期間中$20kg/m^2$を越えることはなかった。また、ナチュにおける積雪重量と積雪深（ルーチン観測値）から求めた積雪密度は$0.1-0.4g/cm^3$であった。

凍結深度の観測値とルーチン観測値を比べたところ、凍土の発達過程では概ね一致するものの、最大凍結深は過小評価されることが判明した。この原因として、地中の温度勾配が小さいために、わずかな温度の誤差や場所による違いによって凍結深の値が大きく変わる可能性、ならびにセンサー直上の地上部に制御・記録部の収納箱があるという構造上の問題点が示唆された。

本観測と並行して気象研究所が行っている気象観測の結果を用い、ナチュにおける凍土の発達過程（90日間）の平均的な熱収支を、土壌の熱物理定数と含水率を推定して求めた。この結果、土壌は乱流熱輸送により冷却していて、正味放射はこの冷却を妨げていることが明らかになった。また、土壌水分の凍結による潜熱の放出量が貯熱量の変化に匹敵することが明らかとなった。

チベット高原東部の気象官署のルーチンデータを解析した結果、最大凍結深は標高とともに増大するが、南東部のリンチとチャンドゥではこの傾向からはずれることが分かった。この２地点では冬期の日照が少ないため、前述の放射が凍土の発達を抑制する作用が弱いことがこの原因として考えられる。また、モンスーン活動度の指標の一つである夏期（７～８月）の降水量、地表面温度から求めた積算寒度Ｉ、最大凍結深Ｄの関係を解析した。この結果、夏期の降水量が多い年の翌冬は暖冬傾向にあること、及びＤ／√Ｉで定義される係数α（凍上の発達度の目安）が大きな官署においては、αは前の夏の降水量が多いと大きくなる傾向にあることを見出だした。

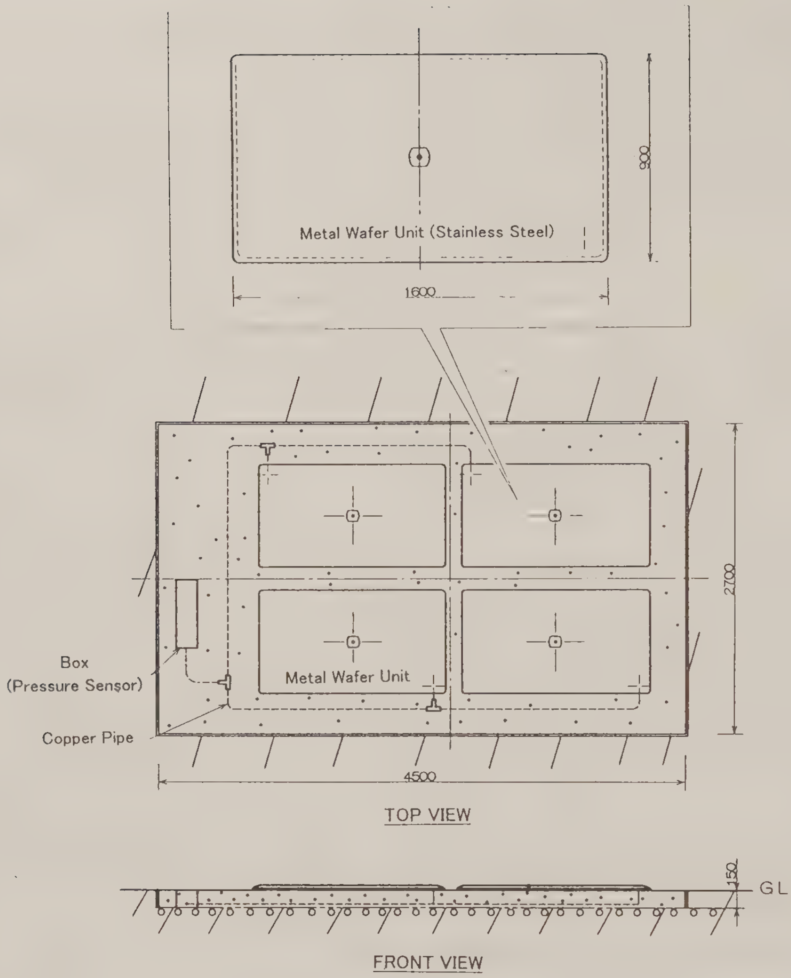


Figure 1 Snow weight meter.
積雪重量計.

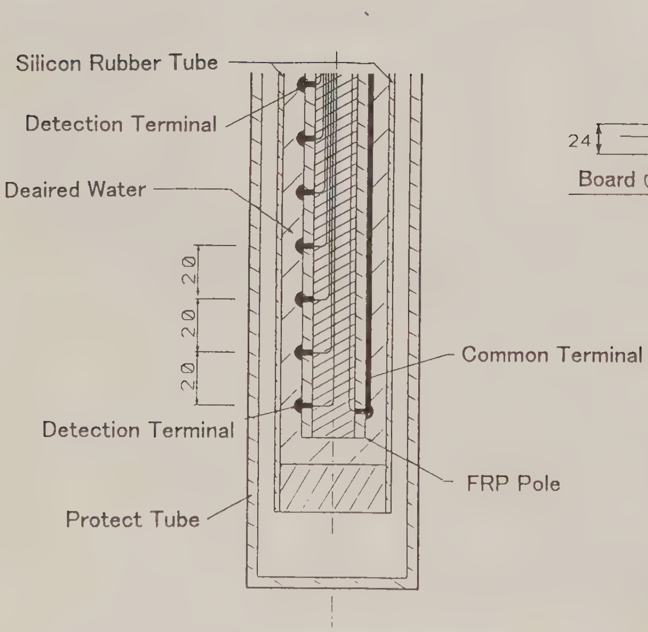


Figure 2 Sensor unit of frozen ground depth meter (FDM2).
凍結深度計のセンサーユニット (FDM2).

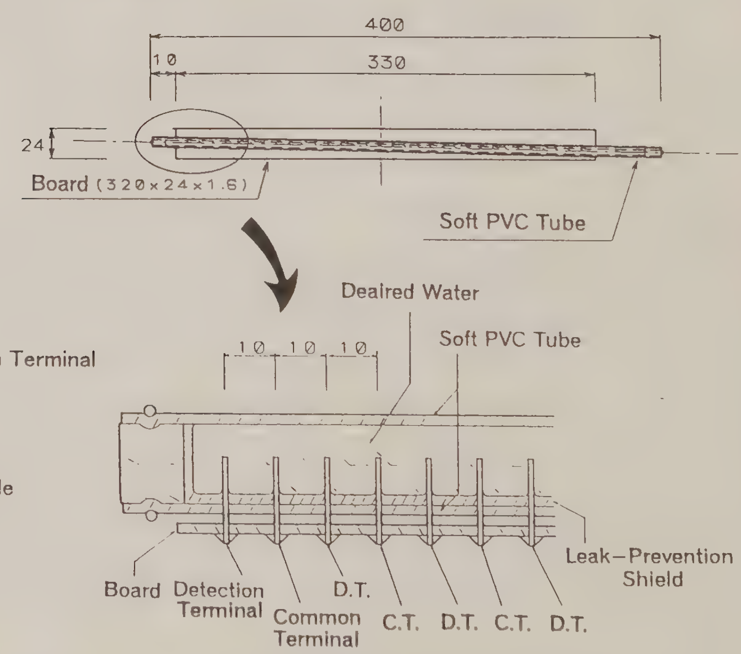


Figure 3 Sensor unit of frozen ground depth meter (FDM3).
凍結深度計のセンサーユニット (FDM3).

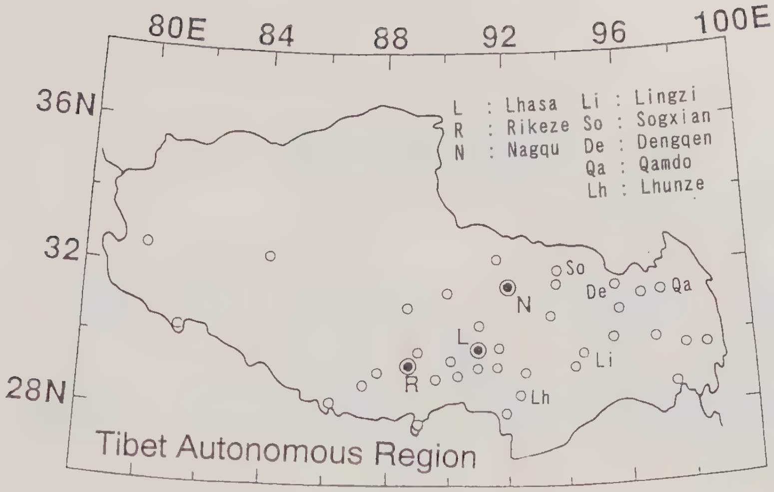


Figure 4　Locations of observation sites (◉) and meteorological stations belonging to the Tibet Autonomous Meteorological Bureau (○).
観測地点 (◎)とチベット気象局の気象官署 (○).

Table 1　Locations and altitudes of observation sites.
観測地点の位置と標高

Site	Long.(E)	Lat.(N)	Altitude(m)
Lhasa	91°08′	29°40′	3649
Rikeze	88°53′	29°15′	3836
Nagqu	92°04′	31°29′	4507

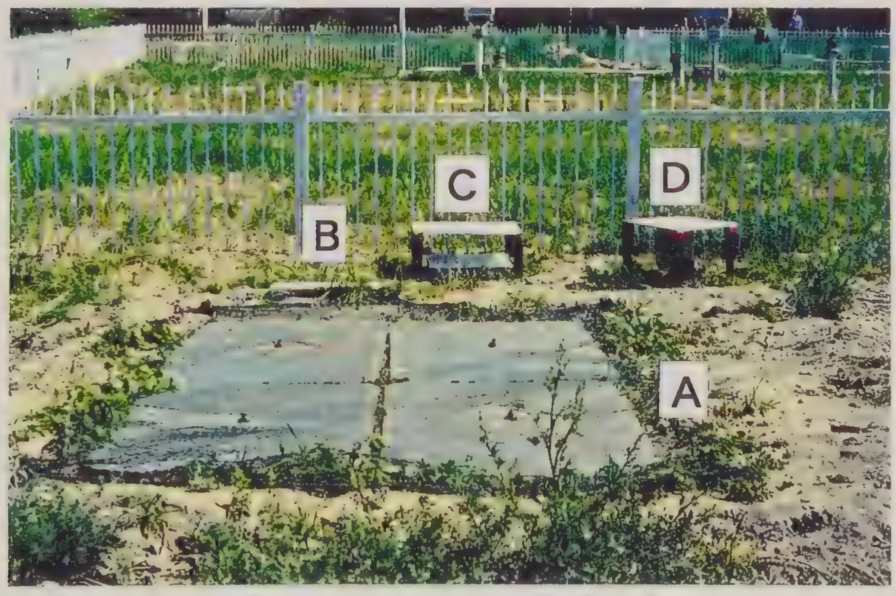


Photo 1　Snow weight meter (A-C) and frozen ground depth meter (D) at Lhasa.
A: metal wafer unit, B: pressure sensor, C: container box.
ラサに設置した積雪重量計 (A-C) と凍結深度計 (D).
A: メタルウェハーユニット, B: 圧力センサー, C: 収納箱.

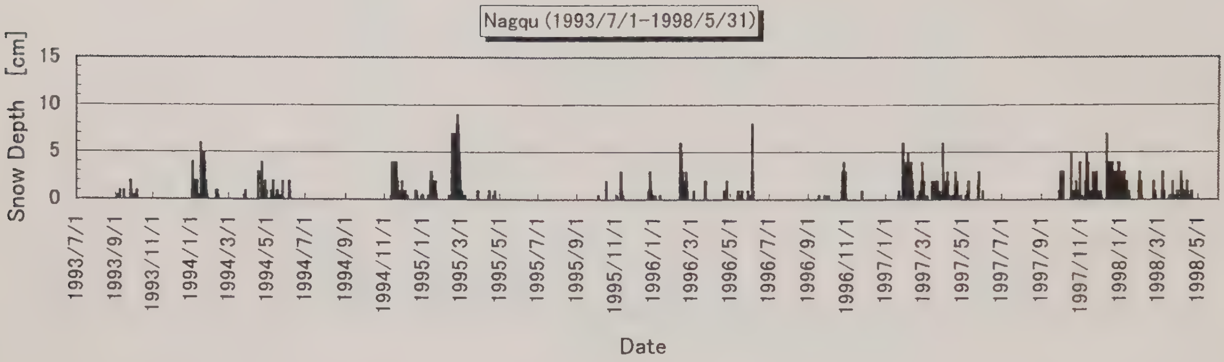


Figure 5 Time series of snow depth measured routinely at Nagqu.
ナチュにおける積雪深の変化(ルーチン観測).

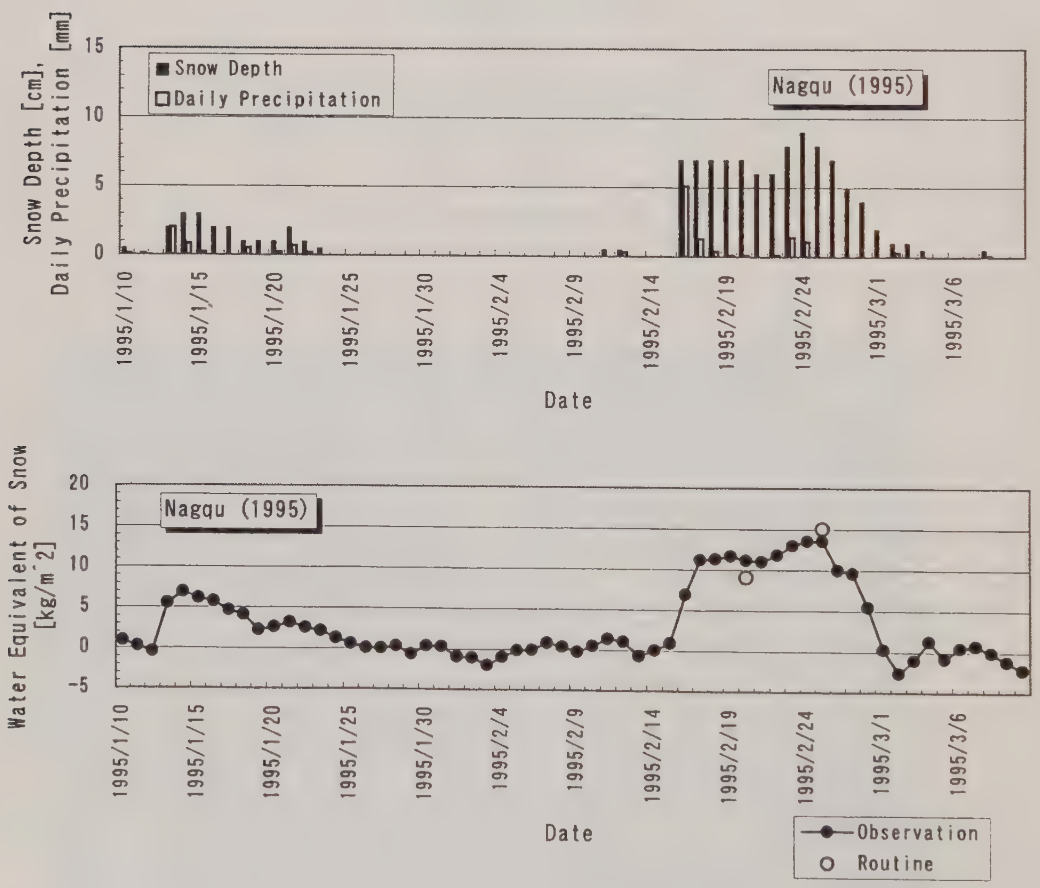


Figure 6 Time series of snow depth, daily precipitation (upper) and snow weight (water equivalent of snow)(lower) at Nagqu from January to March 1995.
1995年1月～3月のナチュにおける積雪深及び日降水量(上図)と積雪重量(積雪相当水量)(下図).



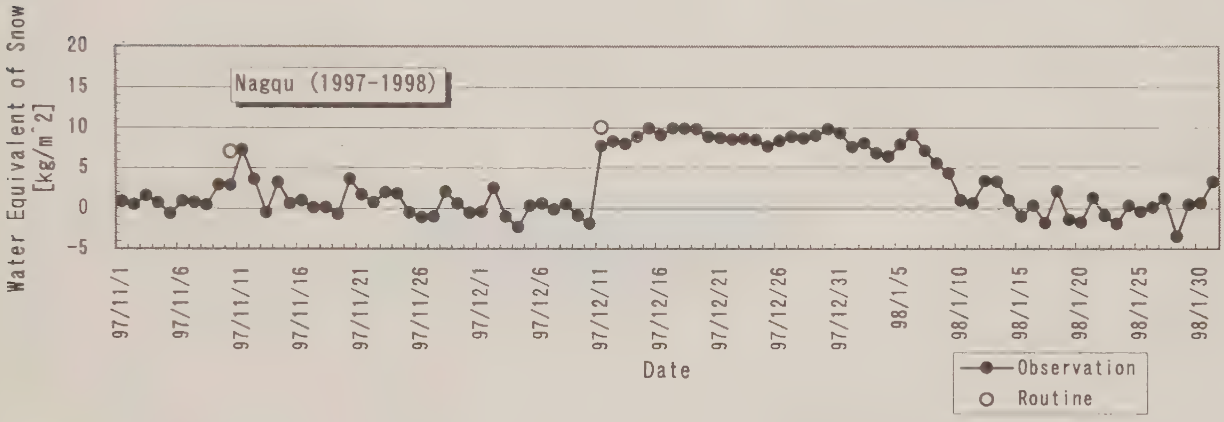


Figure 7　Time series of snow depth, daily precipitation (upper) and snow weight (water equivalent of snow)(lower) at Nagqu from November 1997 to January 1998.
1997年11月～1998年1月のナチュにおける積雪深と日降水量(上図)
及び積雪重量(積雪相当水量)(下図).

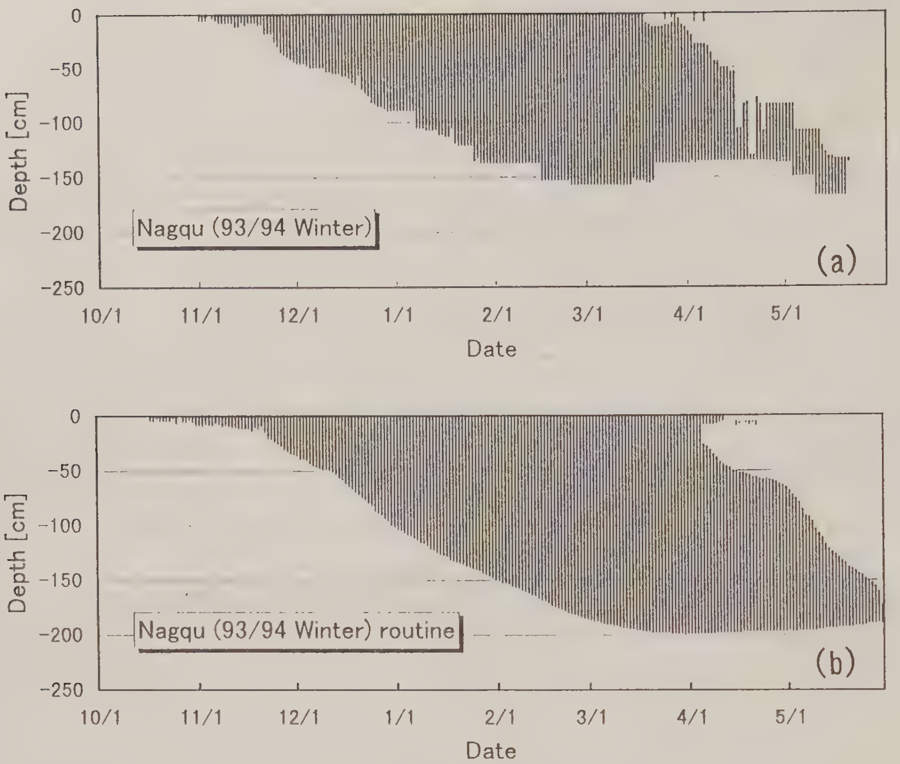


Figure 8 Seasonal variation of the frozen ground observed with FDM2 (a) and that routinely measured (b) at Nagqu in 93/94 winter.
93/94冬期にナチュでFDM2により観測した凍結深度(a)とルーチン観測による凍結深度(b).

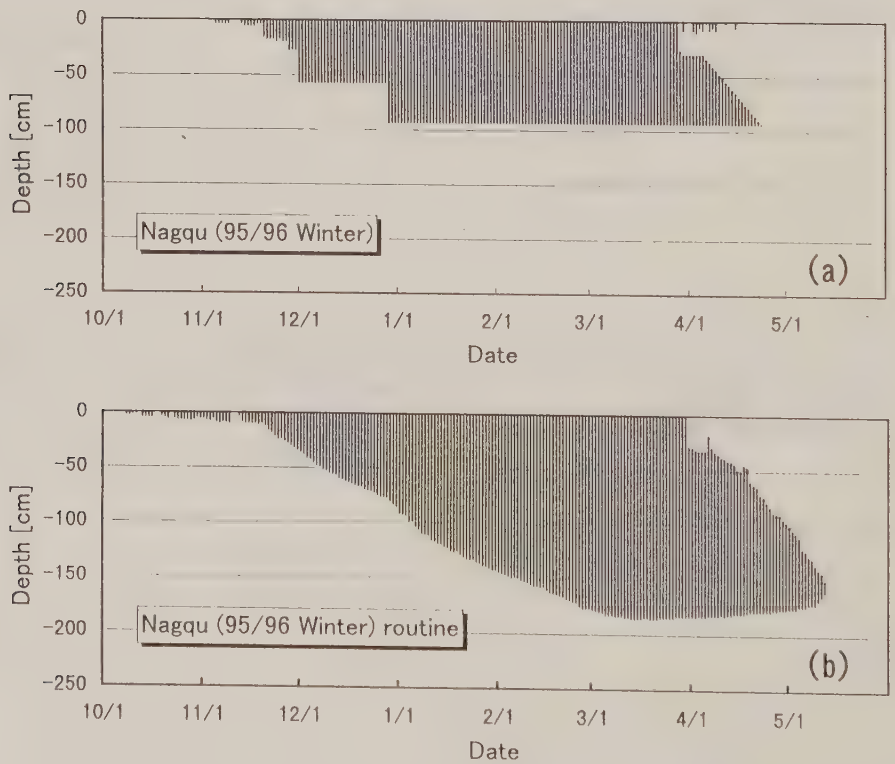


Figure 9 Seasonal variation of the frozen ground observed with FDM3 (a) and that routinely measured (b) at Nagqu in 95/96 winter.
95/96冬期にナチュでFDM3により観測した凍結深度(a)とルーチン観測による凍結深度(b).

Table 2　Summary of the maximum frozen ground depth.
最大凍結深度のまとめ

Site / Winter	Lhasa		Rikeze		Nagqu	
	Obs.	Routine	Obs.	Routine	Obs.	Routine
93/94	-	13	12	35	158	200
94/95	0	15	12	42	134	177
95/96	12	12	-	26	94	186
96/97					96	195
97/98					84	199

- : lack of data due to instrumental errors.

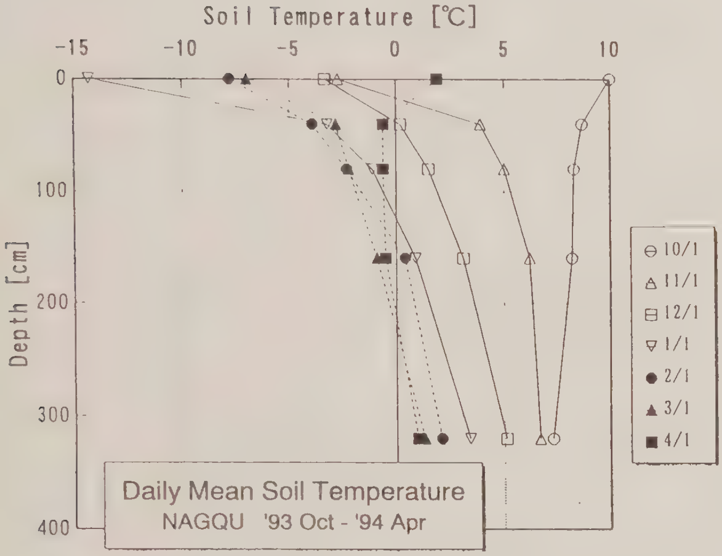


Figure 10　Routinely measured ground temperature profile at Nagqu in 93/94 winter.
93/94冬期のナチュにおける地温分布(ルーチン観測).

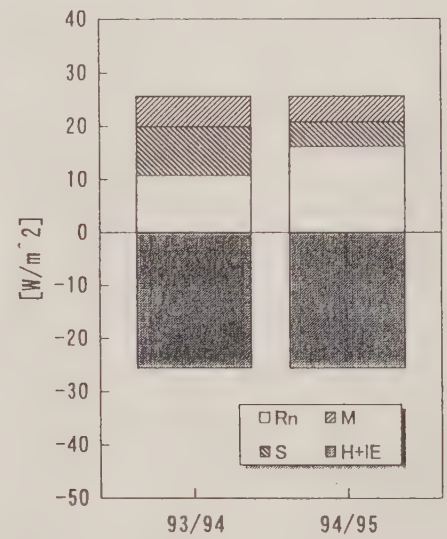


Figure 11 Heat budget of the ground during the freezing stage (Nagqu).
Rn: net radiation, S:heat storage, M:latent heat of freezing, H+lE: sum of the turbulent sensible and latent heat fluxes.
ナチュにおける凍土発達期の熱収支
Rn:正味放射, S:貯熱量, M:凍結潜熱, H+lE:顕熱と潜熱の和.

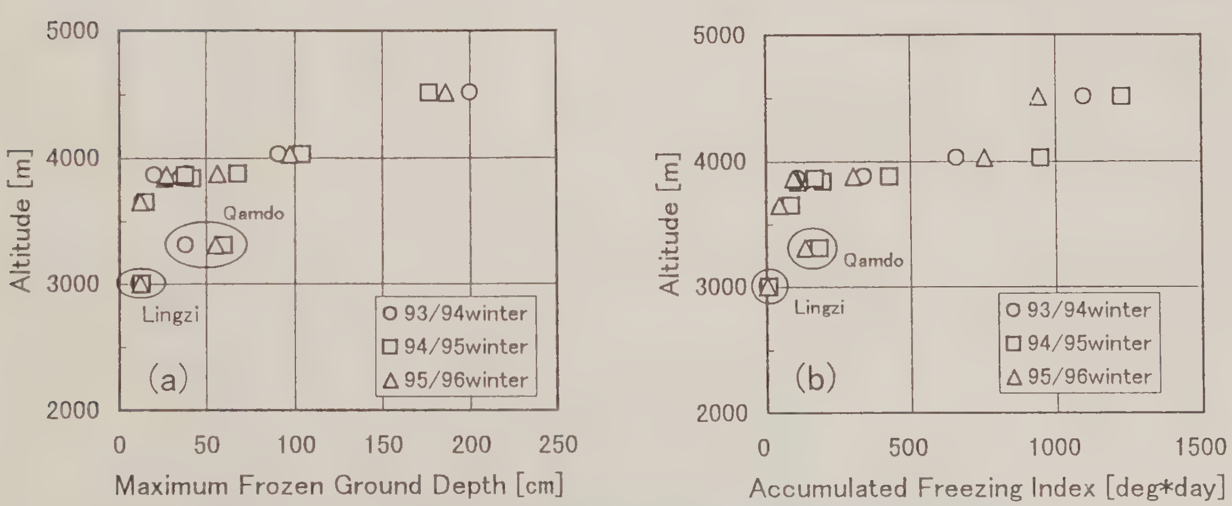


Figure 12　The relationship between the maximum frozen ground depth and the altitude of meteorological station(a) and that between the accumulated freezing index and the altitude(b) .
気象官署の最大凍結深と標高の関係(a)及び積算寒度と標高の関係(b).

Table 3 Summary of accumulated freezing index, the maximum frozen ground depth, coefficient α and precipitation in the preceding summer. Values are routinely measured.
ルーチン観測から得られた積算寒度、最大凍結深、係数 α 及び前年夏の降水量のまとめ.

Station Name	Altitude (m)	93/94winter				94/95winter				95/96winter			
		Accumulated Freezing Index (deg*day)	Maximum Frozen Ground Depth (cm)	α	1993 Jul-Aug Precipitaion (mm)	Accumulated Freezing Index (deg*day)	Maximum Frozen Ground Depth (cm)	α	1994 Jul-Aug Precipitaion (mm)	Accumulated Freezing Index (deg*day)	Maximum Frozen Ground Depth (cm)	α	1995 Jul-Aug Precipitaion (mm)
Lhasa	3650	75	13	1.5	289	86	15	1.6	167	44	12	1.8	300
Rikeze	3837	135	35	3.0	228	197	42	3.0	123	110	26	2.5	288
Nagqu	4508	1099	200	6.0	241	1230	177	5.0	67	940	186	6.1	247
Lingzi	3001	0.3	11	20.1	333	8	13	4.5	203	2	12	7.7	290
Sogxian	4023	656	91	3.6	328	950	104	3.4	105	752	97	3.5	234
Dengqen	3874	340	39	2.1	357	427	68	3.3	89	302	56	3.2	273
Qamdo	3307	154	38	3.1	350	183	60	4.4	84	132	55	4.8	190
Lhunze	3861	108	20	1.9	109	171	38	2.9	163	93	27	2.8	123

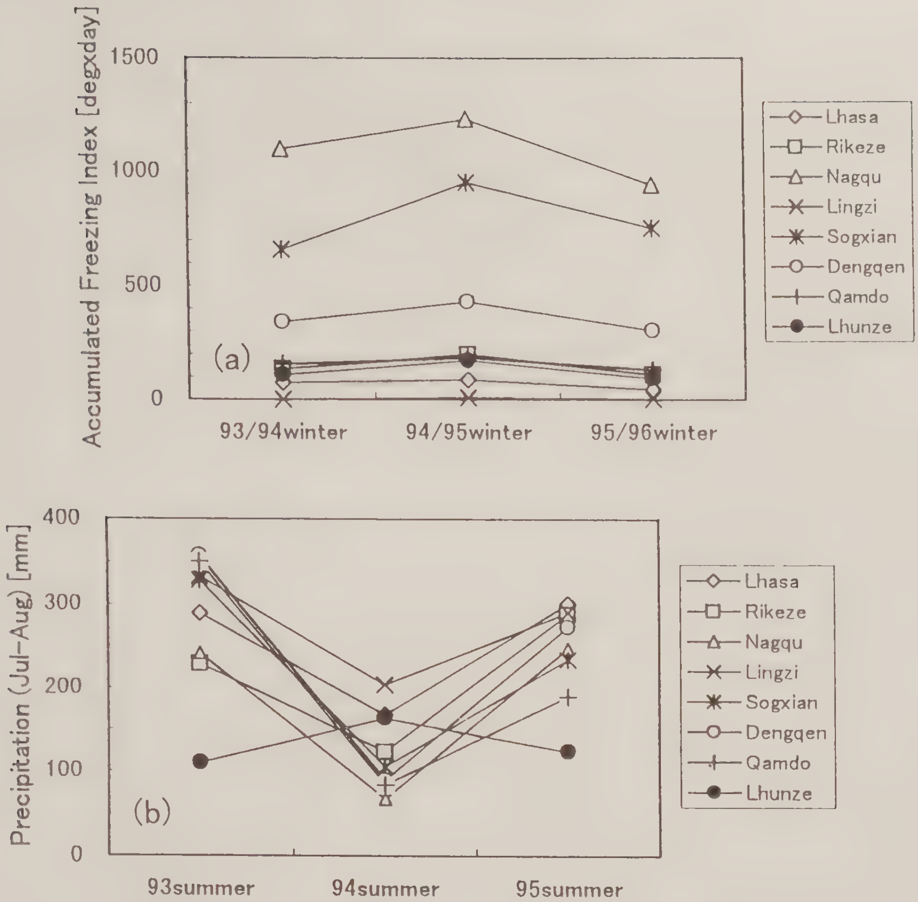


Figure 13　Inter-annual variations of the accumulated freezing index (a) and the amount of precipitation in summer (Jul.-Aug.)(b). The precipitation data at Lhunze may be bad.
積算寒度(a)と前年夏(7月－8月)の降水量(b)の年々変動.
Lhunzeの降水量は不良データかもしれない.

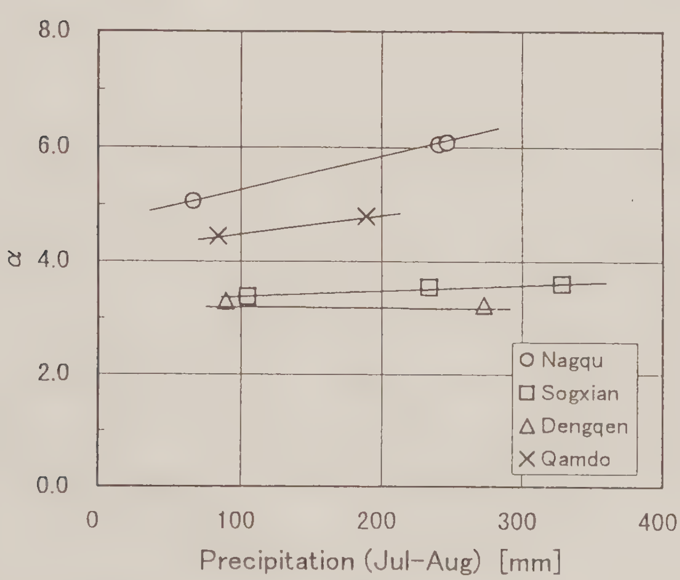


Figure 14　Relationship between the coefficient α and the amount of precipitation in the preceding summer (Jul.-Aug.) at the stations where the maximum frozen ground depth exceeds 40cm.
最大凍結深が40cmを越える気象官署における係数αと前年夏(7月－8月)の降水量の関係.

I. 大気・海洋・陸域相互作用の諸過程に関する観測・解析研究

I. Observation and analysis on the process of atmosphere-ocean-land interactions

3. 陸面における諸過程に関する観測・解析研究

3. Observation and analysis of over the land

(2) 地表面熱収支に関する観測研究

(2) Observational study of ground surface heat budgets

郵政省通信総合研究所

Communications Research Laboratory

Ministry of Posts and Telecommunications

増田 悦久, 大野 裕一, 足立 樹泰

Yoshihisa Masuda , Yuichi Ohno, and Tatsuhiro Adachi

Abstract

The Communications Research Laboratory (CRL) has been developed five boundary layer radars (BLR) for continuous monitoring of vertical profiles of wind velocity vectors and virtual temperature in the atmospheric boundary layer with good time-height resolution. We have observed wind profiles by a BLR at Bangkok, Thailand, since 1993, as a cooperative research with the King Monkut's Institute of Technology Ladkrabang (KMITL). In this paper, we will show seasonal and diurnal variability of the wind profiles and discuss activity of the Asian monsoon.

1. Objectives

A boundary layer radar (BLR) is a remote sensor measuring a height profile of wind velocity and virtual temperature in the atmospheric boundary layer. The most significant feature of the BLR is superior time-height resolution, which enables us an approach to smaller scale (meso- and micro-scale) phenomena. Recently small atmospheric waves such as gravity waves are considered to play an important role in global atmosphere dynamics. We believe that a study of detailed atmospheric structure can be a key to further understanding of the global atmosphere. Our purpose of this study is to demonstrate utility of the BLR for continuous monitoring of atmosphere dynamics such as Asian monsoon.

2. Methods

The BLR is one of the Doppler radars, which can detect Doppler frequency shift

proportional to the radial (line-of-sight) velocity of the radar targets such as atmospheric turbulence and rain-drops. By steering an antenna beam of the BLR into at least three directions, we can derive three components of a wind velocity vector of the targets from the projection components measured by the each beam direction. The BLR can derive vertical profiles of three dimensional wind velocity and turbulence intensity from clear air turbulence, and horizontal wind velocity, rain intensity, and rain drop-size distribution from precipitation particles, respectively. Table 1 shows a basic specification of the BLR [1].

Table 1: Specification of the BLR.

Frequency	1357.5 MHz (L-band)
Transmit peak power	1 kW
Averaged power	50 W
Range resolution	75 m, 150 m, 300 m
Radar type	Monostatic pulse Doppler radar
Antenna type	Parabolic Antenna (4 m in diameter)
Antenna beam width	3.9 °
Beam direction (Azimuth °, Zenith °)	(0, 0), (90, 15), (0, 15)
Time resolution	5 min for three beam directions
Location	KMITL, Bangkok, Thailand

The BLR is a monostatic pulse Doppler radar with a parabolic antenna of 4 m in diameter, which is operating 1327.5 MHz in the L-band with a peak power of 1 kW. Time-height resolution is typically 5 min and 150 m, respectively by mechanically steering the antenna beam into one vertical and two oblique directions.Height coverage of the BLR reaches typically 3 km and more than 6 km for the targets of clear air turbulence and precipitation particles, respectively. The lowest boundary of the height coverage depends on transition time required for transmission-reception (TR) switching. For the BLR, the lowest height range is about 300 m. The height coverage is also affected by intense spurious signals due to ground and sea clutters, insects, birds, air plain and so on.

3. Results

Measurement Accuracy of the BLR

We carried out simultaneous observations of the BLR and radiosondes to verify measurement accuracy of wind velocity by the BLR during November 15-23, 1993. The radiosonde could measure a wind velocity profile by tracking the position based on the omega navigation system. We launched the radiosondes from CRL, Tokyo, which was the BLR site during the observations.

Figure 1 shows scatter plots comparing eastward and northward wind velocity

components between the BLR and radiosondes, where 1370 data points were obtained

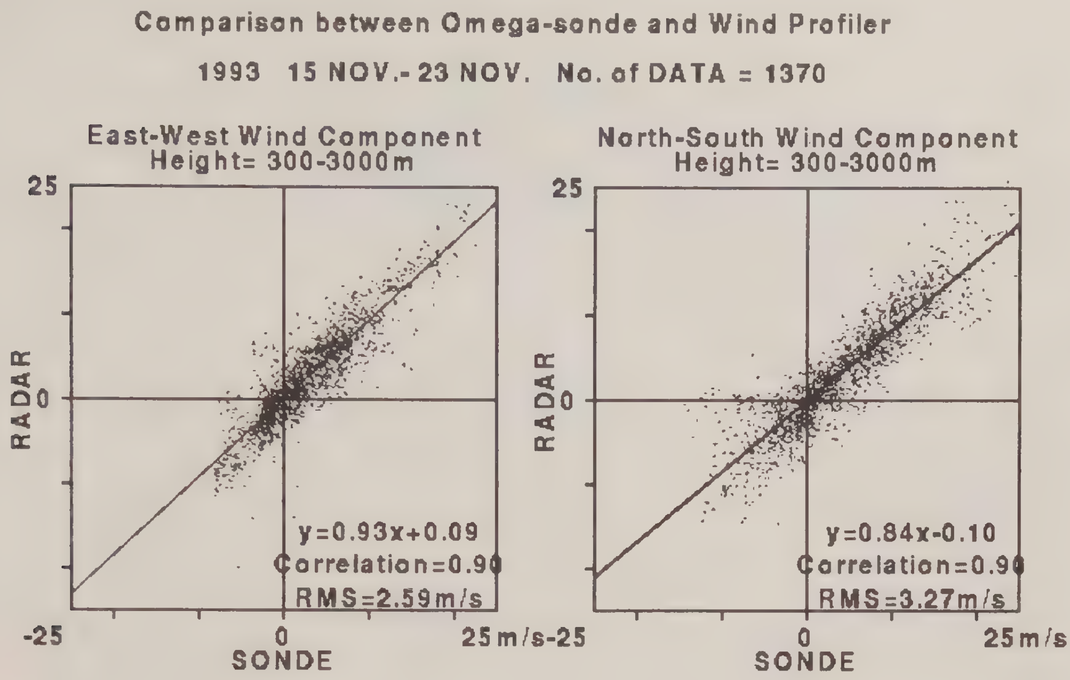


Figure 1: Comparison of wind velocity derived from the BLR and radiosondes.

from 300 m to 3000 m in altitude. The result by the two sensors agreed quite well, although some outliers were seen. A solid line indicates a good linear correlation of the two, where the correlation coefficient was 0.9. We consider that the measurement accuracy will be enhanced, when a sophisticated data processing algorithm is developed to screen off the outliers.

Seasonal Variation of Wind Profiles at Bangkok

In this section, we investigate seasonal variation of wind profiles at Bangkok. Annual climate at Bangkok can be classified into rainy and dry seasons, which are from April to September, and from October to March, respectively. The Asian monsoon generally blows southwestward during the dry season, inversely, northeastward during the rainy season.

Figure 2 shows the seasonal variation of wind velocity vectors averaged over 10 days at Bangkok from 1994 to 1996. Some data blanks were due to low signal to noise ratio or system troubles. We clearly found that a dominant wind direction was eastward from May to September, and westward from November to March. Transition of the wind directions occurred in April and October. These characteristics were consistent with a general model of the Asian monsoon. The wind speed was larger during the rainy season rather than during the dry season. which was probably due to active thermodynamic

phenomena excited by much solar heating during summer in the Northern Hemisphere. As for inter-seasonal variation, we could see a significant year to year variability. The

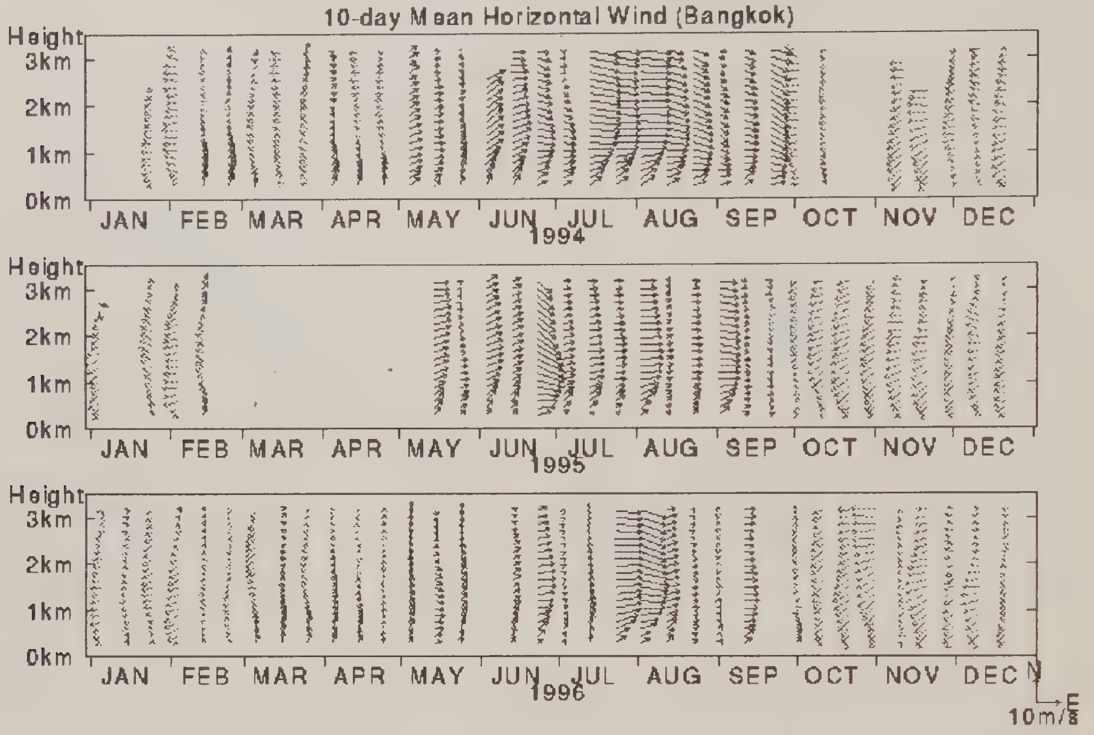


Figure 2: Time-height cross-section of horizontal wind velocity at Bangkok from1994 to 1996.

wind speed of the rainy season in 1994 was generally larger than that of any other seasons, however that in 1996 was quite small except from the end of July to the beginning of August. We could find an oscillating fluctuation of the wind speed with a period of about a month in the rainy season in 1995. The inter-seasonal variability could be related to some larger scale phenomena such as the El Nino activity.

Diurnal Variation of Wind Profiles at Bangkok

We here focus on diurnal variation of wind velocity profiles during the rainy and dry seasons at Bangkok. Figure 3 shows a time-height cross-section of horizontal wind velocity vectors, where every vector of the same local time and altitude was averaged during the rainy and dry seasons, respectively. The wind direction above 1 km in altitude agreed with the direction of the Asian monsoon, however, northward components became dominant for both the rainy and dry seasons below 1 km, suggesting that a local circulation near the surface. The northward components were small in the daytime and large in the nighttime, which was inconsistent with a land-sea breeze theory that a sea breeze occurred during daytime, because the radar site located

at the north of the gulf of Thailand. We considered that a local terrain effect produced the northward components.

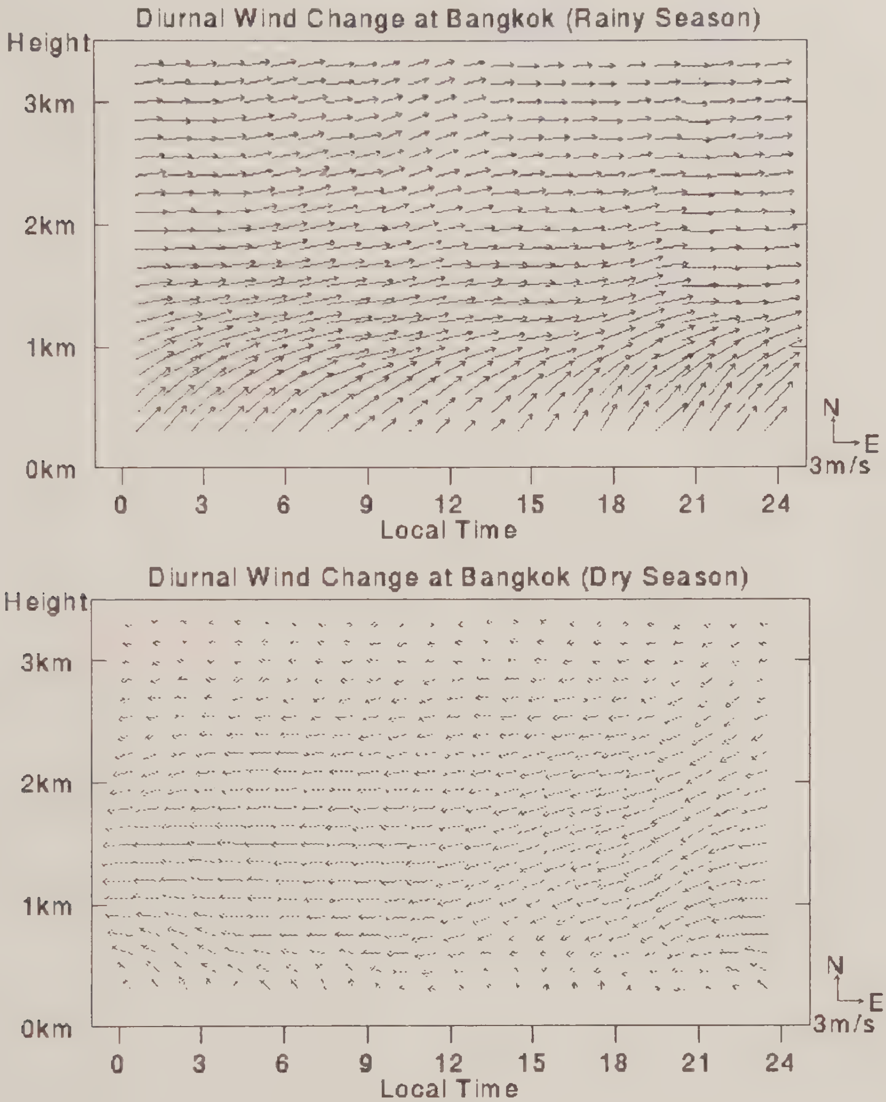


Figure 3: Time-height cross-section of diurnal wind velocity.

4. Discussions

This paper proved that the BLR was a useful remote sensor for observing wind velocity profiles in the atmospheric boundary layer. We have observed the wind velocity profiles at Bangkok Thailand since 1993, and found that the seasonal variation of wind velocity generally agreed with a typical model of the Asian monsoon, however the inter-seasonal variation had significant year to year variability especially during the rainy season. The diurnal variation of wind velocity suggested a local circulation below 1 km in altitude.

We consider that the BLR can measure momentum flux and sensible heat flux transported to upper atmosphere by using an eddy correlation method. However, we have not obtained reliable flux values, because it is still difficult to reject the outliers due to ground and sea clutters and spurious signals from insects, birds and so on. It is a further subject to develop sophisticated radar hardware and software which can determine turbulence and precipitation echo signals with better accuracy.

Acknowledgement

This paper is based on a cooperative study between King Monkut's Institute of Technology Ladkrabang (KMITL), Thailand, and CRL, Japan. The authors are deeply grateful to the staff of KMITL.

5. References

[1] Y. Masuda, K. Okamoto, K. Nakamura, T. Ihara, and T. Onishi; J. Remote Sensing Soc. Japan, vol.12, No.1, pp.43-56, 1992.

6. Publications

(1) Y. Ohno, Y. Masuda, and K. Nakamura; Extended Abstract of Third International Symposium on Tropospheric Profiling, pp. 310-312, 1994.

(2) Y. Ohno, A. Manyano, N. Leelauji, N. Hemmakon, and Y. Masuda; Proc. Seond International Study Conference on GEWEX in Asia and GAME., p. 121, 1995.

(3) Y. Rangsanseri and Y. Ohno; Research and Development Report on the Co-operative Environment Observation by MPT and KMITL, pp. 9-14, 1995.

(4) Y. Ohno, A. Manyano, N. Leelaruji, and N. Hemmakon; Proc. COST-76 Profiler Workshop 1997 in Switzerland, pp. 78-81, 1997.

(5) Tatsuhiro Adachi, Yoshihisa Masuda, and Ken'ichi Okamoto: Proc. 8th International workshop on Technical and Scientific Aspects of MST Radar in Bangalore, India, 1997.

7. International Cooperation

For the study of the Asian monsoon, CRL has already installed the BLR at the King Monkut's Institute of Technology Ladkrabang (KMITL) at Bangkok, Thailand, and the National MST Radar Facility (NMRF) at Tirupati, India.

要約

郵政省通信総合研究所は(CRL)、1991 年に L バンド大気境界層観測用レーダ(BLR)を開発し、その後、タイ国キングモンクット工科大学(1993 年)、CRL 沖縄電波観測所(1994 年)、CRL 小金井本所(1992 年、1995 年)、インド共和国国立 MST レーダ施設(1997 年)にそれぞれ展開してきた。これらのレーダは大気境界層の風速・乱流強度・降雨強度の高度分布及び RASS (Radio Acoustic Sounding System)を付加することで仮温度の高度分布の観測が可能である。本研究では、BLR をラジオゾンデと比較した結果、良好な測定精度が得られることがわかった。タイに設置した BLR で得られた風速プロファイルからアジアモンスーンによる季節変動、年変動及び日変化の特徴を調べた結果、季節変動はおおむねアジアモンスーンのモデルと合致するが、特に雨期においては年変動が大きく、約 1 ヶ月周期で振動する季節内変動も見られた。日変化は、高度 1km 以下で局所循環の影響を受け、北向き風速が卓越することがわかった。

Ⅰ. Observation and analysis on the process of the atmosphere-ocean-land interactions
大気・海洋・陸域間相互作用の諸過程に関する観測・解析研究
3. Observation and analysis on the process over the land
陸域における諸過程に関する観測・解析研究
(2) Observation on Regional Surface Heat Budget
地表面熱収支に関する観測研究

Meteorological Research Institute,
Japan Meteorological Agency
S. Haginoya and H. Naoe
気象庁 気象研究所
萩野谷 成徳・直江 寛明

(Abstract)

In order to clarify the mechanism of the Asian Monsoon caused through Air-Sea-Land interactions, the large-scale heat budgets over two different areas should be estimated: Tibetan-Himalaya Mountains Area and the Indian Ocean-South China Sea Area. This study aims to collect the basic meteorological data and to estimate large-scale heat budgets over the two areas.

Field observations were carried out in the Tibetan Plateau and Indian Ocean. This paper describes the following results through the observations.

(1) Tibetan Plateau

The six sets of Automatic Weather Station (AWS) have been installed in the Tibetan area and continued observation. Four of them (Lhasa, Rikeze, Nagqu and Lingzi) are located in the central and eastern Tibet since summer 1993. Two of them (Gaize and Shiquanhe) are located in the western Tibet since fall 1997. Soil samples in each site were collected and measured soil water content and soil parameters.

The following results were obtained through the data analysis.

There are clear daily variations of meteorological elements such as wind speed, air temperature, pressure and so on.

Angstrom's turbidity coefficient was estimated and its value is from 0 to 0.02. This fact shows the atmosphere over Tibetan Plateau is very clear. To estimate daily accumulated global solar radiation from duration of sunshine that was provided by China Meteorological Administration, the empirical formula was made. Daily global solar radiation at routine meteorological stations in the Tibetan Plateau were estimated from the empirical formula. The negative correlation is found between the total amount of rainfall and the average of daily global solar radiation.

The data of western AWS installed at Gaize and Shiquanhe from September 1997 to August 1998 were analyzed. Sensible heat flux and latent heat flux are estimated from net radiation, soil heat flux and Bowen ratio. The results were checked by water balance method. Both methods are consistent. The heat and water balance model for bare soil surface was checked by AWS data. It is confirmed that the model can apply the surface heat balance analysis with routine data over the Tibetan plateau. This model was applied to estimate the heat balance in the eastern Tibet. The Bowen ratio in the eastern Tibet is about 1.5. That in the western Tibet is about 8.

(2) Indian Ocean

AWS observations were made on Osaka-Maru (31,382 GT) from October 1991 to October 1995. She made round trips between Japan and Republic of South Africa through the South China Sea, the Strait of Malacca and the Indian Ocean every two months. The averaged net heat energy into the sea from 20 degrees north to 20 degrees south through the course in 1993 is 55.6W/m^2, that in 1994 is 13.4W/m^2. That from 1991 to 1995 is 24.9W/m^2.

Atmospheric boundary layer was observed by Hakuho-Maru's (3,987 GT) Omega sonde in the Indian Ocean. Mixed layer heights were estimated by virtual potential temperature profile and specific humidity profile. Height of mixed layer in the low latitude (20S-20N) is below 1000m and is nearly equal to the results that were obtained in the equatorial Pacific Ocean.

1. Objectives

In order to clarify the mechanism of the Asian Monsoon caused through Air-Sea-Land interactions, the large-scale heat budgets over two different areas should be estimated: Tibetan-Himalaya Mountains Area and the Indian Ocean-South China Sea Area. Because of the vastness of the areas and of their unsuitable conditions for observations, observatories or ships in these areas are very sparsely distributed. Therefore the basic meteorological data to clarify the mechanism of the Asian Monsoon has been lacking. This study aims to collect these basic data and estimate large-scale heat budgets over the two areas.

2. Methods

Since the heat budgets in two areas are studied by different methods, they are described separately. The following observations were made.

(1) Tibet

The four sets of Automatic Weather Station (AWS) were installed in the eastern part of Tibetan area in summer of 1993. Figure 1 (a) shows the outline of eastern AWS. AWS can collect basic meteorological data necessary for estimating surface heat balance. Observation sites are Lhasa, Rikeze, Nagqu and Lingzi (see Table 1 and Figure 2). The observation were carried out continued from 1993. Japanese scientist visited some of them every year. He investigated the observation sites and around topography. He also supported data collection and AWS maintenance. Chinese side took a picture twice a week, checked AWS every month and collected data twice a year (summer and winter). Collected data were sent to Japan by mail. To keep the data quality, all of the AWS sensors except soil sensors were exchanged and sent to Japan for re-calibration.

The two sets of AWS were installed in the western part of Tibetan area (Gaize and Shiquanhe see Table 1) in September 1997. Figure 1 (b) shows the western AWS.

The barometer was installed at the middle of the mountain area near Lhasa site in summer of 1996. Its elevation is about 4700m above the mean sea level. The aim of this observation is to estimate the regional averaged sensible heat flux from the time and height variation of pressure. The barometer was removed and data was collected in summer of 1997. Soil samples were collected in each site and soil water content and soil parameter were measured. Routine meteorological data in Tibetan area were also collected.

(2) Indian Ocean

AWS observation was made on the Osaka-Maru (31,382 GT), which made six times round trips between Japan and Republic of South Africa through the South China Sea, the Strait of Malacca and the Indian Ocean from October 1991 to October 1995. The data were collected when the Osaka-Maru came back to Yokohama. AWS was exchanged at least once a year for maintenance. 24 times round trip observation were made in total. Another AWS observation was made on Shoyo-Maru (1,363GT) of Fisheries agency from October 1995 to January 1996 in the equator of Indian Ocean and Arabian Sea. Sea surface heat balances are estimated from observation data.

Sea surface heat budget affects atmospheric thermal structure and its motion, especially in the ABL(Atmospheric Boundary Layer). Only surface observation does not obtain enough data to clarify the mechanism of the Asian Monsoon. It should be sounded the vertical structure of atmosphere making use of aerological sonde observation to collect the data of vertical thermal structure of ABL. Omega sonde observation (aerological observation) was carried out on the R/V Hakuho-Maru of University of Tokyo from August 1993 to September 1993 in the Indian Ocean and the Meteorological Observation Ship, Chofu-Maru (430GT) of JMA in October 1994 and 1995 in the East China Sea and the Pacific Ocean. Omega sonde was used to obtain pressure, temperature, relative humidity, wind direction and wind speed up to 500hPa (about 5000m mean sea level). Omega sonde is the instruments that measure the wind using omega navigation networks.

3. Results

(1) Tibet

Table 1 summarized the observation sites. Lhasa is the capital of Tibet Autonomous Region and the biggest city in Tibet. Lhasa site is inside the field of Tibet Meteorological Bureau, which is located at the bottom of valley. The length of valley is 40km in the east and west direction. Its width is 7km to 8km at the bottom and is 25km at the ridgeline of mountains. Average height difference between the bottom and the ridgeline is 1500-2000m. Nagqu is located about 220km north-east of Lhasa. This site is representative place in the central Tibet, which is located in the rural area on the opened plateau. Rikeze is located in a basin bottom, about 230km

west of Lhasa. The horizontal scale of basin bottom is 20km. Lingzi is located in the bottom of valley, 320km east of Lhasa. The length of valley is 30km in the north-west and south-east direction. Its width is 5km at the bottom. Average height difference between the bottom and the around mountain peak is 1500-2000m. This valley is narrower than that of Lhasa. Gaize is located at the middle of western Plateau, about 730km west-north-west of Lhasa. This site is representative place in western Tibet, which is located in the rural area on the opened plateau. There is an undulating plain. Ground surface is bare soil, few grasses and no tree. Gaize climate conditions are characterized by large sunshine duration, strong wind, large amplitude of air temperature and dry air. Shiquanhe is located in the western edge of Tibetan Plateau, about 1000km west-north-west of Lhasa. This site is a representative place in western edge of Tibet, which is located in the small town and surrounding the mountain. Ground surface is bare soil, no grass and no tree. Climate conditions at Shiquanhe are characterized by large sunshine duration, few rainfall and dry air.

(1.1) Daily variation of wind at Nagqu. Figure 3 shows the time series of AWS wind at Nagqu. The daily cycle of wind speed is easily found. Surface wind velocity reaches above 10m/s in the daytime and it becomes below 2m/s in the nighttime. Figure 4 shows the hodograph of 15 days vector average. It changes the clockwise. Diurnal strong wind is westerly. Its direction is nearly the same as 500hPa level at Lhasa. 500hPa level is about 1200m height from Nagqu ground level. It is conceivable that diurnal convective mixing transports the upper layer momentum to the ground surface level. The mechanism of daily cycle is as follows. After sunrise, solar radiation heats up ground surface. Then surface boundary layer is heating and mixed layer develops in the daytime. Momentum of westerly wind is transported downward. Then, the ground surface wind velocity increases. In the nighttime, radiational cooling stabilizes the atmospheric boundary layer. The momentum transfer from the upper layer is stopped, and then wind is weakened. The simple Ekman layer model (Alan and Trevor, 1977) simulated the diurnal variation of wind at Nagqu site.

(1.2) Global solar radiation was measured by two kinds of systems. One system can store the instantaneous value at every 10 or 20 minutes to the memory. Another system can store the hourly accumulated value. To check the data quality, these two observational data were compared each other. The following characteristics are obtained through the time series of the daily mean global solar radiation. In summer period, the fluctuation of solar radiation is large. This is caused by the influence of cloud that indicates convective activity. On the other hand, that in winter period is small. The ratio of solar radiation at the ground surface to that at the top of atmosphere is large in winter because of small water vapor in the air mass. The solar radiation of the western part of Tibet is larger than eastern Tibet. The time variations of calibration coefficient for pyranometer are checked. Its coefficient of some pyranometer varied more than 5 %. This cause is the change of paint property over the sensor element, inclined sensor element and inclined stand. To keep the data accuracy, data should be checked by empirical formula. To check the data quality of global solar radiation, Angstrom's turbidity coefficient (β_{dust}, Kondo and Miura, 1983) was estimated by QXPMEX-79 data (Zhang *et al.*, 1988) and the AWS data. Figure 5 shows the relation between the ratio of sky solar radiation (D) to direct solar radiation on horizontal level ($I\cos\theta$) and inverse of air mass ($1/\cos\theta$). θ is the zenith angle. The line shows β_{dust}. The data are scattered between β_{dust}=0 and 0.02. This means the atmosphere over Tibetan Plateau is very clear. Next global solar radiation data are checked. Figure 6 shows the time series of daily accumulated global solar radiation. In the figure, several lines show the global solar radiation on a fine day. Parameters are β_{dust}. The maximum value of observational data which are considered fine day are scattered around β_{dust}=0.02. This fact shows that the observation data shown in the Figure 6 are not inconsistent.

(1.3) To estimate daily average of global solar radiation *(S)* from routine sunshine duration (N_J), we made the following empirical formula. $S/S_0=a+b^*(N_J/N_0)$, where S_0 is daily average of global solar radiation at the top of atmosphere, N_J is daily sunshine duration measured by Jordan's sunshine recorder, N_0 is daily possible sunshine duration, *a* and *b* are empirical constants. We use S_0 instead of S_{0f}, which is daily average of global solar radiation at the surface on a fine day. Because the magnitude of scatter between S/S_{0f} and N_J/N_0 is as same as S/S_0 and N_J/N_0, and the calculation method is simpler than S_{0f}. Daily global solar radiation was estimated from sunshine duration data using the empirical formula. Figure 7 shows the result at 13 routine meteorological stations in the Tibetan Plateau. There is a good negative correlation between solar radiation and

rainfall amount. Solar radiation in western Tibet is larger than eastern Tibet. On the other hand, amount of rainfall in western Tibet is smaller than eastern Tibet. Solar radiation of central and eastern Tibet in 1993 is smaller than that in 1994. The average variation of solar radiation and rainfall are about $17W/m^2$, 116mm, respectively. These are also equal to 6% of solar radiation and 35% of rainfall, respectively. The remarkable difference between 1993 and 1994 is not found at western station "S" which is Shiquanhe.

(1.4) The following equation shows the surface heat balance.

$$Rn = Sd - Su + Ld - Lu = H + lE + G \quad (1),$$

where *Rn* is net radiation, *Sd* global solar radiation, *Su* reflective solar radiation, *Ld* downward long wave radiation and *Lu* upward long wave radiation. The western AWS can measure the four components of radiation *(Rn)* and soil heat flux *(G)* directory. Sensible heat flux *(H)* and latent heat flux *(lE)* are estimated by Bowen ratio method and water balance method. Bowen ratio *(B)* is defined the sensible heat flux to latent heat flux. This is equal to the ratio temperature difference to specific humidity difference with some assumptions. Once we obtain the Bowen ratio, we can estimate the sensible heat flux and latent heat flux from the following equation.

$$lE = (Rn - G)/(1 + B)$$
$$H = (Rn - G)B/(1 + B) \quad (2)$$

Water balance is equation (3).

$$\Pr = R + P + \Delta(SW) + E \quad (3)$$

If we assume the runoff *(R)* and the penetration *(P)* into the underground below 30cm are zero, we can estimate the evaporation *(E)* from the precipitation *(Pr)* and the variation of soil water content Δ *(SW)*. Sensible and latent heat fluxes were estimated from Bowen ratio method and water balance method with net radiation and soil heat fluxes. The difference of both methods is about $10W/m^2$. The heat and water balance model for bare soil surface (Kondo and Xu, 1997) was checked by AWS data. It is confirmed that the model can apply the surface heat balance analysis with routine data over the Tibetan plateau. The figure 8 shows the results of heat balance. The data are monthly average. Heat balance is calculated by heat balance model in the eastern Tibet and is estimated by Bowen ratio method in the western Tibet. Net radiation in the eastern Tibet is larger than in the western Tibet. This is due to larger amount of rainfall in the eastern Tibet increases the evaporation from the ground surface then the evaporation suppresses the rise of ground surface temperature. Also large amount of rainfall increase the downward long wave radiation. Therefore net radiation became larger in the eastern Tibet. Sensible heat flux occupies the most part of the heat balance equation in the western Tibet. On the other hand, latent heat flux increases in the rainy season and exceeds the sensible heat flux in the eastern Tibet. The average Bowen ratio in the eastern Tibet is about 1.5. That in the western Tibet is about 8. The difference of rainfall amount well corresponds to Bowen ratio.

(2)Indian Ocean

AWS observation were made on the Osaka-Maru (31,382 GT) from October 1991 to October 1995 for four years. Figure 9 shows the cruise course. Figure 10 shows the latitudinal variation of daily heat budget. Sensible and latent heat fluxes are estimated by Kondo's bulk method (Kondo, 1975). In the Indian Ocean (from 25S to the equator), yearly net heat flux is about $+20W/m^2$. This means that net heat flow is from the atmosphere to the Ocean. Heat balances in 1993 and in 1994 are estimated from the observation data. The averaged net heat energy into the sea from 20 degree north to 20 degree south in 1993 is $55.6W/m^2$, in 1994 is $13.4W/m^2$. That from 1991 to 1995 is $24.9W/m^2$. Another AWS observations were made on Shoyo-Maru in 1995.

Atmospheric boundary layer was observed by Hakuho-Maru's Omega sonde in the Indian Ocean. Figure 9 also shows the course of Hakuho-Maru's cruise. Observation was made from August to September in 1993. The vertical structure of virtual potential temperature and specific humidity were obtained from the data analysis. Virtual potential temperature is potential temperature, which is considered influence of water vapor. Figure 11 shows the sample of potential temperature and specific humidity profile. Height of atmospheric mixed layer is defined by the kink of profile (refer to the figure). Another parameters of ABL over the Indian Ocean are also defined in the figure. There is no systematic difference between mixed layer height $h\theta v$ and hq. Potential temperature gradient of upper part of ABL is summarized in Figure 12. Figure 13 shows the latitudinal variation of ABL height. Mixed layer height in the low latitude (20S-20N) is nearly equal to the results that were obtained in the Pacific Ocean (Sugimura Y. et al., 1988 and 1993). Its average height is below 1000m. The potential temperature difference between sea surface and mixed layer is about 3 degree centigrade. The specific humidity difference is about 8.0 g/kg.

4. Discussions

Six AWS observation sites were developed in the Tibetan Plateau and observations were carried out since 1993. AWSs are located various kind of climate conditions. The eastern part of Tibetan Plateau is relatively wet region and the western part is dry region. These data are very useful to estimate an energy balance over the Plateau and to check the heat balance model.

Through the observation, remarkable daily variation is found in wind, temperature, pressure and other elements. They are closely related to the high altitude and the around topography. Solar radiation is the important element of heat balance equation. To maintain the data accuracy, sensors must be calibrated periodically and furthermore observation data should be checked by other available data or theoretical method. The check method shown in this paper is useful. The result of soil water content is very interesting. Soil water content strongly affects on the ground surface condition. Therefore heat balance is affected by soil water content.

If the soil temperature is positive and little rainfall condition, water balance method is suitable for heat balance. There is no large error if we use the assumption that evaporation is equal to rainfall in the dry season. The error is at most $10W/m^2$. The validity of assumption concerning water balance method should be checked.

To estimate the heat balance within reasonable accuracy, we should measure the temperature difference and humidity difference more accurate. For example we use the thermocouple to measure the temperature difference. Also we use the three humidity sensors. Two are used to measure the different level humidity. The rest one is set one level and change the level at regular intervals for calibrate the each sensor. To research the soil water movement, we should measure the soil water content more than three layers.

Osaka-Maru observation accumulated the basic data for estimating heat balance over the Indian Ocean for four years. The results showed that net heat flow towards from the atmosphere to the Ocean. The yearly variation of heat balance should be clarified furthermore. The data of Atmospheric boundary layer over the Indian Ocean was obtained. Height of ABL over the Indian Ocean developed below 1000m. This height is roughly equal to that in the tropical ocean. Parameters of ABL are useful for making the ABL model over the Ocean.

5. References

Alan J. Thorpe and Trevor H. Guymer, 1977: The nocturnal jet. *Quart. J. R. Met. Soc.*, **103**, 633-653.

Haginoya, S. et al., 1990-1998: Observation on Regional Surface Heat Budget. Annual Report of Japanese Experiment on Asian Monsoon, Research and Development Bureau, STA.

Kondo, J., 1975: Air-sea bulk transfer coefficient in diabatic conditions. *Boundary-Layer Meteorol.* **9**, 91-112.

Kondo J. and A. Miura, 1983: Empirical formula of the solar radiation at the ground level and a simple method to examine an inaccurate pyranometer. *Tenki,* **30**, 284-290.

Kondo, J. and J. Xu, Seasonal variations in the heat and water balances for nonvegetated surfaces. *J. Appl. Meteor.*, **36**, 1676-1695, 1997.

Sugimura Y. et al., 1988 and 1993: Precise Observation on Atmospheric Structure and Fluxes. The annual report of Japanese Pacific Climate Studies (JAPACS), Research and Development Bureau, STA, 21-29 (1988) and 23-28 (1993).

Zhang Jijia, Zhu Baozhen, Zhu Fukang, Weng Duming, Sun Guowu, Lu Junning, Peng Yongqing and Wang Yuanzhong, 1988: Advances in the Qinghai-Xizang Plateau Meteorology. The Qinghai-Xizang Plateau Meteorological Experiment (1979) and Research. pp.268.

6. Publications

① Journal with referee

1) Domestic (6 papers)

Haginoya, S. and T. Fujitani, Outline of the Automatic Weather Station 2700 by AANDERAA INSTRUMENTS. *Tenki*, **36**, 747-751, 1989.

Haginoya, S. and T. Fujitani, Heat balance of the atmospheric boundary layer in the tropical Pacific Ocean. *Tenki*, **37**, 397-408, 1990.

Fujitani, T. and S. Haginoya, Method of evaluating surface energy fluxes over open ocean by cruising ship of opportunities. *Tenki*, **38**, 441-447, 1991.

Haginoya, S. and T. Fujitani, Measurement of global solar radiation on board making use of simple pyranometer system. *Tenki*, **38**, 645-648, 1991.

Haginoya, S., N. Obata and N. Kinoshita, Heat budget analysis on daily variation of sea surface

temperature observed by Keifu-Maru cruise (90-02). *Tenki, 40*, 197-205, 1993.
Kondo, J., J. Xu and S. Haginoya, Empirical formula for estimating the solar radiation at an upland from the sunshine duration data. *J. Japan Soc. Hydrol. & Water Resour.*, **9**, 468-472, 1996.
2) International (2 paper)
Li Guoping, Duan Tingyang, Wan Jun, Gong Yuanfa, Shigenori Haginoya, Chen Longxun and Li Weiliang, Determination of the Drag Coefficient over the Tibetan Plateau. ADVANCES IN ATMOSPHERIC SCIENCES, China Ocean Press Beijing, p511-518, 1996.
Li Guoping, Duan Tingyang, Shigenori Haginoya, Chen Longxun and Li Weiliang, Estimate of the bulk transfer coefficients and surface fluxes over the Tibetan Plateau using AWS. (in preparation)
② Others
1) Domestic (14 papers)
Haginoya, S., On the processes of surface heat exchange. Heat engineering in the future technology (Report of "Branch of science on the problem of heat engineering in the future technology", Mechanical engineering society of Japan), 79-82, 1989.
Haginoya, S. et al., Observation on regional surface heat budget. Japanese Experiment on Asian Monsoon (JEXAM) Annual Report, Research and Development Bureau, Science and Technology Agency, 1990～1998 (9 reports)
Haginoya, S., Observation on Regional Surface Heat Budget. -Plan, preliminary results and review of analysis method-. Study of Asian Monsoon in Japan and China, Edited by M. Murakami and Ding Yihui, 70-91, 1992.
Haginoya, S., Automatic Weather Station for Vessels using automatic observation of the regional sea surface heat budget. Symposium on "New observation system", Conference of Meteorological Society of Japan in 1992, 41-42, 1992.
Haginoya, S. and N. Kinoshita, Thermal structure of atmospheric boundary layer over the Indian Ocean. Preliminary Cruise Report, R/V Hakuho-maru KH93-3 Research Cruise, July 8 - September 17, 1993, 165-183, 1995.
Haginoya, S. and H. Naoe, Observation on Regional Surface Heat Budget, Research and Development Bureau, Science and Technology Agency, Recent Progress in Studies of Asian Monsoon Mechanism, 1-16, 1999.
2) International (4 papers)
Li Yuehong, Li Weiliang, Li Xiaowen and Shigenori Haginoya, Analysis of AWS Data on Tibetan Plateau from 1994 to 1995. The Recent Advances in Asian Monsoon Research. -The Proceedings of P.R.China-Japan Cooperation Research Project on Asian Monsoon Mechanism, Meteorological press, 15-24, 1996.
Li Yuehong, Li Weiliang, Ding Xiaorong, Ren Chuansen and Shigenori Haginoya, Characteristics of The Surface Layer Turbulent Fluxes in Lhasa from July to September, 1993. The Recent Advances in Asian Monsoon Research. -The Proceedings of P.R.China-Japan Cooperation Research Project on Asian Monsoon Mechanism, Meteorological press, 25-36, 1996.
Li Guoping, Duan Tingyang, Shi Youyu and Shigenori Haginoya, Temporal Variation and Response to Weather Processes of the Drag Coefficient over The Tibetan Plateau. The Recent Advances in Asian Monsoon Research. -The Proceedings of P.R.China-Japan Cooperation Research Project on Asian Monsoon Mechanism, Meteorological press, 37-44, 1996.
Zhu Keyun, Qiao Yongjun, Duan Tingyang and Shigenori Haginoya , Research on the Surface Total Radiation of Tibetan Plateau. The Recent Advances in Asian Monsoon Research. -The Proceedings of P.R.China-Japan Cooperation Research Project on Asian Monsoon Mechanism, Meteorological press, 45-53, 1996.

7. International cooperation

Meteorological observation over the Tibetan Plateau is carried out the cooperative study with China Meteorological Administration. Japanese scientists visited Tibetan Plateau every year since 1993 to research the field and to collect the AWS data in cooperation with Chinese side. Meteorological Research Institute invited 10 Chinese scientists since 1993. Japanese and Chinese sides discussed the Tibet observation and examined the results. They summarized the results of discussion as "Working Plan" in each year. Details concerning the "Working Plan" are summarized in the Appendix 1 of "SUMMARY REPORT ON THE 1st to 7th WGM OF JAPAN-PRC COOPERATIVE PROGRAM ON ASIAN MONSOON".

要旨

本研究は，大気を媒体として海洋と陸面間の相互作用として発現しているアジアモンスーンの機構を解明する

ため、2つの異なる地域における広域のエネルギー収支を評価するものである。そのうちの1つはチベット・ヒマラヤの山岳地帯の地表面フラックス, もう1つはインド洋・東南アジア地域の海面フラックスである。これらの地域において、熱収支解析に必要な気象要素を現地観測により収集し, それに基づいて広域熱収支解析を行うことを目的としている。

(1) チベット関連:

6 基の山岳用自動気象観測装置(AWS)をチベット高原に設置して、長期観測を行った。そのうちの 4 基は、東チベットの拉薩(ラサ)、日喀則(シガセ)、那曲(ナチュ)および林芝(ニンチ)に設置し、1993 年夏以降観測を行っている。他の 2 基は西チベットの改則(ガイゼ)と獅泉河(シーチョワンホー)に設置して、1997 年秋以降観測を行っている。それぞれの地点において土壌資料を採取して、土壌水分量や土壌パラメータを求めた。1998 年まで毎年、日本から研究者が現地に行き、中国側と共にAWSデータの回収・保守点検を行った。このほか、チベット地域のルーチン観測所のデータ(地上、高層および放射量)の入手、さらに中国人研究者を毎年日本に招聘し、共同研究の打ち合わせ等を行った。

1998 年までに得られたデータを解析した結果、以下の成果が得られた。

風速、気温、気圧などの気象要素に顕著な日変化が見られた。

オングストロームの大気混濁係数を求め、その値が 0 から 0.02 の間にあることがわかった。これは、チベット高原上の大気が大変清澄であること示す。ルーチン観測で得られている日積算日照時間データから、日平均全天日射量を推定する実験式を作った。本実験式を用いて、チベット高原上のルーチン観測所の日平均全天日射量を求めた。日平均全天日射量と積算雨量との間には負の相関が見られた。

西チベットのガイゼとシーチョワンホーに設置したAWSで得られた、1997 年 9 月から 1998 年 8 月までのデータを解析した。顕熱と潜熱を正味放射量と地中伝導熱およびボーエン比から求めた。得られた結果を水収支法で検討したところ、妥当な結果であった。AWS データを用いて、裸地面上の熱・水収支モデルを検証した。本モデルとチベット高原上のルーチンデータから、地表面の熱収支解析を行うことができることが確認された。本モデルを用いて東チベットの熱収支解析を行った。東チベットの年平均ボーエン比は約 1.5、西チベットは約 8 であった。

(2) インド洋関連:

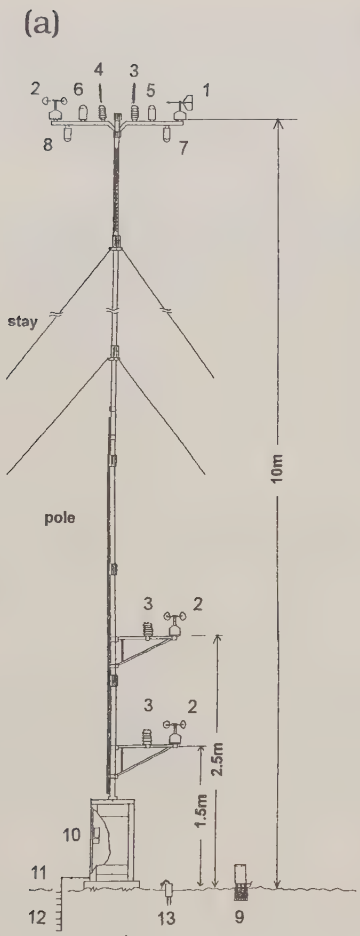
船舶用 AWS を 1991 年 10 月から 1995 年 10 月まで、大阪商船三井船舶株式会社の定期コンテナ船「大阪丸(31.382GT)」に搭載して観測した。本船は、南シナ海、マラッカ海峡、インド洋経由で日本と南アフリカのケープタウンを 2 ヶ月に 1 往復のペースで航行している。得られたデータを解析した結果、北緯 20 度から南緯 20 度の海域において、1993 年は海面に入る正味の平均熱量は約 56W/m^2、1994 年は約 13W/m^2 であることが分かった。1991 年から 1995 年までの期間平均熱輸送量は約 25W/m^2 である。

白鳳丸のオメガゾンデを用いて、インド洋上の大気境界層の観測を行った。大気混合層高度は仮温位と比湿の鉛直分布から求めた。低緯度地帯(南緯 20 から北緯 20 度)における混合層高度は、1000m 以下で、太平洋赤道海域で得られた結果とほぼ同じであった。

Table 1 Summary of the AWS sites.

site name	Lhasa	Nagqu	Rikeze	Lingzi	Gaize	Shiquanhe	Lhasa-P
latitude	29°40'N	31°29'N	29°15'N	29°34'N	32°18'N	32°30'N	29°44'N
longitude	91°08'E	92°04'E	88°53'E	94°28'E	84°03'E	80°05'E	91°07'E
altitude(m)	3,649	4,507	3,836	3,000	4,420	4,279	4,690
around the topography	bottom of valley	flat hill	bottom of basin	bottom of valley	flat	flat	slope
conditions around the site	city	rural town	rural town	rural	rural	rural town	middle of mountain
ground surface conditions	short grass	bare soil (gobi)	irrigated vegetable field	short grass	bare soil	bare soil	rock
observation period	from July 1993	from July 1993	from July 1993	from July 1993	from Sept. 1997	from Sept. 1997	from June 1996 to Aug. 1997
Pressure(hPa)	652.7	587.2	638.1	709.5	590.8	604.4	
Temparature(C)	8.5	-0.6	6.9	9.1	0.1	1.2	
Relative humidity(%)	43.5	54.5	44.5	64.5	34.0	34.9	
Rainfall(mm)	468.9	406.4	419.8	739.2	108.3	51.5	

Note: Lhasa-P is pressure measurement site whose data is used to estimate average sensible heat flux around the valley. Rainfall at Gaize and Shiquanhe is from September 1997 to August 1998.



	Element	Sensor
0	Wind direction & speed	Windmill anemometer
1	Wind direction	Wind vane
2	Wind speed	3-cup anemometer
3	Air temperature	Thermometer
4	Relative humidity	Hygrometer
5	Global solar radiation	Pyranometer
6	Downward total radiation	Total radiometer
7	Reflective solar radiation	Pyranometer
8	Upward total radiation	Total radiometer
9	Precipitation	Rain gauge
10	Pressure	Barometer
11	Ground surface temperature	Thermometer
12	Soil temperature	Thermometer
13	Soil water content	Soil water content meter
14	Soil heat flux	Heat plate
15	Ground surface temperature	Radiation thermometer
16	Downward long wave radiation	Long wave radiometer
17	Upward long wave radiation	Long wave radiometer

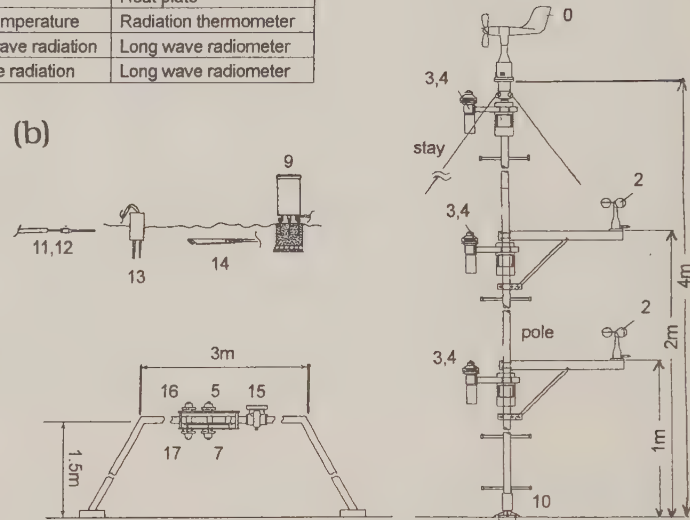


Fig. 1 Schematic views of Automatic Weather Station (AWS). (a) was installed at eastern Tibet, (b) was at western Tibet.

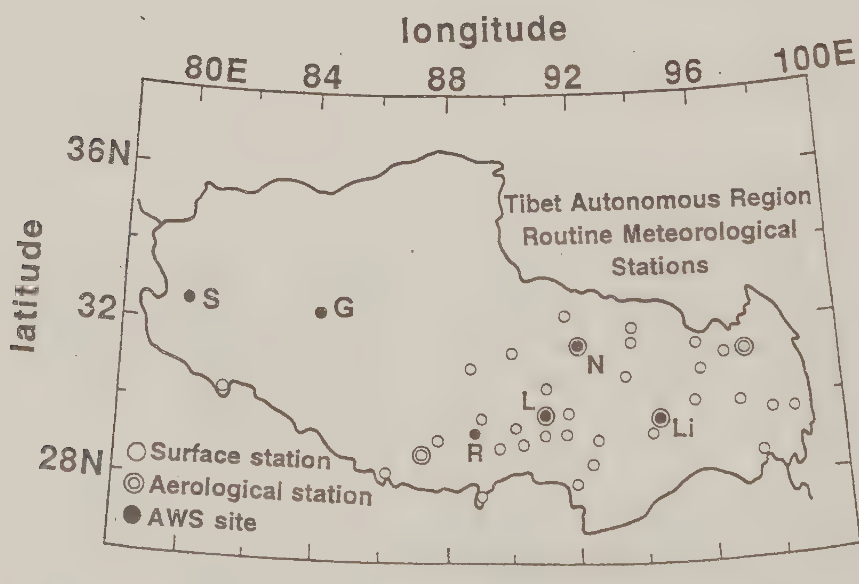


Fig. 2 Meteorological observatory in Tibet autonomous region. Alphabets show the first letter of stations.

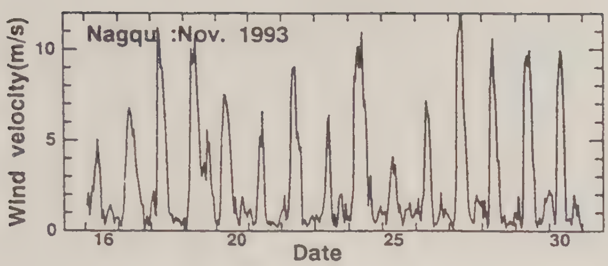


Fig. 3 Wind speed of 10m height at Nagqu. Data are hourly average.

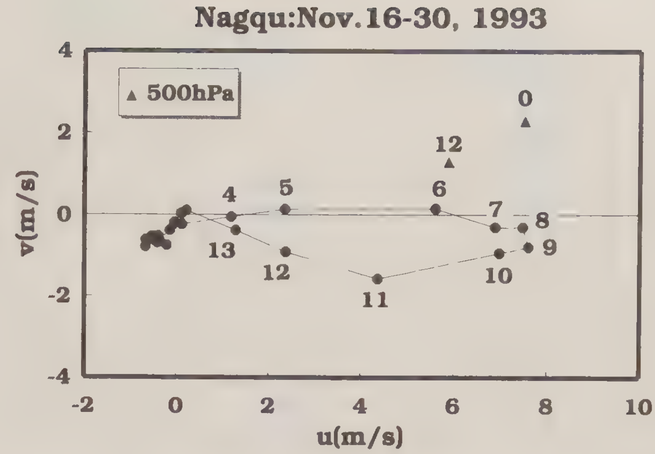


Fig. 4 The hodograph of observation at Naqgu (●). ▲ show 500hPa wind at Lhasa. The number indicates GMT. Local time is GMT+6.

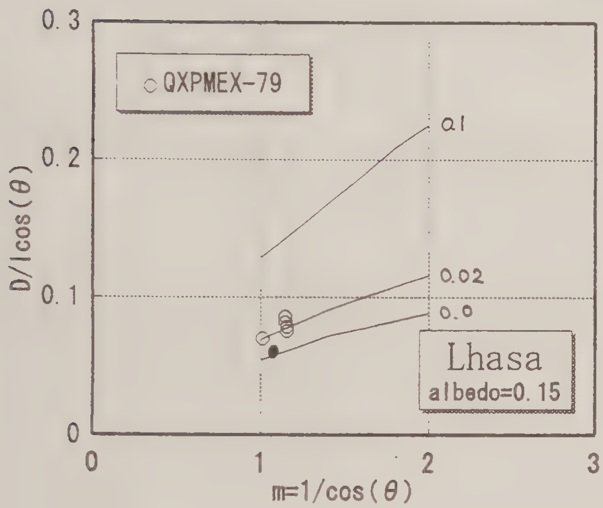


Fig. 5 The relation between the ratio of sky solar radiation (D) to direct solar radiation on horizontal level (Icos θ) and inverse of air mass (1/cos θ). Open marks show QXPMEX-79 data, filled mark AWS data. Line parameters are β_{dust}.

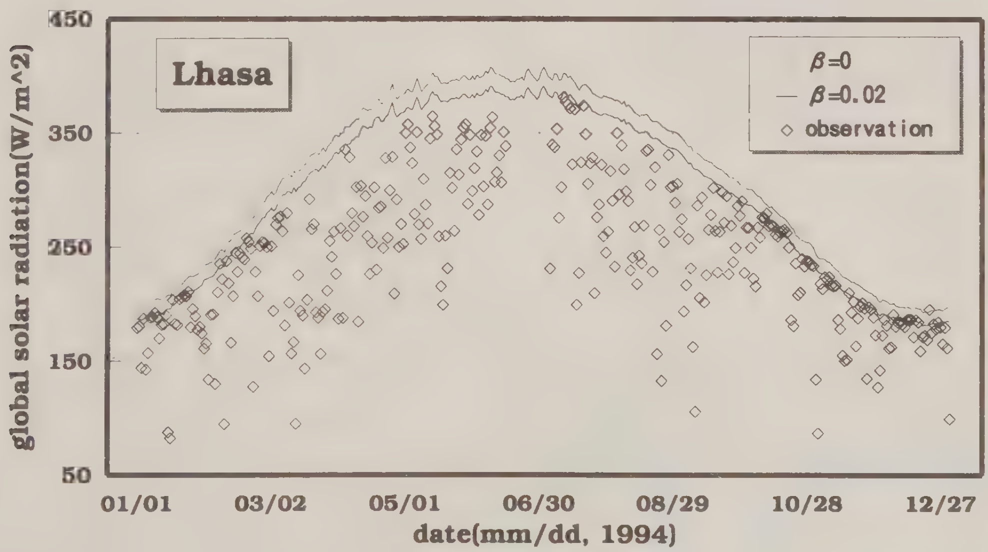


Fig. 6 Variation of daily mean global solar radiation. Mark "◇" indicates observation data. Lines indicate empirical value at fine day. Parameters are β_{dust}.

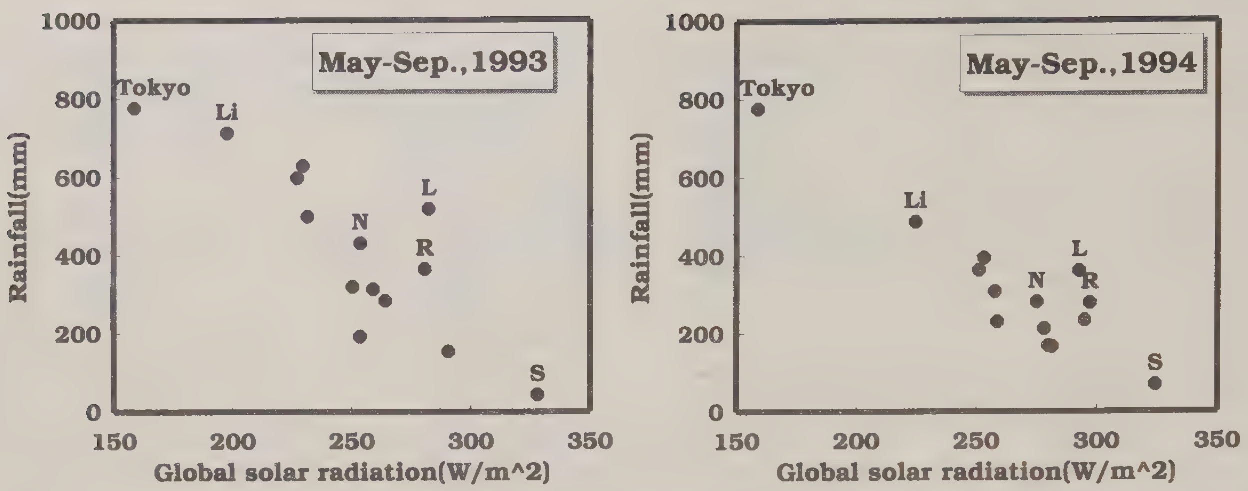


Fig. 7 The relation between global solar radiation and rainfall. The data are routine observatories inside the Tibet Autonomous Region. Global solar radiation is calculated by empirical formula with sunshine duration. Tokyo is average for 30 years from 1961 to 1990.

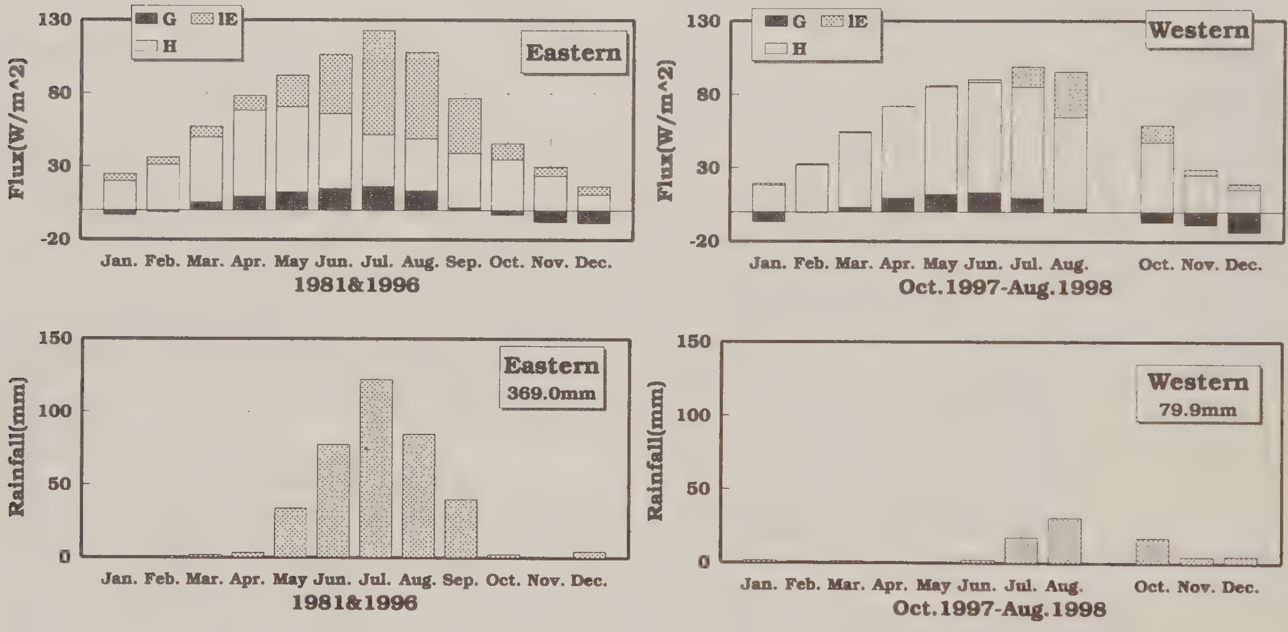


Fig. 8 Monthly heat balance and rainfall in the Tibetan Plateau. Easter is average of Lhasa and Rikeze, western is Gaize and Shiquanhe.

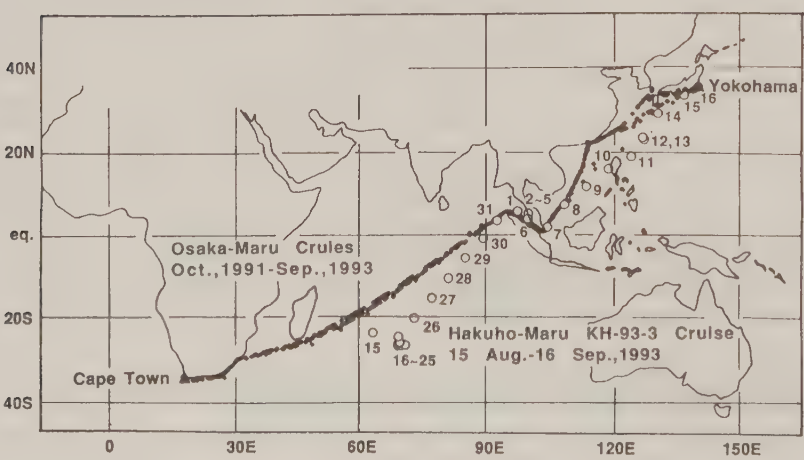


Fig. 9 The cruise course. The marks indicate the position at noon JST. Open circle indicate the Hakuho-Maru, closed square the Osaka-Maru. The number indicates the date of JST.

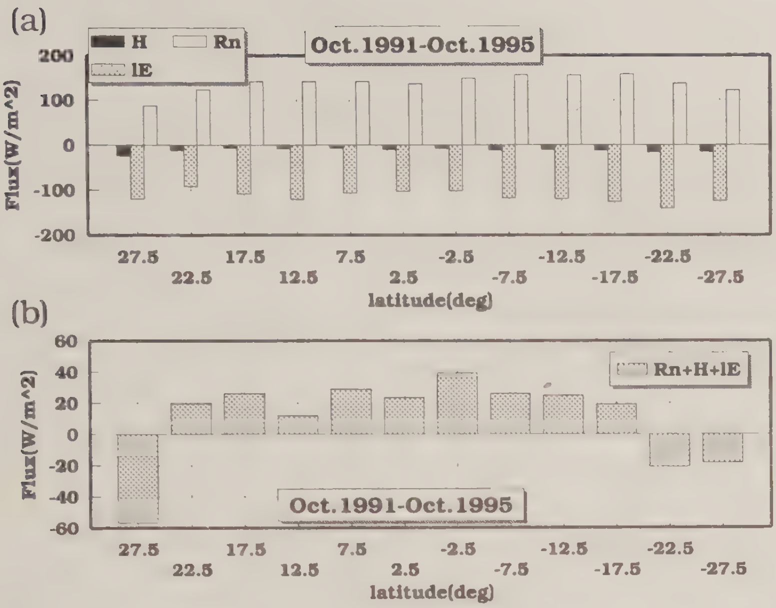


Fig. 10 (a) Latitudinal variation of averaged energy fluxes. H: sensible heat flux, lE: latent heat flux and Rn: net radiation flux. Positive fluxes show the direction from the atmosphere to the ocean.
(b) Same as (a) but Rn+H+lE that means net flux into the ocean.

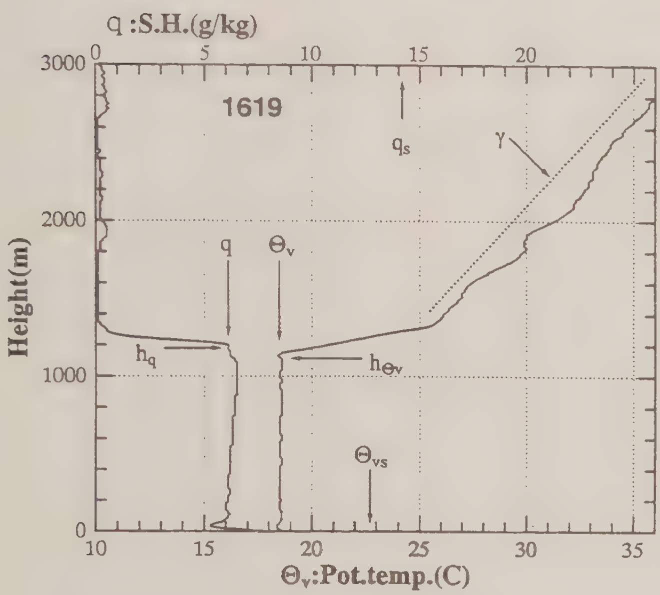


Fig. 11 Example of virtual potential temperature profile and specific humidity. Symbol indicates the characteristic parameter of ABL. $h_{\theta v}$: height of mixed layer defined by virtual potential temperature. h_q: height of mixed layer defined by specific humidity. γ : virtual potential temperature gradient of upper part of ABL(dotted line). θ_v: virtual potential temperature of mixed layer. q: specific humidity of mixed layer. θ_{vs}: virtual potential temperature corresponded to SST. q_s:saturated specific humidity corresponded to SST.

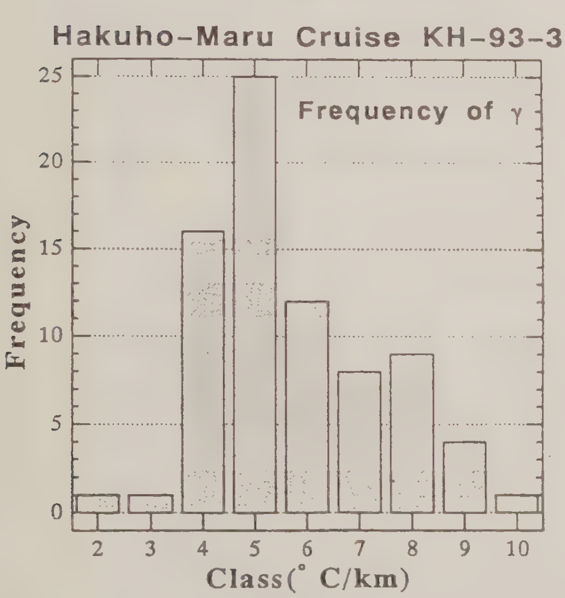


Fig. 12 The frequency distribution of γ .

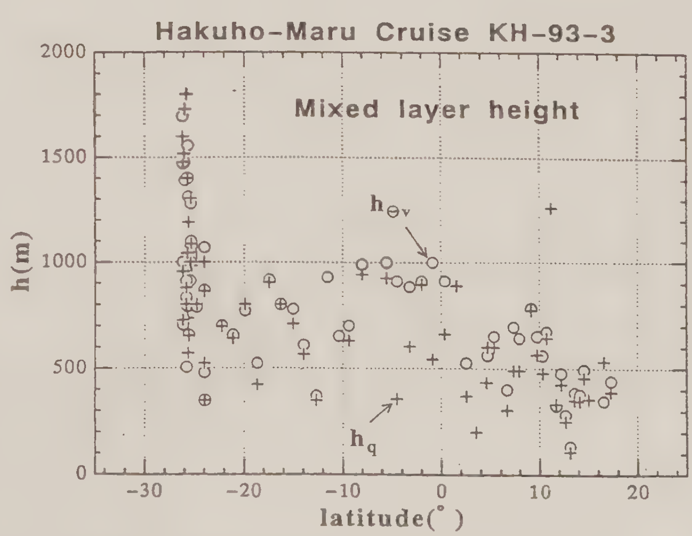


Fig. 13 latitudinal variation of mixed layer height $h_{\theta v}$ and h_q.

I. 大気・海洋・陸面間の相互作用の諸過程に関する観測・解析研究

Observation and Analysis on the Process of the Atmosphere-Ocean-Land Interactions

3. 陸面における諸過程に関する観測・解析研究

Observation and Analysis on the Process over the Land

(3) モンスーン循環広域条件及び雪氷変動状況に関する研究

Analysis on Environmental Conditions and Snow-Ice Cover Changes Affecting Monsoon Cycle in Asia

防災科学技術研究所　矢崎 忍、中根 和朗、諸星 敏一、宋 献方

National Research Institute
for Earth Science and Disaster Prevention
YAZAKI Shinobu

(abstract)

One of the purpose of this study is to make periodical image data set of environmental conditions over Asia and the other is to clarify relation between the conditions and Asian monsoon activity.

Two kinds of image data set have been compiled with multi-channel meteorological satellite data: weekly data set which cover whole Asia except polar region and daily data set which cover center of Asian continent. Both images are consist of visible, near infrared and thermal infrared bands.

Methods to detect several items of condition are developed. Sea and land surface temperature and vegetation index can be detected with weekly data set and images are obtained for every month. Methods to detect snow cover with daily data set is also developed. Snow cover image are obtained for every ten days.

1. Objectives

Purposes of this study is to make periodical data set of earth surface image with satellite data over Asia, to develop methods for detection of various environmental conditions with the image data and finally to clarify relation between those conditions and Asian monsoon activity.

2. Methods

Two kinds of image data set have been made with polar orbital multi-channel

meteorological satellite data: weekly data set which cover whole Asia except polar region and daily data set which cover central Asian continent. Both images are consist of reflectivity data in visible, near infrared band and thermal radiation data in far infrared bands.

Methods to detect several items of condition are developed. Sea and land surface temperature and vegetation index can be detected with weekly data set and images are obtained for every month.

Especially on later half of the research period effort was made to develop a method to detect changes of snow cover area over Asian continent with daily data set. For each pixel channel data over one snow season are used to detect the beginning and the expiration of snow period. Utilizing the method snow cover images are made for every month.

3. Results

(1) Compilation of environmental image data set

The environmental data set are made with NOAA-AVHRR/GAC data through the following process.

Original pixel value that is incident energy to the sensor is converted to physical values: percent albedo for channel 1(visible) and channel 2(near infrared) and brightness temperature in degree centigrade for channel 3 to 5(thermal infrared). Correction for solar zenith angle is included in the process.

The data are then geometrically corrected and resampled on the equal longitude and latitude grid. Geometrical correction is done systematically with satellite orbit data first then errors of the resultant image are detected by referring GCP data and the image is re-corrected with the error information.

Two kind of data set are being made. Specifications of each data set are

Data set I

range:	30E - 160E, 20S - 60N	
pixel size:	1/30 degree × 1/30 degree	
image size:	3900 pixel × 2400 line	
data interval:	seven days	
band:	band 1	AVHRR channel 1
	2	channel 2
	3	channel 3
	4	channel 4(low mode)
	5	channel 5(high mode)

	6	channel 5 - channel 4 (resolution 0.1 degree)	
period:	1989 - 1993		

Data set II

range:	60E - 120E, 15N - 55N		
pixel size:	1/30 degree × 1/30 degree		
image size:	1800 pixel × 1200 line		
data interval:	one day		
band:	band 1	AVHRR channel 1	
	2	channel 2	
	3	channel 4	
period:	1993 - 1995 (continuing)		

(2) Analysis of environmental conditions

Methods to analyze various environmental conditions of land surface are developed with weekly data set. Four successive images of weekly data set are used to make monthly image

Sea surface temperature with correction to water vapor absorption is estimated with channel 4 and channel 5 data by means of split window method. Monthly image of SST is composed of the maximum value among four images. Same coefficients are expediently applied to estimate ground surface temperature. Image of both sea and land surface temperature are made for every month.

NDVI is calculated with channel 1 and channel 2 data of one image. Monthly NDVI image is also made with a similar method to SST image.

(3) Detection of snow cover

The method to detect snow cover for each day with daily data set is developed .

At first the characteristic of object in each channel is investigated.

<u>Channel 1 reflectivity</u>(unit in percent albedo)

Cloud free pixel corresponding to ground surface without snow (hereafter called snow-less pixel) gives 5 to 20. Those with vegetation gives 5 to 10 while those without vegetation that is bear soil such as desert surface gives 15 to 20.

A pixel which is completely covered with snow gives 40 to 50. A certain portion of the pixel is covered with snow but the rest is not it gives medium value between the both.

Cloud makes reflectivity higher. Reflectivity of cloud depends on its thickness and height and the value varies continuously. The highest cloud reaches up to

almost 70.

Channel 4 radiation(unit in degree centigrade)

Ground surface temperature varies much with time in a year and location. Since the observation time of NOAA is around 14:00(2:00PM) in local time, surface temperature of the ground with neither snow nor cloud is almost above zero regardless of time and place. The temperature of snow surface is nearly -10 to 0. Cloud makes observed temperature lower. The temperature of the thickest and highest cloud reaches to –40 degree C or lower.

For cloud free pixel distinction between snow and snow-less pixel is not difficult both with visible and thermal channel. But distinction between snow and cloud is almost impossible by the reason mentioned above.

Images that starts in September and ends in August of next year are used as a data set for one year. Changes of pixel value of each channel over a year is examined. The value defined by the following relation is estimated as corrected value.

$\overline{X}_1$ = second smallest value among seven days(form three days before to three days later of the day) value of X_1

Similarly, corrected temperature $\overline{T}_4$ is defined by

$\overline{T}_4$ = largest value among seven days value of T_4

The graph of $\overline{X}_1$ and $\overline{T}_4$ is shown in Figure 1.

According to these graphs, channel 1 brightness discontinuously goes up with start of snow cover and discontinuously goes down with snow melting. While channel 4 temperature changes rather continuously.

From these data the threshold value of each channel which distinguish snow pixel and snow-less pixel is determined to be 20(%) for channel 1 and 3(℃) for channel 4 respectively.

To detect the time of start and end of snow cover period, function S(I) defined by the following expression is introduced.

$$S(I) = \sum_{J=1}^{I} s(J) + \sum_{J=I+1}^{365} \{1 - s(J)\}$$

where

$$s(I)=\begin{cases}1 & when\ \ \overline{X}_1(I)\geq 20\ \ and\ \ \overline{T}_4(I)\leq 3\\ 0 & otherwise\end{cases}$$

and I denote serial day count starting from September 1. S(I) at the sample pixel is shown in Figure 2.

Let I which gives the maximum value of S(I) be Is and I which gives the minimum value of S(I) be Ie. Then the snow period is detected as Is≦I≦Ie.

The resultant snow cover distribution obtained with the method given here is shown in Figure 3.

4. Discussions

The study started with making weekly environmental image data set with satellite data. The data frequency is almost sufficient for detection surface temperature or vegetation index.

But for detection of snow cover weekly data was found insufficient for removing cloud from snow. So frequency of the data set is changed from weekly to daily in the halfway of study period.

The study on relationship between such environmental conditions and Asian monsoon activity still remains unsatisfactory. To discuss the relationship long term data is necessary at least five years or more.

As the next step elongation of the data period is first required and then continue the study on the influence to Asian monsoon activity.

5. Reference

6. Publications

矢崎他、 NOAA-AVHRR の広域画像処理 I－地理変換および地図投影
計測・自動制御学会第 16 回リモートセンシングシンポジウム資料

中根他、 NOAA-AVHRR の広域画像処理 II－画像合成
計測・自動制御学会第 16 回リモートセンシングシンポジウム資料

矢崎、 NOAA-AVHRR 画像におけるスペクトル情報を用いた海岸線の検出と画像歪の自動補正、日本リモートセンシング学会第 10 回学術講演会論文集

諸星他、MOS-1 データによるクンブ氷河の表面状態の解析、1990 年度日本雪氷学会講演集

中根他、 NOAA-AVHRR の GAC データを用いた地表環境の季節変化、日本リモートセンシング学会第 13 回学術講演会論文集

Yazaki, Analysis on Environmental Conditions and Snow-Ice Cover Changes affecting to Monsoon Cycle in Asia, Proceedings of International Symposium on Asian Monsoon, 1992

Yazaki, Detection of Snow Cover with Satellite Data over Asia, Recent Progress in Studies of Asian Monsoon mechanism, 1999

7. International Cooperation

The study has been carried out under cooperation with China Satellite Meteorological Center(SMC), China Meteorological Agency. Every year NIED invite one or two researchers from SMC and almost every year one NIED researcher visit SMC to discuss on the method and result of cooperation research especially in the snow cover detection with satellite data.

（アブストラクト）

極軌道衛星のデータを用いて、可視、近赤外および 3 波長の熱赤外の 5 チャンネルからなる広域衛星画像データセットをデータ間隔が 7 日のものと 1 日のものの 2 種類を作成した．地上分解能はいずれも約 4km である．

週データセットを用いて、アジア地域の海面温度、地表温度、植生指標の分布図を 1 月毎に作成する手法を開発した．温度画像と植生指標は 1 月分の 4～5 画像から雲を除去した．一方、積雪分布は日データセットを用いて、チベット地域を中心とするアジア大陸中央部の積雪分布を任意の時間間隔で作成する手法を開発した．雲と雪を識別するため、1 年分のデータを用いて累積積雪指標を定義し、その値から積雪開始日と積雪終了日を決定する手法を開発した．この方法によれば、長期間雲に覆われた地域についても精度よく積雪を検出することができた．

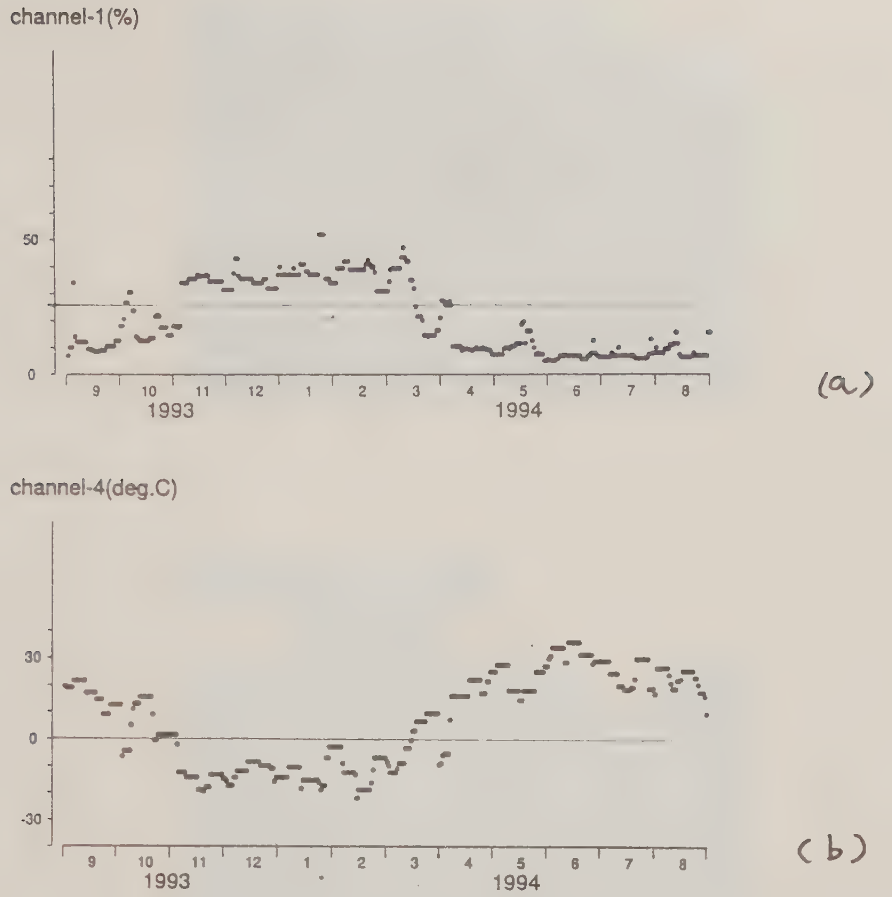


図１　補正した輝度値の変化の例　 (a) チャンネル１　(b) チャンネル４

Fig.1　Chang of pixel value of sample pixel

(a) corrected channel 1: $\overline{X}_1$　　(b) corrected channel 4: $\overline{T}_4$

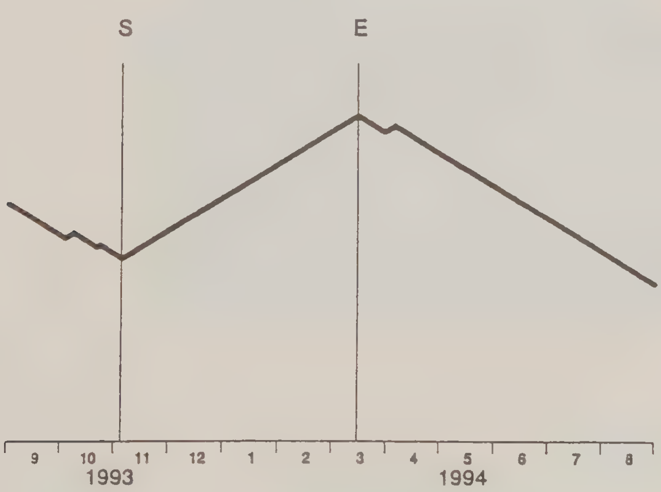


図２　関数 S(I)の一例

Fig.2　Function S(I) for sample pixel

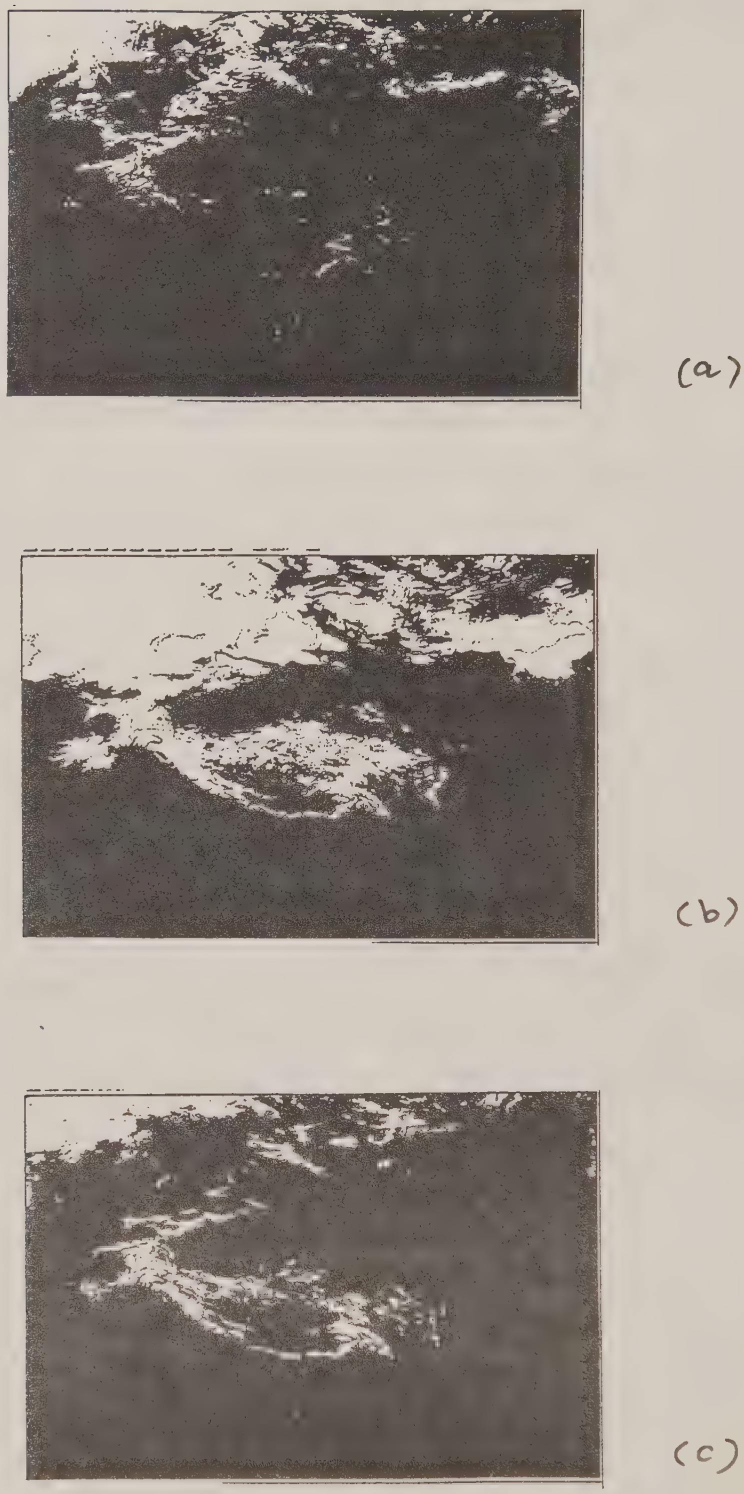


図３　検出された積雪分布

(a) 1993 年 11 月 1 日　(b)　1994 年 2 月 1 日　(c) 1994 年 4 月 1 日

Fig.3　Detected snow cover

(a) Nov.1, 1993　(b) Feb.1, 1994　(c) Apr.1, 1994

I. 大気・海洋・陸域間相互作用の諸過程に関する観測・研究

Observation and analysis on the process of the atmosphere-ocean-land interactions

3. 陸域における諸過程に関する観測・解析研究

Observation and analysis on the process over the land

(4) 地域水収支に関する解析研究

Analytical Study of Water Balance on Representative River Basins

科学技術庁防災科学技術研究所
岸井徳雄、葛葉泰久、矢崎　忍
杉田　文

National Research Institute for Earth
Science and Disaster Prevention,
Science and Technology Agency
T.Kishii, Y. Kuzuha, S.Yazaki, & F.Sugita

(Abstract)

The activity of Asia monsoon is influenced by water cycle and change of water cycle affects Asia monsoon. This study aims to clarify water balance of the regional scale in China. For these purposes hydrological data base, the elements are precipitation, runoff, evaporation, temperature, humidity and wind velocity are made. Using this data base, the characteristics of rainfall, runoff and evaporation is analyzed in the Huai he river basin.

This report shows the result of the hydrological characteristics in the Huai he river basin by the runoff model (Tank model) and the analysis of water balance. As the result, hydrological characteristics of the rainfall-runoff relation, discharge-duration curve, potential evaporation and runoff characteristics was determined in the Huai he river.

1. Objective

This study aims to clarify the characteristics of the runoff in the upstream of the Huai he river in China. This river is located on the area between the Yellow river and the Chang Jiang river. The river basin is strongly affected by the Asian monsoon. Tank model is used for analyzing daily runoff in this river.

The discharge, rainfall and evaporation data from 1983 to 1991 for this analysis used here were given by the Remote Sensing Technology Center, Department of Water Resources in China. Three discharge stations are selected in the middle to upper stream in the Huai he River. The location of the station are shown in the Fig. 1.

Data of temperature for the calculation of potential evapotranspiration come from "The monthly meteorological data in China". are used.

The "Thornthwaite method" is used for the calculation of potential evapotranspiration.

Monthly and seasonal change of hydro-meteorological condition as follow. Rainfall occur's mainly in June to October. Especially much rainfall in June, July and October. Runoff amounts is also large from June to October similar to rainfall. Potential evaporation is larger than 4 mm/day from April to September.

2.Method

The discharge station used here is the "Bengbu"(basin area 121,330 km^2), the Huai pin (16,005km^2) and the Shishen (10,190 k m^2) indicated as Fig.1. The Thank model is used for this analysis.

2-1. Rainfall and runoff relation

The rainfall runoff relation of the Huai He river from 1983 to 1991 was analyzed (Fig. 2). The annual rainfall loss of the basin is 600 mm and the potential evapotranspiration also shows similar value. The result is following. Yearly runoff ratio of Huai He river from 0.22 to 0.48. This indicate that rainfall losses are very large compare to the runoff ratio of the Japanese river basins. Annual rainfall ranges from 600 mm to 1,500 mm.

2-2. Discharge duration curves

The discharge-duration curves in the basin was analyzed.

The runoff (mm/day) of 95 day, 185 day, 275 day and 355 day are calculated. The results are shown by Fig. 1 and Table 1. For example, the 95 day runoff (mm/day) of each stations become to 0.997, 1.555 and 1.543(Table 1.).

The ratio of 95 day runoff to 355 day runoff is about nine times in Huaipin. That ratio of the Tone River basin in Japan, similar area of the Huaipin, is about twice. So the flow regime of the Huai He River is unstable as compared with the Tone River in Japan.

The discharge-duration relation has a tendency that the larger the basin area, the smaller the x day runoff. The amounts of the runoff of 355 day runoff are 0.069 to 0.187mm/month that correspond basins area from 1.2x105km^2 to 1.0x104km^2. The smallest basin area corresponds that of the Tone River in Japan.

2-3.Potential evapotranspiration

The potential evapotranspiration of the year has the value of 832mm. The rainfall loss from the estimation by water balance is 828mm. So both values show one in annual period. But the value in winter season is considerably smaller than that of the value of water balance method. So it is estimated that the

seasonal value is different to the observed one. The result of the calculation of potential evapotranspiration is following. The importance of evapotransopiration on rivers in China is suggested[1),2)].

Monthly potential evaporation ranges from 1.21mm/month in January to 166mm/month. Monthly temperature ranges from 1.5℃ to 27.3℃. The averaged values of potential evapotranspiration of the stations corresponds to 3.77mm/month to 161mm/month as shown by Fig. 4.

2-4. Runoff analysis by Tank model

Four series tank models are used for analyzing runoff of the Huai He river. The analyzed area are the mentioned three stations, that is, Bengbu, Huaipin and Shishen.

Areal rainfall amounts are calculated by arithmetic mean. There are some example[3)] about the method of estimation of the hydrologic quantities . Evapotranspiration for this analysis is used for half amounts of obsserved pan evaporation from results by annual rainfall loss analysis. Three tank models of each basin are determined. The parsmeter of them are shown at Table 2.

Result are following. In summer season, of large amount of discharge, the simulated result is coincided with observed one. But not so good in low flow period (Fig. 5).

3.Result

Annual rainfall in the Huai He river basin ranges from 600 mm to 1500 mm, runoff 160 mm to 700 mm and runoff ratio from 0.22 to 0.48.

From these results, runoff ratio is smaller than that of the river in Japan. That shows evapotranspiration have major role in water balance.

The Annual average rainfall of the year 1,129 mm and 301 mm as the annual runoff.

So the annual rainfall loss becomes 828mm. Otherwise the average potential evapotranspiration shows the amounts of 832 mm per year.

4. Discussion

On the runoff model analysis, the simulated result coincided with the observed one and did not coincide with the observed one of thee low flow period. The part of the cause may be artificial drainage, irrigation for paddy field, cultivated land etc. The effect id more large in the dry season. This bring to be difference between observed and calculated runoff in the dry season. Runoff coefficients of the first & the second tank of tank model of the upstream basins are larger than that of the down stream basin (Table 2.). It means that rapid runoff component of upstream basin is larger than that of downstream basin.

The parameters of the model are considerably small compared to that of the Japan river.

5. Reference

1) Kishii, T., Kuzuha, Y. and Yan, C.X.(1996a): Evapotranspiration in the Huai He River Basin.

Proceedings of the International workshop on Macro-scale Hydrological Modeling : 54-56.
2) Kishii, T., Kuzuha, Y. and Cao, S. (1996b) : Comparison of Yearly Water Balance between Huai He River in China and Experimental Basin in Japan (in Japanese). Proceedings of Hydraulic Engineering, No. 40, 87-92.
3) Shin, S. and Sawamoto, M. (1995) : Analysis of spatial characteristics for hydrologic quantities in the Han Gang Basin. Jounal of Japan Society of Hydrology & Water Resources, Vol. 8, No. 6, 560-567.

6. Publication

① Journal of Society

1) in Japan (1)

T. Kishii, Y. Kuzuha and.S. Cao (1996):Comparison of annual water balance between Huai He river in China and rivers in Japan. Journal of Hydroulic Engineering, Japan Society of Engineers, Vol. 40, pp.87-92.

T. Kishii(1997):Runoff analysis of the Huai He River in China. Proceedings of the International Symposium on Hydro-Environment in Asia.

2) International (3)

T. Kishii (1993):A brief look at rainy season precipitation in China 1982-1988. Proceedings of the IAHS Symposium, IAHS Pub. No. 216.

T. Kishii, Y. Kuzuha and C.X. Yan (1996):Evapotranspiration in the Huai He River Basin. Proceedings of the International Workshop on Macro-scale Hydrological Modeling.

T. Kishii and Y. Kuzuha (1998):Water balance of the Huai He River in China. Proceedings of the Second International Conference on Climate and Water.

7. Cooperation

Two researcher are invited to our institute from 5 to 19 February 1999 and cooperative sudy was done about the method of analysis of water balance. One researcher visited China from 23 February to 14 March 1999 and attended the final meeting of Japan and China working group and the workshop. Furthermore, the final discusion to researchers of the Remote Sensing Technology Application Center was carried out about the water balance on the representative river basin.

和文要旨

本研究の目的の１つであるデータベースの構築については、1971～1983年の中国の196地点での気温、降水、風速、蒸発量等の日単位データをＦＤに収録した。

ついで、中国の代表流域の淮河における水収支及び流況について解析した。

その結果、水収支解析によると年損失量は、600mm～800mmに達する大きい値を示した。また、この値は可能蒸発散量にほぼ等しい。又、流況曲線を利用した解析の結果、流域面積の増大と共に、流況は良好となる。わが国の河川との比較では、淮河代表流域の流況は良好でない。

さらに、タンクモデルを利用した淮河の流出解析により、本流域は、早い流出成分が卓越していることがが

Table 1. Discharge duration curve in the Huai he river in China

	A:Bengbu	B:Huaipin	C:Shisen
95 day runoff	0.997	1.505	1.543
185 day runoff	0.512	0.724	0.752
275 day runoff	0.241	0.449	0.463
355day runoff	0.069	0.172	0.187

Table 2. Parameters of tank model of three stations

	A:Bengbu	B:Huaipin	C:Shisen
First tank	0.31	0.40	0.70
Second tank	0.11	0.15	0.25

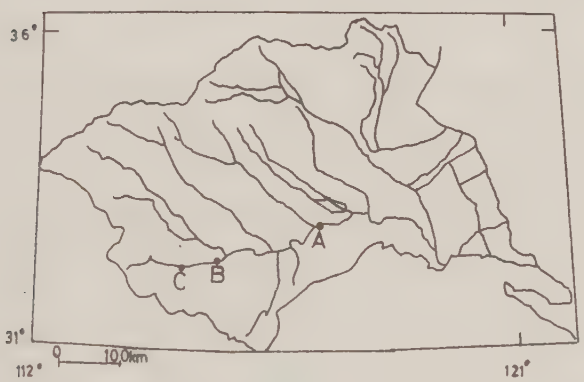


Fig.1. Location of the hydrological stations in the Huai he river basin
(A: Bengbu, B: Huaipin, C: Shi shen, D: Shanghai)

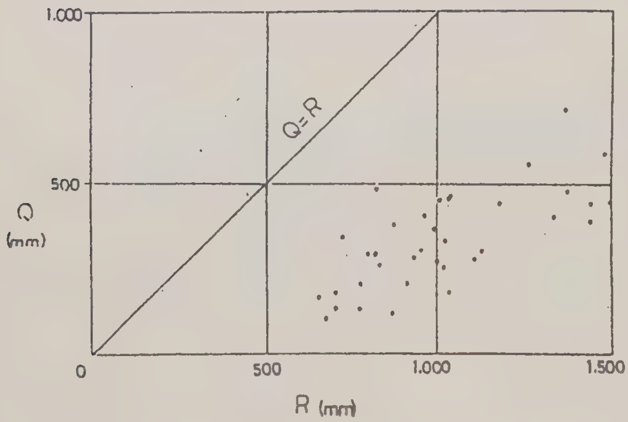


Fig. 2. Rainfall runoff relation in the Huai he river

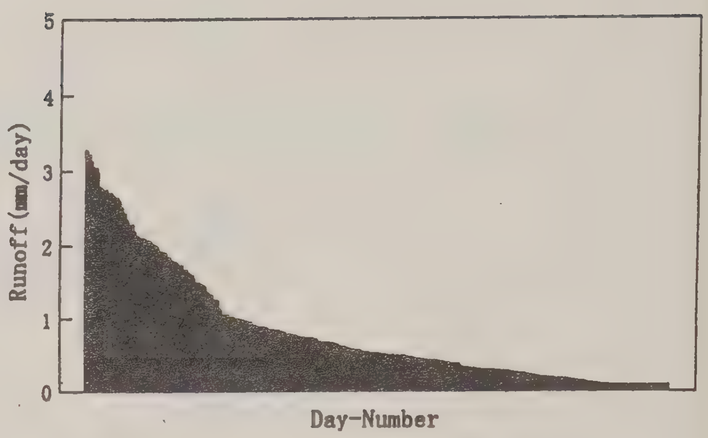


Fig. 3. Discharge duration curve (Bengbu)

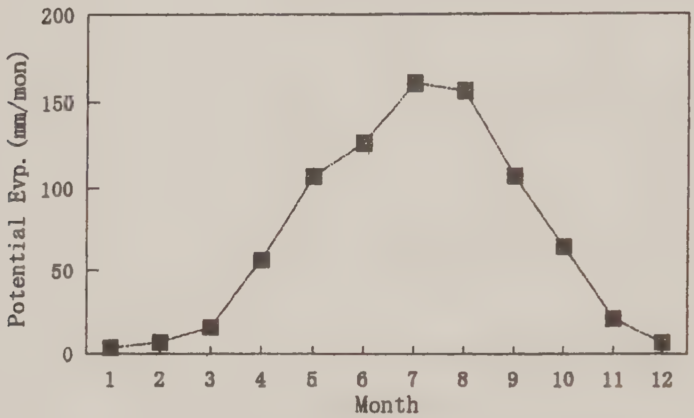


Fig. 4. Potential evapotranspiration (Bengbu)

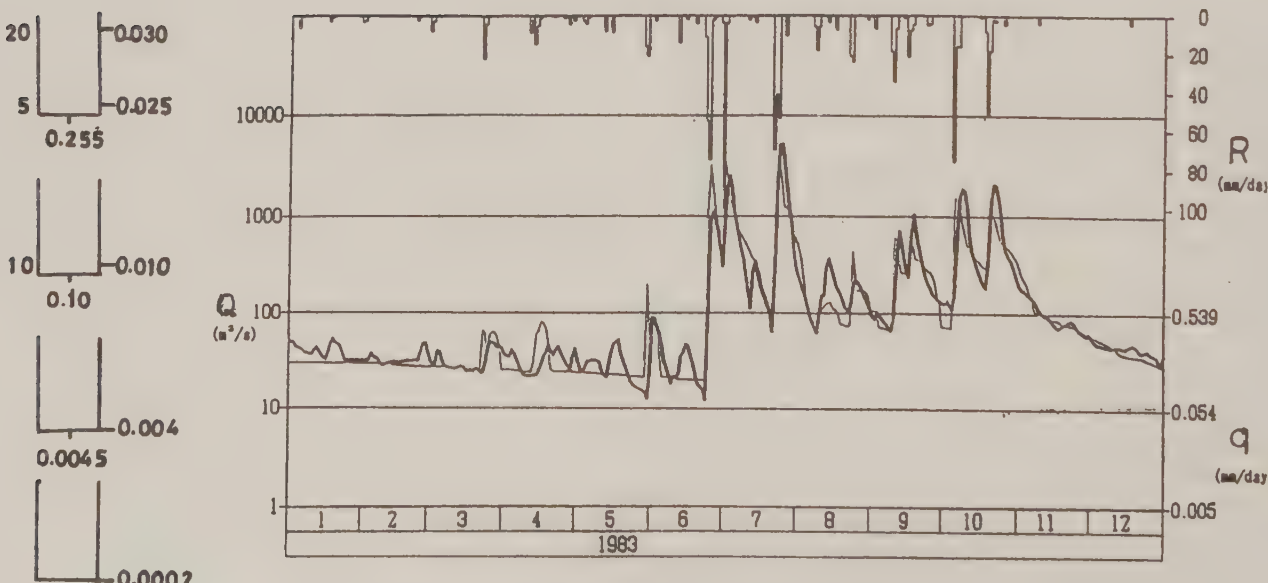


Fig. 5. Daily runoff analysis by Tank model (Bengbu)

Ⅱ．数値モデルによる大気・海洋・陸域間相互作用の実験研究
Experiment of the Atmosphere-Ocean-Land Interactions by the Use of Numerical Model

1．数値モデルによる４次元資料同化システムの開発に関する研究
Development of the Four Dimensional Data Assimilation System by the Use of Numerical Model

気象庁　予報部
竹内義明、隈健一、北川裕人、経田正幸、露木義
Forecast Department,
Japan Meteorological Agency
Yoshiaki Takeuchi, Ken-ichi Kuma, Hiroto Kitagawa,
Masayuki Kyouda and Tadashi Tsuyuki

(Abstract)

For the purpose of understanding the physical mechanism of the Asian monsoon, we carried out, 1) compilation of global data set from four dimensional data assimilation (4DDA) system of Japan Meteorological Agency (JMA) for Asian monsoon diagnosis, 2) Validation of the 4DDA system with global satellite data and in-situ observation in the Tibetan plateau, and 3) Improvement of global model used in the 4DDA system.

To investigate the physical mechanism of Asian monsoon quantitatively, we compiled a global physical parameter data set, which includes 20 parameters closely related to energy flux and water mass flux. The grid size of the data set is 2.5 deg x 2.5 deg in latitude and longitude and the temporal resolution is 6 hours, the specification of the data set enables us to study the diurnal variation of the water circulation around Asian monsoon area. The data set from April 1996 through March 1999 was distributed to domestic and foreign researchers on Asian monsoon.

Through the validation of the 4DDA system with satellite data, we found that deficiency of water vapor observations used in the 4DDA system and systematic error of global model caused some inconsistency of long-term water balance. To verify the 4DDA system with ground based observation, the 4DDA analysis was compared with Automatic Weather Station (AWS) data at Nagqu in the Tibetan plateau for April-September 1996. The AWS data were provided by 'Observation on Regional Surface Heat Budget", one of the research items of JEXAM. It was found that 4DDA data and AWS observation showed good agreement, which implied that the 4DDA system was well functioned. However, there were some differences of diurnal variation of temperature between 4DDA data and AWS observation depending on weather conditions such as precipitation and cloudiness. The result implied further progress of 4DDA system might be expected by improving spatial and temporal resolution and accuracy of cloudiness forecast.

An experiment showed cloud parameterization affected the forecast characteristics of Asian monsoon because less cloudiness enhances thermal gradient between land and ocean, which results in the intensification of Asian monsoon. Then, in order to improve the global numerical prediction model used in the 4DDA system, one-month forecast experiments for the Asian summer monsoon were carried out by using the model with inclusion of effects of aerosols and modified parameterization schemes for cloud cover. Different vertical profiles and optical properties of aerosols between over the land and ocean were used. The indirect effect of aerosol was considered by reducing the effective radii of cloud droplets over the land. Diagnostic parameter of cloud cover was set different between over the land and ocean. Results showed that the above modifications reduce surface downward radiation over the Eurasian continent. This reduction suppresses the continental heat low, modifies horizontal moisture transports, delays the seasonal march of Asian summer monsoon and affects the

activities of Baiu front.

Finally, we revised the cumulus convection scheme of global model and carried out forecast experiments. New scheme named modified Arakawa-Schubert scheme in which the coupling between dynamics and cumulus convection is enhanced by allowing the time scale for the adjustment toward the equilibrium to vary according to the vertical motion near the top of the mixed layer. Results from some forecast experiments proved that the new scheme can simulate realistic Madden-Julian oscillation and precipitation distribution.

1. Objectives

As was studied by many scientists, large-scale water circulation is one of the key factors to understand the Asian summer monsoon. Land-sea heat contrast and high mountain region induce large moisture convergence and then enormous precipitation occurs southeast of the Asia. Thus, the monsoon research must place high priority in the construction of high quality data set of water circulation.

The four dimensional data assimilation (4DDA) system produces a uniformly spaced and well-defined meteorological and hydrological parameters through the objective analysis and model diagnostics. This data set will be used for understanding the mechanism of the monsoon and for upgrading the long-range forecasts.

Main objective of this study are to produce a global data set on energy and water circulation parameters from the 4DDA system and to distribute the data set to Asian monsoon researchers for Asian monsoon diagnosis. We also validate the 4DDA system with global satellite data and in-situ observation and improve the global model used in the 4DDA system.

2. Methods

2.1 Products of 4-DDA system

We have produced the global physical parameter data set for the period of April 1996 through March 1999 and compiled the data onto CD-ROM (2 disks per year) with a browse software. To make the data set volume on the CD-ROM compact, we selected 20 elements, all of which are two-dimensional properties, as shown in Table 1. The grid of the data is 2.5 deg x 2.5 deg and the time resolution is 6 hours.

2.2 Validation of 4-DDA products with global satellite data and in-situ observation in Tibet

1) Validation with satellite data

Using preliminary 4DDA data, we checked the consistency of long-term water balance and validated the data set with SSM/I (Iwasaki et al., 1995). First, consistency of long-term water balance was checked by comparing the first guess and observation. Secondly, objective analyses of total precipitable water are compared with the SSM/I derived data. The SSM/I data, which is not used in the operational analysis, may give independent information on the performance of the 4DDA.

2) Validation with in-situ data

In order to verify the quality of the 4DDA system, the outputs from the system were compared with Automatic Weather Station (AWS) data at Nagqu in the Tibetan plateau for April-December 1996. The AWS observation is hourly and was operated under “Observation on Regional Surface Heat Budget”, one of the research items of JEXAM. Nagqu is located in a rather flat area of the Tibetan plateau, so it is suited for comparison with the analysis data. The analysis data from 4DDA system were prepared on a 1.25deg x 1.25deg grid at 6-hour intervals, and bilinearly interpolated to the location of Nagqu. AWS data used are 10m temperature and wind.

2.3 Improvements of numerical model used in 4-DDA system

The NWP model used in our experiments is a global NWP model (GSM9603) at JMA. It has a truncation wave number of T63 in the horizontal and 30 levels up to 10hPa in the vertical. Details of this model are found in the publication available from JMA (1997).

1) Aerosol and cloud parameterization

In order to study systematic impacts of aerosol and cloud radiation on Asian summer monsoon, we have made one-month forecasts from 5 initial conditions at 12 UTC, 31 May 1991- 1995. The control model does not include any effects of aerosols and uses the same cloud diagnostic scheme both over the land and ocean.

Regarding aerosol and cloud radiation, the control model is modified in the following ways.

(a) We consider only two types of vertical profiles and optical properties of aerosols, which are different between over the land and ocean. The size of aerosol is dependent on relative humidity.

(b) The indirect effect of aerosol is considered by reducing the effective radii of cloud droplets over the land because the concentration of cloud condensation nuclear is higher over the land than over the ocean.

(c) Diagnostic parameter of cloud cover is set different between over the land and ocean. This modification increase cloud cover over the land in particular for low cloud.

2) Convection scheme

Deep cumulus convection in the model is parameterized by an economical prognostic Arakawa-Schubert scheme (Randall and Pan, 1993). In the original version of the scheme (AS1), the time scale for the adjustment toward the equilibrium value for the cloud work function is set to a constant. In the modified version of the scheme (AS2), the time scale is allowed to vary according to the vertical motion near the top of the mixed layer. If downward motion is found here, the time scale is increased so as to suppress cumulus convection. It should be noted that we have a stronger coupling between dynamics and cumulus convection in the AS2 scheme than in the AS1 scheme. We carried out seven-month time integration from 30 May 1990, and compared the results focusing the simulation of the Madden-Julian oscillation (MJO), which is one of the key targets for extended-range prediction of Asian monsoon because of its long time scales (30-60days).

To resolve the problem that AS1 shows unnatural precipitation distribution around Asian monsoon region, we also carried out one month time integration from 1 July 1997 focusing precipitation distribution.

3. Results

3.1 Products from 4-DDA system

The global physical parameter data set for the period of April 1996 to March 1999 were released and distributed to more than fifty Asian monsoon researchers. The data set is compact and saved on to CD-ROM with browsing software, so the researcher can treat it with ease. Fig.1 shows global water circulation data set on CD-ROM and an example of global distribution of precipitable water extracted from the data set.

3.2 Validation of 4-DDA products with global satellite data and in-situ observation in Tibet

1)Validation with satellite data

Fig.2 shows diurnal cycles of precipitation and evaporation averaged over 3 months, June, July and August. Around the monsoon Asia, precipitation has a large diurnal cycle with its maximum in the evening, where the moisture is mainly supplied by convergence. The diurnal cycle around the monsoon Asia may play an important role in the atmospheric global circulation.

Fig.3 shows monthly means of SSM/I-derived (top) and analyzed (bottom) total precipitable water

around the tropical Pacific region in July 1994. East of 170W, near the ITCZ and SPCZ total precipitable water obtained from the 4DDA is overestimated in comparison with the SSM/I data. This kind of error is not found west of 170W. The difference between the eastern and western sides of 170W is attributed to the moisture data retrieved from the GMS (Geostationary Meteorological Satellite) infrared images (Baba, 1987). Outside of the GMS observing area (east of 170W), we get temperature observation from the SATEM, i.e. temperature data retrieved from sounder instrument on the NOAA satellites, but few data of the moisture over the ocean. There appear unrealistic feedback between the observed temperature and the first guess of relative humidity, because the current operational NWP model has climate drifts of cooling and moistening biases in the tropics. The SATEM data may correct low-level cooling bias in the objective analysis and activate the convection in the course of time integration. Accordingly, enhanced horizontal convergence increases total precipitable water in the first guess. This feedback is avoidable when moisture observation is simply introduced into the objective analysis.

2) Validation with in-situ data in Tibet

Fig.4 shows time sequences of surface air temperature and wind at Nagqu from the 4DDA data denoted as 'GANAL' and the AWS data for 1-10 April 1996. It is found that the analyzed surface air temperature and observed temperature shows good coincidence but analyzed surface air temperature shows less diurnal variation. Since maximum temperature occurred around 08UTC at Nagqu, the 4DDA system, the temporal resolution of which is six hours, can not correctly estimate the amplitude of diurnal variation. Furthermore we can find small negative temperature biases of the 4DDA analysis. The bias may be caused by ambiguity of temperature correction in height because model surface used in the 4DDA system and ground surface is different particularly in plateau regions. Wind data also shows good coincidence and the 4DDA system represents typical diurnal variation of wind though the amplitude is less than the AWS observation.

Fig.5 shows temperature difference between 06UTC and 00UTC between analyzed surface air temperature and observed air temperature for two periods. In summer, several small temperature difference are observed by the AWS associated with rainy days. On the other hand, we can find large temperature difference in late fall associated with clear days. The relationships between the 4DDA analysis and AWS observation varies with seasons and weather conditions. These variations may be attributed to model biases associated with diurnal variation near surface over the mountain regions because we have less observation at 06UTC.

The results suggested that our 4DDA system is well functioned and improvements of temporal and spatial resolution and cloudiness forecast are essential to realize further improvement of 4DDA system.

3.3 Improvements of numerical model used in 4-DDA system

1) Aerosol and cloud parameterizations

Fig.6 indicates that in the test run land-cloud enhancement effectively increases cloud cover over the land. Both aerosols and increased cloud covers enhance the atmospheric albedo and reduce the atmospheric absorption. The reduction of surface downward shortwave radiation is about 50 W/m^2 over the land around the monsoon Asia. Surface longwave radiation is shown to increase over the regions where cloud cover increases. The reduction of net downward shortwave radiation takes over the increase in downward longwave radiation. As responses to that, upward longwave radiation, sensible heat and latent heat decrease over the land. The reduction of these heat fluxes significantly lower the low-level temperature over the Eurasian continent.

Fig.7 shows the monthly averaged forecast error of the earth's absorbed solar radiation compared with observational data provided by NOAA satellites. The control run overestimates the absorbed solar radiation over the continent but underestimates it over the ocean. Both errors are reduced in the experimental run as is easily expected from the modification of the cloud scheme.

2) Convection scheme

Fig. 8 shows the time-longitude cross section for 200hPa velocity potential along the equator as well as the location in longitude of tropical cyclones in the Northern Hemisphere. A time filter which only passes period of 30-60 days is applied for the velocity potential field. This figure indicates that the model using the AS1 scheme does not well simulated the MJO and the tropical cyclone activity is weak in comparison with the analysis and the model using the Kuo scheme (Kuo, 1974). The model using the AS2 scheme significantly improves the simulation of MJO and tropical cyclone activity.

Fig.9 shows monthly mean precipitation distribution in July 1997. The AS2 scheme shows realistic distribution of precipitation around western part of India and northern part of Bengal sea due to proper parameterization of cumulus convection by coupling it with upward motion forced by topography

4. Discussions

The global physical parameter data set compiled in this study is compact and enables us to study diurnal variation of the water circulation around Asian monsoon area. In near future we will need three-dimensional parameters to investigate vertical structure of water and energy circulation and need higher spatial and temporal resolution to investigate phenomena associated with Asian monsoon in details.

To make detailed analysis of the Asian monsoon, many kinds of observation should be assimilated to 4DDA system. In particular to increase the number of moisture observations is essential to improve the analysis of water circulation. Satellite measurements have no-doubt to be promising ways of observing global moisture with appropriate retrieved methods. In the JMA, a retrieval method of TOVS data has been developed using one-dimensional variational method. Our preliminary result shows the implementation of the method have positive impacts on the temperature and moisture analysis. The SSM/I data, which is used only for validation in this study, has a great potential to be assimilated. We should implement the SSM/I data to the 4DDA system after establishing a real-time ingest system of the SSM/I data. Key problems of real-time assimilation SSM/I data are large data volume and the complexity of assimilation method.

Regarding to assimilation of in-situ observation, some problems (e.g. inhomogenuity of the observation, height correction between model surface and truth ground surface) have been recognized. Unless these problems are not resolved, we cannot assimilate the valuable surface truth data into the 4DDA system in optimum way. The preliminary comparison shows significant dependency of temperature and wind on the weather condition and topography in the Tibetan plateau.

In one-month forecast experiments for Asian summer monsoon, the newly introduced parameterization schemes reduce surface downward radiation over the Eurasian continent successfully. This reduction suppresses the continental heat low, modifies horizontal moisture transports, delays the seasonal march of Asian summer monsoon and affects the activities of Baiu front. Many uncertainties remain in the direct and indirect effects of aerosol. Furthermore, there are other important physical processes to cause systematic errors of land-ocean heat contrast in the model. The real reasons for underestimation of land-ocean contrast do not have been confirmed yet. We need further studies on the cloud formation mechanism associated with land-ocean contrast.

The result of experiments on convective scheme suggests that we have to include the effect of coupling between the vertical motion at the top of the mixed layer and cumulus convection for successful simulation of MJO, the tropical cyclone activity, and realistic precipitation distribution. Some encouraging results of this study should contribute the improvement of our operational 4DDA system in near future.

5. References

Baba,A., 1987: Improvement of estimation method of moisture data from satellite cloud sounding. JMA/NPD technical report No.16, 54pp.

Iwasaki,T., K.Kuma, T.Nakazawa, and A.Shibata, 1995: Annual Report (FY1994) of Japanese Experiment on Asian Monsoon (JEXAM). Science Technology Agency, 129-136.

JMA, 1997: Outline of the operational numerical weather prediction at the Japan Meteorological Agency. 126pp.

Kuo,H., 1974: Further studies of the influence of cumulus convection on large scale flow. J.Atmos.Sci., **31**,1232-1240.

Randall,D. and. D.Pan, 1993: Implementation of the Arakawa-Schubert cumulus parameterization with a prognostic closure. Meteorological Monograph/ The representation of cumulus convection in numerical models. J.Atmos.Sci., **46**, 137-144.

6. Publications

(1)Scientific Journals

Iwasaki,T. and H.Kitagawa, 1998: A possible link of aerosol and cloud radiations to Asian summer monsoon and its implication in long-range numerical weather prediction. J.Meteor.Soc.Japan, 76, 965-982.

(2)Reports

Iwasaki,T., 1995: An estimation method of atmospheric water balance with 4-dimensional data assimilation., Proceeding of 'Second International Symposium on Assimilation of Observations in Meteorology and Oceanography', TOKYO JAPAN, 13-17 March 1995.

Iwasaki,T., 1996: Impacts of parameterization scheme of cloud formations on one-month dynamical forecast of the Asian summer monsoon. Proceedings of the International Workshop on the Climate System on Monsoon Asia, 3-7 December 1996, Kyoto, Japan, 164-167.

Iwasaki,T., 1996: Annual Report (FY1995) of Japanese Experiment on Asian Monsoon (JEXAM). Science Technology Agency, 123-130.

Iwasaki,T. and H.Kitagawa, 1997: Extended forecast experiment of the Asian monsoon using a global model with a cloud scheme different over between the land and ocean. The First WMO International workshop on Monsoon Studies, 24-28 February 1997, Bali, Indonesia.

Iwasaki,T. and H.Kitagawa, 1998: A possible link of aerosol and cloud radiations to Asian summer monsoon and its implication in long-range numerical weather prediction. Seminar/Workshop on Short-term Climate Prediction, 2-4 March 1998, Tokyo, Japan.

Iwasaki,T. and H.Kitagawa, 1998: A possible link of aerosol and cloud radiations to Asian summer monsoon and its implication in long-range numerical weather prediction. JMA/NWP Technical Report, JMA, 33, 22pp.

Iwasaki,T., H.Kitagawa and T.Tsuyuki, 1998: Annual Report (FY1997) of Japanese Experiment on Asian Monsoon (JEXAM). Science Technology Agency, 107-114.

Iwasaki,T., K.Kuma, H.Kitagawa and T.Tsuyuki, 1997: Annual Report (FY1996) of Japanese Experiment on Asian Monsoon (JEXAM). Science Technology Agency, 101-108.

Iwasaki,T., K.Kuma, T.Nakazawa, and A.Shibata, 1995: Annual Report (FY1994) of Japanese Experiment on Asian Monsoon (JEXAM). Science Technology Agency, 129-136.

Kuma,K., 1996: The Madden-Julian oscillation and the onset of Asian summer monsoon – Prelude to numerical prediction of monsoon onset -. Proceedings of the International Workshop on the

Climate System on Monsoon Asia, 3-7 December 1996, Kyoto, Japan, 202-205.
Kuma,K., 1996: The convection schemes and the Madden-Julian oscillation. The WGNE Workshop on Numerical Weather Prediction and Data Assimilation for Climate, 23-25 October 1996, Tokyo, Japan.
Tsuyuki,T., K.Kuma, H.Kitagawa, M.Kyouda, Y.Takeuchi, 1999: Development of the four dimensional data assimilation system by the use of numerical model, Recent Progress in Studies of Asian Monsoon Mechanism, Meteorological Research Institute, 295-308.

7. International Cooperation

None

（和文アブストラクト）

本研究では、1) ４次元資料同化システムによるアジアモンスーン診断資料の作成・配布、2) 4 次元資料同化システムから得られた水循環データの全球衛星データおよびチベット特別観測データによる検証、3) ４次元資料同化システムに用いられている数値モデルの改良を行った。

まず、アジアモンスーン機構を定量的に理解するために、気象庁の４次元資料同化システムから水フラックスやエネルギーフラックスなど（20 要素）の全球２次元物理モニターファイル（空間分解能 2.5°×2.5°、時間分解能 6 時間）を作成した。作成期間は 1996 年 4 月から 1999 年 3 月であった。本データセットは、時間分解能が高いため、チベット、東南アジア地域の日変化を良く表現することが可能で、アジアモンスーンの研究にとって有益であった。本データセットは、汎用の画像化ユーティリティと合わせて CD-ROM（２枚／年）に格納され、「アジアモンスーン機構に関する研究」の研究担当者、研究検討委員会委員のみならず、国内外のアジアモンスーン研究者計 58 名に配布され、アジアモンスーン研究に広く利用された。

また、４次元資料同化システムを改善するために、本システムから得られた全球水循環データを GMS や SSM/I の衛星データを用いて検証した。全球水循環データから計算された長期水循環はわずかに収支が合わないが、４次元資料同化システムに入力される水蒸気データが少ないことが一因であることが衛星データによる検証から分かった。その他、予報モデルの系統的誤差も収支不一致の原因であり、水蒸気の全球衛星観測データの利用および予報モデルの改良の必要性が示された。

一方、観測データの少ないチベット域における４次元資料同化システムの性能を評価するために、「アジアモンスーン機構に関する研究」の「地表面熱収支に関する観測研究」により実施されているチベット特別観測の自動気象観測データを用いて、検証を行った。地形が比較的平坦な Nagqu における 1996 年４～12 月の地上観測データと４次元資料同化システムで得られた解析値を、地上気象要素（気温、風）について比較した。両者はよく対応しているが、気温の日較差に降水、雲量に起因する違いが見られた。この結果から、４次元資料同化システムが良好に機能していること、システムをさらに改良するために、時間空間分解能の向上、雲量の予報精度向上が必要であることが示された。

アジアモンスーンの長期予報を改善するために、雲量のパラメタリゼーションが予報精度に及ぼす影響を調べた。雲は地表面での日射を減らし（アルベド効果）、その結果陸面からの熱フラックスを減少させる。１ヶ月予報実験の結果、雲量を減らすことによってアジアモンスーンが強化されることが見出された。この理由は、雲量の減少によりユーラシア大陸と太平洋との間に大きな気圧傾度が形成され、極東方面への水蒸気輸送量が増えるためである。この実験で、雲量のパラメタリゼーションは大気陸面相互作用を通じてアジアモンスーンの予報特性に大きな影響を与えることが分かった。

４次元資料同化システムに用いられている全球モデルを改良するために、エーロゾルの効果を組み込み、かつ雲量のパラメタリゼーションを変更して、夏季アジアモンスーンに対する１ヶ月予報実験を行った。海上と陸上で異なるエーロゾルの鉛直分布と光学的性質を用いた、陸上で雲粒の有効半径を減少させることによってエーロゾルの間接効果を考慮した。さらに雲量の診断的パラメタを海上と

陸上で変えた。1ヶ月予報実験の結果、これらの変更によってユーラシア大陸上の雲量が増加し、下向きの地表面放射フラックスが減少することがわかった。この減少は、大陸上の熱的低気圧の発達を抑え、水蒸気の水平フラックスを変形し、アジアモンスーンの季節進行を遅らせ、梅雨前線の活動に影響することがわかった。また、大気と地表面による太陽放射の全吸収量にみられたモデルの系統的誤差が大きく減少した。

さらに、全球モデルに使用されている積雲対流スキームを改良し、予報実験を行ってそのインパクトを調べた。積雲対流スキームにおいて対流の起こりやすさを混合層上端における上昇流に応じて変化させた。その結果、力学と積雲対流の相互効果を強めて、マデン・ジュリアン振動や、熱帯低気圧の活動の表現が改善した。さらに、積雲対流スキームにおける地形性強制上昇流への感度も強まり、現実に近いアジアモンスーン領域の月平均降水量分布が再現できるようになった。

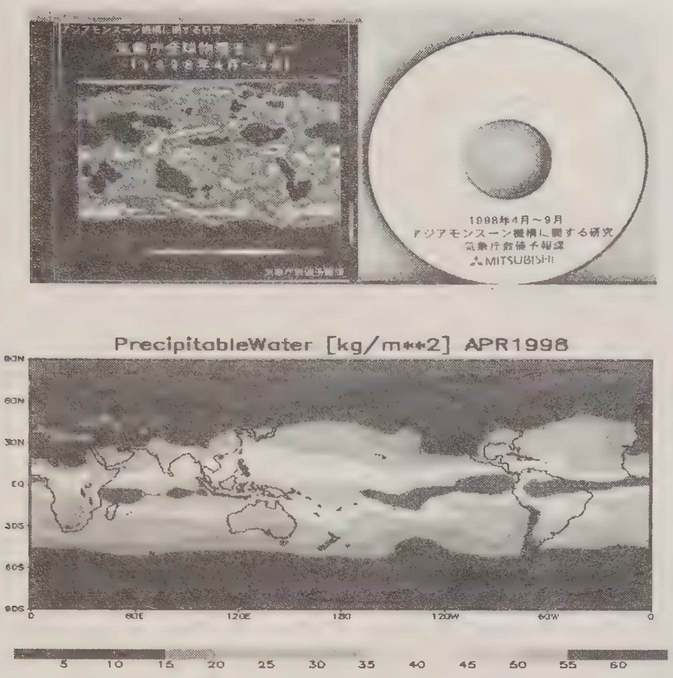


Fig.1 Global water circulation data set on CD-ROM and an example of global distribution of precipitable water extracted from the data set.

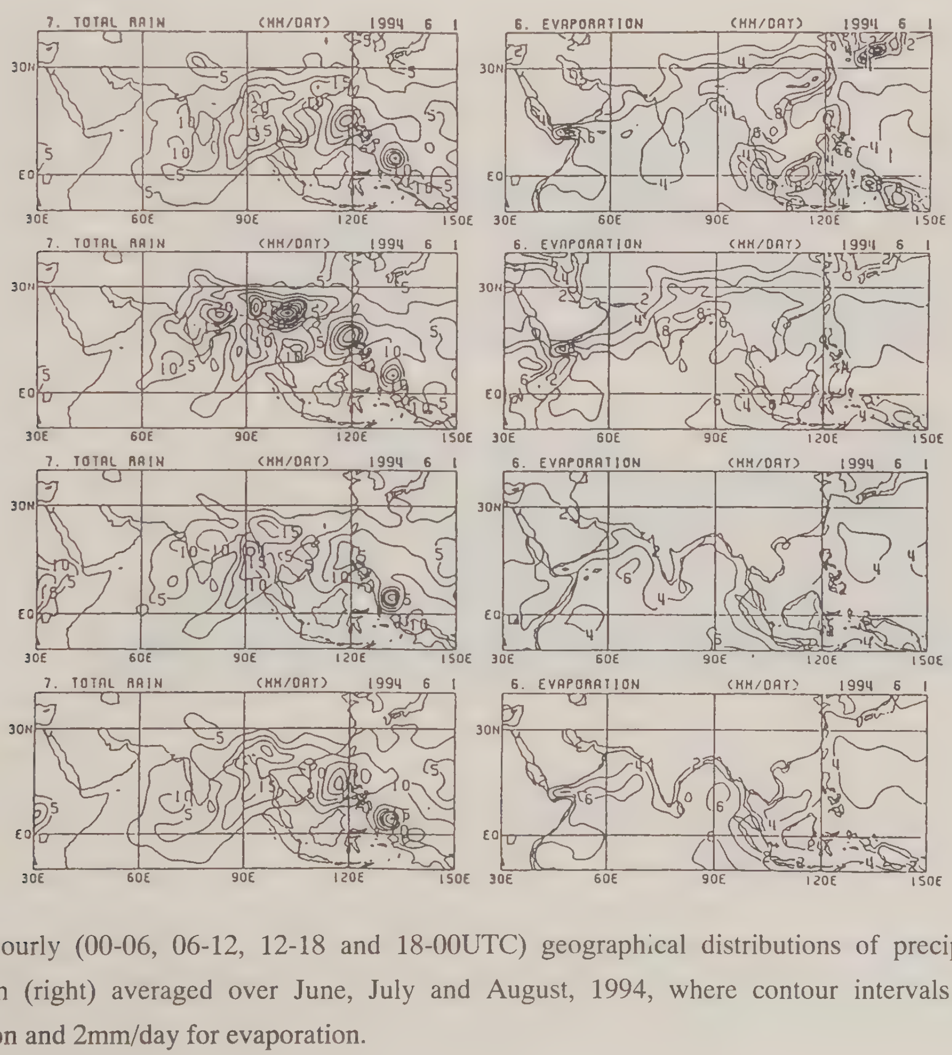


Fig.2 6-hourly (00-06, 06-12, 12-18 and 18-00UTC) geographical distributions of precipitation (left), and evaporation (right) averaged over June, July and August, 1994, where contour intervals are 5mm/day for precipitation and 2mm/day for evaporation.

Element Name	Content	Unit
ROF	Run off	m/day
FLLH	Latent heat flux	W/m**2
FLSH	Sensible heat flux	W/m**2
LTRS	Transpiration	W/m**2
LINT	Interception loss	W/m**2
RRC	Rain rate (convection)	mm/day
RRL	Rain rate (large scale convection)	mm/day
UWV	Horizontal flux of water vapor (eastward)	m/s
VWV	Horizontal flux of water vapor (northward)	m/s
RSUB	Radiation flux at surface (shortwave, upward)	W/m**2
RSDB	Radiation flux at surface (shortwave, downward)	W/m**2
RLUB	Radiation flux at surface (longwave, upward)	W/m**2
RLDB	Radiation flux at surface (longwave, downward)	W/m**2
RSUT	Radiation flux at the top of atmosphere (shortwave, upward)	W/m**2
RSDT	Radiation flux at the top of atmosphere (shortwave, downward)	W/m**2
RLUT	Radiation flux at the top of atmosphere (longwave, upward)	W/m**2
CLA	Total cloudiness	Non unit
RCSB	Cloud radiative forcing (shortwave, surface)	W/m**2
RCLB	Cloud radiative forcing (longwave, surface)	W/m**2
TPW	Precipitable water (snap shot)	kg/m**2

Table 1 Parameter list of the JMA global physical parameter CD-ROM.

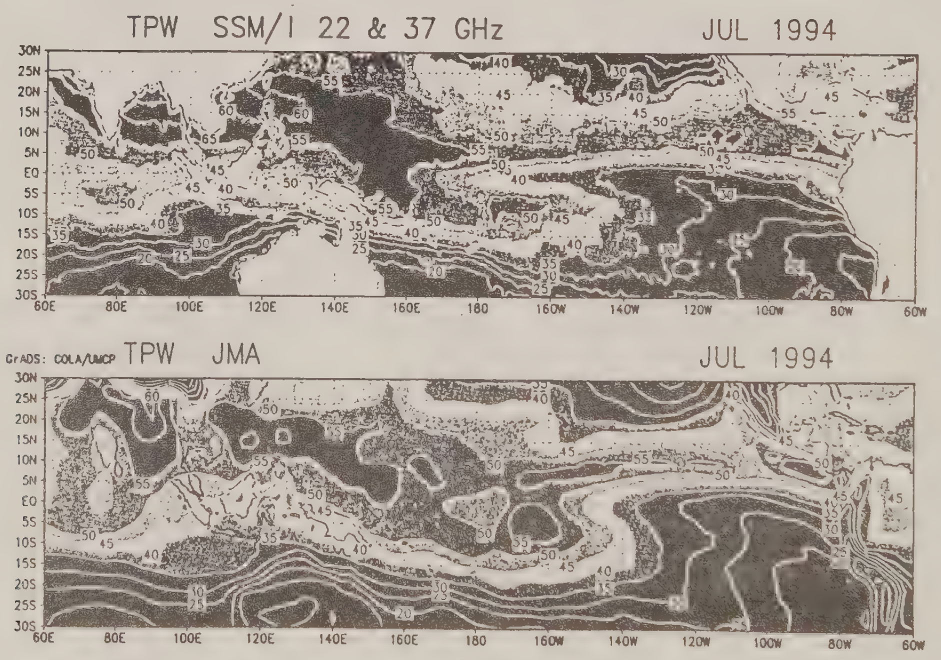


Fig.3 Total precipitable water (mm) averaged over July 1994. Top and bottom panels show results of SSM/I and 4DDA, respectively. The contour interval is 5mm/day.

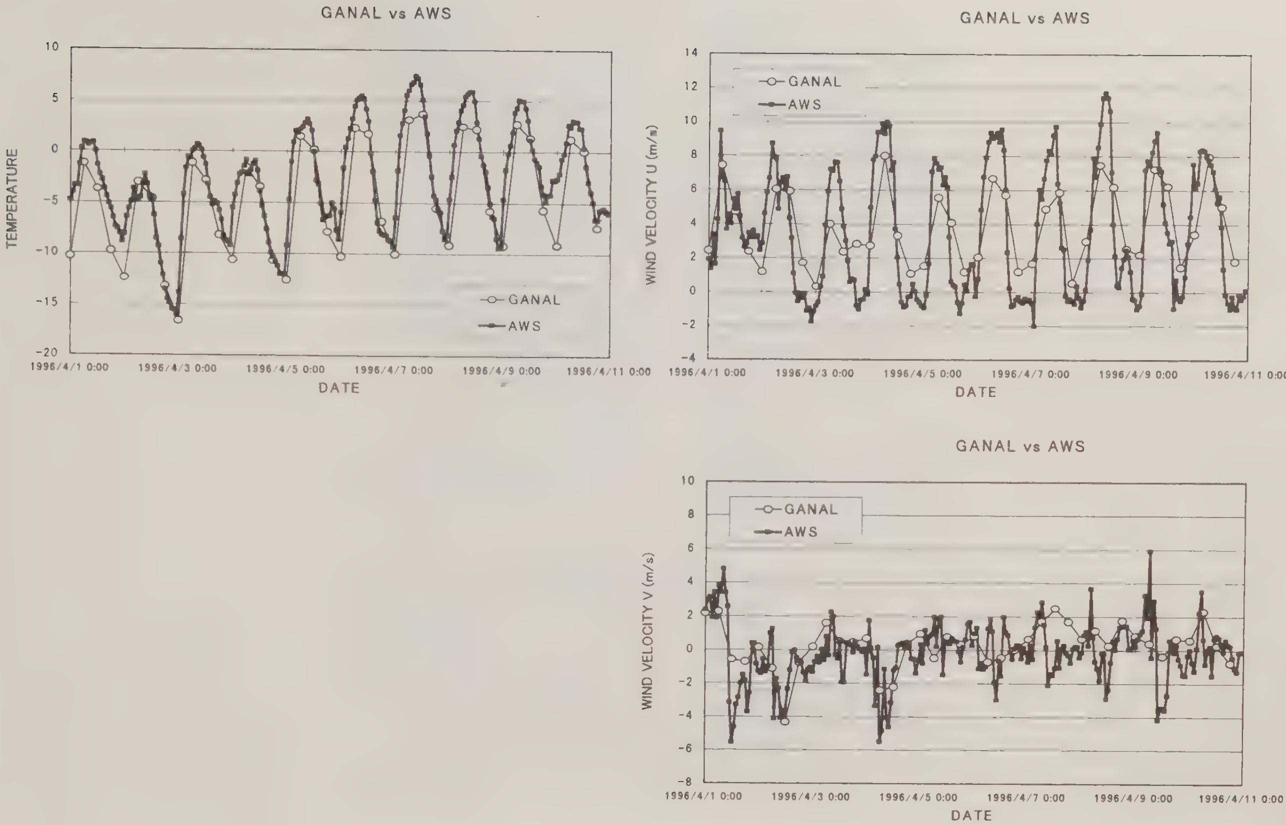


Fig.4 Time sequences of surface air temperature (℃) and wind velocities U, V (m/s) at Nagqu from the 4DDA data (○) denoted as 'GANAL' and the AWS data (■) denoted as 'AWS' for 1-10 April 1996.

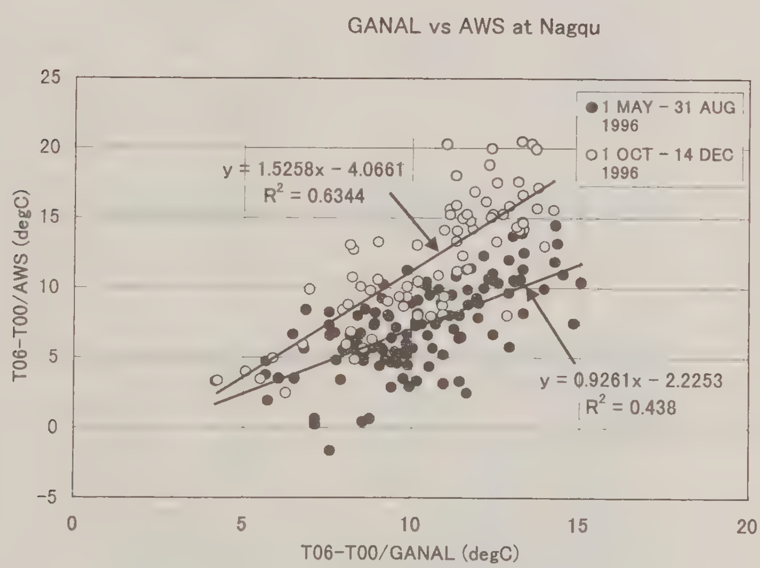


Fig.5 Temperature difference between 06UTC and 00UTC analyzed by 4DDA analysis (denoted as 'GANAL') and AWS observation (denoted as 'AWS'). Closed circles are results for the periods from 1 May through 31 August 1996 and open circles are results for the periods from 1 October through 14 December 1996.

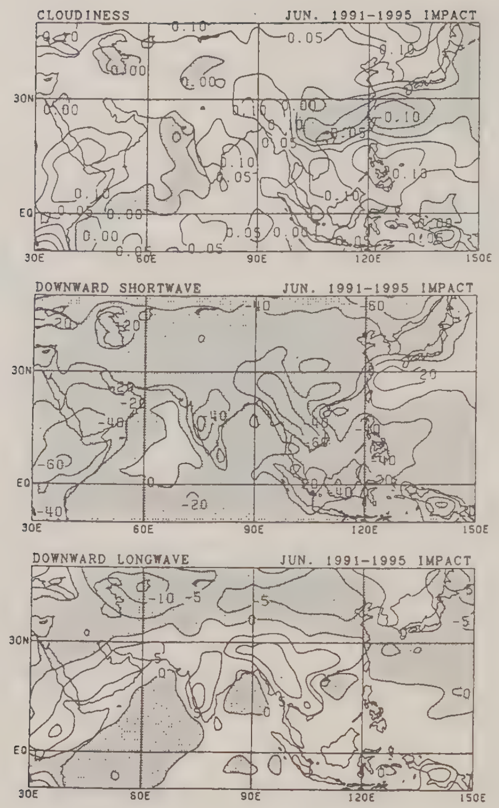


Fig.6 Monthly mean differences (test run and control runs) averaging over June in 1991-1995, where the test run includes the direct and indirect effects of aerosols and land-ocean difference in cloud formation. Negative impacts are shaded. Upper panel: Total cloud cover with a contour interval of 0.05, Middle panel: Downward short wave radiation at the surface with a contou interval of 20W/m^2, Lower panel: Downward long wave radiation at the surface with a contour interval of 5W/m^2.

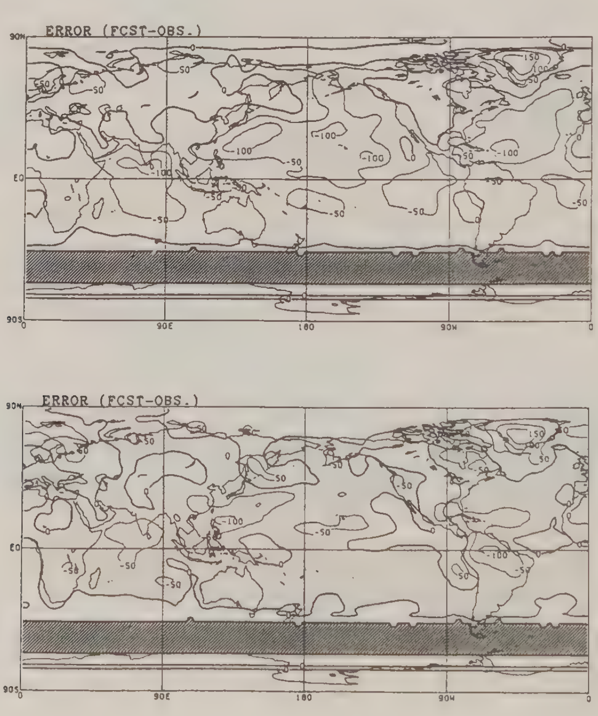


Fig.7 Monthly averaged forecast error of the total earth's absorbed solar radiation. Upper and lower panels show the control run and the experimental run, respectively. Contour interval is 50W/m^2 and negative area is shaded. Observational data are missing south of 45 ° S

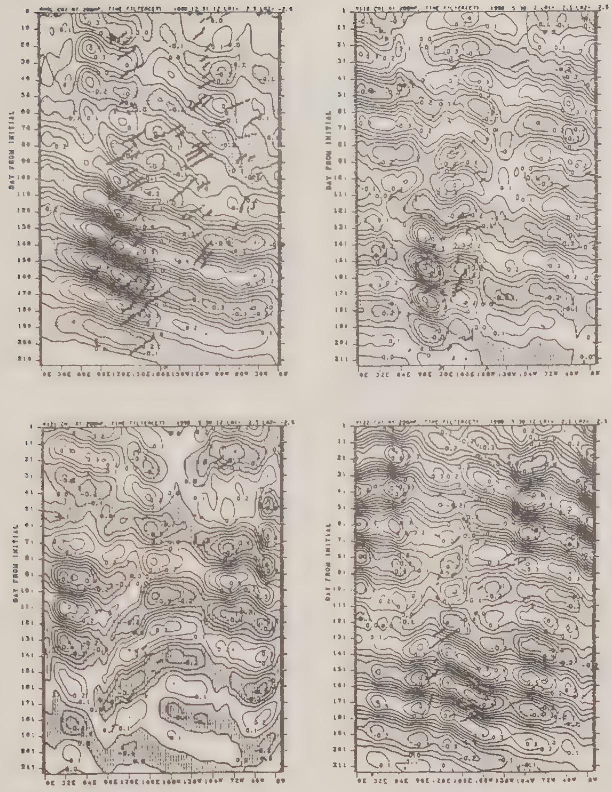


Fig.8 Time-longitude cross section of 200hPa velocity potential ($x10^7 m^2/s$) along the equator as well as the location (○) in longitude of the tropical cyclones in the northern hemisphere. Contour interval is $0.1x10^7 m^2/s$. Negative area is shaded. See text for details. Upper left: JMA analysis and Navy best track.. Upper right: Kuo scheme. Lower left: AS1 scheme. Lower right: AS2 scheme.

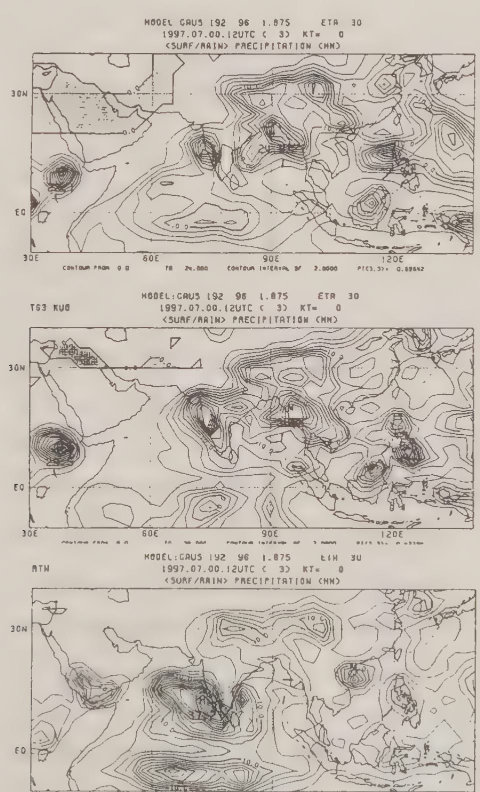


Fig.9 Monthly mean precipitation distribution in July 1997. Upper: AS2 scheme. Middle: Kuo scheme. Lower: AS1 scheme. AS2 scheme and Kuo scheme represent realistic precipitation distribution.

II. 数値モデルによる大気・海洋・陸域間相互作用の実験研究

Experiment of the atmosphere-ocean-land interactions by the use of numerical models

2. 広域水収支モデルの開発に関する研究

Development of water balance model over the wide area

科学技術庁防災科学技術研究所

中根 和郎、幾志 新吉

National Research Institute for Earth Science and Disaster Prevention,Science and Technology Agency.

K. Nakane and S. Kishi

(Abstract)

The purpose of this study is to develop the **R**egional **W**ater **Ba**lance model based on the **T**ank Model(RWBaT) for assessing the variation of water resources and soil moisture over the wide area due to the fluctuation of Asian Monsoon activity. The RWBaT model predicts hydrological regime, which are river discharge, water contents in the soil, storage amount of water in the ground, snow deposit, snow melt and actual evapotranspiration on each grid area with 0.5 degrees x 0.5 degrees in latitude and longitude from observed data of precipitation, evaporation and air-temperature. The product of the atmospheric general circulation model(AGCM) is also available for input data of the model. The model is composed of many field models representing hydrological responses in the grid areas with 0.5 degrees x 0.5 degrees and river models simulating river discharge at each river points in simplified river system. The characteristic of the model is parameters are determined by topographic condition. The prototype of the RWBaT model had been developed and applied to Chaophraya River basin(110 thousand km^2) in Thailand and Huaihe River basin(121 thousand km^2) in China. Reasonable estimations were obtained in both basins. In these simulations, same parameters of the model were used for two basins, though climate, topography and vegetation in two basins are different each other.

The **A**sian **R**egional **W**ater **Ba**lance model based on the **T**ank Model(ARWBaT) advanced from the RWBaT model was also developed. The ARWBaT model was applied to the Asian Continent covering area from 60° N to 20° S in latitude and from 30° E to 160° E in longitude. Simulation using AGCM data in 1970 were carried out for checking the model working. The ARWBaT model worked well to estimate the river discharge and water contents in the surface ground on each grid area with 0.5 degrees resolution. However, the accuracy of the results is not clear in this time. More detail analyses are necessary for both results and input data.

The model requires huge conventional observed data, such as precipitation, evaporation and air-temperature. However, it is difficult to acquire these data over the wide area densely, especially evaporation. Therefore, the study estimating evaporation in wide area by using satellite data was carried out. Evaporation has strong relation with air-temperature. The air-temperature could be derived from split window data of infrared channel on NOAA AVHRR GAC data potentially. The new regression equation estimating the monthly mean air-temperature(M-AT) had been developed. The equation has four coefficients. These coefficients are derived from the function of

the latitude and the altitude of target points. The equation was applied to estimate the M-AT over the Asian Continent, and gave reasonable estimations with 2 minutes resolution.

1. Objectives

The purpose of this study is to develop the regional water balance model with 0.5 degrees resolution for assessing the variation of water resources and soil moisture over the wide area due to the anomaly of Asian Monsoon activity. The regional water balance model predicts river discharge, water contents in the soil, water storage in the ground as potentially utilizable water, snow deposit, snow melt and actual evapotranspiration on each grid area with 0.5 degrees x 0.5 degrees in latitude and longitude from observed daily data on precipitation, evaporation and mean air-temperature. The study had started with developing the prototype of the **R**egional **W**ater **Ba**lance model based on the **T**ank Model(RWBaT). As the final goal of this study, the **A**sian **R**egional **W**ater **Ba**lance model(ARWBaT) calculating the hydrological regime over the Asian continent was developed.

2. Methods

The regional water balance model, which produces river discharge, water content in the soil, storage amount of water in the ground as potentially utilizable water, snow deposit, snow-melt and actual evapotranspiration, is made on the basis of the concepts of Tank Model(Sugawara, 1984). The Tank Model is the simple concept and representing adequate hydrological responses on a basin, which had been applied to various river basins in the world, such as tropical humid area, snow covered area, semi-arid area, etc. In the model, analyzing area are represented by grid areas with 0.5 degrees x 0.5 degrees in longitude and latitude, and complicated river system are also simplified to ideal river networks, which mainly represent main streams and major tributaries. As shown in Figure 1, the RWBaT model is composed of many field models and river models, which represent

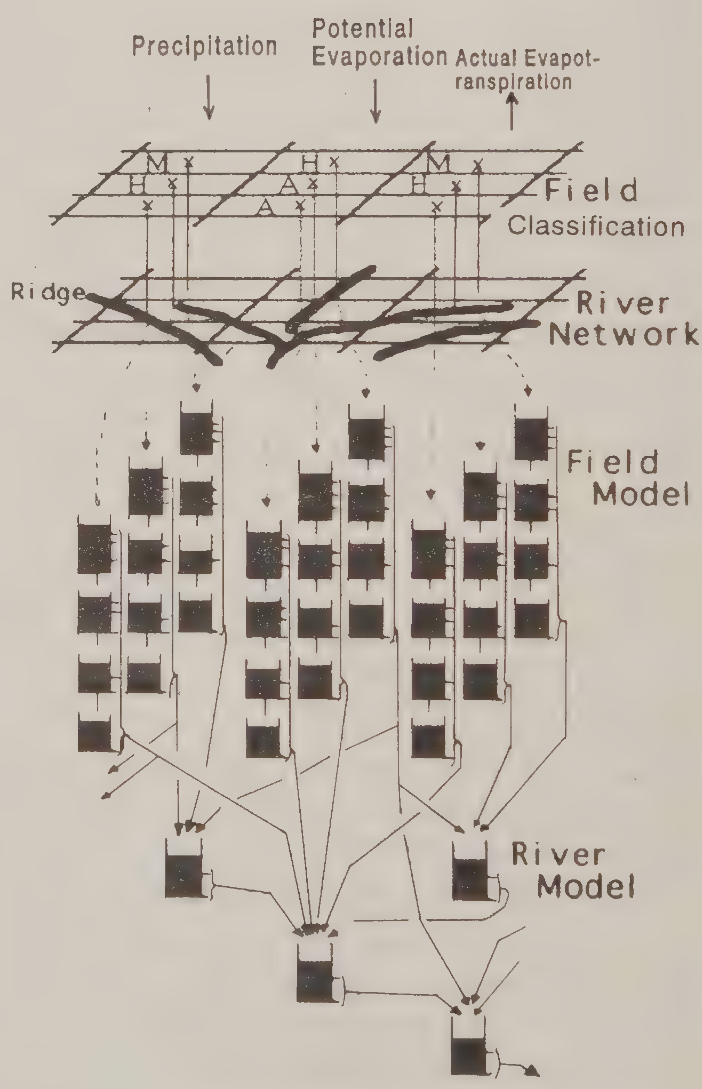


Fig.1 Outline of the Regional Water Balance Model.

hydrological responses in the grid areas and simulate river discharge in each river points of the simple river system respectively. The field models, which are composed of four tanks arranged vertically in series and two kinds of surface soil zones in the Top Tank, are applied to each grid areas. These grid areas are simply categorized into four types according to the topography of grid areas, such as mountainous type, hilly type, diluvial terrace type and alluvial plain type. River models are composed of one tank representing the effects both of storage and smoothing to river discharge at each river points. River models are also categorized into three types according to river conditions, such as mountainous type, plain type and swampy type. These field models connect to river models in the downstream and river models link each river models in the downstream like a tree structure. Calculation is carried out from field models. These calculated discharge are input to each connected river models. Then, calculated discharge from river models are input to each connected river models in the downstream. These calculation are continued to the most downstream of the river point. The prototype of the RWBaT model had been developed and was applied to Chaophraya River basin with 110 thousand km^2 in Thailand and Huaihe River basin with 121 thousand km^2 in China.

The ARWBaT model was developed for calculating hydrological regime on a daily bases over the Asian continent covering area from 60° N to 20° S in latitude and from 30° E to 160° E in longitude with 0.5 degrees resolution. Parameters of the model were same as the RWBat model. Field types and river types of each grid areas in the model were determined by using both average and standard deviation of elevations on the ETOPO 5 data-set in each 0.5 degrees grid areas. The model also requires many data-set on river systems, which represent flow direction and linkage of each river points, for calculating river discharge at each points. Therefore, major 45 river systems in the Asian Continent were made from the digital river network data on the World Data Bank II. The prototype of the model was developed. Simulation using AGCM data in 1970 were carried out for checking the model working.

The model requires huge conventional observed data, such as precipitation, evaporation and air-temperature. However, it is difficult to acquire these data over the wide area densely, especially evaporation. Therefore, the study estimating evaporation in wide area by using satellite data was carried out. Evaporation has strong relation with air-temperature (Thornthwaite, 1948). The air-temperature is potentially derived from split window data of infrared channel on NOAA AVHRR(Advanced Very High Resolution Radiometer) GAC(Global Area Coverage) data. In the study of Analysis on Environmental Conditions and Snow-Ice Cover Changes Affecting Monsoon Cycle in Asia, Weekly Regional Satellite Image(W-RSI) data covering the area from 60° N to 20° S in latitude and from 30° E to 160° E in longitude were made from NOAA AVHRR GAC data on a weekly basis(Yazaki, 1990 and Nakane, 1990). The map projection of W-RSI data is a grid coordinate system with 2 minutes equal intervals of latitude and longitude. W-RSI data unfortunately contain many cloud, which prevent to transmit information from land surface to satellite because of absorption and reflection of radiation from the land. Therefore, Monthly Regional Satellite Image(M-RSI) data are made by composing data of cloud free area on W-RSI data during a month. M-RSI data could be used for estimating monthly mean air-temperature(M-AT) successfully(Nakane, 1991). The new regression equation described in Equation 1 had been

developed for estimating the M-AT from M-RSI data.

$$M\text{-}AT = K1 \times SR3 + K2 \times Tch4 + K3 \times (Tch4 - Tch5) + K0 \qquad ----(1)$$

$$SR3 = SR \times L \times \tan^{-1}(\sqrt{(1 - Dul \times Dul)}/Dul) \times 2.0/\pi$$

$$SR = \cos(\theta - \delta)$$

$$\delta = 0.4093 \times \sin(0.01698 \times (JDAY - 80))$$

$$L = 1.0 + 0.033 \times \cos(360/370 \times JDAY)$$

$$Dul = -0.045/\cos(\theta)/\cos(\delta) - \tan(\theta) \times \tan(\delta)$$

Where, Tch4 and Tch5 are brightness temperature(unit: degree Celsius) of Channel 4(wave band: 10.5～11.5 μm) and Channel 5(wave band: 11.5～12.5 μm) on NOAA AVHRR data respectively, SR3 and θ are the seasonal coefficient of outer solar radiation and latitude at a target point respectively, δ is declination, JDAY is Julian Days. K0, K1, K2 and K3 are coefficients of regression equation.

The equation has four coefficients, which were derived from the function of the latitude and the altitude of the target point. The regression equation gave reasonable estimations of M-AT with 2 minutes resolution over the Asian Continent.

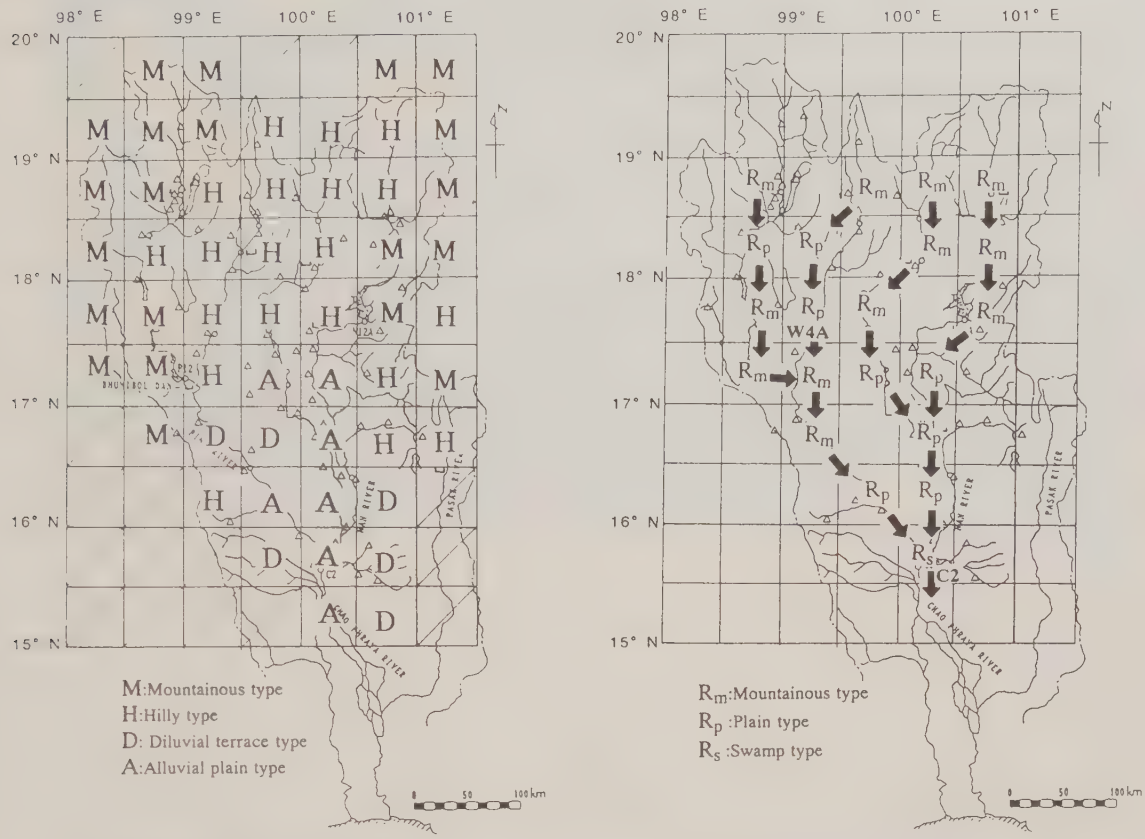
3. Results

In the study, it were carried out the development of the Regional Water Balance model, the Asian Regional Water Balance model and the new regression equation estimating M-AT from NOAA AVHRR GAC data, which were applied to Chaophraya river basin, Huaihe River basin and the Asian continent. These results are summarized as follows;

(1)Application of the RWBaT model to the Chaophraya River basin and the Huaihe River basin.

The prototype of the RWBaT model had been developed and applied to the Chaophraya River basin in Thailand and the Huaihe River basin in China, where the analyzing catchment areas are 110 thousand km^2 and 121 thousand km^2 respectively. Climate and topography in two basins are different, though two basins are fertile agricultural regions. Figure 2 and Figure 3 show the classification of the basin and simplified river systems in the Chaophraya River basin and the Huaihe River basin respectively. These figure show topography of two basins are very different. Estimations were carried out on a daily basis from 1982 to 1985 in the Chaophraya River basin and from 1983 to 1989 in the Huaihe River basin. In these calculations, 43 precipitation data measured by rain gauges, 15 evaporation data measured by the Class A pan and discharge data just below of two huge dams were used for input data in the Chaophraya River basin, and 38 precipitation data measured by rain gauges, 15 evaporation data measured by evaporation pan with 20 cm diameter and discharge data just below of 6 big dams were used in the Huaihe River basin. Areal precipitation and evaporation on grid areas were estimated by weight mean method using above observed data in this time. In calculations, the extra coefficient depending on the altitude for both precipitation and evaporation were not used because of little information for the dependency on the latitude. The important thing of these experiments is same parameters of both field models and river models in two basins were used. Figure 4 shows estimations for monthly discharge from April 1982 to March 1986 at W4A station, where the catchment area is 10,507 km^2, and C2

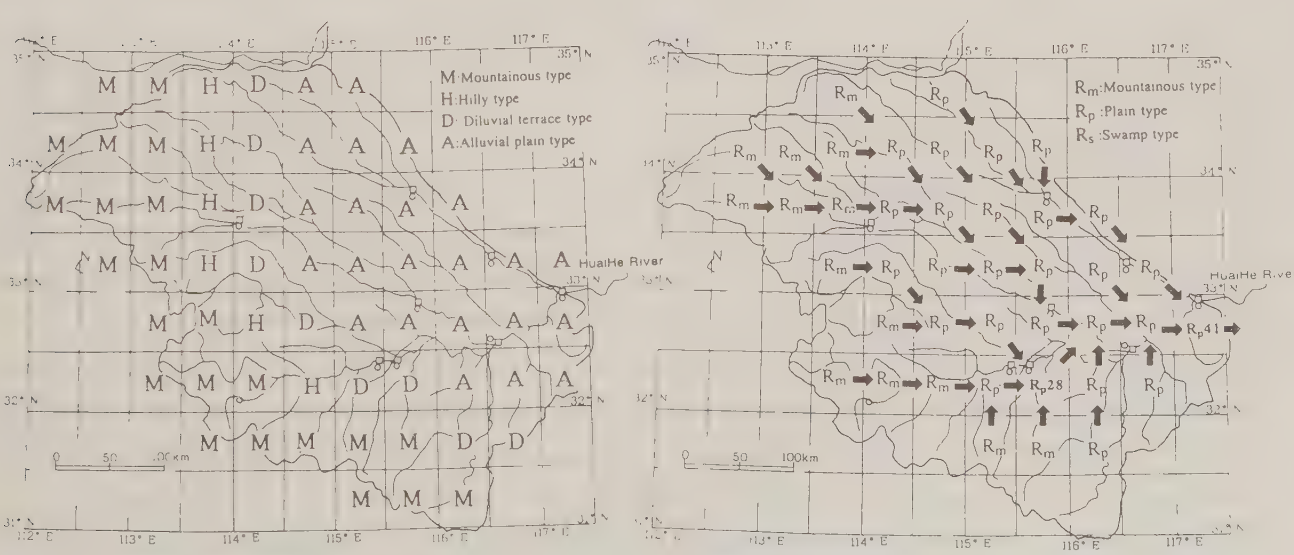
station, where the catchment area is 110,569 km2, in the Chaophraya River basin. These estimations are reasonable as a whole.



Classification of the basin

Simplified river system

Fig.2 Classification of the basin and simplified river system in Chaophraya River basin.



Classification of the basin

Simplified river system

Fig.3 Classification of the basin and simplified river system in Huaihe River basin.

Figure 5 shows estimations for monthly discharge from 1983 to 1989 at WangJiaba station, where the catchment area is 30,630 km^2, and BengBu station, where the catchment area is 121,330 km^2, in the Huaihe River basin. These estimations are also reasonable as a whole. In detail, estimation for low flow and flood shape are not adequate. The cause seems to arise from irrigation and flood control.

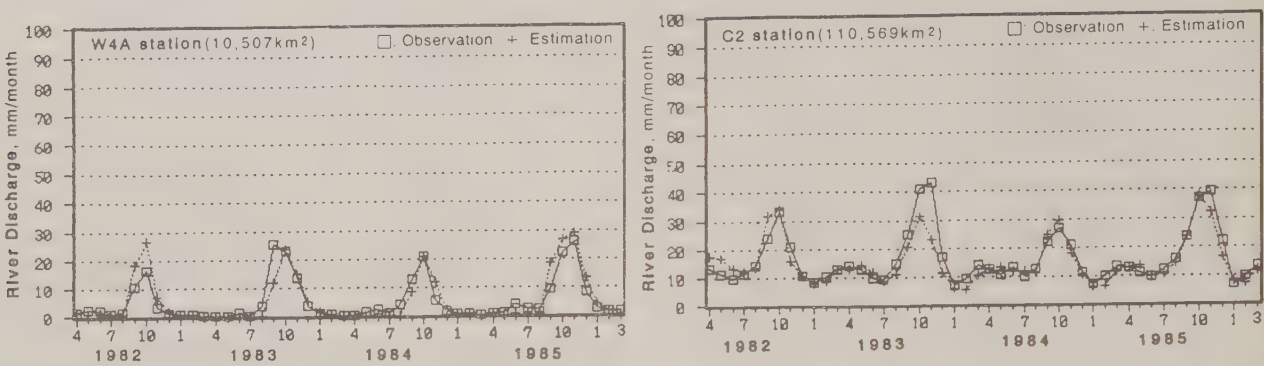


Figure 4 Estimations for monthly discharge in Chaophraya River basin.

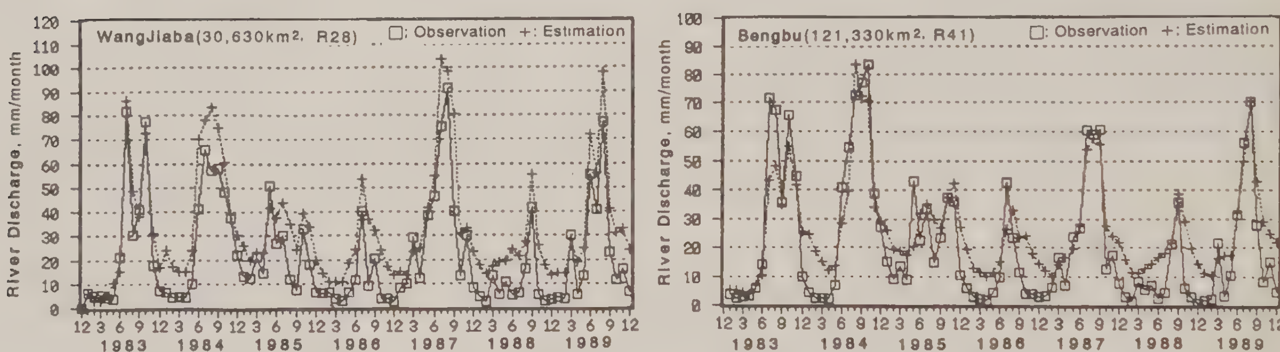


Figure 5 Estimations for monthly discharge in Huaihe River basin.

(2) Application of the ARWBaT model to the Asian Continent.

The prototype of the ARWBaT model was developed and applied to the Asian Continent covering area from 60° N to 20° S in latitude and from 30° E to 160° E in longitude. Figure 6 shows field types of each 0.5 degrees x 0.5 degrees grid areas over the Asian Continent, which were made by using both average and standard deviation of elevations on the ETOPO 5 data-set in 0.5 degrees grid areas. River types of each grid areas in the model were also determined by the same method. River networks, which represent flow direction and linkage of each river points, were made from the digital river network data on the World Data Bank II. As shown in Figure 7, major 45 river systems in the Asian Continent were made. Simulation using AGCM data in 1970 were carried out for checking the model working. The AGCM data were 6 hourly products with 1 degree resolution (Sugi.et al, 1990). Daily data on precipitation and air-temperature were made by the interpolation in space and the integration/average in time. Daily integration of equilibrium evaporation data, which are made from net-radiation and surface air-temperature on 6 hourly data, were used as input data of daily evaporation. Figure 8 shows the preliminary result of river discharge at four major rivers in the Asian Continent by the ARWBaT model.



Fig.6 Distribution of field types for each grid areas with 0.5 degrees resolution over the Asian Continent covering area from 60° N to 20° S in latitude and from 30° E to 160° E in longitude, which were made by using both average and standard deviation of elevations on the ETOPO 5.



Fig.7 Major 45 river systems in the Asian Continent, which were made from the digital river network data on the World Data Bank II.

In this simulation, human activity was not considered such as dam control and irrigation, because it was difficult to acquire these data. Therefore, estimated hydrograph similar to natural river flow. As these figure show, the ARWBaT model worked well to estimate the river discharge.

However, the accuracy of results is not clear in this time. More detail analyses are necessary for both results and input data.

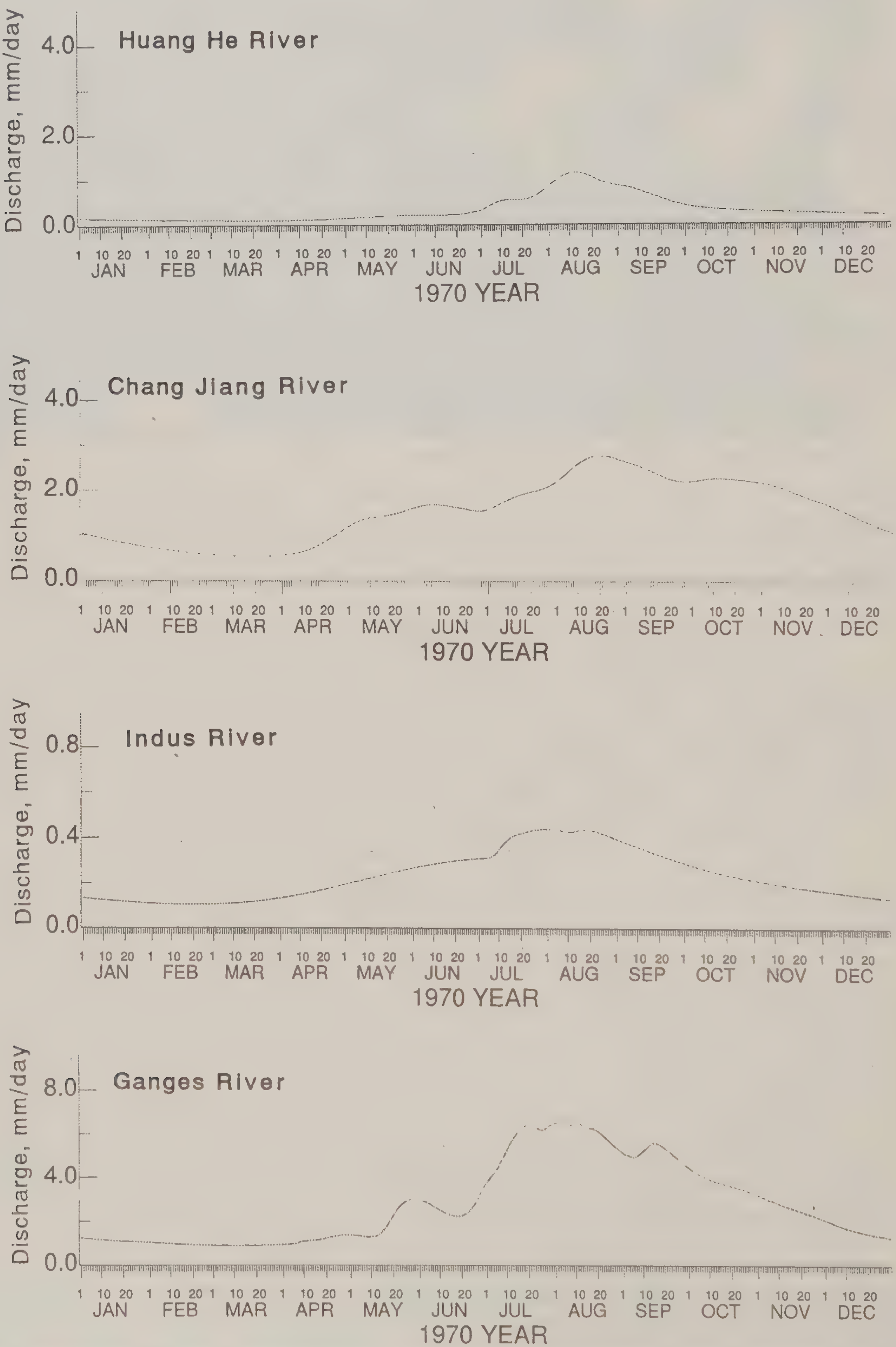
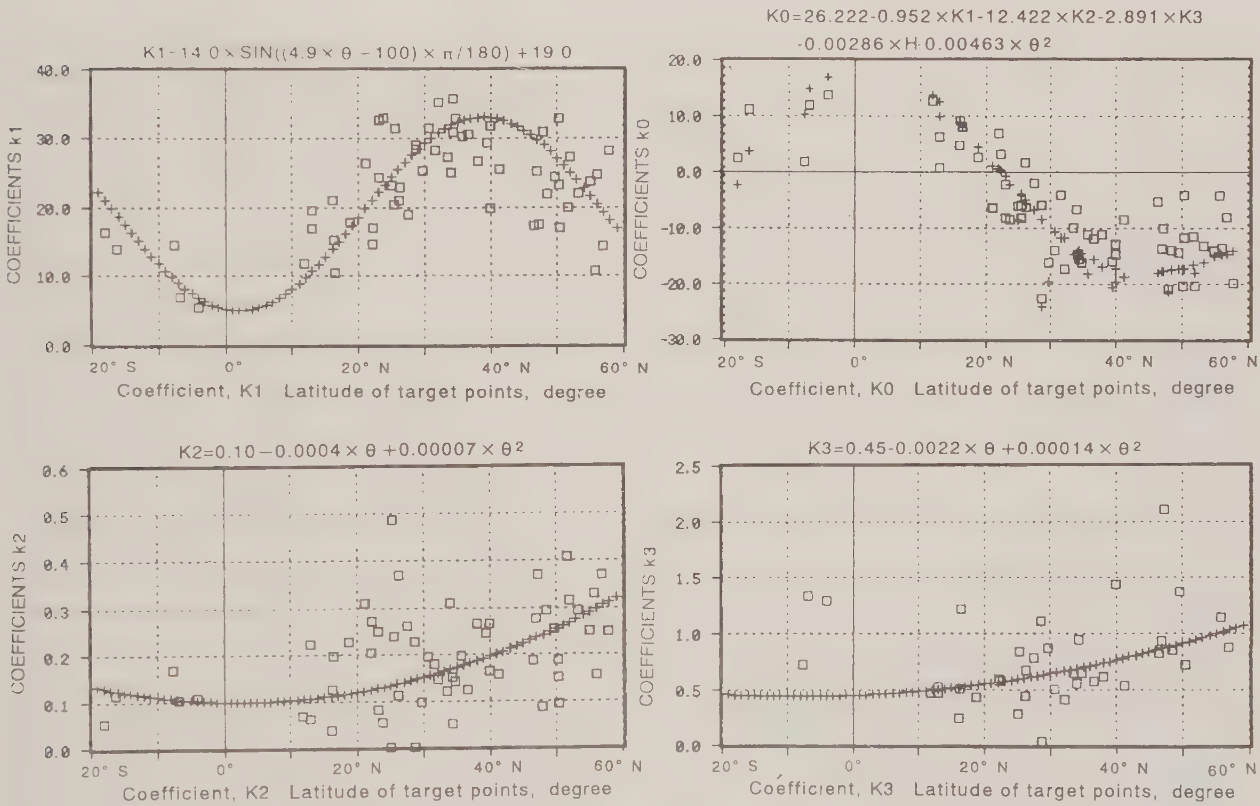


Fig.8 Preliminary result of river discharge at four major rivers in the Asian Continent.

(3)Application of the new regression equation estimating M-AT to the Asian Continent by using M-RSI data.

The regression equation, which derives M-AT by using M-RSI data, was developed. The solar term in the equation was considered both of the distance between sun and earth and the duration of sun shine as well as seasonal change of the sun angle. The regression equation has 4 coefficients. From the regression analysis in 59 stations over the Asian Continent, 47 desirable coefficients were obtained. Though these coefficients were different from place to place, it was found the relation between coefficients and both of the latitude and the altitude. Figure 9 shows the relation as well as functions dediving coefficients using the latitude and the altitude. From these functions, applicable coefficients in wide area were obtained. Figure 10 shows estmated M-AT in several points, which are agree with observed data. Figure 11 shows estimated M-AT in April and June, 1990 over the Asian Continent. From these figures, it was found the regression equation gave reasonable M-AT estimations with 2 minutes resolution in wide area.



++++ : Derived by the function of latitude θ and altitude H, □ : Derived by the regression analysis between observed M-AT and M-RSI data at each target points

Fig.9 Relation between latitude and derived coefficients(K0, K1, K2 and K3) by the regression analysis between observed M-AT and M-RSI data at each target points(Eq. 1), and by the function of the latitude and the altitude.

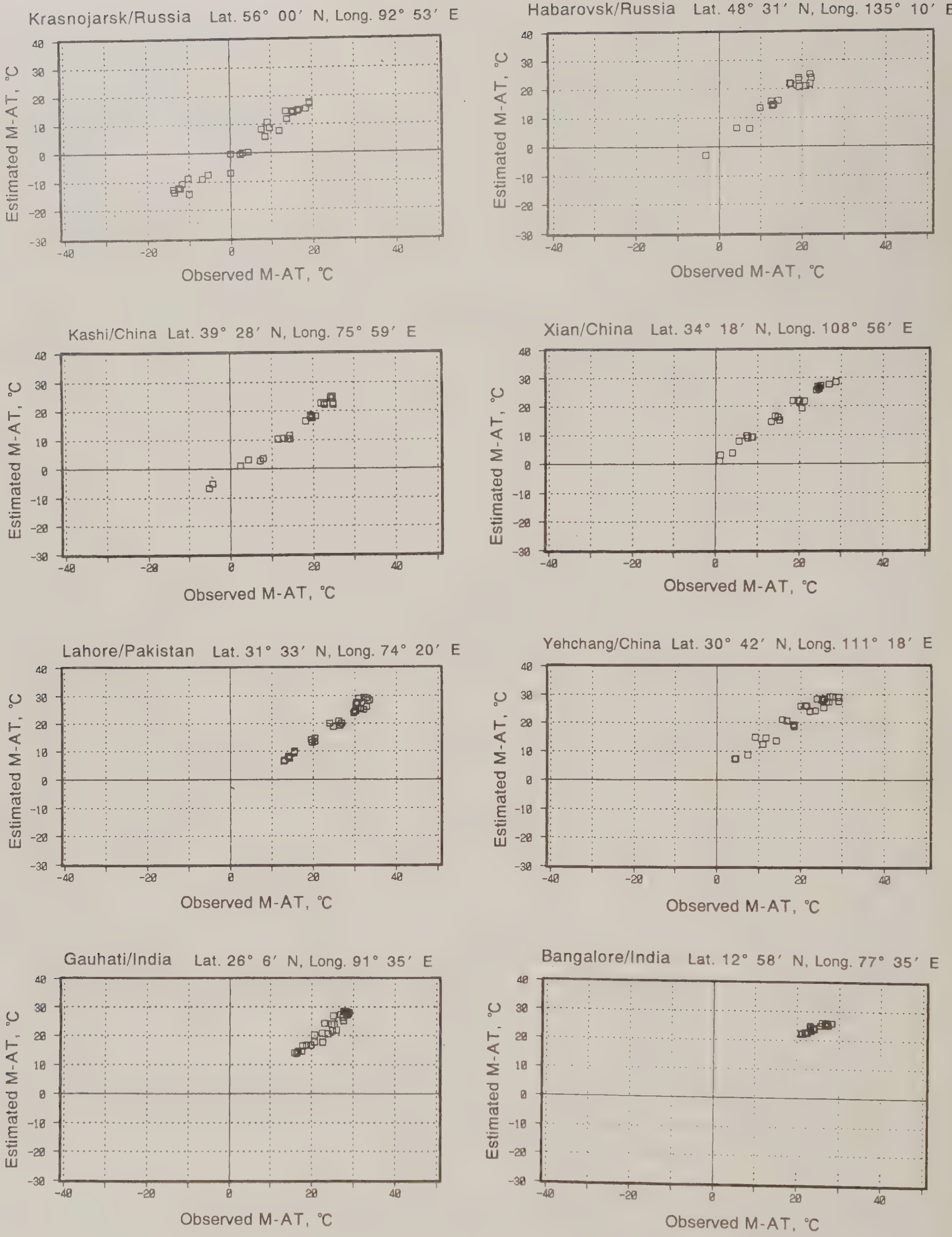


Fig.10 Estimation of M-AT in several points over the Asian Continent by using coefficients (K0, K1, K2 and K3) derived by functions of the latitude and altitude at target point.

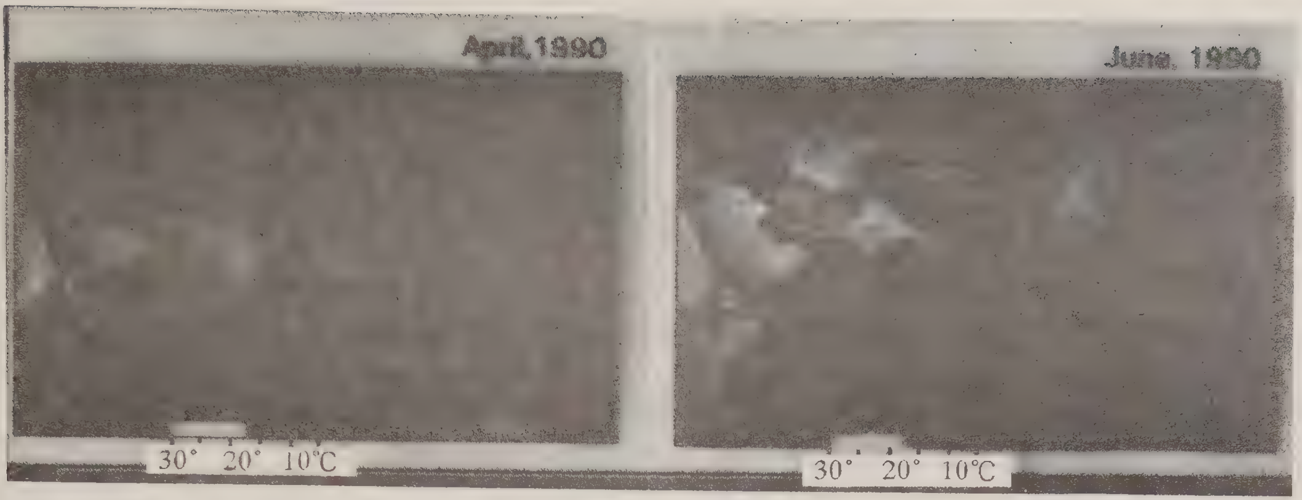


Fig.11 Estimation of M-AT over the Asian Continent with 2 minutes resolution by using coefficients (K0, K1, K2 and K3) derived by functions of the latitude and altitude at target point.

4. Discussions

The RWBaT model and the ARWBat model, which was made on the basis of the Tank Model, were developed. The RWBaT model were applied to the Chaophraya River basin(110 thousand km^2) and the Huaihe River basin(121 thousand km^2), and the ARWBat model were applied to the Asian Continent covering area from 60° N to 20° S in latitude and from 30° E to 160° E in longitude with 0.5 degrees resolution. Estimations were carried out on a daily basis from 1982 to 1985 in the Chaophraya River basin and from 1983 to 1989 in the Huaihe River basin. Estimations were reasonable as a whole, though same parameters of the model in two basins were used. In some detail points, estimation were not adequate. The cause seems to arise from irrigation and flood control. These problem will be clear through the further detail estimation using data on irrigation and flood control in the basin.

For the ARWBaT model, field types and river types of each grid areas were determined by using the digital elevation data, and major 45 river systems in the Asian Continent were made from topographic data. The prototype of the model was applied to the Asian Continent. the model worked well to estimate the river discharge and water contents in the surface ground on each grid area with 0.5 degrees resolution. However, more detail analyses are necessary for evaluating the accuracy of the results. Parameters of the model are determined by only topographic condition in this time. These parameters also depend on a surface soil type and landuse. After this, parameters of the model and basin's condition will be investigated in more detail.

The new regression equation was developed for estimating the M-AT. The regression equation has four coefficients, which are derived from functions of the latitude and the altitude at each target point. The regression equation gave adequate estimations on a whole. However, in desert area, estimated M-AT became lower than observed data. To find out the season, the relation between errors of estimated M-AT and surface weather condition was investigated. The reason, however, was still not clear. If cloud of sand occurs around 2 p.m. of the local time, when NOAA satellite passes through, the reason seems to be the absorption of the radiation from the surface by

the cloud sand. This is a assumption. So, the father detail research is necessary.

5. References

1) K. Nakane et al.; Regional Image Processing for NOAA AVHRR data Part II-Composition of the wide Regional Image(in Japanese), Report on the 16th Remote Sensing Symposium, pp67-70, 1990.

2) K.Nakane; Estimation of Monthly Mean Air Temperature over Asian Area using GAC Data of NOAA AVHRR(in Japanese), Journal of Japan Remote Sensing Vol.13 No.1, pp14-26, 1993.

3) K. Nakane; Regional water balance model based on the concept of the Tank Model: Development and application for Huaihe River Basin and Chaophraya River Basin, Proceedings of the Third International Study Conference on GEWEX in Asia and GAME, GAME International Science Panel, pp180-185, 1997.

4) K. Nakane, S. Yazaki and S.Kishi; Estimation of Monthly Mean Air-temperature over the Asian Continent using NOAA AVHRR GAC data, Proceedings of International Workshop on Global Change and Terrestrial Environment in Monsoon Asia, University of Tsukuba, pp164-167, 1997.

5) M. Sugawara et al.; Tank Model with Snow Component, Research Notes of the National Research Center for Disaster Prevention No.65, pp1-293, 1984.

6) M. Sugi et al.; Description and performance of the JMA operational global spectral model(JMA-GSM88), Geophysical Magazine Vol.43 No.3, pp105-130, 1990.

7) C.W. Thornthwaite; An Approach Toward a Rational Classification of Climate, Geographical Review Vol.38, pp55-94, 1948.

8) S. Yazaki et al.; Regional Image Proceeding for NOAA AVHRR data Part I Geometric Correction and Map Projection(in Japanese), Report on the 16th Remote Sensing Symposium, pp63-66, 1990.

6. Publication

1) National academic journal 1

K.Nakane; Estimation of Monthly Mean Air Temperature over Asian Area using GAC Data of NOAA AVHRR(in Japanese), Journal of Japan Remote Sensing Vol.13 No.1, pp14-26, 1993.

2) Proceedings of International Conference 2

K. Nakane; Regional water balance model based on the concept of the Tank Model: Development and Application for Huaihe River Basin and Chaophraya River Basin, Proceedings of the Third International Study Conference on GEWEX in Asia and GAME, GAME International Science Panel(1997).

K. Nakane, S. Yazaki and S.Kishi; Estimation of Monthly Mean Air-temperature over the Asian Continent using NOAA AVHRR GAC data, Proceedings of International Workshop on Global Change and Terrestrial Environment in Monsoon Asia, University of Tsukuba,164-167(1997)

7. International Cooperation

The study was carried out cooperatively with RSTAC/MWS(Remote Sensing Technology Application Center, Ministry of Water Resources in China) and SMRI/SMR/CMA(Satellite

Meteorology Research Institute, Satellite Meteorology Center, China Meteorological Administration). We cooperated with RSTAC/MWS to analyzing land surface conditions related to hydrological factors using MOS-1 data on Huaihe River basin and visited Ohyodo River basin for making data-set of RWBAT Model. We also cooperated with SMRI/SMR/CMA to analyzing land surface conditions related to hydrological factors using NOAA AVHRR GAC data over the China.

和文抄録

本研究は広域にわたるアジアモンスーン地域を対象として、降水、積雪・融雪、蒸発散、河川流出等の水文過程を的確にモデル化し、アジアモンスーンの変動が地域の水資源及び土壌水分に与える影響を0.5度×0.5度(約50km×50km)の等緯度経度の分解能で詳しく評価できる広域水収支モデルの開発を目的としている。本研究で開発する広域水収支モデルは広域の地表を０.５度×０.５度の領域にメッシュ分割し、降水量、蒸発量及び気温から任意の地域の河川流量、雨水の流域貯留量（土壌水分量、地下水量など）、実蒸発散量等を計算するモデルであり、高分解能の広域水資源情報を提供する。この広域水収支モデルはタンクモデルの概念を基本に構築されている。初期的な広域水収支モデルは乾期と雨期のある熱帯域に位置するタイのチャオプラヤ川流域（解析対象面積１１万ｋm2）及び温帯湿潤地域に位置する中国の淮河流域（解析対象面積１２万ｋm2）に適用し、良好な予測結果を得た。また、アジア全域（範囲：北緯６０°～南緯２０°、東経３０°～東経１６０°）を対象とし、５分分解能の標高データ（ETOPO５）を用いて、領域モデル及び河川モデルのタイプ分けを行うと共に、河川網データ（World Data Bank II）及び標高データ（ETOPO５）を用いて、大陸の主要な４５河川の河川網及び尾根線データを作成し、最終目標であるアジア広域水収支モデルを構築した。このモデルの性能を評価するため、大気大循環モデルの１９７０年の計算結果を用いてアジア地域の水文諸量を推定した。結果は妥当で有ったたが、その精度評価については入力データの問題とモデル自体が抱える問題があり、今後、多くの事例を重ねる必要がある。

アジア広域水収支モデルは入力データとして膨大な観測データを必要とするが、これら広域データを密に収集するのは困難である。特に、蒸発量データは困難である。そのため、衛星データを用いた蒸発量の推定研究も行った。蒸発量は気温と密接に関係しており、NOAA AVHRR GACデータを用いた月平均気温の新しい推定手法を開発した。この手法は太陽高度、距離及び日照時間とNOAA AVHRR GACの熱赤外２チャンネルのデータを説明変数とした４つの定数を持つ回帰式で現される。この４つの定数は緯度及び標高と密接な関係があり、それらの関数として求めている。この手法により推定したアジア大陸各地の月平均気温は全体的に妥当な推定値を示した。しかし、砂漠地域や寒冷地域で推定誤差が大きくなる傾向があり、この原因究明には地表の気象条件及び砂塵等の影響を考慮した詳しい解析が必要である。

III. Synthetic Study on the Atmosphere-Ocean-Land Interactions
大気・海洋・陸面間の相互作用に関する総合研究

1. Experiment of the Atmosphere-Ocean-Land Interactions by the Use of General Circulation Models
大規模モデルによる大気・海洋・陸面間の相互作用に関する実験研究

Meteorological Research institute,
Japan Meteorological Agency
A. Kitoh, T. Tokioka, A. Noda, M. Sugi,
Y. Nikaidou, K Mabuchi and T. Ose
気象庁気象研究所
鬼頭　昭雄、時岡　達志、野田　彰、
杉　正人、二階堂義信、馬淵　和雄、
尾瀬　智昭

(Abstract)

Climatological features and interannual variability of the Asian summer monsoon simulated by a global coupled atmosphere-ocean GCM is investigated. The overall monsoon region as defined by the seasonal change of wind direction and convection proxy agrees with the observed. Simulated Indian summer monsoon rainfall anomaly is negatively correlated with equatorial Pacific SST anomaly, being consistent with the observed one. Ground temperature is significantly warmer in central Asia in spring preceding a good monsoon. The model shows a strong signal of the tropospheric biennial oscillation (TBO) of the South Asian monsoon system. In the strong phase of TBO, area of strong convective maximum, which is located over South Asia in spring to summer, moves southeastward to Indonesia in autumn to winter season. This movement superimposes on its climatological seasonal cycle. As a response to the equatorial monsoon convection anomaly in northern winter, a stationary Rossby wave is established over the South Asian region. This is a favorable condition for bringing cold air advection over the Eurasian continent and reducing land-sea temperature contrast to set up the following weak South Asian summer monsoon.

The large scale background fields associated with the interannual variability of SST anomaly over the South China Sea is also studied by the statistical analysis of the observational data and GCM experiments. The South China Sea SST anomaly can be recognized as a unique index for the Asian monsoon and the El Nino/Southern Oscillation (ENSO) system because of its special geographical location for that system.

1. Objectives

The monsoon is an essential part of climates in the Asian countries by contributing to establish an annual cycle in many meteorological elements. For some contries the monsoon is the climate. And the interannual variability of the Asian monsoon affects climate variations not only in Asia but also in larger parts of the globe because the Asian monsoon region is located close to the ocean with the warmest sea surface temperature and is the most vigorous heating source of the atmospheric general circulation.

The purposes of the present study are to clarify the mechanism of atmosphere-ocean-land interactions in an Asian monsoon region including the Pacific and the Indian Oceans and the Eurasian continent by performing a series of numerical experiments.

2. Methods

Observational studies show a strong relationship between the monsoon intensity and the tropical SST, particularly in the Pacific. The monsoon is also related with the Eurasian snow cover. In order to investigate the monsoon variability in the context of coupled ocean-atmosphere-land system, we look for this relationship in a long integration of the MRI coupled atmosphere/ocean general circulation model (CGCM). We also investigate the mechanism of the tropospheric biennial oscillation (TBO) of South Asian monsoon which is an essential part of the tropical atmosphere-ocean system particularly in the South Asian monsoon region (Meehl, 1993, 1994). Using the lag-lead regression analysis technique for the biennial component of monsoon index, we discuss the possible role of the Asian monsoon in the TBO seasonal cycle concerning the interactive processes with other global phenomena through the global scale circulations.

We also made the statistical analysis using the observational data in order to clarify the relationship between the South China Sea (SCS) SST and circulation changes associated with El Nino/Southern Oscillation (ENSO) phenomenon.

3. Results

(1) Model climate

We use the 70-year integration data of the Meteorological Research Institute (MRI) CGCM (Yukimoto et al., 1996; Kitoh et al., 1998). The atmospheric model has 15 layers between the surface to the model top at 1 hPa with its horizontal resolution of $4^\circ \times 5^\circ$. The oceanic model has 21 vertical levels with a realistic ocean bottom topography. Its horizontal resolution is 0.5°-$2.0^\circ \times 2.5^\circ$. The latitudinal grid spacing is reduced near the equator to better simulate El Nino. This model has been used for a transient CO_2 experiment (Tokioka et al. 1995). Some of the results of the 70-year control run are analyzed by Kitoh et al. (1996) and Yukimoto et al. (1996).

Figure 1 shows the simulated monsoon region diagnosed by two methods, together with

the distribution of precipitation and 850 hPa winds. Large dots in Fig. 1a are the grid points where the summertime OLR is less than 240 W m^{-2} and the seasonal change of monthly mean OLR is greater than 60 W m^{-2}. Compared to the observation (Fig. 1 of Murakami and Matsumoto 1994), the monsoon area extends northward of 20N in the model over the western Pacific. This corresponds to a northward shift bias of the subtropical anticyclone. The hatched area is where the monthly mean wind direction between January and July shifts more than 120 degrees at 850 hPa. This broadly agrees with the observation (see Fig. 3 of Kitoh and Tokioka 1987). One of discrepancy is that the SCS is not classified as the monsoon region in the model. This is because the summertime 850 hPa winds flow along the Tibetan plateau from the Indian Ocean to China and the westerlies do not penetrate well into the SCS (Fig. 1c, d). Simulated precipitation in the SCS is thus depressed in the model (Fig. 1b). It is also noted that the peak values of the simulated cross-equatorial Somali jet is weaker than observed.

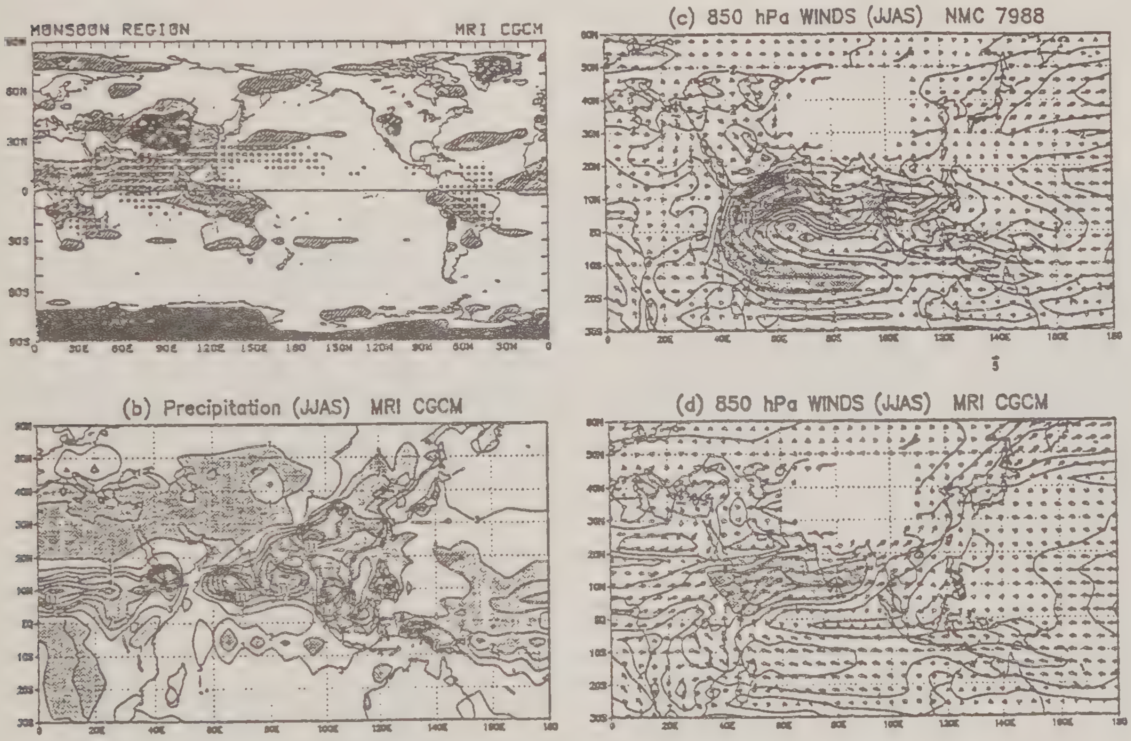


Fig. 1 (a) Monsoon region in the model. See text for definition. (b) Simulated June-September (JJAS) mean precipitation. (c) Observed JJAS wind vector at 850 hPa. (d) Simulated JJAS wind vector at 850 hPa.

(2) Interannual variability

The MRI CGCM has simulated some aspects of El Nino (Yukimoto et al. 1996) with dominant peak periods of 3 to 6 years. The SST averaged for the NINO3 region for JJAS is shown in Fig. 2. Also shown is the South Asian monsoon index defined as the difference of zonal winds between 850 hPa and 200 hPa averagred over 40E-110E, 0N-20N for JJAS. The monsoon wind index is significantly negatively correlated with the NINO3 SST.

Figure 3a-c shows the simultaneous correlations between the precipitation in South Asia (land area in 60E-120E, 10N-30N) and SST (or ground temperature over land), 850 hPa zonal wind and precipitation in JJAS. There is a dipole precipitation anomaly between India and China. Precipitation in India is negatively correlated with the equatorial Pacific SST. There is a potitive SST anomaly in the North Pacific. This simulated SST pattern in the Pacific captured the observed SST anomaly pattern with respect to El Nino. Negative ground temperature anomaly over India is related with wetter ground surface and more cloudiness due to heavier local precipitation. Westerly wind anomaly is found over the Arabian Sea, indicating a stronger monsoon flow. There is an easterly wind anomaly over the equatorial western Pacific, which is consistent with La Nina type SST anomalies. Therefore, the overall relationship between circulation patterns and the SST distribution in the model is consistent with the observed one (i.e., good monsoon is associated with La Nina).

Lagged correlations are calculated for surface conditions over land in the preceding season. Correlations for snow mass in March-May (MAM) (Fig. 3d) show that spring snow is less extensive in western Eurasia in the year when summer monsoon is stronger than normal. At this time, ground is drier although statistical significance is not large. Cloudiness is less and upper tropospheric temperature is warmer in the 30N-50N belt over Eurasia. Cold SST anomalies, however, are already prevailing at this time in the tropical Pacific. Therefore this study does not show if there is an influence of land surface conditions and monsoon variability on tropical Pacific SST changes.

(3) Tropospheric biennial oscillation in the model

The MRI CGCM shows a strong signal in the biennial component of the South Asian monsoon (Ogasawara et al., 1998). As an index of the South Asian monsoon, we use area averaged summer June-August (JJA) precipitation in the South Asian region (60E-90E, 4N-26N). The power spectrum of monsoon index shows a significant peak around 2 years, as well as a peak around 4 to 8 years corresponding to ENSO.

At first, all of the monthly model output data were bandpass filtered into 15-30 month band. The filtered monsoon index was then regressed against the seasonal mean model parameters such as SST or u and v wind component at each grid point. Lagged regression relationships for seasonal mean value during the northern spring season (MAM) prior to a strong monsoon (lag = -1 season) to the following spring season (lag = +3 season), prior to a weak monsoon, are used to examine the evolution of convection and circulation signals corresponding to the TBO of South Asian monsoon.

Based on these lagged regression maps, a schematic of the seasonal evolution of the

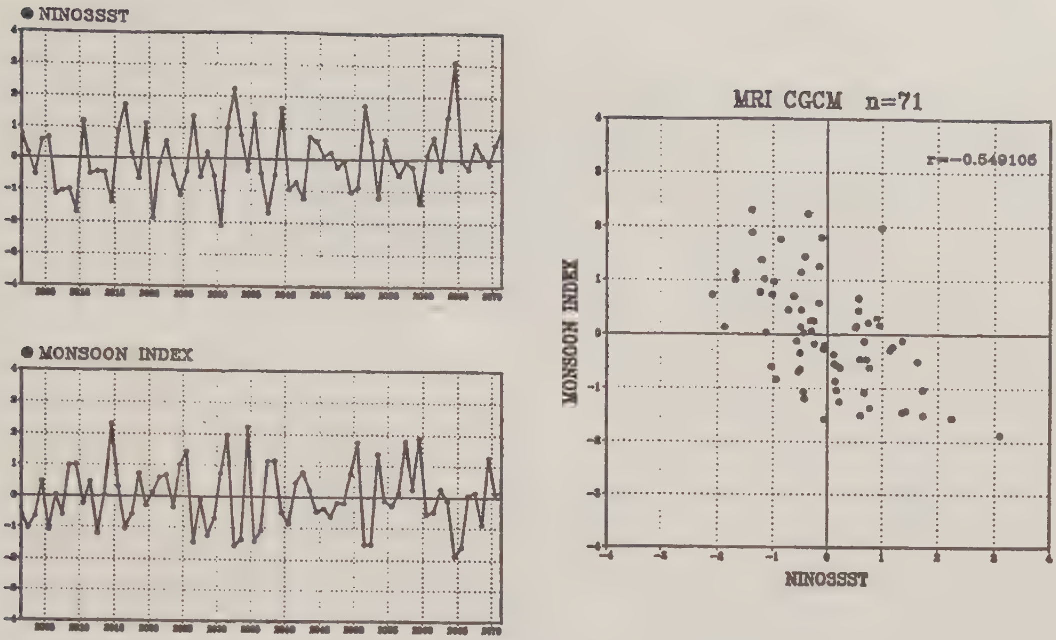


Fig. 2 Interannual variations of JJAS mean NINO3 SST and monsoon index. Both the NINO3 SST and the monsoon index is the normalized values.

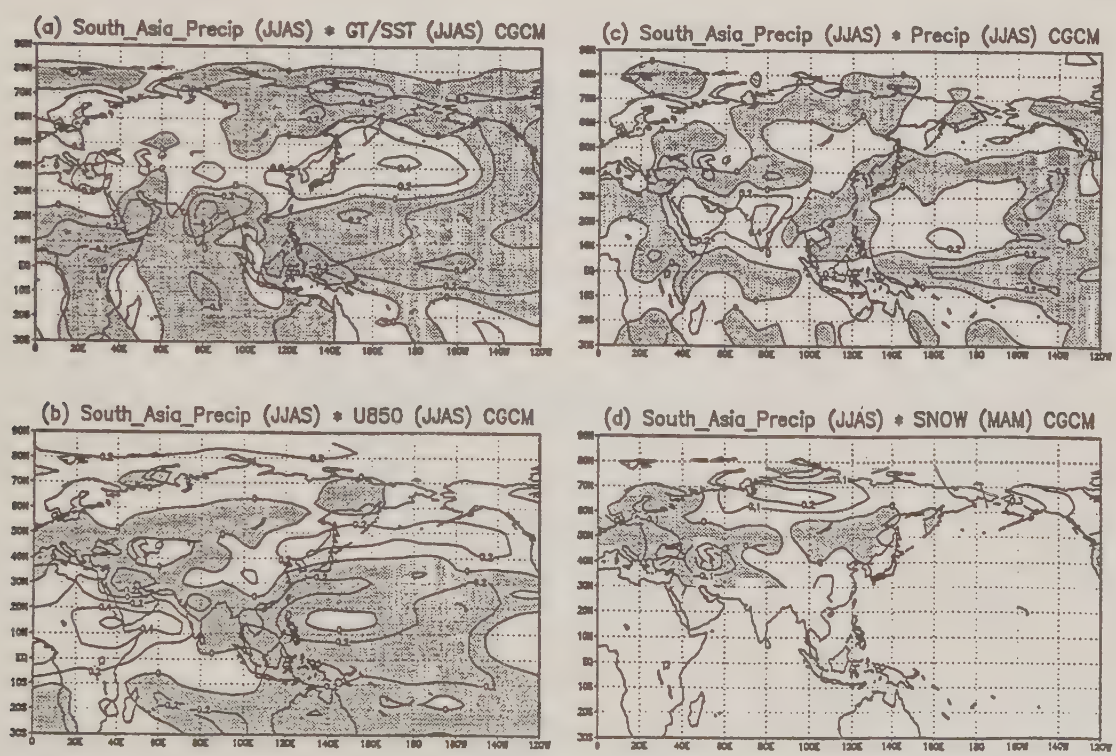


Fig. 3 (a-c) Simultaneous correlations in JJAS. Precipitation in South Asia and (a) sea surface/ ground temperature, (b) zonal wind at 850 hPa, (c) precipitation. (d) Lagged corelation between the precipitation in South Asia in JJAS and snow mass in MAM.

TBO is obtained from northern summer to following spring season for the strong monsoon phase (Fig. 4).

In the northern summer (JJA) season (Fig. 4a), anomalous monsoon westerly flow appears over the Arabian Sea. At the same time, noticeable easterly anomalous flow extends from the central equatorial Pacific to the Bay of Bengal, contributing to the stronger South Asian monsoon precipitation. The SST and convective activity is below normal over the central Pacific and there is a global scale east-west Walker circulation anomaly between South Asia and the equatorial Pacific.

In the following autumn September-November (SON) to winter December-February (DJF) season (Fig. 4b, c), westerly wind anomaly spreads over the entire South Asia. This corresponds to the southeastward movement of relatively strong precipitation maximum from South Asia (10N, 70E) to around Indonesia (0N, 100E). This movement of convection activity superimposes on its seasonal cycle. The anomalous state of east-west Walker circulation persists during summer to winter season. In the central to eastern Pacific region, there appears westerly anomalous winds due to the secondary circulation associated with downward motion at eastern periphery of the Walker circulation. Because the westerly anomalous flow is against the climatological easterly trade wind, reduced latent heat flux at ocean surface and weakened upwelling motion by the Ekman pumping or reduced upper ocean mixing reads to warm the SST there. This negative feedback in the Pacific atmosphere/ocean coupled system dissipates the TBO variability over there by the end of the winter season.

Associated with the persistent Walker circulation anomaly, convective activity also lasts during the entire monsoon season over the Indonesia and northern Australian monsoon region. As a Matsuno-Gill type stationary Rossby wave response to this equatorial convection anomaly in the Indian sector, there forms an anticyclonic circulation anomaly at the upper level and a cyclonic circulation at the lower level over South Asia. The cyclonic circulation over the Eurasian continent in winter season, after the strong Asian monsoon, is a favorable condition to cool the land surface temperature through the cold air advection and more snowmass (Fig. 4c). Cold surface temperature around Middle East to central Asia persists through the whole winter to spring season to reduce the land-sea temperature contrast and then, setup the weak South Asian monsoon in the following spring (Fig. 4d). Relatively cool SST over the Arabian Sea also contributes to keep weak monsoon by the reduced evaporation and less convection. As the simulated TBO of the South Asian monsoon is tightly phase locked with the seasonal cycle and its phase reverses in spring, the TBO extratropical/tropical interaction in the Indian sector is realized mainly at northern spring through the onset of South Asian monsoon.

(4) SST in the South China Sea

Interannual variability of the SST anomalies (SSTA) over the SCS is recognized as a unique index for the Asian monsoon and ENSO system because of its special geographical location for that system (Ose et al., 1997). The following results are obtained by the statistical analysis of the observational data and the atmospheric general circulation model (AGCM) experiments.

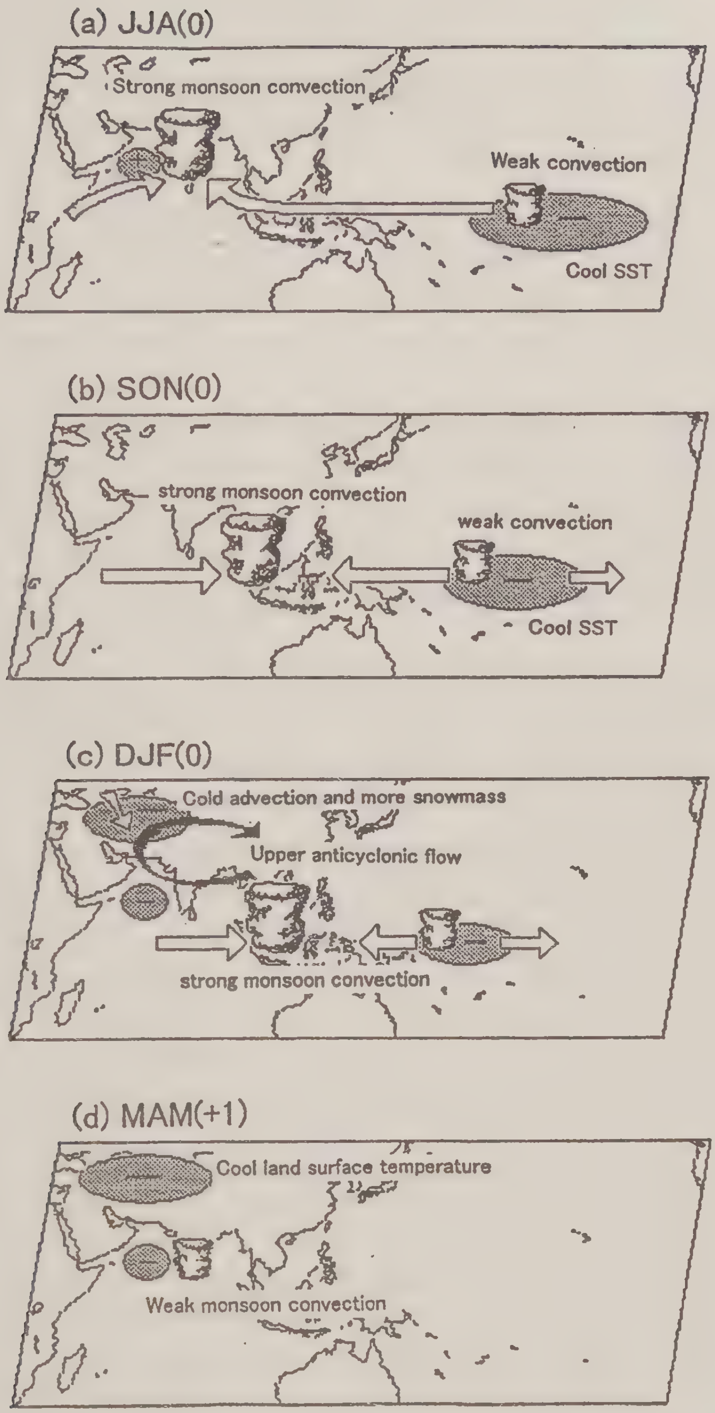


Fig. 4 Schematic illustration of the TBO during its strong phase, from (a) summer through (d) spring. Shaded areas in the figure indicate the anomalous states of SST or land surface temperature. White/black arrows means the anomalous states of lower/upper level circulation.

(1) The northern summer SCS SSTA do not play the active role on the summer Asian monsoon in a viewpoint of the global scale. The summer SCS SSTA seem to be controlled by in-situ low-level wind anomalies. The weak South Asia monsoon jet is related to the weak low-level wind speed over the SCS, and furthermore the warm SCS SSTA. The westerly wind anomalies in East Asia and the easterly anomalies east of the Philippines are also found at 850 hPa in the case of the warm SCS SSTA.

(2) All years are classified into 'the BO-type years' and 'the LF-type years' by the combination of the polarities of the SCS SSTA and the NINO4 SSTA in the northern winter season. The defined two type years are considered as the in-phase and out-of-phase composition of the biennial mode and the low-frequency mode. The features of the biennial mode can be found in the BO-type years.

(3) In the northern winter, the LF-type years are distinguished from the BO-type years by a small westward shift of the global low-level vorticity anomalies under a given polarity of the tropical eastern Pacific SSTA. The SSTA with a dominant biennial oscillation are found in the regions where the directions of the low-level wind anomalies are quite sensitive to that longitudinal shift across the SCS of the vorticity anomalies. The SCS SSTA are the most typical case.

(4) Tropical eastern Pacific SSTA change significantly during the northern spring for the BO-type years. On the other hand, they tend not to change for the LF-type years. The low-level wind anomalies over the tropical western Pacific in winter may be important factors to determine the change of NINO3 SSTA during the following spring.

(5) In the northern summer, the detailed interannual variability of the SCS SSTA is associated with the fluctuations of the three major low-level wind branches over South Asia, East Asia, and the western Pacific. The typical BO-type years are distinguished from the LF-type years by the strength of zonal wind anomalies and associated geopotential height anomalies at 850 hPa in the western Pacific.

4. Discussions

The MRI coupled model showed interannual variations, similar to the observation that a good monsoon is associated with La Nina type SST anomalies. It is also found that snow is less and the ground is generally dry in western Eurasia in spring preceding a good monsoon. However, whether land surface conditions and monsoon variability could have an impact on tropical Pacific SST changes needs further sensitivity studies.

The mechanism of the TBO discussed above includes two types of interaction, one is between the monsoon and air-sea coupled system in the Pacific during summer to winter season, and another is interaction between the monsoon and land surface condition during winter to spring season. In this point of view, the Asian monsoon plays an important role in the TBO cycle. As is suggested by the above discussion, the TBO of Asian monsoon seems to consist of complicated interactions with other global phenomena through global scale circulations. Then it is natural that other variablity, such as ENSO in the tropical Pacific or chaotic behavior

of the middle latitude circulation patterns, modulates the TBO cycle as noted by Yasunari and Seki (1992).

With respect to the data analysis of the SCS SST, we confirm that the tropical atmospheric circulation anomalies are closely coupled with the SSTA. The characteristic anomalies in the tropical atmosphere are simulated by the AGCM with the observed tropical SSTA. The tropical atmospheric anomalies seem to explain the corresponding SSTA. We have neither challenged to analyze the tropical ocean data nor to use the atmosphere-ocean coupled model in order to explore the oceanic state. This work may be made in the future.

5. References

Kitoh, A. and T. Tokioka, 1987: A simulation of the tropospheric general circulation with the MRI atmospheric general circulationmodel. Part III: The Asian summer monsoon. J. Meteor. Soc. Japan, 65, 167-187.

Kitoh, A., H. Koide, K. Kodera, S. Yukimoto and A. Noda, 1996: Interannual variability in the stratospheric-tropospheric circulation in a coupled ocean-atmosphere GCM. Geophys. Res. Lett., 23, 543-546.

Kitoh, A., S. Yukimoto and A. Noda, 1998: ENSO-monsoon relationship in the MRI coupled GCM. (Submitted to J. Meteor. Soc. Japan)

Meehl, G.A., 1993: A coupled air-sea biennial mechanism in the tropical Indian and Pacific regions: Role of the ocean. J. Climate, 6, 31-41.

Meehl, G.A., 1994: Coupled land-ocean-atmosphere processes and South Asian monsoon variability. Science, 266, 263-267.

Murakami, T. and J. Matsumoto, 1994: Summer monsoon over the Asian continent and western North Pacific. J. Meteor. Soc. Japan, 72, 719-745.

Ogasawara, N., A. Kitoh and T. Yasunari, 1998: Tropospheric biennial oscillation in the MRI coupled GCM. (Submitted to J. Meteor. Soc. Japan)

Ose, T., Y. Song and A. Kitoh, 1997: Sea surface temperature in the South China Sea - an index for the Asian summer monsoon and ENSO system. J. Meteor. Soc. Japan, 75, 1091-1107.

Tokioka, T., A. Noda, A. Kitoh, Y. Nikaidou, S. Nakagawa, T. Motoi, S. Yukimoto and K. Takata, 1995: A transient CO2 experiment with the MRI CGCM - Quick report -. J. Meteor. Soc. Japan, 73, 817-826.

Yasunari, T. and Y. Seki, 1992: Role of the Asian monsoon on the interannual variability of the global climate system. J. Meteor. Soc. Japan, 70, 177-189.

Yukimoto, S., M. Endoh, Y. Kitamura, A. Kitoh, T. Motoi, A. Noda and T. Tokioka, 1996: Interannual and decadal variabilities in the Pacific in the MRI coupled GCM. Clim. Dyn., 12, 667-683.

6. Publications

Kitoh, A, 1991: Interannual variations in an atmospheric GCM forced by the 1970-1989 SST. Part

I: Response of the tropical atmosphere. J. Meteor. Soc. Japan, 69, 251-269.
Kitoh, A, 1991: Interannual variations in an atmospheric GCM forced by the 1970-1989 SST. Part II: Low-frequency variability of the wintertime Northern Hemisphere extratropics. J. Meteor. Soc. Japan, 69, 271-291.
Bhaskar Rao, D. V., K. Yamazaki and A. Kitoh, 1991: Some GCM experiments of the Asian summer monsoon related to land boundary conditions. Pap. Met. Geophys., 42, 127-143.
Kitoh, A., 1992: Simulated interannual variations of the Indo-Australian monsoons. J. Meteor. Soc. Japan, 70, 563-583.
鬼頭昭雄, 1992: インド／オーストラリア・モンスーンの年々変動. グロースベッター, 30, No.2, 48-56.
Kitoh, A., 1992: GCM studies of the Asian summer monsoons at the MRI. Japanese Experiment on Asian Monsoon (JEXAM): Studies of Asian Monsoon in Japan and China,111-134.
Kitoh, A., 1992: Simulated interannual variations of the Indo-Australian Monsoons. Simulation of Interannual and Intraseasonal Monsoon Variability, WMO/TD-No.470, 2.87-2.92.
鬼頭昭雄, 1993: １０年スケールの大気・海洋変動について. 海と空, 68, 191-202.
鬼頭昭雄, 1994: 熱帯海面水温変動と北半球の夏の循環. 平成５年度全国長期予報技術検討会資料, 平成６年１月, 気象研究所, 43-53.
鬼頭昭雄, 1994: 大気大循環モデルを用いた大気の長周期変動に関する研究　１９９３年度日本気象学会賞受賞記念講演 . 天気, 41,No.8, 447-458.
鬼頭昭雄, 1994: 海面水温変動の大気への影響について. 気象, 38, No.11, 8-12.
Kitoh, A., 1994: AGCM experiments on Tibetan snow and monsoon. Proceedings of the International Conference on Monsoon Variability and Prediction, July 1994, WCRP-84 (WMO/TD-No.619), 661-665.
Kitoh, A., 1995: Observation and simulation of the relationship between the global sea surface temperature variability and the 500 hPa height in the northern summer. J. Meteor. Soc. Japan, 73, 247-253.
Kitoh, A., S. Yukimoto, A. Noda, S. Nakagawa and T. Motoi, 1997: Asian monsoon in the MRI coupled GCM. Proceedings of the Third International Study Conference on GEWEX in Asia and GAME (Seogwipo KAL Hotel, Cheju, Korea, 26-28 March 1997), 373-376.
Kitoh, A., Yukimoto, S., A. Noda and T. Motoi, 1997: Simulated changes in the Asian summer monsoon at times of increased atmospheric CO2. J. Meteor. Soc. Japan, 75, 1019-1031.
Ose, T., Y. Song and A. Kitoh, 1997: Sea surface temperature in the South China Sea - an index for the Asian monsoon and ENSO system -. J. Meteor. Soc. Japan, 75, 1091-1107.
Ogasawara, N., A. Kitoh and T. Yasunari, 1998: Tropospheric Biennial Oscillation (TBO) in the MRI Coupled GCM. CAS/JSC WGNE Research Activities in Atmospheric and Oceanic Modelling, Report No.27, WMO/TD-No.865, 9.12-9.13.
Chandrasekar, A. and A. Kitoh, 1998: Impact of Localized Sea Surface Temperature Anomalies over the Equatorial Indian Ocean on the Indian Summer Monsoon. J. Meteor. Soc. Japan, 76, 841-853.
Kitoh, A. and. T. Ose, 1999: Experiment of the atmosphere-ocean-land interactions by the use of general circulation models. Recent Progress in Studies of Asian Monsoon Mechanism,

Japan-China Cooperative Program on Asian Monsoon Mechanism, 357-365.

7. International Cooperation

· Two researchers of the Chinese Academy of Meteorological Sciences (CAMS) were invited to Japan Meteorological Research Institute (MRI) for 15 days from 1 September 1994 to 15 September 1994 for the exchange of the technical information.
· One researcher of the MRI was invited to Beijing and Guangzhou for 12 days from 27 October 1994 to 7 November 1994 to attend the Workshop and Symposium on the Asian Monsoon.
· One researcher of the MRI was invited to Beijing and Chengdu for 16 days from 13 June 1995 to 28 June 1995 to attend the workshop and discuss research results.
· One researcher of the CAMS was invited to the MRI for 32 days from 1 October 1995 to 1 November 1995 to carry out an SST anomaly experiment with the MRI GCM. The model output was provided to the CAMS. Discussion on the study results was made by e-mail between the MRI and the CAMS.
· One researcher of the MRI was invited to Beijing and Nanjing for 9 days from 25 April 1997 to 3 May 1997 to attend the workshop.
· Two researchers of the CAMS were invited to the MRI for 15 days from 14 October 1997 to 29 October 1997 for the exchange of the technical information.

要旨

全球大気・海洋結合モデルのモンスーン循環の解析を行い、アジアモンスーン域の面的な表現がほぼ再現されていることを確認した。モデルで再現されたエルニーニョとモンスーン強度には、観測と同様に有意な負相関がある。夏季のモンスーンが強い年の、春の中央アジアの積雪は少ない傾向にあるものの有意性は大きくない。またモデルにはユーラシア大陸から西太平洋にかけて、対流圏2年振動が明瞭に現れていることがわかった。

エルニーニョの偏差分布によって、西太平洋の下層の風向が逆になりうることを、データ解析及び大気大循環モデル実験から示し、南シナ海のSST偏差が熱帯の大気・海洋系の年々変動にとって特異な海域であることを明らかにした。

III. Synthetic study of the monsoon circulations
大気・海洋・陸面間の相互作用に関する総合研究

2. Analysis of the energy balance of monsoon
モンスーンのエネルギー収支に関する解析研究

Meteorological Research Institute (MRI)
Japan Meteorological Agency
Tomoaki Ose
気象庁気象研究所
尾瀬　智昭

(Abstract)

Summer Asian monsoon was studied from a viewpoint from atmospheric energy budget and radiative flux budget at the top of atmosphere.Two diabatic heating contrasts are created as the response to the strong shortwave incident from spring through summer. One is the contrast between northern land and ocean, and another is between upper and lower atmosphere over land. Monsoon circulation moderates these heating contrasts; southerly warm advection over northern ocean, northerly cold advection in the lower layer over land and warming in the upper layer over land due to downward motion were analyzed.

Role of diabatic heat source in a forming of monsoon circulation was studied using a simple model, suggesting that condensational heat sources in southern and eastern Asia contribute to a forming of the above characteristics of monsoon circulation. The study also suggested that the weakening of zonal mean wind in the northern extratropics from June to July and the appearance of deep convection over the tropical western Pacific in August are important for the seasonal evolution of Asian monsoon circulation, including East Asia climate.

A GCM study showed that Eurasian surface condition, specifically additional snowmass in early spring, can influence summer Asian monsoon circulation and the associated precipitation in southern Asia. Based on surface energy flux budget in the experiment, the necessary conditions for snowmass anomalies influential to monsoon evolution are considered. The conditions include latitude and altitude of snow area and climatological ground wetness beneath, which are involved with effectiveness of snowmass anomalies and melt water anomalies and their longevity.

The inter-relationship among radiative flux, surface heating, condensational heating and monsoon circulation in Asian summer monsoon system was shown in the above studies.

1. Objectives

Asian monsoon is formed basically by the solar heat difference between land and ocean. In order to understand the mechanism of Asian monsoon activities including its onset, it is important to analyze the energy budget associated with Asian monsoon.

In this study, the Earth radiation budget (ERB) observed by satellites was analyzed in space and time. The ultimate purpose is to clarify the mechanism for formation, maintenance and variation of Asian monsoon by combining the ERB and atmospheric energy budget analysis.

2. Methods

Spatial distribution of ERB and its seasonal change are studied in association with Asian summer monsoon, using monthly mean radiative flux data (ERBE-S4) from 1985-87. An atmospheric energy budget is calculated from the ECMWF re-analysis upper air data set for 1985-87. Heat and moisture budget are obtained in almost the same way as Hoskins et al. (1989). The analysis is made twice a day (0000 and 1200 UTC). See details in Ose (1999).

Roles of heat sources in the formation of Asian monsoon are studied using a simple model with the obtained heat sources and observed zonal mean wind (Hoskins et al., 1995). Details are mentioned in Ose (1998).

Asian summer monsoon simulations by the MRI-GCM-I (Tokioka et al., 1984) are analyzed from a viewpoint of surface energy budget. The details for the experiments are seen in Ose (1996).

3. Results

3.1 Asian Summer Monsoon Viewed from Energy Budget (Ose, 1999)

Asian summer monsoon was studied viewed from energy budget by analyzing the radiative flux budget at the top of the atmosphere and the atmospheric heat budget. (a) The contrast of heat sources in northern summer between land and sea and between the upper and lower atmosphere over land, and (b) atmospheric heat advection moderating these contrasts are summarized as follows;

The net radiative flux at the top of the atmosphere (NET) over land dominates that over the ocean in mid and high latitudes during northern summer. The NET land-ocean contrast is created by stratus clouds over the ocean in high latitudes after snow cover mostly disappears over land.

Seen from the vertically integrated atmospheric energy budget (Figure-1(b)), seasonal change similar to that of NET (Figure-1(a)) is found in sensible heating over land in high latitudes. In mid-latitudes, sensible heating is dominant from spring to early summer, and evaporation is active in late summer. Energy estimated exceeding NET is transported from the atmosphere to the ocean in high latitudes besides NET in July-August.

Before the onset of the summer monsoon circulation (in April), sensible heating near the surface (Figure-2(c)) contributes to increase the low-level temperature over land (Figure-2(a)), especially under the downward motion (Figure-2(e)) of Hadley circulation and extratropical

stationary waves (Iran Plateau and northern China).

After the onset of summer monsoon circulation (in June), the heat source due to precipitation in Southeast Asia dominates sensible heating over the Eurasian Continent. Upward motion balances this condensational heat source.

Strengthened downward motion (Figure-2(f)) warms upper-level air over central Asia (Figure-2(b)) and sensible heating near the surface (Figure-2(d)) is canceled by northerly cold advection. Strengthened warm southerly advection contributes to troposphere warming over the Tibetan Plateau and the northwestern Pacific in the mid-latitudes. Condensational heating in both of the above regions appears to contribute to the strengthening of the lower-level southerly flow.

3.2 Seasonal Change of Asian Summer Monsoon Circulation and Heat Source (Ose, 1998)

The Asian summer monsoon circulation, especially its climatological seasonal change, is studied as the model response to the prescribed zonal mean field and the prescribed diabatic heat source from the observation. The obtained results are summarized as follows.

During the Asian summer monsoon season, the prescribed deep heat sources in the southern part of Asia (Figure-3(a)) form the Tibetan High, the monsoon trough, the low-level circulation over South Asia, and furthermore, the downward motion in the western part of the Eurasian Continent. The heat sources near surface over the central Asia also induce downward motions aloft.

In early summer (June), the deep heat sources in the southern part of Asia (Figure-3(a)) tend to form southwesterly low-level flows and upward motion southeast of Japan. Those are considered to be the background for the Baiu formation in East Asia as well as heat lows produced in the southern part of Asia. The mid-latitude heat sources associated with the Baiu precipitation (Figure-3(a)) produce low-level jet south of that.

Climatological seasonal change from early summer (June) to mid-summer (July) is characterized by air temperature increase in the whole Northern Hemisphere and northward shift of weakened westerly jet. When zonal mean field in June is replaced by that in July in the model, the major characteristics of the seasonal change are obtained qualitatively; low-level jets and upward motion areas in South Asia and East Asia shift from ocean side of the coasts toward land side. This change of vertical motion is consistent with the seasonal change of deep heat sources from June to July (Figure-3(b)).

Climatological seasonal change from mid-summer (July) to late summer (August) is characterized by enhanced convective activity in the extended area of the subtropical western Pacific (Figure-3(c)). When deep heat sources in July are replaced by those in August only over the western Pacific, the major characteristics of the seasonal change over the Pacific and the Indian Ocean are obtained. The expansion of the Tibetan High at upper-level and the Pacific High at low-level over Japan is also simulated only by the seasonal change of the western Pacific heat sources.

3.3 The Comparison of the Simulated Response to the Regional Snowmass Anomalies over Tibet, Eastern Europe, Siberia (Ose, 1996)

The atmospheric response to the regional snow mass anomalies in early spring over Tibet, Eastern Europe, and Siberia is compared by the general circulation model ensemble experiments. The positive snow mass anomalies over Tibet produce the largest cooling anomalies in the atmosphere from spring to early summer. Almost no significant forcing anomalies are systematically formed by the snow mass anomalies over Eastern Europe and Siberia.

The model experiments show that the cooling source over Tibet works significantly to delay the seasonal transition from spring to summer in the Northern Hemisphere. It is confirmed by the simulated weak Asian monsoon ; weak lower tropospheric monsoon jet in South Asia, weak large-scale divergence center at the upper troposphere in Southeast Asia, negative lower-layer geopotential height anomalies in the North Pacific and the North Atlantic, and the weak Walker circulation in the equatorial Pacific are simulated.

The above noticeable response of the atmosphere to the snow mass anomalies over Tibet is associated with the following characteristics of Tibet as compared with Eastern Europe and Siberia;

(1) The small snow melt speed over Tibet, probably due to its high elevation, maintains the early spring additional snow mass until almost the end of the climatic snow melt season.

(2) The snow albedo is effective because of large solar incident and relatively small cloudiness over Tibet.

(3) The existence of the anomalous snow cover works to cut the upward sensible heat flux rather than the evaporation over Tibet because of its dry ground condition.

(4) The dry ground over Tibet makes it possible that all the anomalous snow melt water is not drained as runoff, but a part of it is stored in the ground.

(5) As pointed out by many researchers, the Tibetan Plateau plays an important role in the establishment of Asian monsoon.

The above conditions (1)-(5) for the effective snow mass anomalies are found in the model Tibet, but these conditions would be satisfied by the real regions where the snow mass anomalies affect the atmosphere efficiently.

4. Discussions

The purpose of this study is to claryfy the energy budget of the Asian summer monsoon. Precise estimation of energy budget, particularly, surface energy budget could not be done, but the characteristics of energy budget in the Asian summer monsoon are captured from the estimation of radiative flux budget and atmospheric heat budget . By combining model studies, the internal relationship between radiative flux budget, surface heating, condensational heating and monsoon circulationis is shown partialy. In the above sense, the purpose of this study is basically accomplished.

Concern is that the analysis was not expanded to a year-to-year variability of the energy budget.

The study did not cover surface energy budget.

5. References

1) Hoskins, B.J., H.H. Hsu, I.N. James, M. Masutani, P.D. Sardeshmukh and G.H. White, 1989; Diagnostics of the global atmospheric circulation based on ECMWF analysis 1979-1989. WMO/TD. No.326. 217pp.

2) Hoskins, B.J. and M. J. Rodwell, 1995: A model of the Asian summer monsoon. Part I: the global scale. J. Atmos. Sci., 52, 1329-1340.

3) Ose, T., 1996: Seasonal change of Asian summer monsoon circulation and its heat source. J. Meteor. Soc. Japan, 76, 1045-1063.

4) Ose, T., 1997: Sea surface temperature in the South China Sea -an index for the Asian monsoon and ENSO system-. J. Meteor. Soc. Japan, 75, 1091-1107.

5) Ose, T., 1999: Asian summer monsoon viewed from energy budget. Pap. Met. Geophys., (in print).

6) Tokioka, T., K. Yamazaki, I. Yagai and K. Kitoh, 1984: A description of the Meteorological Research Institute atmospheric general circulation model (The MRI-GCM-I). Tech. Rep. of the MRI. No.13. 249pp.

6. Publications

1) Two English papers on J. Meteor. Soc. Japan

Ose, T., 1996: Seasonal change of Asian summer monsoon circulation and its heat source. J. Meteor. Soc. Japan, 76, 1045-1063.

Ose, T., 1997: Sea surface temperature in the South China Sea -an index for the Asian monsoon and ENSO system-. J. Meteor. Soc. Japan, 75, 1091-1107.

2) Three English papers on other magazines

Sugi, M., 1992: Study of earth radiation budget in relation to Asian monsoon. Studies of Asian monsoon in Japan and China, M. Murakami and D. Yihui, Eds., MRI/JMA and CAMS/SMA, 151-158.

Ose, T., 1999: Analysis of the energy balance of monsoon. Recent progress in studies of Asian monsoon, M. Murakami, N. Yamazaki, C. Longxun and D. Yihui, Eds., MRI/JMA and CAMS/NMC, 323-338.

Ose, T., 1999: Asian summer monsoon viewed from energy budget. Pap. Met. Geophys., (in print).

7. International Cooperation

None

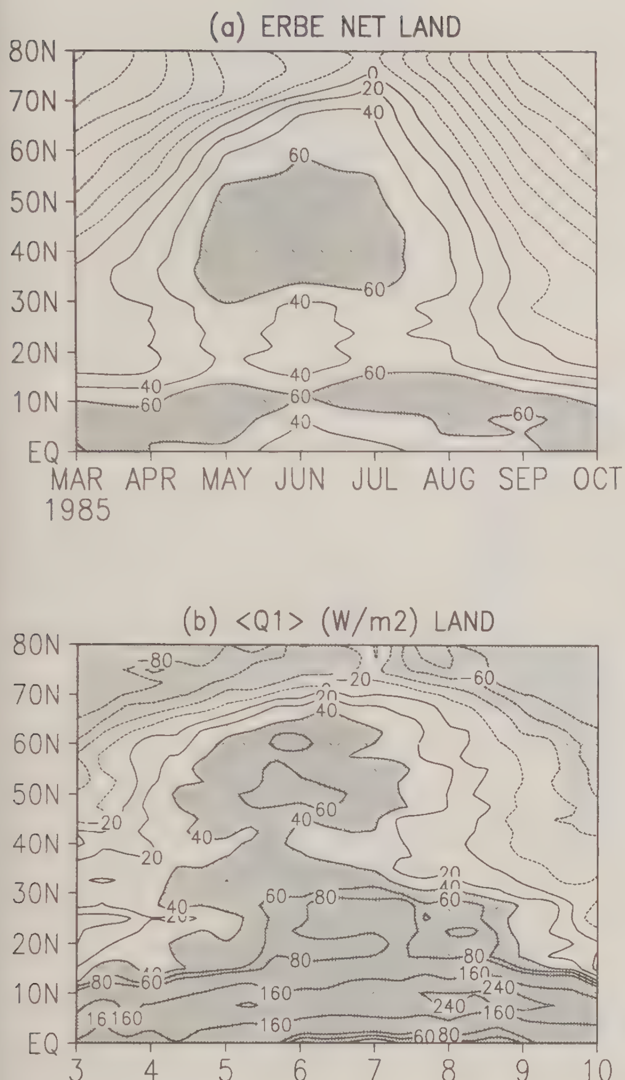
和文要旨

大気のエネルギー収支と大気上端での放射収支から、夏のアジアモンスーンを調べた。春から夏にかけての強い太陽入射に対する応答として、２つの加熱のコントラストが生成される。一つは北方の大陸と海洋間であり、他の一つは陸上の上層下層間である。モンスーン循環は、これらの加熱のコントラストを緩和する。すなわち、北方海洋上での南風による暖気移流、陸上下層での北風による寒気移流、陸上上層での下降流による昇温が解析された。

非断熱加熱のモンスーン循環形成に果たす役割が簡単なモデルを使って調べられた、南方アジア及び東アジアの凝結熱がモンスーン循環の上記の特徴の形成に貢献していることを示した。また、６月から７月にかけて弱まる北半球中緯度での帯状平均東西風と８月に現れる熱帯西部太平洋での深い対流は、東アジアの気候を含む、アジアモンスーン循環の季節変化に対して重要であることを示した。

GCM 実験による研究は、ユーラシア大陸の地表面状態、特に早春に付加した積雪偏差が、夏のモンスーン循環及び関連する南方アジアの降水に影響を及ぼしうることを示した。地表面におけるエネルギーフラックスの収支から、モンスーンの発展に影響を与える積雪偏差の条件が考察された。この条件には、積雪地域の緯度と高度、気候的な土壌水分量が含まれていて、これらは積雪偏差とその融水の影響度と寿命に関連する。

以上の研究で、夏のアジアモンスーンにおける、放射収支、地表面での加熱、降水による凝結熱、モンスーン循環の相互関係が、示された。



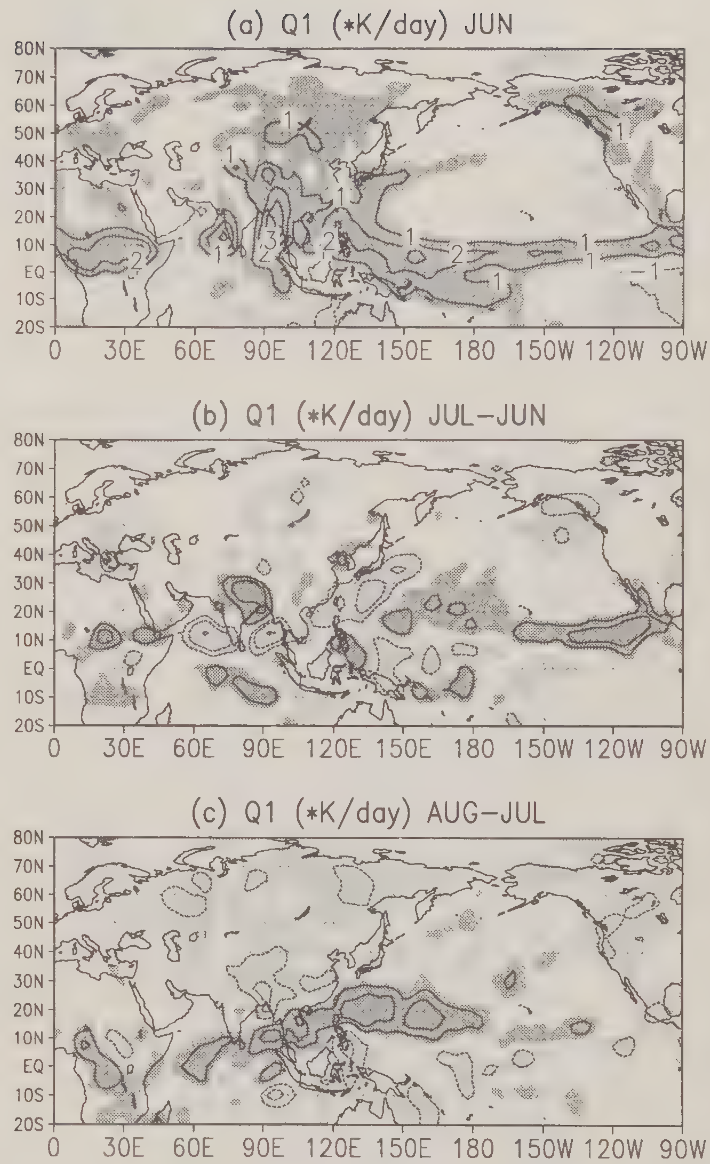


図１（左図）(a) 陸上で帯状平均した大気上端正味放射（W/m2）の季節変化。(b) 陸上で帯状平均し鉛直積分した大気中の非断熱加熱（W/m2）の季節変化。

Fig.1. (left) (a) Seasonal change of net radiative flux at the top of the atmosphere (W/m2) over land. (b) seasonal change of vertically integrated (85 hPa-surface) diabatic heating rate (W/m2) over land.

図３ （右図）(a) ６月の鉛直平均した非断熱加熱（K/day）、(b) ６月から７月にかけての変化（K/day）、(c) ７月から８月にかけての変化（K/day）

Fig.3. (right) (a) Vertically averaged heat source in June (K/day), (b) itsl change from June to July, and (c) from July to August.

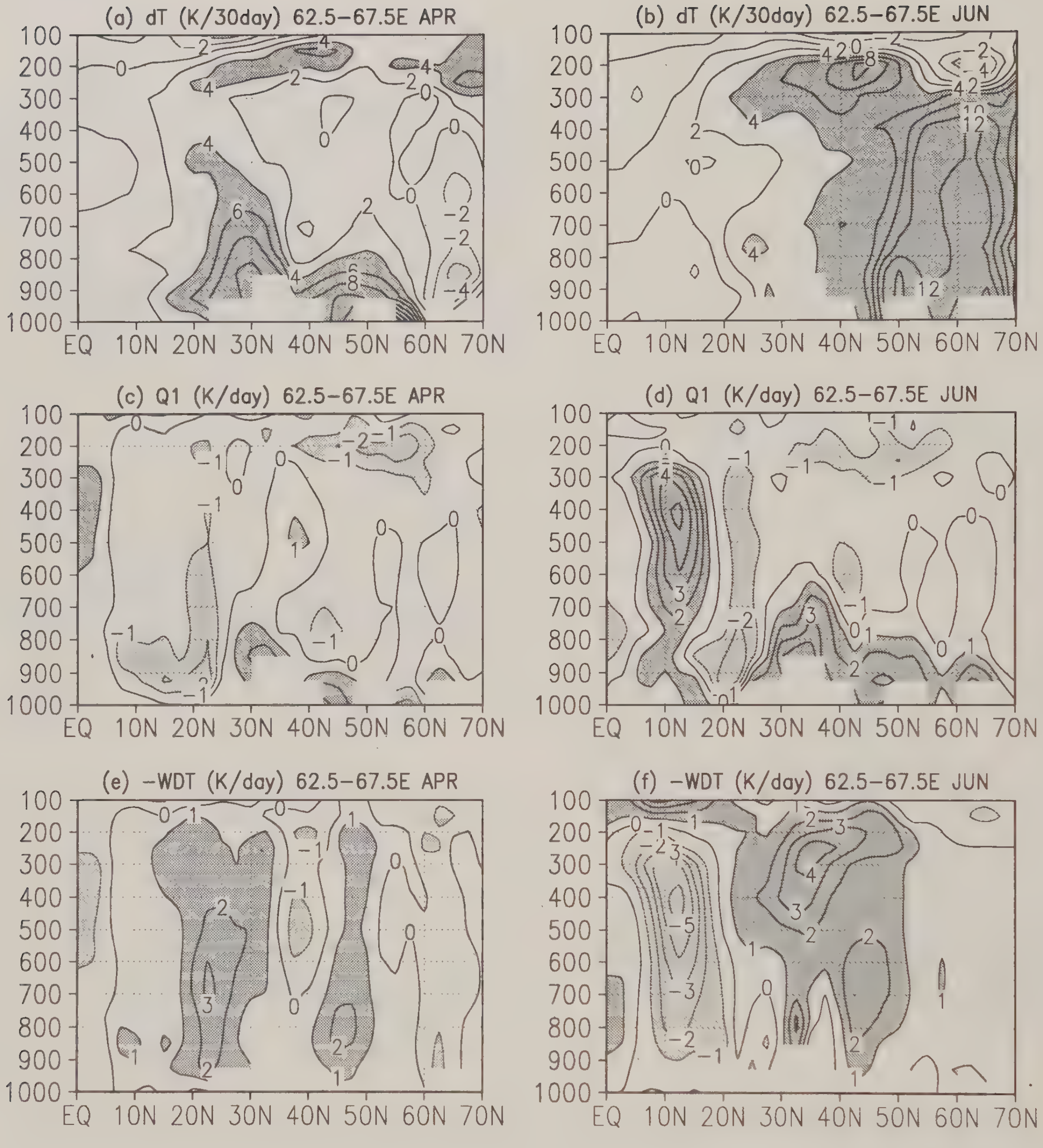


図２　62.5-67.5E 平均の鉛直緯度断面図

(a)　４月の平均昇温、(c) ４月の平均非断熱加熱、 (e)　４月の下降流による平均昇温。(b) (d) (f)は、６月の結果。

Fig.2. The latitude-height section of the atmospheric heat budget along 62.5-67.5－E for April. (a) temperature increase rate (dT), (c) diabatic heat source (Q1), (e) vertical advection plus adiabatic compression (-WDT). (b), (d) and (f) are the same as (a), (c) and (e) except for June. Units are K/day except that K/30day in (a) and (b).

Ⅲ．大気・海洋・陸面間の相互作用に関する総合研究
Synthetic study on the atmosphere-ocean-land interactions
3．モンスーン循環系の総合解析
Synthetic study of the monsoon circulations

気象庁気候・海洋気象部
藤川典久、礒部英彦、小澤芳郎、
工藤達也、青木孝、多田一正、木村吉宏
Climate and Marine Department
Japan Meteorological Agency
N. Fujikawa, H. Isobe, Y. Kozawa,
T. Kudo, T. Aoki, K. Tada, Y. Kimura

(Abstract)

The interannual variability of the Asian summer monsoon circulation and its impact on the Japanese and the world climate is studied through data analysis. For this purpose, three indices are defined to measure the activity of the Asian summer monsoon using outgoing longwave radiation flux. They represent the total convective activity in the monsoon area as well as the meridional and zonal shifts of the active convection areas. Year-to-year variations of the monsoon from 1979 to 1998 are given using the indices.

The impact of monsoon variations on atmospheric circulation on a worldwide scale is investigated through correlation analyses between the monsoon indices and atmospheric variables such as geopotential height and zonal wind velocity. Statistically significant relationships are obtained between the monsoon variations and the location of subtropical jets, the intensity of the Tibetan high pressure, and the intensity of the subtropical high pressure around Japan. Special attention is given to convective activity around the Philippines and its impact on the summer climate in Japan. Features of the summer climate in East Asia and Asian monsoon activity during the years 1993,1994, and 1998 are also studied.

The correlation between the monsoon indices and the Eurasian snow cover and the sea surface temperature of the Indian and Pacific Oceans is calculated in order to find precursors to monsoon variations. Some relationships are found to be statistically significant. However the physical mechanisms linking the correlated variations are subject to future study.

1. Objectives

The Asian monsoon circulation shows variations on a time scale of several days through several years. Its variations significantly influence the climate in Japan and in the world through the global atmospheric circulation system. The purpose of this study is to provide clarification about the long-term variations of the Asian summer monsoon as well as to assess their influence on the Japanese and the world climate through data analysis.

2. Methods

First, the interannual variability of the Asian summer monsoon circulation is studied. In order to represent the monsoon activity quantitatively we define monsoon indices. Precipitation amounts observed over the Indian subcontinent and the vertical shear of zonal wind between 200 hPa and 850 hPa in the monsoon area are often used to define the monsoon intensity (e.g.,

Parthasarathy, 1994; Webster and Yang, 1992). Here, however, we use monthly mean outgoing longwave radiation (OLR) flux on a 2.5° x 2.5° grid from the NOAA polar orbital satellites. OLR data is superior to precipitation data in covering evenly the whole area relevant to the Asian monsoon circulation. In the tropics, lower OLR values can be translated into more active convection, and further into stronger energy sources for the atmospheric circulation. The OLR flux, therefore, more specifically identifies the intensity of the convection associated with the monsoon circulation than the vertical wind shear.

Second, the impact of the variations of the Asian monsoon on the climate on a worldwide scale is examined. For this purpose, correlation coefficients are calculated between the monsoon indices and the stream function at 850 hPa and 200 hPa, zonal wind velocity at 850 hPa and 200 hPa, and geopotential height at 500 hPa and 100 hPa for the summer seasons from 1979 to 1996. Additional analyses are applied to convective activity around the Philippines, its impact on the summer climate in Japan, and the summer climate in East Asia in 1993, 1994 and 1998.

Third, possible external factors contributing to the interannual variability of the Asian summer monsoon are considered. The monsoon circulation is driven by thermal difference between continents and oceans. Its variability is, therefore, affected to some extent by thermal conditions of the lower boundary. Two external factors which are thought to contribute to monsoon variations: the snow cover in the Eurasian continent and sea surface temperature (SST) in the Pacific and Indian Oceans, are brought into consideration. Correlation is, initially, calculated between the monsoon indices and Eurasian spring (April, May, June) snow coverage on a 2° x 2° grid for the period from 1979 to 1997. Here the monthly snow coverage is defined as the proportion of days covered with snow to the total days of the month, and calculated from the CPC/NOAA digital data on weekly northern hemisphere snow cover. Correlation is, then, calculated between the monsoon indices and SST in the Indian and Pacific Oceans.

3. Results

3.1 Indices of Asian summer monsoon activity and their interannual variations

Figure 1 shows the summer (June, July, August) mean OLR flux averaged over the period from 1974 to 1996. Minimum values of less than 210 W/m^2 are located over the Bay of Bengal, Indochina and the Philippine Islands. They indicate the presence of organized deep cumulus convection. Therefore, the heating of atmosphere by cumulus convection in the mean field may be the most intense in region W and region E shown in Fig. 2. Using OLR(W+E) which represents the summer mean OLR flux averaged over region W and region E, we define an index to represent the total convective activity in the monsoon area by the equation:

$$\mathrm{SAMOI(A)} = -\mathrm{OLR(W+E)}.$$

SAMOI stands for “Summer Asian Monsoon OLR Index”.

An empirical orthogonal function (EOF) analysis was applied to the summer mean OLR flux from 1979 to 1996 for the region surrounded by bold lines in Fig. 1 to identify spatial structures of interannual variations. The first EOF (Fig. 10) is nearly zero in the active convection area of Fig. 1 where the OLR flux is less than 210 W/m^2. The second EOF is roughly characterized by a contrast between east and west: the sign is opposite between region W and region E. The third EOF is characterized by a contrast of north and south: the sign is opposite between the region south of 5° N and the region from northern India to the northern part of the South China Sea. Referring to the second and third EOF patterns, we define two indices to measure the meridional and zonal shifts of the active convection areas as:

$$\mathrm{SAMOI(N)} = -(\mathrm{OLR(N)} - \mathrm{OLR(S)}),$$
$$\mathrm{SAMOI(W)} = -(\mathrm{OLR(W)} - \mathrm{OLR(E)}).$$

Here OLR(X) is obtained first by averaging the OLR flux over summer and region X, next by subtracting from the average its mean for 1979 to 1996, and finally by dividing the anomaly by the standard deviation. The indices are standardized with respect to their means and standard deviations, and used in the following analyses. Hereafter SAMOI(A), SAMOI(N) and SAMOI(W) indicate the standardized values.

Figure 3 shows year-to-year variations of the monsoon indices. The behaviors of SAMOI(A), which represents the total convective activity, and the monsoon intensity index defined by Webster and Yang (1992) (figure not shown) are found to be fairly similar (correlation coefficient +0.55). On the other hand, SAMOI(A) has no correlation (coefficient +0.05) with the Indian summer monsoon rainfall (ISMR) (Parthasarathy, 1994), which is a monsoon index defined using precipitation amounts from June through September averaged over the Indian subcontinent.

In terms of SAMOI(A) using the standard deviation as a threshold value, we can classify the years 1984, 1985 and 1994 as years of strong monsoon, and the years 1979, 1983 and 1993 as years of weak monsoon. As for the location of active convection, the years 1981, 1994 and 1997 are classified as years of northward shift, the years 1983, 1992 and 1996 as years of southward shift, the years 1980, 1995, 1996 and 1998 as years of westward shift, and the years 1979 and 1981 as years of eastward shift.

It is noted that the quasi-biennial oscillation-like signals which were pointed out in several studies (e.g., Yasunari, 1990) as being dominate in climate variations in the tropics are not found in any of the indices.

3.2 Impact of Asian monsoon variations on the climate in Japan and in the world

(1) Impact on the climate on a worldwide scale

Figure 4 shows the correlation between (a) SAMOI(A) and 200 hPa stream function, (b) SAMOI(A) and 200 hPa zonal wind velocity, (c) SAMOI(A) and 500 hPa height, and (d) SAMOI(W) and 500 hPa height. The correlation coefficient which is significant at the 5% level is 0.48.

Figure 4 (a), in which positive correlation dominates in the northern hemisphere and negative correlation dominates in the southern hemisphere except for the low latitudes, indicates that the stream function globally tends to have anticyclonic anomalies when the monsoon is strong, and cyclonic anomalies when the monsoon is weak. In particular, the coefficient is larger than +0.72 from Arabia to the Tibetan Plateau. This suggests that the Tibetan high pressure is likely to be strong in strong monsoon years, and weak in weak monsoon years. Positive correlation of more than +0.72 seen around Japan both in Fig. 4 (a) and (c) suggests that a barotropic high pressure tends to develop around Japan when the monsoon is strong.

Figure 4 (c) further indicates that 500 hPa height in the northern tropics has a tendency to be lower than normal in strong monsoon years, and higher in weak monsoon years.

Figure 4 (b), in which negative values are found along 30° N and positive values are found between 40° N and 50° N, indicates that subtropical jets tend to shift poleward when the monsoon is strong, and equatorward when the monsoon is weak. A similar distribution is also seen in the southern hemisphere.

In Fig. 4 (d), a large positive-value region is located along 20° N in the western North Pacific and a negative-value region is located east of Japan. This suggests that the subtropical high pressure is likely to become more intense south of Japan when the active convection areas

shift westward, and near Japan in the case of an eastward shift. The relationship is supported by the correlation pattern between SAMOI(W) and zonal wind velocity at 850 hPa (figure not shown).

Other relationships identified are summarized as follows:

a) When the monsoon is strong, zonal wind anomalies at 850 hPa tend to be easterly in the eastern tropical Pacific, and westerly in the case of a weak monsoon.

b) When the active convection areas shift northward, the Tibetan high pressure tends to be strong (weak in the case of a southward shift), and geopotential height anomalies at 500 hPa and 100 hPa tend to be positive (negative in the case of a southward shift) in middle latitudes, such as over the Mediterranean and from Korea to northern Japan, and in polar areas.

c) When the active convection areas shift westward, subtropical jets tend to shift southward around Japan, and northward in the case of an eastward shift.

It should be noted that the relationships derived from simultaneous correlation analyses do not necessarily provide us with information relating to the cause and result of phenomenon. Further study is needed to reveal links between the factors involved in the above relationships.

(2) Convective activity around the Philippines and its impact on the climate in Japan

It was shown above that the subtropical high pressure tends to intensify itself around Japan when the convective activity is strong in region E rather than in region W. Kurihara and Tsuyuki (1987) suggested through an experiment with a linear shallow-water equation model that the development of a barotropic high pressure around Japan is associated with energy propagation of barotropic Rossby waves excited by intensified convection around 20° N north of the Philippines. These indicate that the convective activity in region E is closely linked to the interannual variations of the subtropical high pressure around Japan.

Figure 5 shows the simultaneous correlation of the intensity of convective activity around the Philippine Islands in August with 500 hPa height in Asia and the western North Pacific, based on data between 1978 and 1993. Here, HCPH which is defined as the normalized anomaly of high-cloud amount in the region 10-20° N and 110-140° E observed by the Geostationary Meteorological Satellite was used as an index for the intensity of convective activity. Strong positive correlation is found from the Korean Peninsula to central Japan.

A correlation analysis demonstrates that the convective activity intensity around the Philippine Islands is related to SST both in the Pacific Ocean and in the Indian Ocean: HCPH is positively correlated with SST in the western equatorial Pacific and negatively correlated with SST in the Indian Ocean. According to our study in FY1992, statistically significant correlation does not exist between SST in the Indian Ocean and in the western equatorial Pacific. The relationships are combined into one as in Fig. 6, where WEST-IND is the difference of the SST anomalies normalized after they were made into an average value for the region EQ.-14° N and 130-150° E and a value which was obtained following the same method for the region EQ.-10° N and 60-100° E. The correlation coefficient is 0.74, which exceeds the significance level of 1%.

It should be noted that the above results do not deny the influence of convective activity in region W on the climate in Japan. In fact, a positive correlation exists between OLR flux in region W and 500 hPa height around Japan for the summer seasons from 1979 to 1996 (figure not shown). It is also noted that the positive correlation between SAMOI(A) and WEST-IND is larger than the correlation between each of the convective activities in region W and in region E and WEST-IND.

(3) Summer climate in 1993, 1994 and 1998

Summer 1993 was characterized by significantly cool and wet weather in most parts of Japan and Korea due to continual appearance of anticyclones around the Sea of Okhotsk and prolonged frontal activities. The Asian monsoon was weak in 1993 as is shown in Fig. 3. The summer mean 500 hPa height shown in Fig. 7 (a) indicates that the subtropical high pressure was weaker than normal around Japan. Another analysis shows that subtropical jets shifted to the south of the normal position almost everywhere in the northern hemispheric.

Contrary to 1993, Japan and Korea experienced record-breaking hot and dry conditions in the summer of the 1994 year. Analyses of geopotential height data indicate that Japan and Korea were dominated by a stable positive pressure anomaly which extended from the lower troposphere to the upper troposphere during July and August (Fig. 7 (b)). The analyses also indicate that the Tibetan high pressure was stronger than normal and subtropical jets shifted to the north of the normal position. In 1994 the Asian summer monsoon was strong and the active convection area was located northward compared to the normal position (Fig. 3).

In summer 1998 an extreme amount of precipitation was observed in East Asia: over the basin of the Yangtze River from June through July and in Korea, northeastern China and northern Japan in August. Figure 8 shows that convection was weaker than normal around the Philippines and stronger than normal over the Indian Ocean. That is, the active convection areas associated with the monsoon shifted to the west and to the south of the normal position, though the southward shift is not reflected in the value of monsoon index SAMOI(N) (Fig.3). This is because the convective activity was especially strong in the area off the west coast of Java, which is south of region S used to define SAMOI(N) (Fig.2). Another analysis shows that subtropical jets were weaker than normal and located south of the normal position during the second half of the summer in East Asia.

The features of the climate in East Asia and of the Asian monsoon activity noted in the analysis of these three summers are consistent with the findings given in (1) above.

3.3 Possible factors contributing to Asian monsoon variations

(1) Eurasian snow cover

Figure 9 presents the correlation coefficients between the monsoon indices and Eurasian spring snow coverage. The correlation coefficient which is significant at the 5% level is 0.46. The results are summarized as follows:

a) Figure 9 (a) indicates that statistically significant correlation does not exist between SAMOI(A) and the snow coverage except for a small area in eastern Kazakhstan, where the coefficient is about -0.4.

b) In Fig. 9 (b), the negative correlation coefficients of -0.4 to -0.6 found in central Siberia indicate that the active convection areas tend to shift northward when the snow coverage is smaller than normal, and southward when the snow coverage is larger.

c) In Fig. 9 (c), the negative correlation coefficients of -0.4 to -0.6 seen in the northwestern part of Russia indicates that the active convection areas tend to shift westward when the snow coverage is smaller than normal, and eastward when the snow coverage is larger.

It has been pointed out in many studies (e.g., Hahn and Shukla, 1976) that negative correlation exists between Eurasian spring snow cover and Indian summer monsoon intensity. The result a) does not confirm the existence of negative correlation. However, the relationship might be reflected in the result b), because SAMOI(N) is positively correlated with the Indian

monsoon intensity index (ISMR).

(2) SST in the Indian and Pacific Oceans

A few relationships of statistical significance are found between the monsoon indices and spring (March, April, May) SST and summer (June, July, August) SST in the Indian and Pacific Oceans. However, referring to relationships between the monsoon indices and OLR flux, some of them are thought to indicate that the SST variations play passive roles, because OLR flux and SST are positively correlated. The other relationships, which are significant at the 5% to 15% level, are as follows:

a) Spring SST in the central and eastern equatorial Pacific is positively correlated with SAMOI(W).

b) There is a negative correlation between SAMOI(A) and summer SST in the eastern equatorial Pacific.

c) There is a positive correlation between SAMOI(W) and summer SST in several parts of the Indian Ocean, where the simultaneous correlation between SST and OLR flux is negative.

In addition, there is a positive correlation between SAMOI(A) and WEST-IND as is pointed out in 3.2 (2). Further study is needed to examine the linkage between the monsoon variations and the SST variations.

4. Discussions

(1) In this study, we defined new indices of Asian summer monsoon activity using OLR flux and described its interannual variability. Many studies have related the interannual variability of Asian monsoon to the El Niño-Southern Oscillation (ENSO) phenomenon (e.g., Webster and Yang 1992; Yasunari 1990). However, our indices do not have statistically significant correlation with SST in NINO.3 and NINO.4. The first EOF mode of summer mean OLR flux in the region surrounded by bold lines in Fig. 1 exhibits variations associated with ENSO: the correlation between the time coefficient of the first mode and the SST in NINO.3 is 0.69. In the spatial pattern of the first mode (Fig. 10) are seen the two fluctuation patterns of high-cloud amount found by Nitta (1986). One pattern is an east-west oscillation along the equator between the maritime continent and east of 140° E. Another pattern is a north-south oscillation between the western North Pacific along 20° N and the middle latitude across Japan. Figure 10 indicates that the convection intensity north and south of region E varies in phase. The interannual variability of the first mode and its impact on the climate in the world are topics for future study.

(2) This study confirmed that convective activities associated with the Asian summer monsoon are closely related with the climate not only in the monsoon region but also in the middle latitudes, especially around Japan. The impact on the climate in Japan is obvious in Fig. 11 which shows relationship between SAMOI(A) and summer mean temperature anomalies in northern Japan. Therefore, the predictability of the Asian summer monsoon is crucial to the forecast of summer climate in Japan. The relationships with a time-lag given in subsection 3.3 could potentially be suitable for statistical bases of monsoon prediction in summer. Further study is needed to explore the feasibility of this.

(3) Our study in FY1993 pointed out that when July and August SST averaged over the region (10° S-10° N; 60° E-100° E) in the Indian Ocean is higher than normal, 500 hPa height in July and August tends to be lower than normal over Japan. This relationship should be reexamined in terms of a linkage through variations of the Asian monsoon. The relationships given in 3.2 (2) and

3.3 (2) might be clues to the linkage.

5. References

1) Hahn, D.G. and J. Shukla, 1976: An apparent relationship between Eurasian snow cover and Indian monsoon rainfall. *J. Atmos. Sci.*, 33, 2461-2462.
2) Kurihara, K. and T. Tsuyuki, 1987: Development of the barotropic high around Japan and its association with Rossby wave-like propagations over the North Pacific: Analysis of August 1984. *J. Meteor. Soc. Japan*, 65, 237-246.
3) Nitta, T., 1986: Long-term variations of cloud amount in the western Pacific region. *J. Meteor. Soc. Japan*, 64, 373-390.
4) Parthasarathy, B., A.A. Munot and D.R. Kothawale, 1994: All-India monthly and seasonal rainfall series: 1871-1993. *Theor. and Appl. Climatol.*, 49, 217-224.
5) Webster, P.J. and S. Yang, 1992: Monsoon and ENSO: Selectively interactive systems. *Quart. J. Roy. Meteor. Soc.*, 118, 877-926.
6) Yasunari, T., 1990: Impact of Indian monsoon on the coupled atmosphere/ocean system in the tropical Pacific. *Meteor. & Atmos. Phys.*, 44, 29-41.

6. Publications

1) Sakai S., F. Watanabe, K. Kurihara, K. Hayashi, H. Isobe, N. Fujikawa, R. Yamagiwa, 1996: Low rainfall and high temperatures－from the beginning of May through the middle of October 1994－. *Technical Report of the Japan Meteorological Agency*, 118, 117-137. (in Japanese)
2) Wakahara K. and N. Fujikawa, 1997: Features of the climate in Japan and atmospheric circulation in the cool summer of 1993 and in the hot summer of 1994. *Kishou Kenkyuu Note*, 189, 2-69. (in Japanese)

7. International Cooperation

None

アブストラクト

夏のアジアモンスーンの年々変動とそれが日本及び世界の天候に与える影響をデータ解析により調べた。この調査に使用するため、夏のアジアモンスーンの活動度を表す3つの指数（モンスーン域全体の対流活動度、対流活動活発域の南北シフト及び東西シフト）を外向き長波放射量を用いて作成した。この指数を用いて1979～1998年の年々のモンスーン活動の特徴を把握できた。

アジアモンスーンの変動が全球規模の大気循環に及ぼす影響を把握するため、特定気圧面の高度、東西風速等とモンスーン指数の相関係数を求めた。その結果、亜熱帯ジェットの位置、チベット高気圧の強さ、日本周辺での亜熱帯高気圧の強さとモンスーンの活動との間に、統計的に有意な関係が得られた。また、フィリピン周辺の対流活動とそれが日本の夏の天候に及ぼす影響に特に着目した解析を行うとともに、1993·1994·1998年の夏の事例について、東アジアの天候とモンスーン活動の特徴を調べた。

さらに、モンスーンの変動を引き起こす要因として考えられるユーラシア大陸の積雪分布、インド洋・太平洋の海面水温とモンスーン指数との間に、統計的に有意な関係をいくつか得た。しかし、相関関係の物理的メカニズムについては今後の調査が必要である。

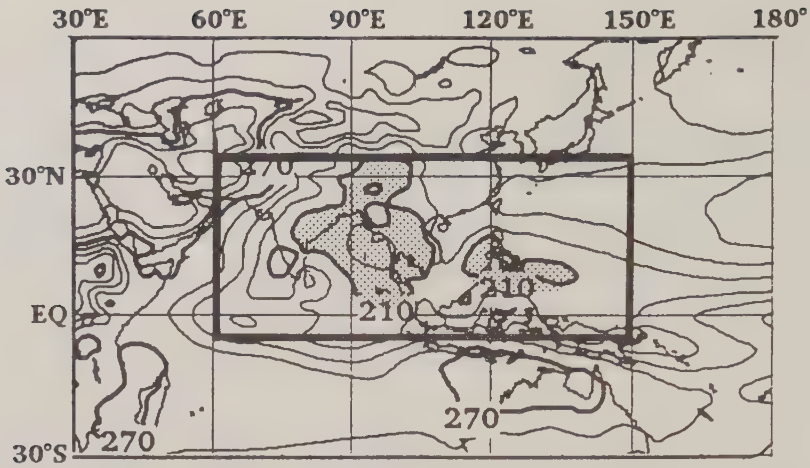


Fig. 1 Summer (June, July, August) mean OLR flux averaged over 23 years (1974-1996) Contour interval is 15 W/m². Areas with the OLR flux of less than 210 W/m² are shaded.

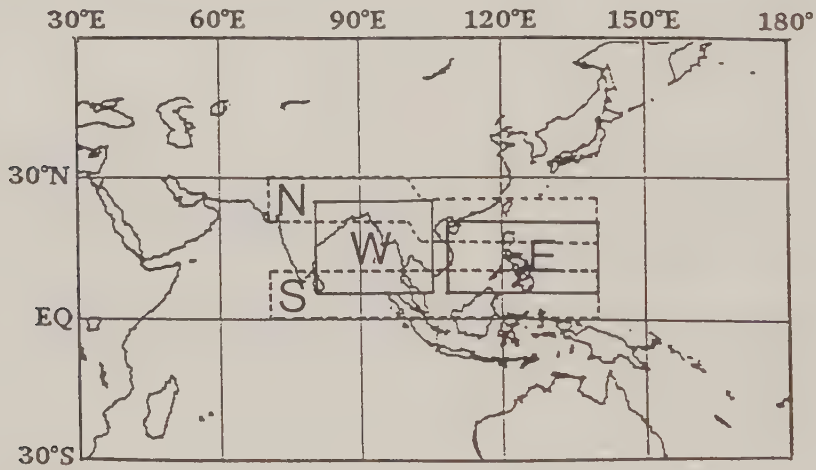


Fig. 2 Regions chosen to define the monsoon indices

E area: (107.5-140° E, 5-20° N)

W area: (80-105° E, 5-25° N)

N area: (70-100° E, 20-30° N)+(102.5-140° E, 15-25° N)

S area: (70-140° E, EQ.-10° N)

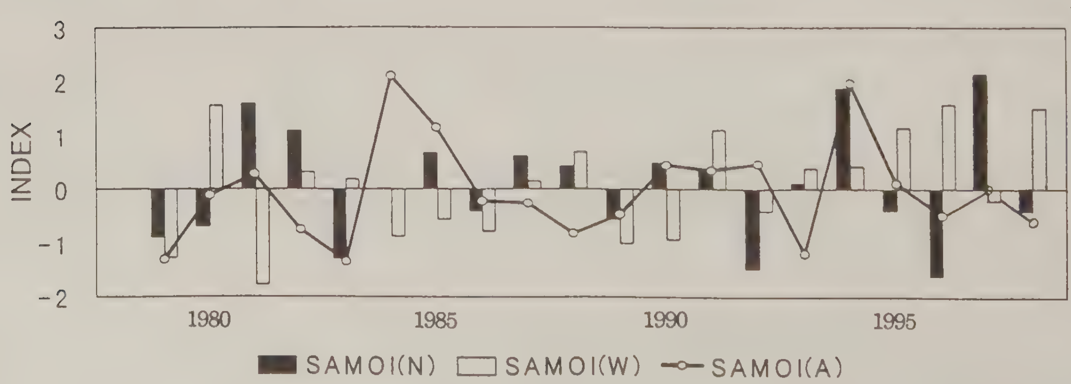


Fig. 3 Time series of the monsoon indices (1979-1998)

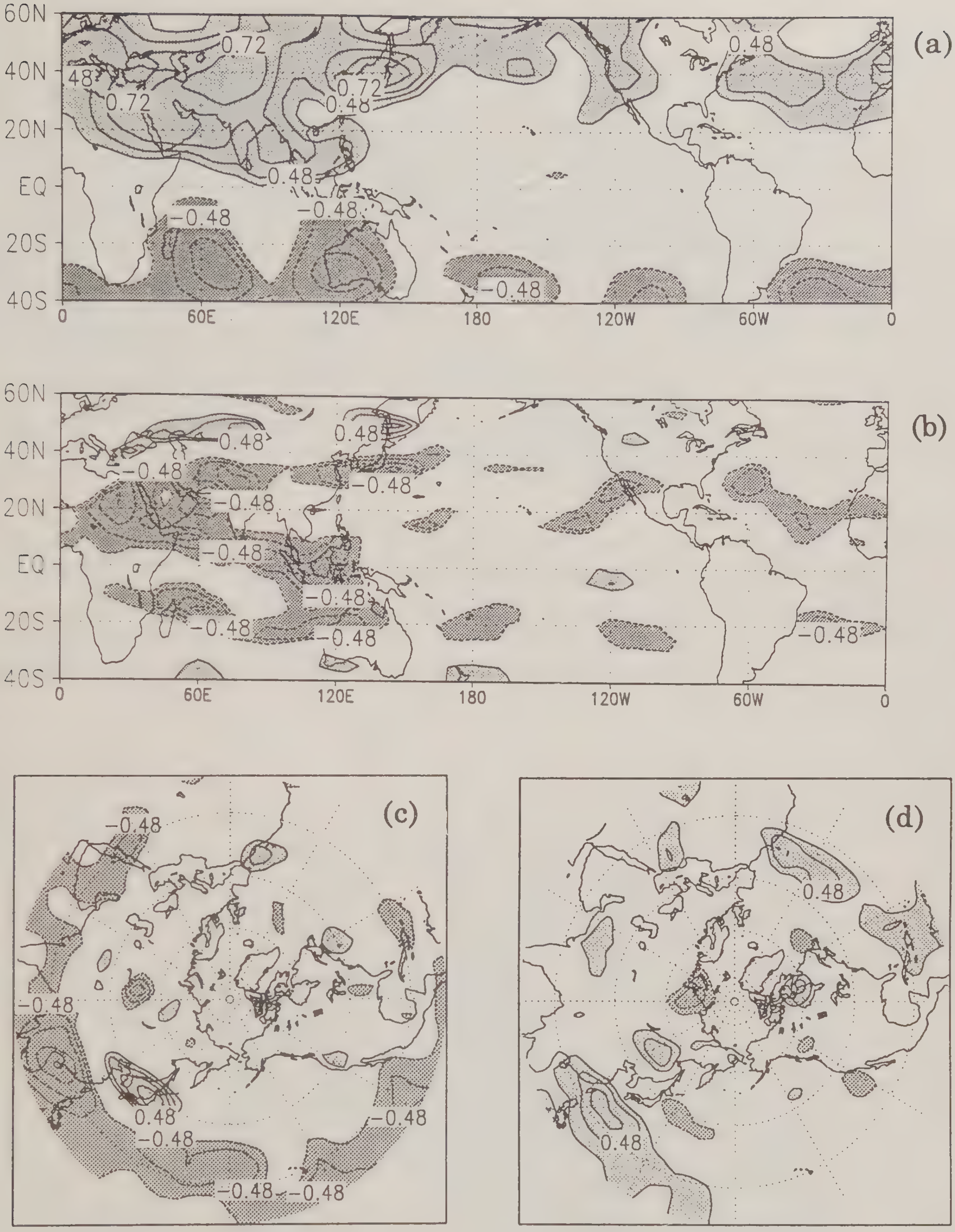


Fig. 4 Correlation coefficients between (a) SAMOI(A) and stream function at 200 hPa, (b) SAMOI(A) and zonal wind velocity at 200 hPa, (c) SAMOI(A) and geopotential height at 500 hPa, and (d) SAMOI(W) and geopotential height at 500 hPa

Contour interval is 0.12 and contours between −0.24 and +0.24 are excluded. Regions with positive correlation greater than 0.36 are lightly shaded, and those with less than −0.36 are heavily shaded.

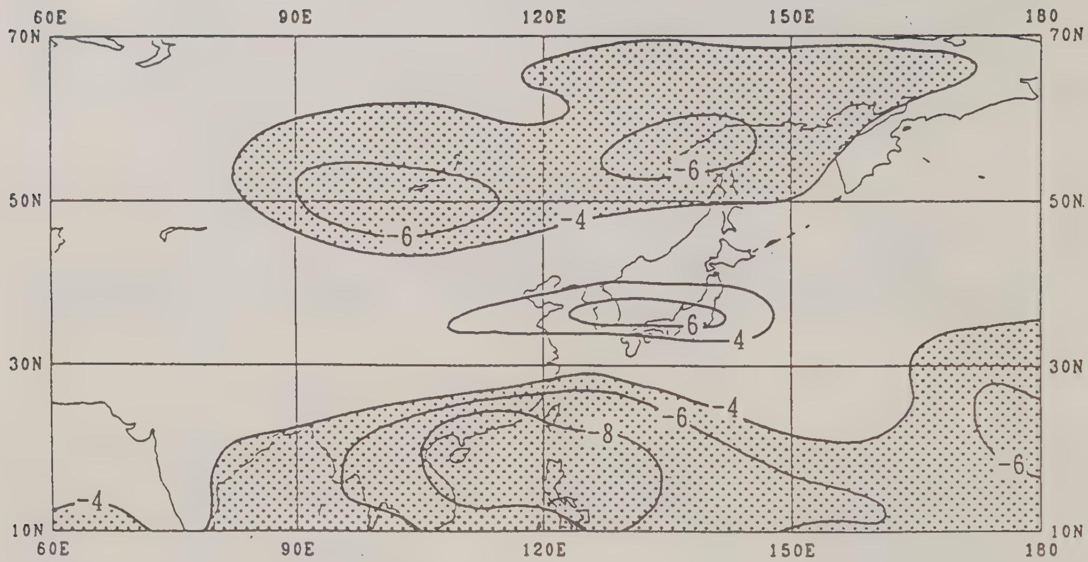


Fig. 5 Correlation coefficients (x10) between HCPH and geopotential height at 500 hPa
Contour interval is 2 and contours of –2, 0 and +2 are excluded.
Coefficient is less than –0.4 in the shaded areas.

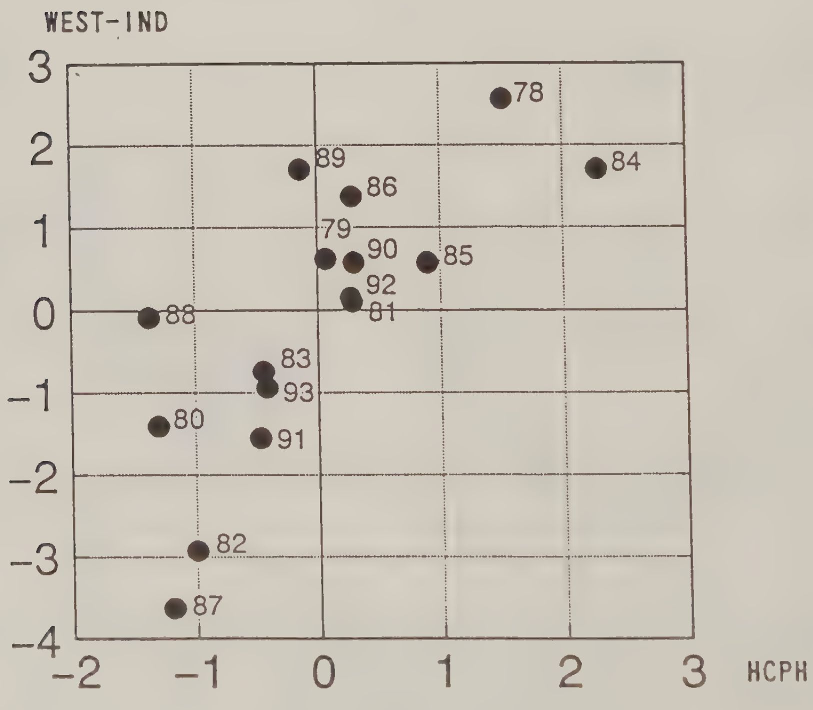
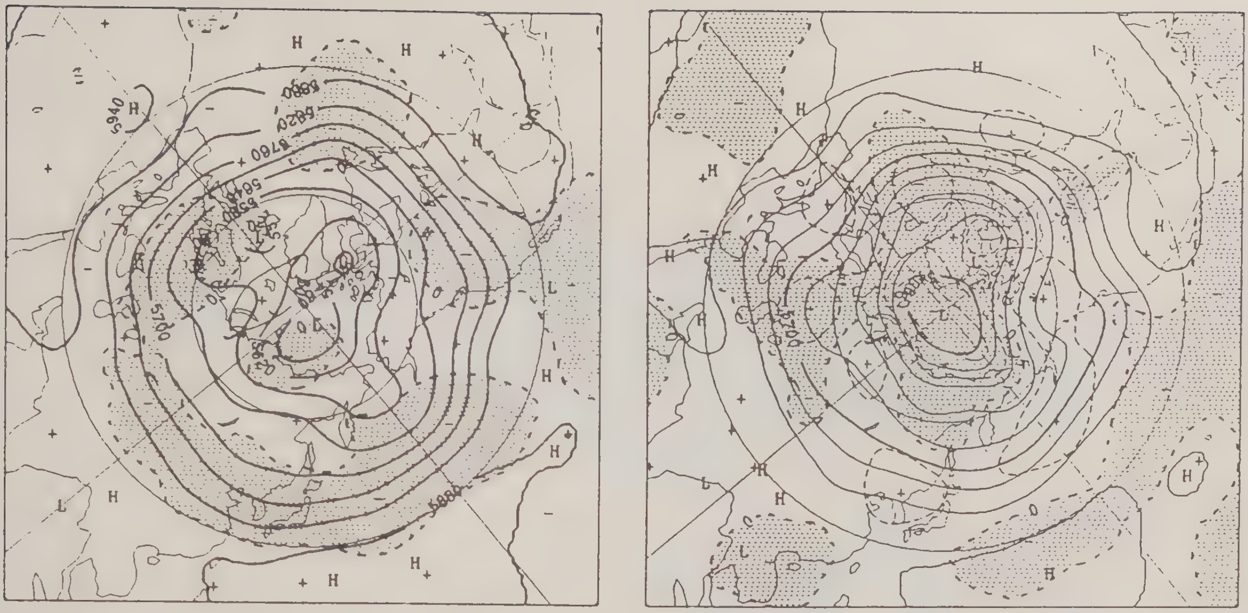


Fig. 6 Scatter diagram of HCPH versus WEST-IND in August
Numbers attached to the dots indicate the years.



(a) (b)

Fig. 7 Summer mean geopotential height at 500 hPa and its anomaly
(a) 1993, (b) 1994

Solid lines indicate the geopotential height: contour interval is 60 m. Dashed lines indicate its anomaly: contour interval is 30 m. Areas of negative anomalies are shaded.

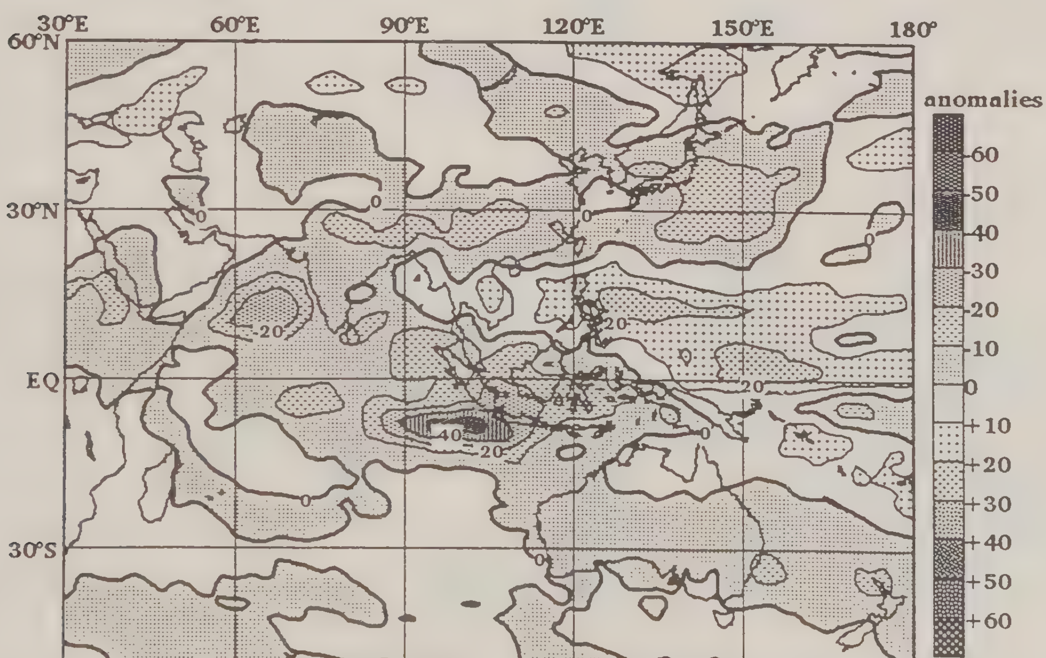


Fig. 8 Summer mean OLR anomaly of 1998
Contour interval is 10 W/m^2. Base period for normal is 1979-1996.

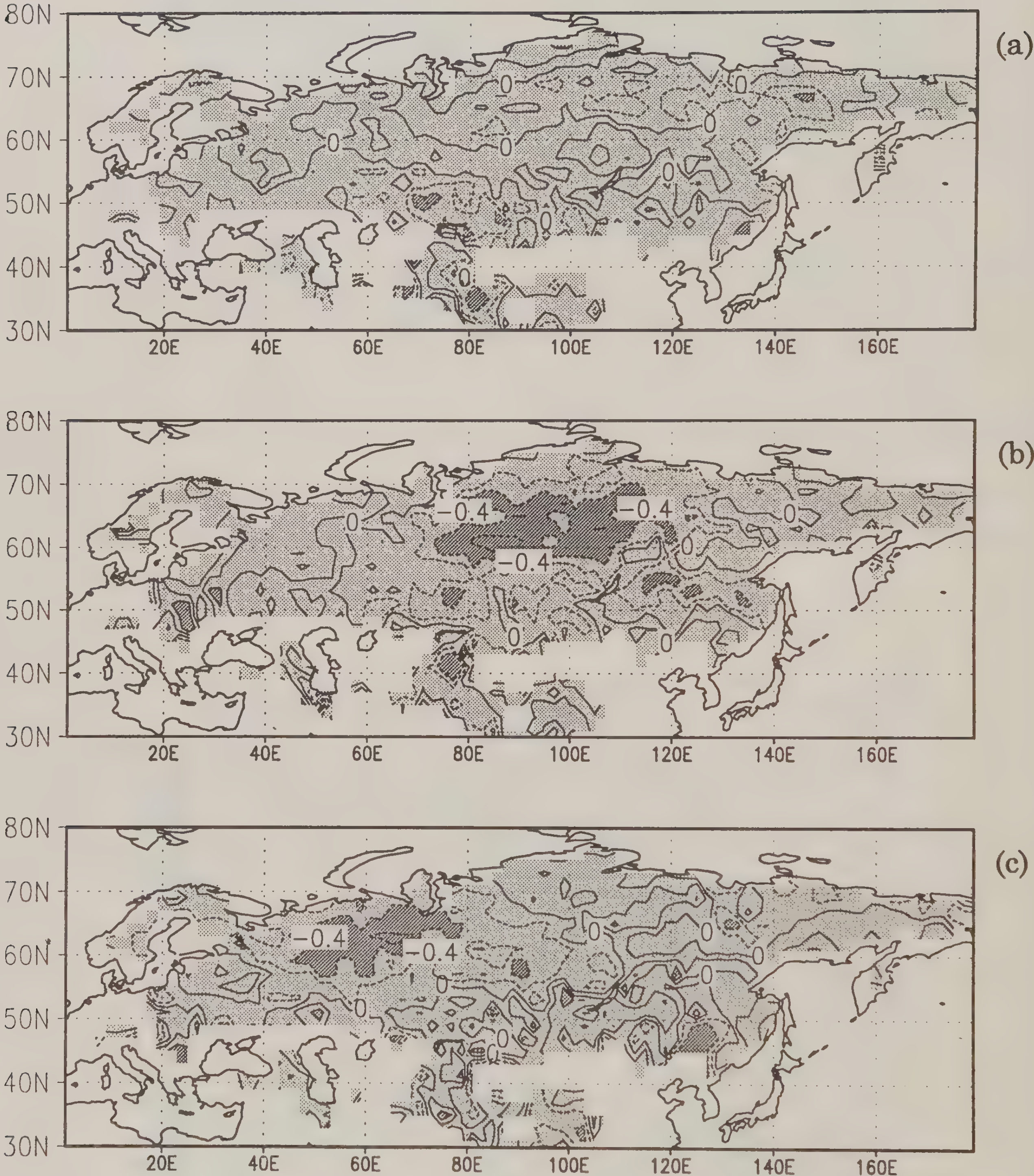


Fig. 9 Pointwise correlation of the snow coverage averaged from April through June with the monsoon indices, (a) SAMOI(A), (b) SAMOI(N), and (c) SAMOI(W)

Contour interval is 0.2. Dashed lines indicate a negative correlation. Regions with negative correlation less than –0.4 are heavily shaded.

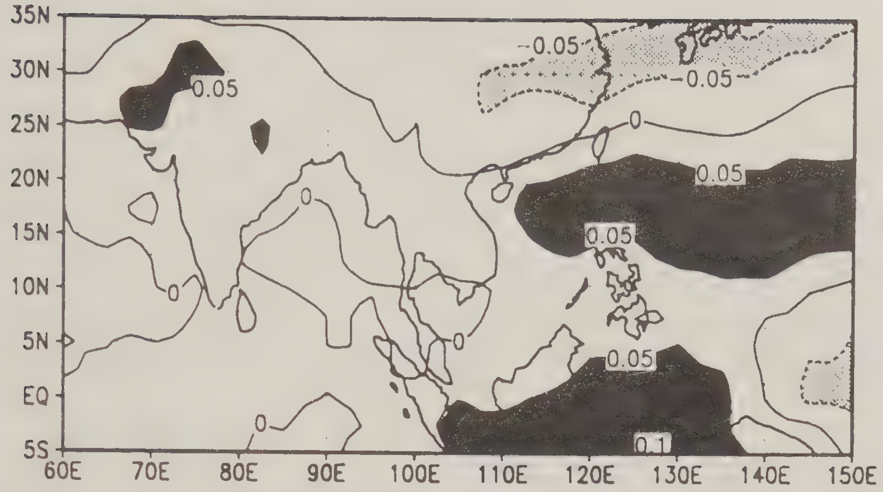


Fig. 10 Spatial pattern of the first EOF mode of summer mean OLR flux Unit is arbitrary. Areas of more than +0.05 are heavily shaded and areas of less than –0.05 are lightly shaded.

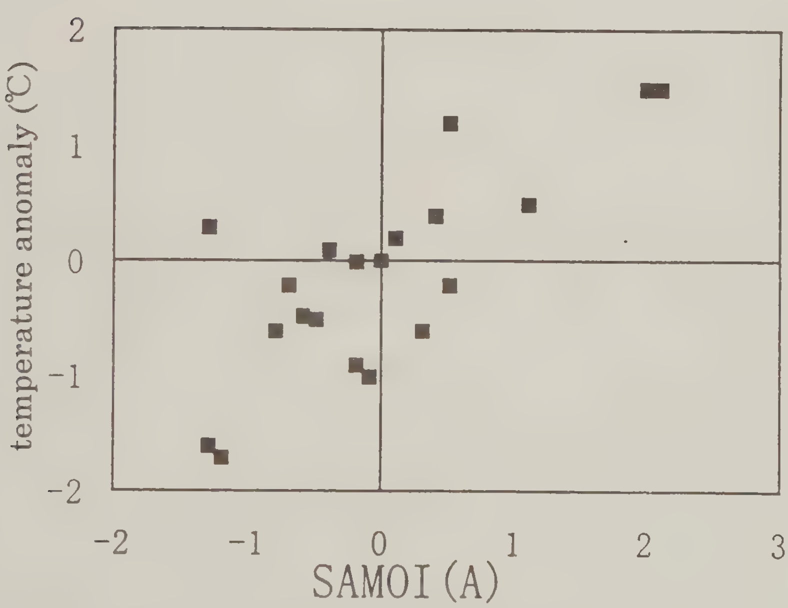


Fig. 11 Scatter diagram between summer mean temperature anomalies (℃) in northern Japan and SAMOI(A) for the 1979-1998 period
The correlation coefficient is +0.77, which is significant at the 0.1% level.

観測・解析研究ディレクトリー

Directory of Observation/Analysis Data Set

List of Directory Entry Titles

1. Directory Entry Title :

GMS IR Histogram

2. Directory Entry Start and Stop Date

Start Date : 1980-01-01
Stop Date : 1998-12-31

3. Sensor Name

VISSR

4. Source Name

GMS

5. Investigator, Technical Contact, and Author

(1) Investigator

Last name : Yamazaki
First name : Nobuo
Email : nyamazak@mri-jma.go.jp
Phone : +81-298-53-8668
Address : M.R.I.,1-1 Nagamine,Tsukuba,Ibaraki 305-0052, Japan

(2) Technical Contact

Last name : Kiyoshi
First name : Sasamoto
Email :
Phone :
Address : Meteorological Satellite Center, 3-235 Nakakiyoto
Kiyose-City ,Tokyo 204-0012, Japan

(3) Author

Last name :
First name :
Email :
Phone :
Address :

6. Data Center

(1) Data Center Name : ＭＲＩ＞Meteorological Research Institute
(2) Dataset ID :
(3) Data Center Contact

Last Name :
First Name :
Email :
Phone :
Address :

7. Originating Center

8. Campaign or Project

ＪＥＸＡＭ＞Japanese Experiment on Asian Monsoon

9. Storage Medium 130 CCT's 13 G Bytes
10. Parameter Measured Earth Radiative Process > IR equivalent black body temperature
11. Discipline Keywords Earth Science > Atmosphere
12. Coverage Minimum Latitude: 50S Maximum Latitude: 50N Minimum Longitude: 80E Minimum Longitude: 160W
13. Location Keywords Western Pacific
14. General Keywords
15. Revision Date
16. Science Review Date
17. Future Review Date
18. References
19. Summary Available on the basis of cooperative research

1. Directory Entry Title : GMS Water vapor Channel Histogram
2. Directory Entry Start and Stop Date Start Date : 1995-06-01 Stop Date : 1995-12-31
3. Sensor Name VISSR
4. Source Name GMS
5. Investigator, Technical Contact, and Author (1) Investigator Last name : Yamazaki First name : Nobuo Email : nyamazak@mri-jma.go.jp Phone : +81-298-53-8668 Address : M.R.I.,1-1 Nagamine,Tsukuba,Ibaraki 305-0052, Japan (2) Technical Contact Last name : Kiyoshi First name : Sasamoto Email : Phone : Address : Meteorological Satellite Center, Tokyo, Japan (3) Author Last name : First name : Email : Phone : Address :
6. Data Center (1) Data Center Name : ＭＲＩ＞Meteorological Research Institute (2) Dataset ID : (3) Data Center Contact Last Name : First Name : Email : Phone : Address :
7. Originating Center
8. Campaign or Project ＪＥＸＡＭ＞Japanese Experiment on Asian Monsoon

9. Storage Medium

130 CCT's 13 G Bytes

10. Parameter Measured

Earth Radiative Process > Water vapor Channel

Equivalent black body temperature

11. Discipline Keywords

Earth Science > Atmosphere

12. Coverage

Minimum Latitude: 50S
Maximum Latitude: 50N
Minimum Longitude: 80E
Minimum Longitude: 160W

13. Location Keywords

Western Pacific

14. General Keywords

15. Revision Date

16. Science Review Date

17. Future Review Date

18. References

19. Summary

Available on the basis of cooperative research

1. Directory Entry Title : Gridded Brightness Temperature from NOAA-11 AVHRR
2. Directory Entry Start and Stop Date Start Date : 1986-05-01 Stop Date : 1986-08-31 Start Date : 1987-05-01 Stop Date : 1987-08-31 Start Date : 1988-05-01 Stop Date : 1988-08-31 Start Date : 1991-05-01 Stop Date : 1991-08-31 Start Date : 1996-05-01 Stop Date : 1996-08-31
3. Sensor Name AVHRR > Advanced Very High Resolution Radiometer
4. Source Name NOAA-11
5. Investigator, Technical Contact, and Author (1) Investigator Last name : Inoue First name : Tosiro Email : tinoue@mri-jma.go.jp Phone : +81-298-53-8669 Address : M.R.I.,1-1 Nagamine,Tsukuba,Ibaraki 305-0052, Japan (2) Technical Contact Last name : First name : Email : Phone : Address : (3) Author Last name : First name : Email : Phone : Address :
6. Data Center (1) Data Center Name : ＭＲＩ >Meteorological Research Institute (2) Dataset ID : (3) Data Center Contact Last Name :

First Name : Email :
7. Originating Center
8. Campaign or Project J E X A M>Japanese Experiment on Asian Monsoon
9. Storage Medium 4 MT, 400M Bytes
10. Parameter Measured Brightness Temperature of Split Window
11. Discipline Keywords Earth Science> Atmosphere
12. Coverage Minimum Latitude: 40S Maximum Latitude: 40N Minimum Longitude: 40E Minimum Longitude: 150E
13. Location Keywords Indian Ocean, South Asia
14. General Keywords
15. Revision Date
16. Science Review Date
17. Future Review Date
18. References
19. Summary This data set contains brightness temperature of split window data and satellite zenith angle data from AVHRR. These data are available at 0.1° latitude/longitude grid. Available on the basis of cooperative research

1. Directory Entry Title :
Daily rainfall in India

2. Directory Entry Start and Stop Date
Start Date : 1988-01-01
Stop Date : 1990-10-31

3. Sensor Name

4. Source Name

5. Investigator, Technical Contact, and Author
(1) Investigator
Last name : Tanaka
First name : Minoru
Email : mtanaka@mri-jma.go.jp
Phone : +81-298-53-8667
Address : M.R.I.,1-1 Nagamine,Tsukuba,Ibaraki 305-0052, Japan
(2) Technical Contact
Last name :
First name :
Email :
Phone :
Address :
(3) Author
Last name :
First name :
Email :
Phone :
Address :

6. Data Center
(1) Data Center Name : ＭＲＩ>Meteorological Research Institute
(2) Dataset ID :
(3) Data Center Contact
Last Name :
First Name :
Email :
Phone :
Address :

7. Originating Center

8. Campaign or Project
ＪＥＸＡＭ>Japanese Experiment on Asian Monsoon

9. Storage Medium 1 Floppy Disk
10. Parameter Measured Atmospheric Dynamics > precipitation
11. Discipline Keywords Earth Science > Atmosphere
12. Coverage Minimum Latitude: 8N Maximum Latitude: 36N Minimum Longitude: 70E Minimum Longitude: 90E
13. Location Keywords
14. General Keywords Precipitation
15. Revision Date 1994-03-25
16. Science Review Date 1994-03-25
17. Future Review Date
18. Reference
19. Summary Daily rainfall data for 80 stations in India Data not available, outside of J X E A M J E X A M>Japanese Experiment on Asian Monsoon Available on the basis of cooperative research

1. Directory Entry Title :

Gridded Brightness Temperature from INSAT

2. Directory Entry Start and Stop Date

Start Date : 1991-05-01

Stop Date : 1991-09-30

3. Sensor Name

AVHRR

4. Source Name

INSAT

5. Investigator, Technical Contact, and Author

(1) Investigator

Last name : Takahashi

First name : Kiyotoshi

Email : ktakahas@mri-jma.go.jp

Phone : +81-298-51-7111

Address : M.R.I.,1-1 Nagamine,Tsukuba,Ibaraki 305-0052, Japan

(2) Technical Contact

Last name :

First name :

Email :

Phone :

Address :

(3) Author

Last name :

First name :

Email :

Phone :

Address :

6. Data Center

(1) Data Center Name : ＭＲＩ＞Meteorological Research Institute

(2) Dataset ID :INSATIR-910505

(3) Data Center Contact

Last Name :

First Name :

Email :

Phone :

Address :

7. Originating Center

Indian Meteorological Department

8. Campaign or Project

ＪＥＸＡＭ＞Japanese Experiment on Asian Monsoon

9. Storage Medium 1 Magnetic Tape
10. Parameter Measured Earth Radiative Process > Brightness Temperature
11. Discipline Keywords Earth Science > Atmosphere
12. Coverage Minimum Latitude: 60S Maximum Latitude: 60N Minimum Longitude: 40E Minimum Longitude: 120W
13. Location Keywords Indian Ocean
14. General Keywords El Nino phase
15. Revision Date 1992-02-04
16. Science Review Date
17. Future Review Date
18. References
19. Summary This dataset is a 3 hourly 1° ×1° mean TBB file observed by INSAT Available on the basis of cooperative research

1. Directory Entry Title :

China Monthly Surface Bulletin

2. Directory Entry Start and Stop Date

Start Date : 1971-01

Stop Date : 1995-12

3. Sensor Name

4. Source Name

Chinese Meteorological Administration

5. Investigator, Technical Contact, and Author

(1) Investigator

Last name : Yamazaki

First name : Nobuo

Email : nyamazak@mri-jma.go.jp

Phone : +81-298-53-8668

Address : M.R.I.,1-1 Nagamine,Tsukuba,Ibaraki 305-0052, Japan

(2) Technical Contact

Last name :

First name :

Email :

Phone :

Address :

(3) Author

Last name :

First name :

Email :

Phone :

Address :

6. Data Center

(1) Data Center Name : ＭＲＩ＞Meteorological Research Institute

(2) Dataset ID :

(3) Data Center Contact

Last Name :

First Name :

Email :

Phone :

Address :

7. Originating Center

8. Campaign or Project

ＪＥＸＡＭ＞Japanese Experiment on Asian Monsoon

9. Storage Medium

Books, 288 volumes

10. Parameter Measured

Surface elements:wind,temperature,humidity,pressure, precipitation, and soil temperature

11. Discipline Keywords

Earth Science> Atmosphere

12. Coverage

Minimum Latitude: 25N
Maximum Latitude: 50N
Minimum Longitude: 80E
Minimum Longitude: 130E

13. Location Keywords

China

14. General Keywords

15. Revision Date

16. Science Review Date

17. Future Review Date

18. References

19. Summary

Available on the basis of cooperative research

1. Directory Entry Title : GMS multi-level cloudiness
2. Directory Entry Start and Stop Date Start Date : 1984-01-01 Stop Date : 1998-12-31
3. Sensor Name VISSR
4. Source Name GMS
5. Investigator, Technical Contact, and Author (1) Investigator Last name : Takahashi First name : Kiyotoshi Email : ktakahas@mri-jma.go.jp Phone : +81-298-53-8670 Address : M.R.I.,1-1 Nagamine,Tsukuba,Ibaraki 305-0052, Japan (2) Technical Contact Last name : Takahashi First name : Kiyotoshi Email : ktakahas@mri-jma.go.jp Phone : +81-298-53-8670 Address : M.R.I.,1-1 Nagamine,Tsukuba,Ibaraki 305-0052, Japan (3) Author Last name : First name : Email : Phone : Address :
6. Data Center (1) Data Center Name : ＭＲＩ>Meteorological Research Institute (2) Dataset ID : (3) Data Center Contact Last Name : First Name : Email : Phone : Address :
7. Originating Center
8. Campaign or Project

9. Storage Medium 4.7GB/year
10. Parameter Measured Earth Radiative Process > multi-level clouduness
11. Discipline Keywords Earth Science > Atmosphere
12. Coverage Minimum Latitude: 60S Maximum Latitude: 60N Minimum Longitude: 80E Minimum Longitude: 160W
13. Location Keywords Eastern Asisa and Western Pacific
14. General Keywords
15. Revision Date
16. Science Review Date
17. Future Review Date
18. References
19. Summary Available on the basis of cooperative research

1. Directory Entry Title JEXAM Doppler radar data on convective clouds in cloud clusters
2. Directory Entry Start and Stop Date Start Date 1990-8-27 Stop Date 1992-9-22
3. Sensor Name X-band Doppler radar
4. Source Name X-band Doppler radar of Meteorological Research Institute, Japan
5. Investigator, Technical Contact, and Author (1) Investigator Last name : Sakakibara First name : Hitoshi Email : hsakakib@mri-jma.go.jp Phone : 0298-53-8671 , Facsimile : 0298-53-8735 Address : M.R.I., 1-1 Nagamine, Tsukuba, Ibaraki 305-0052, Japan (2) Technical Contact Last name : Tanaka First name : Yoshinobu Email : ytanaka@mri-jma.go.jp Phone : 0298-52-9183 , Facsimile : 0298-53-8735 Address : M.R.I., 1-1 Nagamine, Tsukuba, Ibaraki 305-0052, Japan (3) Author Last name : Sakakibara First name : Hitoshi Email : hsakakib@mri-jma.go.jp Phone : 0298-53-8671 , Facsimile : 0298-53-8735 Address : M.R.I., 1-1 Nagamine, Tsukuba, Ibaraki 305-0052, Japan
6. Data Center (1) Data Center Name : MRI > Meteorological Research Institute (2) Dataset ID : MIYAKO90-92 (3) Data Center Contact Last name : Sakakibara First name : Hitoshi Email : hsakakib@mri-jma.go.jp Phone : 0298-53-8671 , Facsimile : 0298-53-8735 Address : M.R.I., 1-1 Nagamine, Tsukuba, Ibaraki 305-0052, Japan

7. Originating Center MRI
8. Campaign or Project JEXAM > Japanese Experiment on Asian Monsoon
9. Storage Medium 4mm DAT , 8 G Bytes
10. Parameter Measured Atmospheric Dynamics > Precipitation Atmospheric Dynamics > Winds
11. Discipline Keywords Earth Science > Atmosphere
12. Coverage Minimum Latitude : 24 N Maximum Latitude : 25 N Minimum Longitude: 125 E Maximum Longitude: 126 E
13. Location Keywords Asia > Japan > Okinawa > Miyakojima
14. General Keywords Typhoon, Baiu front
15. Revision Date
16. Science Review Date
17. Future Review Date
18. References
19. Summary Available on the basis of cooperative research.

1.Directory Entry Title JEXAM-Miyako92 (NIED) Doppler radar observation
2.Directory Entry Start and Stop Date 27 May 1992 - 19 June 1992、 2 September 1992 - 3 September 1992、 19 September 1992 - 24 September 1992
3.Sensor Name Doppler radar
4.Source Name original data of the special observation
5.Investigator, Technical Contact, and Author NAKAI, S (NIED)
6.Data Center NIED (Investigator)
7.Originating Center NIED (Investigator)
8.Campaign or Project JEXAM
9.Storage Medium 8mm data cartridge
10.Parameter Measured equivalent radar reflectivity factor, mean Doppler velocity, Doppler velocity variance
11.Discipline Keywords Asian monsoon, subtropical precipitation, mesoscale, radar
12.Coverage within 64km radius centered at 24° 54'N, 125° 16'E
13.Location Keywords Miyako, Okinawa, Japan
14.General Keywords Subtropical Rainfall
15.Revision Date Date of Observation
16.Science Review Date
17.Future Review Date
18.References
19.Summary Cooperative observations on the structure of convective clouds were made in June 1992 by Meteorological Research Institute (MRI) and National Research Institute for Earth Science and Disaster Prevention (NIED). Portable X-band Doppler radars were placed at Miyako Island, and synchronized three-dimensional observations were done for dual-Doppler analyses. Radar coverage area was approximately an oval shape with a major axis of 150 km and a minor axis of 130 km. Each of the dual-Doppler lobes had a diameter of about 40 km. The length of the baseline was about 21 km. RHI and vertical incidence data were also obtained by NIED Doppler radar. Observation period was divided into two, Baiu observation period (from May 25 to Jun 20) and Typhoon observation period (from August 21 to September 23). Observations were done when precipitating cloud systems appeared. Amount of observation data of NIED Doppler radar reached 51 volumes of 6250 BPI, 2400 ft magnetic tapes. Observed phenomena includes various types of precipitation in Asian Monsoon region, such as isolated precipitation, severe convective precipitation with echo top at a height of 15 km, very shallow precipitation. This data set is available on the basis of cooperative research.

1.Directory Entry Title GMS S-VISSR and some other operational data
2.Directory Entry Start and Stop Date March to July 1997, March 1998 to March 1999
3.Sensor Name S-VISSR etc.
4.Source Name GMS-5 etc.
5.Investigator, Technical Contact, and Author NAKAI, S (NIED)
6.Data Center NIED (Investigator)
7.Originating Center NIED (Investigator)
8.Campaign or Project JEXAM, MeDRS-NIED
9.Storage Medium 8mm data cartridge
10.Parameter Measured
11.Discipline Keywords
12.Coverage full disk / Japan
13.Location Keywords
14.General Keywords
15.Revision Date
16.Science Review Date
17.Future Review Date
18.References
19.Summary IR TBBs obtained by GMS spacecraft are archived in the form of one file per channel (IPC format). The S-VISSR data are received from GMS at NIED, and visible data is omitted because of mass storage capacity. IR data including water vapor channel are archived as it received. The data is basically hourly. Special observation data at 30-minute intervals are also archived. The following data of the same period are archived in the same tapes: 3-hourly GOES IR images, 6-hourly Meteosat IR images (both are full disk images). AMeDAS station data, and JMA radar echo level data. Visual data list is available. This data set is available on the basis of cooperative research.

1.Directory Entry Title NOAA AVHRR LAC compatible data around Japan
2.Directory Entry Start and Stop Date June to August 1996, March to July 1997, February and March 1998
3.Sensor Name AVHRR
4.Source Name NOAA-12,14
5.Investigator, Technical Contact, and Author NAKAI. S (NIED)
6.Data Center NIED (Investigator)
7.Originating Center NIED (Investigator)
8.Campaign or Project JEXAM, MeDRS-NIED
9.Storage Medium archived in a 2.4 T byte mass storage
10.Parameter Measured
11.Discipline Keywords
12.Coverage around Japan
13.Location Keywords
14.General Keywords
15.Revision Date
16.Science Review Date
17.Future Review Date
18.References
19.Summary Brightness levels of NOAA/AVHRR are archived. LAC compatible (IPC format) raw data and 1024x1024 geometrically converted data are archived. Currently the data is in the mass storage of the receiver system so that copying into 8mm data cartridge is necessary before using the data. Visual data list is available. This data set is available on the basis of cooperative research.

1. Directory Entry Title
Temperature/Depth data in the indian Ocean

2. Directory Entry Start and Stop Date
Start Date : 1989-04-01
Stop Date : 1997-12-31

3. Sensor name
CBT > Compact Bathytermgraph, XBT > Expendable Bathytermgraph,
MBT > Memory Bathytermgraph, CTD > Conductivity, Temperature and Depth Senser
XCTD > Expendable Conductivity, Temperature and Depth Senser

4. Source Name
SOP > Ships of Opportunity

5. Investigator, Technical Contact, and Author
(1) Investigator
Voluntary Ships
(2) Technical Contact
None
(3) Autor
Last name : Inagake
First name : Denzo
E-mail : ina@enyo.affrc.go.jp
Phone : +81-543-36-6064
Address : National Research Institute of Far Seas Fisheries, Fisheries Agency
5-7-1, Orido, Shimizu, Sizuoka, 424-8633, Japan

6. Data Center
(1) Data Center Name : NRIFSF > National Research Institute of Far Seas Fisheries, Fisheries Agency
(2) Data set ID
(3) Data Center Contact
Last name : Inagake
First name : Denzo
E-mail : ina@enyo.affrc.go.jp
Phone : +81-543-36-6064
Address : National Research Institute of Far Seas Fisheries, Fisheries Agency
5-7-1, Orido, Shimizu, Sizuoka, 424-8633, Japan

7. Originating Center

8. Campaign or Project
Project : JEXAM > Japanese Experiment on Asian Monson

9. Storage Medium
DOS Formatted 3.5 inch Magneto Optical Disk

10. Parameter Measured Hydrologic Patameters > Temperature
11. Discription Keywords Earth Science > Ocean
12. Coverage Minimum Latitude : 30 S Maximum Latitude : 10 N Minimum Longitude : 40 E Maximum Longitude : 120 E
13. Location Keywords Indian Ocean > Tropical Indian Ocean
14. General Keywords Asian Monsoon
15. Reversion Date 1998-11-12
16. Science Review Date 1998-11-12
17. Future Review Date 2000-03-31
18. References
19. Summary National Research Institute of far Seas Fisheries have participated in JEXAM program, and has deployed observation network of subsurface temperature in the Indian Ocean by voluntary ships. Maximum depth of tempetature is depends on a ship but mostly expends up to 400-500 m. Each 10 m temperature is reported for an individual observation. Location, time, and temperature data are quality controled. the data are to be sent to JODC annually.

1. Directory Entry Title XBT observation between the South China Sea and the Persian Gulf
2. Directory Entry Start and Stop Date Start Date : 07 Oct. 1990 Stop Date :
3. Sensor Name XBT > Expendable bathythermograph
4. Source Name Kashimasan Maru
5. Investigator, Technical Contact, and Author (1) Investigator (Last Name) (First Name) (Middle Name) Name : Tadashi Asoh Email : tasoh@met.kishou.go.jp Phone : +81-3-3212-8341 Ext. 5165 Address : Oceanographical Division Climate and Marine Department, Japan Meteorological Agency 1-3-4 Otemachi, Chiyoda-ku, Tokyo 100-8124, Japan (2) Technical Contact Name : Satoshi Sugimoto Email : s_sugimoto@met.kishou.go.jp Phone : +81-3-3212-8341 Ext. 5129 Address : Oceanographical Division Climate and Marine Department, Japan Meteorological Agency 1-3-4 Otemachi, Chiyoda-ku, Tokyo 100-8124, Japan
6. Data Center (1) Data Center Name : Global Subsurface Data Center (2) Dataset ID : (3) Data Center Contact (Last Name) (First Name) (Middle Name) Name : Fabri Marie-Claire Email : Marie.Claire.Fabre@ifremer.fr Phone : +33-02-98-22-46-44 Address : IFREMER/ORSTOM PB 70, 29280 Plouzane, France
7. Originating Center
8. Campaign or Project Campaign : TOGA > Tropical Oceans and Global Atmosphere Campaign : WOCE > World Ocean Circulation Experiment
9. Storage Medium magnetic disks
10. Parameter Measured Ocean Dynamics > Temperature

11. Discipline Keywords Earth Science > Ocean
12. Coverage Minimum Latitude : 5N Maximum Latitude : 23N Minimum Longitude : 60E Maximum Longitude : 121E
13. Location Keywords Indian Ocean
14. General Keywords
15. Revision Date
16. Science Review Date
17. Future Review Date
18. References
19. Summary Japan Meteorological Agency is operating a voluntary ship for XBT observations at South China Sea, the Strait of Malacca to Sri Lanka and the Persian Gulf. The ship, "Kashimasan Maru", is a crude oil tanker. About 14 sections per year and 4 casts a day are observed.

1. Directory Entry Title : JEXAM drifting buoy data in teh tropical Indian Ocean
2. Directory Entry Start and Stop Date Start date : Feb. 2, 1990 Stop date : Mar. 31, 1999
3. Sensor Name : Surface drifter with SST sensor
4. Source Name : ARGOS
5. Investigator, Technical Contact and Author (1) Investigator Last Name : Yoritaka First Name: Hiroyuki Email : yoritaka@cue.jhd.go.jp (internet) Phone : +81-3-3541-4387 FAX : +81-3-3541-4397 Address : 5-3-1 Tsukiji, Chuo-ku, Tokyo 104 Japan (2) Technical Contact Last Name : Yoritaka First Name : Hiroyuki Email : yoritaka@cue.jhd.go.jp (internet) Phone : +81-3-3541-4387 FAX : +81-3-3541-4397 Address : 5-3-1 Tsukiji, Chuo-ku, Tokyo 104 Japan (3) Author Last Name : Yoritaka First Name : Hiroyuki Email : yoritaka@cue.jhd.go.jp (internet) Phone : +81-3-3541-4387 FAX : +81-3-3541-4397 Address : 5-3-1 Tsukiji, Chuo-ku, Tokyo 104 Japan
6. Data Center (1) Data Center Name : Japan Oceanographic Data Center (2) Data Set ID : (3) Data Center Contact Last Name : Nagai First Name : Toshio Email : jodc@osman.jhd.go.jp (internet) Phone : +81-3-3541-4295 FAX : +81-3-3545-2885 Address : 5-3-1 Tsukiji, Chuo-ku, Tokyo 104 Japan
7. Originating Center
8. Campaign or Project Project : Japanese Experiment on Asian Monsoon (JEXAM)
9. Storage Medium : MagnetoOptical Disk, 7 Mbyte
10. Parameter Measured : Locations of drifters, SST

11. Discipline Keywords
Earth science > Tropical Indian Ocean > Oceanic currents

12. Coverage
Minimum latitude : 33 S
Maximum latitude : 24 N
Minimum longitude : 38 E
Maximum longitude : 135 E

13. Location Keywords
Indian Ocean > Tropical Region

14. General Keywords
Surface currents > Heat Transport

15. Revision Date
March 31, 1999

16. Science Review Date

17. Future Review Date

18. References

Hydrographic Department of Japan, Surface Currents and Upper Oecan Thermal Structure in the Indian Ocean (small atlas), 1994.

Michida, Y. and H. Yoritaka, Survivability of the surface drifters deployed by Hydrographic Department of Japan for the period from 1988 to 1993, J. Japan Soc. Mar. Surv. Tech. 7(2), 21-28, 1995.

Michida, Y. and H. Yoritaka, Surface currents in the area of the Indo-Pacific throughflow and in the tropical Indian Ocean observed with surface drifters, J. Geophys. Res., 101, 12475-12482, 1996.

1. Directory Entry Title Snow cover and permafrost data
2. Directory Entry Start and Stop Date Start : July 1993 Stop : March 1999
3. Sensor Name Snow weight meter and frozen ground depth meter
4. Source Name
5. Investigator, Technical Contact, and Author Takeshi Sato E-mail : tsato@shinjo.bosai.go.jp Phone : +81-233-22-7550 Fax : +81-233-23-3353 Address : Tokamachi, Shinjo, Yamagata 996-0091, Japan
6. Data Center National Research Institute for Earth Science and Disaster Prevention (NIED), Shinjo Branch of Snow and Ice Studies
7. Originating Center
8. Campaign or Project Japanese Experiment of Asian Monsoon (JEXAM)
9. Storage Medium FD
10. Parameter Measured Snow weight(water equivalent of snow), frozen ground depth, ground temperature
11. Discipline Keywords Earth science, cryosphere
12. Coverage Lhasa : 29° 40′ N, 91° 08′ E Rikeze : 29° 15′ N, 88° 53′ E Nagqu : 31° 29′ N, 92° 04′ E
13. Location Keywords Tibetan Plateau
14. General Keywords Tibetan Plateau, snow weight, water equivalent of snow, frozen ground depth
15. Revision Date
16. Science Review Date
17. Future Review Date
18. Reference
19. Summary

Directory Entry Title	CRL Wind Profiler Data Archive
Directory Entry Start and Stop Date	See summary
Sensor Name	Boundary Layer Radar (BLR) or L-band Wind Profiler Radar
Source Name	Communication Research Laboratory (CRL)
Investigator, Technical Contact, and Author	Yuichi Ohno (ohno@crl.go.jp) Tatsuhiro Adachi (adachi@crl.go.jp) Yoshihisa Masuda (masuda@crl.go.jp)
Data Center	Communication Research Laboratory (CRL)
Originating Center	Communication Research Laboratory (CRL)
Campaign or Project	Project
Storage Medium	WWW (http://www.crl.go.jp/ck/ck121/windprof)
Parameter Measured	Height profiles of wind velocity
Discipline Keywords	Radar remote sensing
Coverage	300 m – 3000 m in altitude
Location Keywords	Bangkok, Thailand, Tokyo, Okinawa, Japan
General Keywords	Wind Measurement, Boundary Layer Radar, BLR, Wind Profiler Radar, Asian Monsoon
Revision Date	
Science Review Date	
Future Review Date	
References	
Summary	This data is research data and was collected with the intent of using it for meteorological research. The Communications Research Laboratory (CRL) and researcher in charge of this page make no warranties as to the accuracy of the data. The CRL will modify the data or may suspend this service at any time. In the case of use of this data for your papers, you should write the source of the data (CRL Wind Profiler Data Archive) clearly in your paper. In the case of use of this data for commercial use, you should inform the Communications Research Laboratory (ohno@crl.go.jp) and ask for permission to use.

1. Directory Entry Title
Surface Meteorological data of AWS

2. Directory Entry Start and Stop Date
Start Date: 6 July 1993
Stop Date:

3. Sensor Name
wind vane, anemometer, thermometer, hygrometer, rain gauge, barometer, soil moisture gauge, pyranometer, radiometer

4. Source Name
AWS > Automatic Weather Station

5. Investigator, Technical Contact, and Author
(1) Investigator
Last Name: Shigenori
First name: Haginoya
E-mail: shaginoy@mri-jma.go.jp
Phone: +81-298-53-8706
Address: M.R.I., 1-1 Nagamine, Tsukuba, Ibaraki 305, Japan
(2) Technical Contact
Last Name:
First name:
E-mail:
Phone:
Address:
(3) Author
Last Name:
First name:
E-mail:
Phone:
Address:

6. Data Center
(1) Data Center Name: MRI > Meteorological Research Institute
(2) Data set ID:
(3) Data Center Contact
Last Name
First name:
E-mail:
Phone:
Address:

7. Originating Center

8. Campaign or Project
JEXAM > Japanese Experiment of Asian Monsoon

9. Storage Medium
3.5" MO disk

10. Parameter Measured
wind direction, wind speed, air temperature, relative humidity, precipitation, air pressure, soil temperature, soil water content, global solar radiation, reflective solar radiation, net radiation.

11. Discipline Keywords
Earth Science > Atmosphere

12. Coverage
Lhasa: 29° 40'N, 91° 08'E
Rikeze: 29° 15'N, 88° 53'E
Nagqu: 31° 29'N, 92° 04'E
Lingzi: 29° 34'N, 94° 28'E

13. Location keywords
Tibetan Plateau

14. General Keywords

15.	Revision Date
16.	Science Review Date
17.	Future Review Date
18.	References
19.	Summary This data set is available to a third party who gets the permission from CMA.

1. Directory Entry Title Sea Surface Meteorological data of AWS
2. Directory Entry Start and Stop Date Start Date: 23 October 1991 Stop Date: 7 October 1995
3. Sensor Name wind vane, anemometer, thermometer, hygrometer, rain gauge, barometer, pyranometer, radiometer
4. Source Name AWS > Automatic Weather Station
5. Investigator, Technical Contact, and Author (1) Investigator Last Name: Shigenori First name: Haginoya E-mail: shaginoy@mri-jma.go.jp Phone: +81-298-53-8706 Address: M.R.I., 1-1 Nagamine, Tsukuba, Ibaraki 305, Japan (2) Technical Contact Last Name: First name: E-mail: Phone: Address: (3) Author Last Name: First name: E-mail: Phone: Address:
6. Data Center (1) Data Center Name: MRI > Meteorological Research Institute (2) Data set ID: (3) Data Center Contact Last Name First name: E-mail: Phone: Address:
7. Originating Center
8. Campaign or Project JEXAM > Japanese Experiment of Asian Monsoon
9. Storage Medium 3.5" MO disk
10. Parameter Measured wind direction, wind speed, air temperature, relative humidity, precipitation, air pressure, sea surface temperature, global solar radiation, long wave radiation.
11. Discipline Keywords Earth Science > Atmosphere
12. Coverage Minimum Latitude:36S Maximum Latitude: 36N Minimum Longitude: 18E Maximum Longitude: 140E
13. Location keywords Indian Ocean
14. General Keywords

15.	Revision Date
16.	Science Review Date
17.	Future Review Date
18.	References
19.	Summary

1. Directory Entry Title
Surface Meteorological data of AWS

2. Directory Entry Start and Stop Date
Start Date: 25 September 1997
Stop Date:

3. Sensor Name
wind vane, anemometer, thermometer, hygrometer, rain gauge, barometer, soil moisture gauge, pyranometer, radiometer, soil heat plate

4. Source Name
AWS > Automatic Weather Station

5. Investigator, Technical Contact, and Author
(1) Investigator
Last Name: Shigenori
First name: Haginoya
E-mail: shaginoy@mri-jma.go.jp
Phone: +81-298-53-8706
Address: M.R.I., 1-1 Nagamine, Tsukuba, Ibaraki 305, Japan
(2) Technical Contact
Last Name:
First name:
E-mail:
Phone:
Address:
(3) Author
Last Name:
First name:
E-mail:
Phone:
Address:

6. Data Center
(1) Data Center Name: MRI > Meteorological Research Institute
(2) Data set ID:
(3) Data Center Contact
Last Name
First name:
E-mail:
Phone:
Address:

7. Originating Center

8. Campaign or Project
JEXAM > Japanese Experiment of Asian Monsoon

9. Storage Medium
3.5" MO disk

10. Parameter Measured
wind direction, wind speed, air temperature, relative humidity, precipitation, air pressure, soil temperature, soil water content, global solar radiation, reflective solar radiation, downward long wave radiation upward long wave radiation, soil heat flux.

11. Discipline Keywords
Earth Science > Atmosphere

12. Coverage
Gaize: 32° 12'N, 84° 24'E
Shiquanhe: 32° 30'N, 80° 05'E

13. Location keywords
Tibetan Plateau

14. General Keywords

15. Revision Date

16.	Science Review Date
17.	Future Review Date
18.	References
19.	Summary This data set is available to a third party who gets the permission from CMA

1. Directory Entry Title. Monthly meteorological data in China
2. Directory Entry Start and Stop Date I January 1971 and 31December 1981
3. Sensor Name Temperature, Humidity, Precipitation etc.
4. Source Name Same as item 3
5. Investigator, Technical Contact, and Author T. Kishii, T. Kishii, and T. Kishii
6. Data Center National Research Institute for Earth Science & Disaster Prevention
7. Oribinating Center Beijing meteorological Center
8. Campaign or Project Analytical study of water balance on representative river basin
9. Storage Medium Floppy Disk
10. Parameter Measured Same as item3
11. Discipline Keywords Hydrology, Meteorology
12. Coverage 196 stations in China
13. Location Keywords Same as item 12
14. General Keywords Hydro-Meteorological data
15. Revision Data 10 May 1999
16. Science Review Date 10 May 1999
17. Future Review Date 10 December 1999
18. References Same as item 1
19. Summary

1.Directory Entry Title JMA global physical parameter data
2.Directory Entry Start and Stop Date Start Date: April 1, 1996 Stop Date: March 31, 1999
3.Sensor Name Operational atmospheric observation
4.Source Name The four dimensional data assimilation system at the Japan Meteorological Agency
5.Investigator, Technical Contact, and Author (1)Investigator (Last Name) (First Name) (Middle Name) Name : Yoshiaki Takeuchi Email : takeuchi@npd.kishou.go.jp Phone : +81-3-3212-8341 ext.3320 Address : 1-3-4 Oote-machi, Chiyoda-ku, Tokyo 100-8122, Japan (2)Technical Contact Name : Masayuki Kyouda Email : kyouda@naps.kishou.go.jp Phone : +81-3-3212-8341 ext.3320 Address : 1-3-4 Oote-machi, Chiyoda-ku, Tokyo 100-8122, Japan
6.Data Center (1)Data Center Name : (2)Dataset ID : (3)Data Center Contact :
7.Originating Center Numerical Prediction Division, Forecast Department, Japan Meteorological Agency
8.Campaign or Project Project: Japanese Experiment on Asian Monsoon (JEXAM)
9.Strage Medium CD-ROM
10.Parameter Measured Atmospheric Dynamics > Heat flux, Radiation flux, Water flux
11.Discipline keywords Earth Science > Global>Atmosphere
12.Coverage Global
13.Location keywords Global
14.General Keywords Assimilation

15.Revision Date
16.Science Review Date
17.Future Review Date
18.References
19.Summary Japan Meteorological Agency has compiled the global water circulation data set onto CD-ROM (2 disks per year) and have distributed them to Asian monsoon researchers. The grid of the data is 2.5 deg x 2.5 deg and the time interval is 6 hours. Parameters of the JMA global physical parameter CD-ROM are run off, latent heat flux, sensible heat flux, transpiration, interception loss, rain rate, horizontal flux of water vapor, radiation flux at surface, radiation flux at the top of atmosphere, total cloudiness, cloud radiative forcing, and precipitable water.

1. Directory Entry Title: Hydrological data in Chaophraya River Basin, Thailand and Huaihe River Basin in China

2. Directory Entry Start and Stop Date
Chaophraya River Basin: April 1982 to March 1986
Huaihe River Basin: January 1983 to December 1989

3. Sensor Name

4. Source Name

5. Investigator, Technical Contact and Author
Technical Contact : Name Kazurou Nakane
e-mail nakane@ess.bosai.go.jp
Phone 81-298-51-1611 ex.541
Fax. 81-298-511610
Address Atmospheric and Hydrospheric Science Division,
National Research Institute for Earth Science and Disaster Prevention
3-1, Tennodai, Tsukuba, Ibaraki, 3050006 Japan

6. Data Center : Non

7. Originating Center: Royal Irrigation Department, Thailand
Ministry of Water Resources, China
State Meteorological Administration, China

8. Campaign or Project: Japanese Experiment on Asian Monsoon(JEXAM)

9. Storage Medium: Floppy Disk

10. Parameter Measured: number presents number of stations
Chaophraya River Basin:Daily discharge 11, daily precipitation 43 and daily evaporation 15
Huaihe River Basin: Daily discharge 17, daily precipitation 38 and daily evaporation 15

11. Discipline Keywords: Hydrology, Water resources

12. Coverage: Chaophraya River Basin, Thailand:110 thousand km^2
Huaihe River Basin, China: 121 thousand km^2

13. Location Keywords: Thailand, Tropics, Warm humid area, Asia

14. General Keywords : Hydrological data

15. Revision Date

16. Science Review Date

17. Future Review Date

18. References

19. Summary

1. Directory Entry Title: Analyzed Monthly Air-temperature over the Asian Continent and(M-AT) , Monthly Regional Satellite Data mosaiced by NOAA AVHRR GAC data (M-RSI)
2. Directory Entry Start and Stop Date M-AT data: January 1989 to April 1992 M-RSI data: January 1989 to December 1993
3. Sensor Name NOAA AVHRR GAC
4. Source Name
5. Investigator, Technical Contact and Author Investigator: Name Kazurou Nakane e-mail nakane@ess.bosai.go.jp Phone 81-298-51-1611 ex.541 Fax. 81-298-511610 Address Atmospheric and Hydrospheric Science Division, National Research Institute for Earth Science and Disaster Prevention 3-1, Tennodai, Tsukuba, Ibaraki, 3050006 Japan Technical Contact : Same as above. Author: Same as above.
6. Data Center : Non
7. Originating Center: NOAA
8. Campaign or Project: Japanese Experiment on Asian Monsoon(JEXAM)
9. Storage Medium: MagnetoOptical Disk
10. Parameter Measured: Estimated monthly air-temperature Regional data of NOAA AVHRR GAC data
11. Discipline Keywords: Air-temperature, Surface environment, Regional scale
12. Coverage: From 60° N to 20° S in latitude and from 30° E to 160° E in longitude with 2 minutes resolution
13. Location Keywords: Asia
14. General Keywords : Regional surface condition
15. Revision Date
16. Science Review Date
17. Future Review Date
18. References
19. Summary

研究評価報告

Report of the Study Evaluation

海洋開発及地球科学技術調査研究促進費
「アジアモンスーン機構に関する研究」
第Ⅱ期（平成５年度～１０年度）
評価報告

［評価の目的］　これまでの研究成果を総括するとともに、この分野の最新の研究状況を鑑みつつ、本研究プロジェクトの終了後に、新規構築すべき研究プロジェクトの指針を見出す。

［評価対象期間］　平成５年度～１０年度

［評　価　者］　研究評価委員会

（主査）　鳥羽良明：海洋科学技術センター　研究顧問
（東北大学名誉教授）

（委員）　小池俊雄：東京大学大学院工学系研究科　教授
松本　淳：東京大学大学院理学系研究科　助教授

［委員会の開催］　第１回終了評価委員会　（平成１２年１月１９日）

研究実施者からヒアリング

第２回終了評価委員会　（平成１２年２月１６日）

研究実施者からヒアリング
評価のとりまとめ

『プロジェクト研究全般に対する評価委員会提言』

プロジェクト研究によって得られた新しい観測データを速やかに公開することと、それを使って世界に先駆けた優れた研究成果を出して発表することとが、両立して進められる方策を推進する必要がある。具体的には次の２項目を提言する。

１．機関間の協力研究、及び研究論文作成の推進について

担当機関が研究所の場合は研究論文を出すことが業務であるが、現業機関であっても、プロジェクトとしての「研究」の担当の仕方、機関間の協力関係、役割分担の考え方、成果の評価の仕方、また、携わる職員個人の、研究発表や研究論文作成を含めた業績評価など、プロジェクトに関わる業務評価を明確にしておく必要がある。

２．地球観測データベース関連業務の推進について

地球環境の時代に、日本が国際社会における役割を良く果たすためには、関係する機関が、それぞれに観測データを世界に流通させるよう、十分機能する必要がある。しかし、いま日本の諸機関は、そのような専任部署、またそれに必要な人員を置く「ゆとりがない」傾向が強い。あるいは、お役所的で、観測データをすぐ公開しない過去の傾向を、ある程度引きずっていることも背景にあるようである。

したがって、国際的に見て、特に米国と比較した場合、データ公開の機能に格段の遅れがある。それは現在の日本の構造的欠陥であり、いま真剣に、国際社会に後れを取らない対策を立てる必要がある。少なくとも、それぞれの機関に、データセンター的な部署と必要な人員を配置し、その機関での観測データベースを作成し、さらに他機関のデータベースと連携しつつ、それを維持・更新することができるようにすべきである。

特にプロジェクト的な研究では、観測データを迅速に利用可能な形に処理して、解析/モデル研究へ提供する（Data Integration）機能を、プロジェクトの企画初期の段階で定義しておく必要がある。

『評点による評価項目』

評価項目	評点	評点の目安
総合評価	a	初期の目標に鑑み極めて優れた研究であり、その成果は極めて高く評価できる
	b	初期の目標に鑑み優れた研究であり、その成果は高く評価できる。
	c	初期の目標に鑑み研究を実施した意義は認められるが、その成果はあまり評価できない。
	d	研究を実施した意義に乏しい。
1．当初想定した成果は得られたか？	a	想定以上の成果が得られた。
	b	想定していた成果が得られた。
	c	成果は必ずしも十分ではなかった。
	d	成果は極めて小さかった。
2．当初想定していない成果は得られたか？	a	当初想定していない大きな成果が得られた。
	b	当初想定していないかなりの成果が得られた。
	c	当初想定していない若干の成果が得られた。
	d	当初想定していない成果は得られなかった。
3．計画どおり進捗したか？	a	計画以上に進捗した。
	b	計画どおり進捗した。
	c	進捗度は必ずしも十分でなかった。
	d	進捗度は極めて低かった。
4．進め方は適切であったか？	a	進め方は適切であった。
	b	進め方は概ね適切であった。
	c	進め方は必ずしも適切ではなかった。
	d	進め方は適切でなかった。
5．目標は適切であったか？	a	目標は適切であった。
	b	目標は概ね適切であった。
	c	目標設定に疑問がある。
	d	目標は適切でなかった。
6．外的条件の変化（外的条件の変化とは，科学技術上または経済，社会上の変化をいう。）	a	研究開発開始当時に比べ、研究開発の対象を巡る外的条件の変化に伴い研究開発の重要性が増加した。
	b	研究開発開始当時に比べ、研究開発の対象を巡る外的条件に特段の変化はない。
	c	研究開発開始当時に比べ、研究開発の対象を巡る外的条件の変化に伴い研究開発の重要性が低下した。

『全体評価』

【評点】

総合評価	:	b（優れた研究）
当初想定した成果	:	b（想定通りの成果）
当初想定しなかった成果	:	b（想定外のかなりの成果）
計画の進捗状況	:	b（計画通り進捗）
研究の進め方	:	c（必ずしも適切でない）
目標設定の適切さ	:	b（概ね適切）
外的条件の変化	:	a（重要性が増加）

【総合評価コメント】

アジアの水資源、農業生産等に重大な影響を与えるアジアモンスーンの変動性の理解と予測の重要度が高まっている現時点から振り返ると、10年前に企画された本研究は、長期的視野に立った先見性のあるプロジェクトであったと、その意義を高く評価する。そして所期の目標に鑑み、個々の研究課題については、概ね優れた成果を出している。

但し、本来総合的な取り組みが必要であったにも関わらず、一部を除き各研究間の連携が不十分で、アジアモンスーンの総合理解に至らなかった点は残念である。

【果たした役割、果たすべきであった役割】

インド洋やチベット高原等、従来、観測データが不十分だった地域で、きちんとした観測がなされ、ある程度の期間のデータ蓄積がなされたことは、10年プロジェクトならではであり、今後のモンスーン研究にも大きく貢献する財産である。

しかし、モデル・観測・解析相互間の連携や、海洋と陸面相互の連関等については、十分な役割を果たせなかった感が強い。

【今後の発展】

本研究の課題の多くは、もともとこれで終わらぬテーマであり、今後ますます長期観測によるデータ取得が不可欠となってくる。そこで、本研究によって確立された長期モニタリングシステムを、継続的に運用できるような仕組みを作る必要がある。それには、観測訓および解析の技術移転、基本的測器の提供等によって、アジア各国との協力体制を培っていく必要がある。また、取得した貴重なデータによるデータベースについては、できる限り継続すると共に、可能なものは広く世界の研究者に公開すべきである。

今後の研究の方向性として、モンスーン活動の広域的・地域的変動を軸に、陸面や海洋のデータを総合的に解析し、モンスーン機構そのものの理解を進めるべきである。そのため、各研究グループを組織し、戦略的に研究を進める体制作りをすべきである。

『課題別評価』

Ⅰ．大気・海洋・陸域間相互作用の諸過程に関する観測・解析研究

1．1　大気における諸過程に関する観測・解析研究

1．1．1　大規模積雲対流活動と降水系に関する解析研究
気象庁 気象研究所

【評点】 総合（ｂ）　想定成果（ｂ）・想定外成果（ｃ）・計画進捗状況（ｂ）
進め方（ｃ）・目標設定（ｂ）・外的条件変化（ａ）

【総合】 衛星データを中心にアジアモンスーン域の日周変化、および季節進行の様相に関する特徴が抽出されるなど、細かい観測事実の記述が種々進んだが、アジアモンスーン全体の形成機構との関係について、中間評価でコメントしたにもかかわらず、ほとんど進展がなかったことは残念であった。

【役割】 GMSヒストグラムデータの整備、研究者への配布及びそれにより明らかになった知見は重要な成果。但し、広域的なモンスーンシステムの中で、数値モデル研究者との相互作用による、全体的なメカニズム理解がほしかった。

【発展】 対流活動、降水量のデータとしては貴重なものが蓄積されたので、それを用いてモンスーンの形成機構そのものに迫る研究をすべきである。ゾンデ観測資料を取り込んだ総合解析が望まれる。

1．1．2　大規模雲域内における対流雲構造に関する観測研究
気象庁 気象研究所

【評点】 総合（ｂ）　想定成果（ｂ）・想定外成果（ｂ）・計画進捗状況（ｃ）
進め方（ｃ）・目標設定（ｃ）・外的条件変化（ｂ）

【総合】 台風及び梅雨期のクラウドクラスター内部の構造を亜熱帯域で初めて詳細に観測できたことは良かった。それなりの結果を出した点は評価できるが、査読付きの雑誌に10年間のプロジェクトで１本も発表がない点は大きな問題点である。

【役割】 日本に来る前の海上における、台風の内側降雨帯の構造については新しい発見があったが、それを台風構造論の中できちんと位置づけなかった点は問題。またアジアモンスーンとの関係も希薄で、ただ観測をしたという感じを否めない。

【発展】 アジアモンスーン域での、水エネルギー輸送におけるメソシステムが果たす役割に焦点をおいた研究が必要である。観測結果を台風もしくは梅雨前線の降水機構の中できちんと位置付け、学術論文として公表することが必要である。

１．１．３　モンスーン域対流雲の維持過程と水収支に関する研究
科学技術庁 防災科学技術研究所

【評点】 総合（ｂ）　想定成果（ｃ）・想定外成果（ｂ）・計画進捗状況（ｃ）
進め方（ｂ）・目標設定（ｂ）・外的条件変化（ｂ）

【総合】 観測に基づき、１例ではあるが、従前のスコールラインとは異なったクラウド・クラスター形成があることを解明できた点は評価できる。しかし対象とした事例が少なく、モンスーン域の代表性の確認が得られていない。

【役割】 梅雨前線帯の中でのクラウドクラスター形成に関して、一定の知見を得た。その知見の一般性､より広域的な梅雨前線帯の中での位置付けなどがなされるべきであった。

【発展】 他の地域の現象との関係などで、一般性を研究することが必要である。レーダー＋衛星による限定域の観測から、衛星データによる広域特性の把握、ひいてはメソ対流系と巨視的なモンスーンとの関係解明へと発展すべきである。

１．２　海洋における諸過程に関する観測・解析研究

１．２．１　表層水温に関する観測研究
気象庁 気候・海洋気象部

【評点】 総合（ａ）　想定成果（ｂ）・想定外成果（ｂ）・計画進捗状況（ｂ）
進め方（ａ）・目標設定（ａ）・外的条件変化（ａ）

【総合】 インド洋の観測データの蓄積に対する貢献は大いに意義深く、Dipole modeの論文のデータになったことは評価できる。また海洋データ同化システムを併用した解析も適切であった。しかし、陸域のアジアモンスーンとの関係にまで踏み込めなかった点は不満が残る。

【役割】 観測の乏しいインド洋での貴重な観測データの蓄積とその解析に対して、重要な役割を果たした。しかし、アジアモンスーンに対するインド洋の役割については、十分に研究が進まなかった。

【発展】 観測の継続およびアジアモンスーンとの関係に踏み込んだ研究の実施が重要である。気象側との連携により、インド洋の変動がモンスーン変動に及ぼす影響を十分に解明すべきである。

１．２．１　表層水温に関する観測研究
水産庁 遠洋水産研究所

【評点】 総合（ｂ）　想定成果（ｂ）・想定外成果（ｂ）・計画進捗状況（ｂ）
進め方（ａ）・目標設定（ａ）・外的条件変化（ｂ）

【総合】インド洋の観測データの蓄積に対する貢献は大いに評価される。また、表層水温の変動特性の解析でも良い成果が得られている。しかし、アジアモンスーンとの関係にまでは踏み込めなかった点については不満も残る。

【役割】インド洋の基本的なデータの取得と提示、並びに季節〜年々変動に関する変動特性の解明に対して重要な成果を得た。XCDT開発に企業と共同するなど、省庁外との共同を進めた点は評価できる。

【発展】観測網の継続とアジアモンスーンに対するインド洋の役割の解明への貢献が期待される。気象庁・水路部等と総合的に共同し、得られたデータに基づく研究を進めて、学術論文として公表するように努めるべきである。

1．2．2　海流循環に関する観測研究
海上保安庁 水路部

【評点】　総合（b）　想定成果（a）・想定外成果（a）・計画進捗状況（b）
　　　　　　　　　　　進め方（b）・目標設定（b）・外的条件変化（a）

【総合】SVPと連動して貴重な2つの成果が得られている。インド洋熱帯域の海洋循環の平均像の提示に貢献した。また、インドネシア通過流に関して、想定以上の成果を出した。

【役割】インド洋の赤道ジェット、南赤道反流、インドネシア通過流の解明に寄与した。論文をJGR('96)に出しており評価できる。しかし、大気観測との連動が不足しており、モンスーンとの関係を含めたメカニズムの解明には至らなかった。

【発展】継続的な観測が望まれる。そして従来とは違った赤道ジェットの発達期の提示が、モンスーン活動などの大気変動とどう関係しているかを解明することを希望する。新しい観測事実などは、学術論文として世界に公表すべきである。

1．2．3　海洋データの標準化及び海洋データ交換の推進
海上保安庁 水路部

【評点】総合（b）　想定成果（a）・想定外成果（a）・計画進捗状況（b）
　　　　　　　　　進め方（b）・目標設定（b）・外的条件変化（a）

【総合】PC通信システムからインターネットシステムへの移行も速やかに行われ、適切なデータ収集配布システムの運営が行われた。しかし、システムの構築としては成功しているが、全体として日常業務的印象を免れなかった。

【役割】「JOIDES」による情報流通体制を確立し、インターネットを利用する体制にしたことは重要な成果であった。しかし、データベースシステムの構築は重要な貢献だが、システムが全体の研究の中で、どのように役立ったかが不明である。また、国際的なデータ交換に関して具体的進展が見えない。

【発展】大気～海洋の包括的データベース作成機能を有するセンターの設立を考えてはどうか。そして、構築されたデータベースの研究への活用の促進と、国際的データ交換の推進を実現すべきである。

1．3　陸域における諸過程に関する観測・解析研究

1．3．1　チベット・ヒマラヤにおける水文変動に関する観測研究
科学技術庁 防災科学技術研究所

【評点】総合（ｂ）　想定成果（ｃ）・想定外成果（ｂ）・計画進捗状況（ｃ）
進め方（ｃ）・目標設定（ｂ）・外的条件変化（ｂ）

【総合】アジアモンスーン機構の研究に連結した陸域の研究で、基礎として有意義であった。困難な観測を実施した点は評価できるが、機器選定などに問題があり、十分な成果を上げられたとは言い難い。得られた貴重なデータを、広域で年々のアジアモンスーンの変動性の観点から研究すべきである。

【役割】困難な遠隔地での観測を実施し、チベット高原での凍土・積雪プロセスと熱収支の基礎的知見を提供した。しかし、広域的なモンスーン活動との関係や、97年の大雪の実態解明には至らなかった。

【発展】諸機関（国内・中国）との連携を密にして、長期観測体制を確立すべきである。少雪地域での積雪量観測方法の確立による広域的積雪情報の取得と、そのモンスーンとの関係の解明が望まれる。

1．3．2　地表面熱収支に関する観測研究
気象庁 気象研究所

【評点】総合（ａ）　想定成果（ｂ）・想定外成果（ｂ）・計画進捗状況（ｂ）
進め方（ｂ）・目標設定（ｂ）・外的条件変化（ａ）

【総合】中国側との粘り強い交渉により、10年プロジェクトでなくてはできない貴重な観測データを取得できたのは大きな成果である。チベット高原での東西の熱・水収支の比較、および年々変動が示され、チベットとアジアモンスーンの変動との関連研究に関する貴重な基礎研究がなされた点は高く評価できる。

【役割】チベット高原という観測が疎で、また観測維持が困難な領域で、観測システムを確立・維持した成果は大きい。チベット高原の地表面熱収支に関して貴重な実測データを提示し、広域的研究への足がかりを得ている。しかし船舶委託の海上気象観測も重要であったが、中断したのは惜しまれる。

【発展】モニタリングシステムの維持により、長期変動の理解に資するデータ収集を目指す

べきである。また、リモートセンシングを含むルーチンデータとモデルを組み合わせて、広域熱収支の長期変動の研究に発展させると共に、得られたデータによる研究成果の公表に力を入れるべきである。

1．3．2　地表面熱収支に関する観測研究
郵政省 通信総合研究所

【評点】総合（b）　想定成果（b）・想定外成果（b）・計画進捗状況（b）
進め方（c）・目標設定（b）・外的条件変化（b）

【総合】境界層レーダ+ RASSシステムの設計・開発に貢献したことは評価できる。但し、観測手法開発が主となってしまい、全体的な研究面への貢献が不十分であった。

【役割】BLRの機器開発に重要な貢献をし、国内のBLR、RASSをリードした。観測場所の選定に関しては問題があった。

【発展】次のプロジェクトに継続して発展してほしい。開発された機器の改良と展開により、アジアモンスーン域の境界層観測のオペレーショナルな観測システムの構築が望まれる。また、対流圏全層が観測可能な測器の開発にも力を入れるべきである。

1．3．3　モンスーン循環広域条件及び雪氷変動状況に関する解析研究
科学技術庁 防災科学技術研究所

【評点】総合（c）　想定成果（b）・想定外成果（c）・計画進捗状況（c）
進め方（c）・目標設定（b）・外的条件変化（b）

【総合】数年分の積雪データセットを作成した点は評価できるが、その成果が他のグループの研究に利用されていないのは残念である。また経年変動などの研究面が不十分であり、査読付きの論文発表がない点は問題である。

【役割】チベット高原で時系列データを用いた積雪アルゴリズムを新たに開発した。広域的な積雪分布のデータセットが完成した点は評価できるが、それを用いた経年変動等の解析で、モンスーン活動との関係を解明すべきであった。

【発展】他の衛星データ等、利用できるものは利用して、さらにデータセットの年数を増やして総合的に発展させるべきである。他の研究グループとの連携を持ってデータが利用されることを希望する。

1．3．4　地域水収支に関する解析研究
科学技術庁 防災科学技術研究所

【評点】総合（b）　想定成果（b）・想定外成果（b）・計画進捗状況（b）
進め方（b）・目標設定（b）・外的条件変化（b）

【総合】アジアモンスーン機構研究の中で位置付けが明確でない。データセットの作成は評価できるが、気象と水文データで期間が合っていないなど、不十分な点がある。

【役割】准河の水文データを取得できた点は有意義である。モンスーン活動など大気側の変動との関係を追求すべきであった。

【発展】1.3.3と結合させて、総合的に解析研究を発展させるべきである。気象データベースを流量データの期間全体に増やし、気候変動と流量等の水文要素の変動との関係を解明することが望まれる。

Ⅱ. 数値モデルによる大気・海洋・陸域間相互作用の実験研究

2．1　数値モデルによる４次元資料同化システムの開発に関する研究
気象庁 予報部

【評点】総合（ｂ）　想定成果（ｂ）・想定外成果（ａ）・計画進捗状況（ｂ）
進め方（ｂ）・目標設定（ｂ）・外的条件変化（ａ）

【総合】４次元資料同化システムのモデル改良による精度向上は非常に大きな成果ではあるが、これは副産物である。目的にあるように、収集された観測データを同化する手法の開発に関する成果を明らかにすべきである。また、全球物理モニターCD-ROMは大変有意義であり、配布した研究者数が若干少ないが、今後の活用が期待される。

【役割】４次元資料同化の成果を広く各研究機関へ配布し、広域解析の貴重な基礎データを提供した。しかし、全球物理モニターデータの提供は有意義だったが、これを利用した研究はなされなかった。また、他の研究の成果がどのようにこのデータに活かされたかもチベットの一部以外では不明である。

【発展】本プロジェクトで指摘された点を踏まえて、全球物理モニターの結果を使ったモンスーンの変動気候解明への取り組みを進めるべきである。

2．2　広域水収支モデルの開発に関する研究
科学技術庁 防災科学技術研究所

【評点】総合（ｂ）　想定成果（ｂ）・想定外成果（ｃ）・計画進捗状況（ｃ）
進め方（ｂ）・目標設定（ａ）・外的条件変化（ａ）

【総合】広域水収支を多数の河川流域について算出できた点は評価できるが、GCMで用いられる陸面スキームとリンクして研究がなされるべきであった。

【役割】大気モデルの出力を使った広域の河川流出量算定により、アジア域の広域水収支モデルを作成した点は重要な役割を果たした。但し、その検証や入力データについては

不十分である。

【発展】入力データの改良や植生効果・人為的影響の組み込みにより、気候変動や地表面状態の変化に伴う水収支の変化の解明を進めるべきである。

Ⅲ. 大気・海洋・陸面間の相互作用に関する総合研究

3．1 大規模モデルによる大気・海洋・陸面間の相互作用に関する実験研究
気象庁 気象研究所

【評点】総合（ａ） 想定成果（ａ）・想定外成果（ｂ）・計画進捗状況（ａ）
進め方（ａ）・目標設定（ａ）・外的条件変化（ａ）

【総合】モンスーンの変動性をGCMを使って総合的に解析し、多くの知見が得られ、数多くの学術論文が出されている。モンスーンの変動に関して正面から取り組んだ感のあるモデル研究で、高く評価できる。

【役割】モンスーン変動の機構解明に対する、モデルによる国際的な先導的研究として位置付けられる。海面水温および陸面状態の変動とモンスーン変動の関係について、モデルの立場からの知見を与えられた点は評価できる。積雪や海水温変動の解析的研究とリンクできなかった点は惜しまれる。

【発展】モデルで得られた知見をもとに、アジアモンスーン全体の変動機構に迫る観測計画の提案・実行を期待する。そして、ENSOとアジアモンスーンの相互作用に関する、さらに深い解明を行うべきである。

3．2 モンスーンのエネルギー収支に関する解析研究
気象庁 気象研究所

【評点】総合（ｂ） 想定成果（ｂ）・想定外成果（ｂ）・計画進捗状況（ｂ）
進め方（ｂ）・目標設定（ｂ）・外的条件変化（ａ）

【総合】解析検討に加えてモデルによる検討も行われ、特に陸面加熱の緩和プロセスが明らかになり、北半球全体の熱収支という視点からアジアモンスーンそのものを全体的に見るという手法から、興味深い知見を得ている。但し、成果の発表が少ないのは問題である。

【役割】大陸・海洋の巨視的熱収支の季節変化の実態を解明したことは意義がある。地上等での観測データとの比較・検討、他の観測研究やモデル研究（課題3.1等）との協力体制がなされなかったのは残念である。

【発展】陸面・海洋での統合的な観測によって作成された４次元同化データを用いて、南北両半球を視野に入れた研究、年々変動のメカニズム解明に切り込む研究等の、精度の高い解析研究が望まれる。

３．３　モンスーン循環系の総合解析
気象庁 気候・海洋気象部

【評点】総合（ｂ）　想定成果（ｂ）・想定外成果（ｂ）・計画進捗状況（ｂ）
進め方（ｂ）・目標設定（ｂ）・外的条件変化（ｂ）

【総合】新しいモンスーン活動のインデックスを作成した点は評価できる。しかし、従来のモンスーンインデックスからの優位性評価や、国際学術論文による情報発信の点で不十分である。

【役割】日本の天候と関係の深い、モンスーンの変動という立場では一定の役割を果たした。但し、他の研究へのアピール不足から、このインデックスを使用した解析が行わなかったのは残念である。

【発展】数値モデル、観測結果（衛星を含む）との連携をとり、新しく相関関係の背後のプロセス解明と、予報への応用を進めるべきである。相関関係を因果関係とするためのメカニズムの考察の深化により、モンスーン変動と日本の天候の関係の理解がより進むものと期待さる。

『研究論文等成果の発表状況』

1）発表件数

	原著論文による発表	論文以外の誌上発表
国内	３０件	５８件
国外	１８件	４１件
計	４８件	９９件

2）受賞等

なし

全般の問い合せ先

〒 100-8966　東京都千代田区霞ケ関２－２－１

科学技術庁研究開発局海洋地球課

Inquiries to:

Ocean and Earth Division,
Research and Development Bureau,
Science and Technology Agency
2-2-1, Kasumigaseki, Chiyoda-ku, Tokyo 100
Japan